



Universiteit  
Leiden

The Netherlands

## **Reactivity of cobalt(II)-dichalcogenide complexes: correlation between redox conversion and ligand-field strength**

Marvelous, C.

### **Citation**

Marvelous, C. (2022, July 5). *Reactivity of cobalt(II)-dichalcogenide complexes: correlation between redox conversion and ligand-field strength*. Retrieved from <https://hdl.handle.net/1887/3421554>

Version: Publisher's Version

License: [Licence agreement concerning inclusion of doctoral thesis in the Institutional Repository of the University of Leiden](#)

Downloaded from: <https://hdl.handle.net/1887/3421554>

**Note:** To cite this publication please use the final published version (if applicable).

# **Reactivity of Cobalt(II)-Dichalcogenide Complexes: Correlation between Redox Conversion and Ligand-field Strength**

Proefschrift

ter verkrijging van  
de graad van doctor aan de Universiteit Leiden,  
op gezag van rector magnificus prof.dr.ir. H. Bijl,  
volgens besluit van het college voor promoties  
te verdedigen op dinsdag 5 Juli 2022  
klokke 10:00 uur

door

**Christian Marvelous**  
geboren te Malang, Indonesië  
in 1994



**Promotores:**

Prof.dr. E. Bouwman

Prof.dr. C. Fonseca Guerra

**Promotiecommissie:**

Prof.dr. H.S. Overkleeft

Prof.dr. S.A. Bonnet

Prof.dr. B. de Bruin (University of Amsterdam)

Dr. C. Duboc (Université Grenoble Alpes, France)

Dr.ing. D.L.J. Broere (Utrecht University)

*“If you wish to succeed in life, make perseverance your bosom friend, experience your wise counselor, caution your elder brother, and hope your guardian genius.”*

Joseph Addison

To my parents and to my future self,  
As a reminder that persistence is almost always rewarding.

# Table of Contents

List of Abbreviations .....	5
Chapter 1      Biomimetic Models of Sulfur-containing Enzymes and a Bioinspired Redox-conversion Reaction .....	7
Chapter 2      Probing The Redox-conversion of Co(II)-disulfide to Co(III)-thiolate Complexes: The Effect of Ligand-Field Strength .....	25
Chapter 3      Cleaner and Stronger: How 8-quinolinolate Facilitates Formation of Co(III)-thiolate from Co(II)-disulfide Complexes.....	47
Chapter 4      Redox-conversion Reactivity of The Chalcogen Family: Selenium vs Sulfur .....	67
Chapter 5      Structural Investigations and Reactivity of Cobalt(II)-Disulfide Complexes.....	89
Chapter 6      Summary, Conclusions, and Outlook.....	107
Appendix I      Supplementary Information for Chapter 2 .....	115
Appendix II      Supplementary Information for Chapter 3 .....	129
Appendix III      Supplementary Information for Chapter 4 .....	143
Appendix IV      Supplementary Information for Chapter 5 .....	157
Samenvatting .....	173
Summary in Indonesian .....	179
Curriculum Vitae .....	185
List of Publications .....	187
Acknowledgements.....	189

# List of Abbreviations

ATP	adenosine triphosphate	mer	meridional
a.u.	arbitrary units	Met	methionine
bpy	2,2'-bipyridine	MO	molecular orbital
br	broad	MS	mass spectrometry
calcd.	calculated	N(nBu <sub>4</sub> )I	tetrabutylammonium iodide
CcO	cytochrome c oxidase	NEt <sub>4</sub> Cl	tetraethylammonium chloride
Cys	cysteine	(NGuaS) <sub>2</sub>	2',2'-(2,2'-dithiodiphenyl)bis(1,1,3,3-tetramethylguanidine)
d	doublet (NMR)	NHase	nitrile hydratase
DCM	dichloromethane	NMR	nuclear magnetic resonance
dd	double doublet	Ph	phenyl
DFT	density functional theory	phen	1,10-phenanthroline
DIPEA	diisopropylethylamine	ppm	parts per million
DMF	dimethylformamide	Py	2-pyridyl
DMSO	dimethylsulfoxide	q	quartet
equiv.	equivalent	Hquin	8-quinolinol
ESI	electrospray ionization	RT	room temperature
fac	facial	s	singlet (NMR), strong (IR)
Glu	glutamic acid	Sec	selenocysteine
His	histidine	Ser	serine
HOTf	trifluoromethanesulfonic acid	SOMO	singly occupied molecular orbital
IR	infrared	t	triplet
Leu	leucine	TDDFT	time-dependent density functional theory
LMCT	ligand-to-metal charge transfer	UV-vis	ultraviolet -visible
m	multiplet (NMR), medium (IR)	vs	very strong
Me	methyl	w	weak



# Chapter 1

---

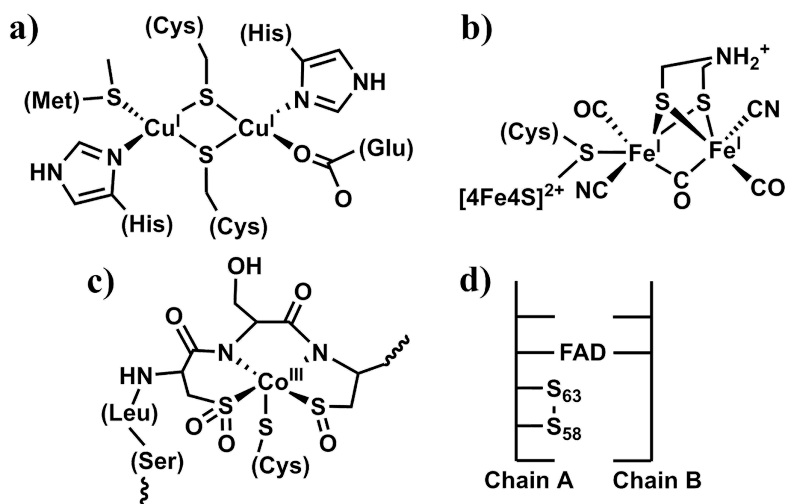
Biomimetic Models of Sulfur-containing Enzymes and a Bioinspired Redox-conversion Reaction

## 1.1. Introduction

### 1.1.1. Sulfur-Containing Enzymes

The presence of the element sulfur in biological systems is prominent, in both structural and functional roles. Due to its chemical versatility, in biological systems sulfur can be present as inorganic sulfur ( $S^{2-}$ ) in iron-sulfur clusters, a thiol group in cysteine (R-SH), a thioether (R-S-R') in methionine, a disulfide e.g. in oxidized glutathione (R-SS-R), or as the partially oxygenated sulfur group (R-SO<sub>x</sub>) in e.g. nitrile hydratases.<sup>1,2</sup>

The sulfur-containing species are utilized by Nature in the form of enzymes, which catalyze various biological processes. Examples of such enzymes are cytochrome *c* oxidase (CcO; **Scheme 1.1.a**), ferredoxin hydrogenase (**Scheme 1.1.b**), nitrile hydratase (NHase; **Scheme 1.1.c**), glutathione reductase (GR; **Scheme 1.1.d**), and many others.<sup>3-12</sup> The CuA site of cytochrome *c* oxidase contains two copper(I) metal centers, each coordinated to a nitrogen atom of histidine moieties and two bridging cysteine thiolates in a diamond-like structure. The structure of the [Fe-Fe] subunit in ferredoxin hydrogenase in the reduced state consists of two iron(I) centers with a bridging CO and an azadithiolate ligand along with several



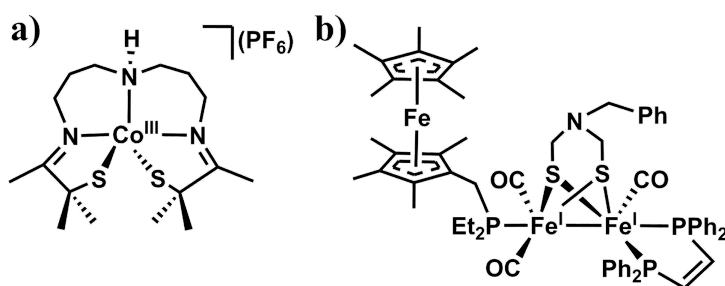
**Scheme 1.1.** Schematic representations of the a) CuA active site in cytochrome *c* oxidase (PDB: 5Z62), b) reduced state of the [Fe-Fe] active site in ferredoxin hydrogenase (PDB: 3C8Y and 1HFE), c) cobalt(III)-containing active site of homology model of nitrile hydratase (PDB: 1IRE), and d) simplified active site of glutathione reductase. Figures are adapted from references<sup>3-12</sup>.

terminal CO and CN ligands. The [Fe–Fe] subunit is also bound to a  $[4\text{Fe}4\text{S}]^{2+}$  cubane cluster. Nitrile hydratases catalyze the conversion of nitriles to amides. Two types of nitrile hydratases have been reported, one with iron(III) as the metal center and the other with cobalt(III). The structures of cobalt NHases are similar to the structure of iron NHase based on the homology model of Fe-NHases, which contains a cobalt(III) center coordinated by two deprotonated peptide nitrogen atoms and two S-oxygenated cysteines.<sup>13-15</sup> The catalytic cycle of glutathione reductase utilizes the reduction of disulfide bonds into thiols and reoxidation to generate the original species.<sup>16</sup>

### 1.1.2. Modelling the Active Sites of Sulfur-Containing Enzymes

The generation of understanding of the working mechanism of enzymes is challenging. Ideally the structure of the enzymes needs to be elucidated, which is an arduous job as crystallization of enzymes is difficult. Even when the structures of enzymes can be determined, correlating the structure to the activity is another immense obstacle. Therefore, in bioinorganic chemistry efforts are made to understand the working mechanism of enzymes using synthetic models. Such synthetic models are usually small molecules that are designed to resemble the structure of the active site of the enzyme of interest. Hence, by studying synthetic models one can potentially clarify the working mechanism of the enzyme of interest.<sup>17, 18</sup>

The group of Kovacs reported the five-coordinated cobalt(III) compound  $[\text{Co}^{\text{III}}(\text{S}_2^{\text{Me}2}\text{N}_3(\text{Pr},\text{Pr}))](\text{PF}_6)$  (**Scheme 1.2.a**) and its analog  $[\text{Fe}^{\text{III}}(\text{S}_2^{\text{Me}2}\text{N}_3(\text{Pr},\text{Pr}))](\text{PF}_6)$  with an accessible binding site for a substrate or inhibitor of the active site of nitrile hydratase.<sup>15</sup>



**Scheme 1.2.** Schematic representations of synthetic models of a) cobalt NHase,<sup>15</sup>  
b) [Fe–Fe] hydrogenase.<sup>21</sup>



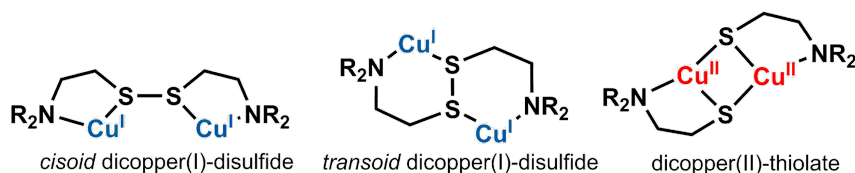
<sup>19, 20</sup> It was reported that several substrates such as azide (NHase inhibitor), ammonia, and thiocyanate (nitrile mimic) can coordinate and subsequently dissociate from the metal center. Other inhibitors such as butyrate or NO (NHase inactivator) did not bind to the cobalt center, but did bind to the iron analog. The results of the study indicated that different mechanisms of enzyme activation and inactivation may be operative for Co-NHase and Fe-NHase, as shown by the binding ability of several biologically relevant substrates towards the model. It was concluded that the thiolate donor *trans* to the vacant site could aid the catalytic process via the *trans* labilizing effect.

An example of a biomimetic model for ferredoxin hydrogenase is depicted in **Scheme 1.2.b**. The dinuclear iron site is highly similar to the [Fe–Fe] subunit of the enzyme, containing two iron(I) centers bridged by an azadithiolate ligand, coordinated with CO and a diphosphine ligand.<sup>7, 21</sup> A ferrocene complex modified with a phosphine group coordinated to one of the iron centers was introduced to mimic the function of [4Fe4S]<sup>2+</sup> group as an electron shuttle. Small molecules such as CO and hydrogen can coordinate to the iron centers, in line with the current proposed catalytic mechanism of [Fe–Fe] hydrogenase.<sup>22, 23</sup>

### 1.1.3. Mimicking Copper(II)-thiolate Active Sites: The Reaction of Cu(I) Salts with Disulfide Ligands

Inspired by the native enzyme cytochrome *c* oxidase, a number of reports describe efforts to construct a synthetic model of the dinuclear copper-bis- $\mu$ -thiolate active site. It is challenging to isolate copper(II)-thiolate species, as generally copper(II) ions in combination with thiolate groups readily undergo an irreversible redox reaction forming copper(I) ions and a disulfide species. The very first dinuclear copper(II)- $\mu$ -thiolate complex containing a single thiolate bridge was reported in 1985.<sup>24</sup> A decade later, the group of Tolman reported the first copper(II)-bis- $\mu$ -thiolate compounds comprising diamond-shaped Cu<sub>2</sub>S<sub>2</sub> cores, using an N<sub>3</sub>S donor ligand as well as an N<sub>2</sub>S donor ligand.<sup>25</sup>

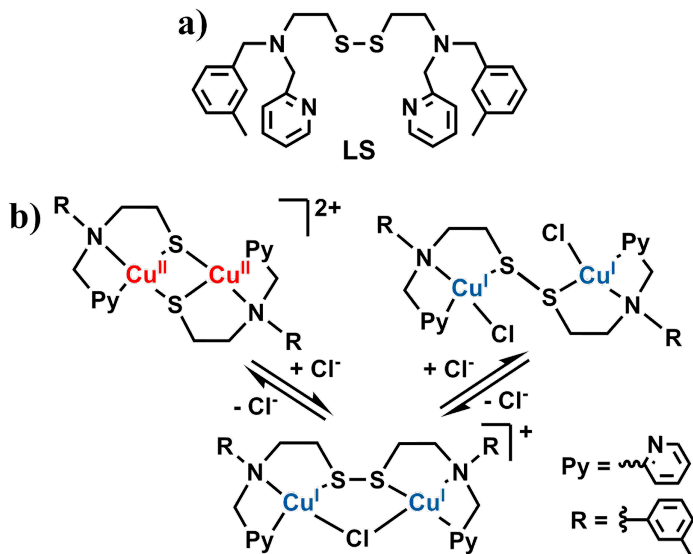
It was not until the early 2000s that the group of Itoh described the unique reverse redox reaction between copper(I) ions and disulfide ligands.<sup>26</sup> It was found that the disulfide bond of a specific chelating ligand can be reduced by copper(I) ions, resulting in the corresponding dicopper(II)-bis- $\mu$ -thiolate species.<sup>26</sup> It was described that slight structural changes of the ligand yielded different species with different coordination geometry, namely either a



**Scheme 1.3.** Different coordination geometries of copper compounds with disulfide and thiolate ligand, adapted from reference <sup>26</sup>.

*cisoid*-dicopper(I)-disulfide, a *transoid*-dicopper(I)-disulfide, or a dicopper(II)- $\mu$ -thiolate compound (**Scheme 1.3**). The structural changes in the ligand affect the donor ability of the pyridine nitrogens of the ligand, consequently influencing the electron density at the copper(I) ions and subsequent electron transfer to the disulfide group.

The discovery of how slight changes of the disulfide ligand affect which copper complex is generated led to a report of the first reversible redox-conversion reaction of a copper(I)-disulfide compound with the corresponding copper(II)-thiolate complex.<sup>27</sup> The reaction in acetone of  $[\text{Cu}(\text{CH}_3\text{CN})_4](\text{ClO}_4)$  with the dissymmetric disulfide ligand **LS**, containing pyridyl and *m*-tolyl groups (**Scheme 1.4.a**) afforded a dicopper(II)-bis- $\mu$ -thiolate complex. The clean conversion of the dicopper(II)-bis- $\mu$ -thiolate complex to



**Scheme 1.4.** a) Schematic drawing of the ligand **LS** used in the first reported redox-conversion reaction of a copper(I)-disulfide to a copper(II)-thiolate complex, b) Chloride-induced redox-conversion reaction between copper(I)-disulfide/copper(II)-thiolate with ligand **LS**.<sup>27</sup>

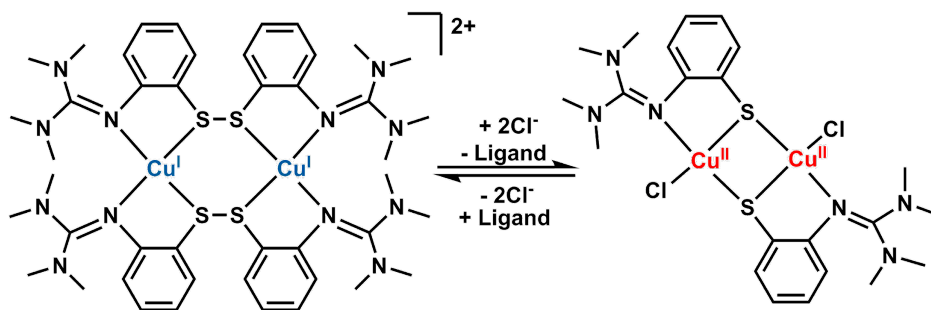
*cisoid*-dicopper(I)-disulfide complex and further to a *transoid*-dicopper(I)-disulfide complex was achieved by stepwise addition of coordinating chloride ions (**Scheme 1.4.b**). Interestingly, the *transoid*-dicopper(I)-disulfide complex can be reverted to the dicopper(II)-bis- $\mu$ -thiolate complex by removal of the chloride ions using a silver salt, showing that this specific redox-conversion reaction is a reversible process.

## 1.2. The Metal-disulfide to Metal-thiolate Redox-conversion Reaction

### 1.2.1. Copper-based Systems

Since the report of the novel redox-conversion reaction between the dicopper(I)-disulfide and dicopper(II)-dithiolate compounds by Itoh in 2002, several attempts to obtain reversible redox systems have been successful, using different ligand systems. The Henkel group reported the synthesis of a dinuclear copper(I)-bis- $\mu$ -disulfide complex upon the reaction of  $[\text{Cu}(\text{MeCN})_4]\text{OTf}$  with one equivalent of the disulfide ligand (NGuaS)<sub>2</sub> in acetonitrile.<sup>28</sup> Upon addition of two equivalents of NEt<sub>4</sub>Cl in dichloromethane, blue crystals of the dinuclear copper(II)-bis- $\mu$ -thiolate species were obtained. This copper(II)-thiolate species is also obtained upon reaction of the disulfide ligand (NGuaS)<sub>2</sub> with two equivalents of copper(I) chloride (**Scheme 1.5**). The reaction from the dicopper(II)-bis- $\mu$ -thiolate compound to copper(I)-bis- $\mu$ -disulfide complex can be achieved by addition of silver tetrafluoroborate, but additional disulfide ligand has to be added to replace the chloride ions.

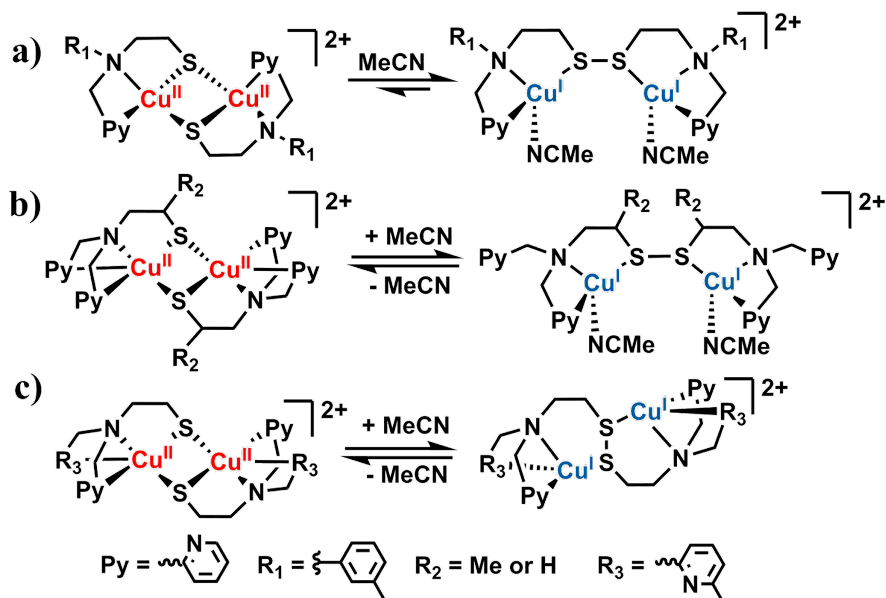
Aside from the addition or removal of chloride ions, the use of solvent has been reported to trigger the redox-conversion reaction between Cu(I)-disulfide and Cu(II)-thiolate complexes. At the time of writing of this Chapter, three reports describe copper compounds of five



**Scheme 1.5.** Schematic representation of the redox-conversion between a Cu(I)-disulfide and a Cu(II)-thiolate compound based on the disulfide ligand (NGuaS)<sub>2</sub> influenced by chloride ions.<sup>28</sup>

different ligands that are either in the Cu(I)-disulfide or Cu(II)-thiolate form, depending on the solvent used during the reaction.<sup>29-31</sup> The group of Itoh reported that a copper(II)-bis- $\mu$ -thiolate compound can be fully converted to the corresponding copper(I)-disulfide complex by changing the solvent (**Scheme 1.6.a**). The copper(II)-bis- $\mu$ -thiolate compound is stable in a relatively nonpolar and non-coordinating solvent such as dichloromethane. Replacement of the non-coordinating solvent by the more polar and weakly coordinating solvent acetone afforded a mixture of the copper(II)-thiolate and copper(I)-disulfide complexes. When the more polar and coordinating solvent acetonitrile (MeCN) was used, the copper(II)-thiolate compound was fully converted to the corresponding copper(I)-disulfide complex.

Similarly, the group of Stack reported the acetonitrile-induced redox-conversion of a Cu(II)-bis- $\mu$ -thiolate complex to the corresponding Cu(I)-disulfide complex (**Scheme 1.6.b**).<sup>30</sup> However, in this reaction two of the coordinating pyridine groups need to

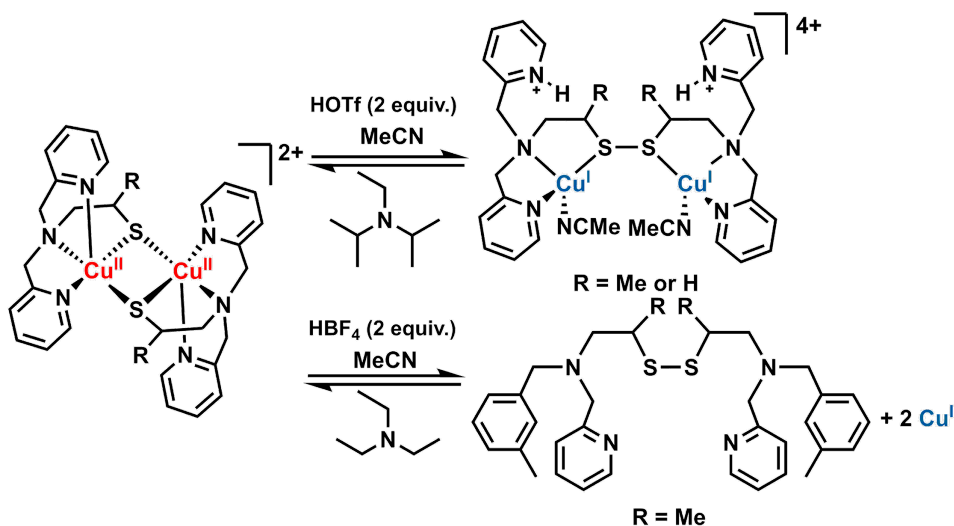


**Scheme 1.6.** Schematic representations of solvent-induced redox-conversion between copper(I)-disulfide and copper(II)-thiolate compounds from a) group of Itoh,<sup>29</sup> b) group of Stack,<sup>30</sup> c) group of Bouwman.<sup>31</sup>

dissociate, and competition between coordination of the pyridine groups and acetonitrile resulted in equilibrium mixtures of the copper(II)-thiolate and copper(I)-disulfide species.

The acetonitrile-induced redox-conversion between copper disulfide and thiolate compounds has also been reported by our group (**Scheme 1.6.c**).<sup>31</sup> However, for the dissymmetric demethylated ligand used in our studies the conversion was not accompanied by the displacement of pyridyl groups with the solvent. The conformation of the resulting Cu(I)-disulfide compound appeared to be *transoid*, in contrast with previous reports where the resulting Cu(I)-disulfide compound is in the *cisoid* conformation. The DFT-calculated formation energy showed that formation of the *transoid* isomer is indeed possible, although the *cisoid* isomer is thermodynamically more stable.

A rather unexplored manner of triggering the redox-conversion process is by using protons. The group of Stack reported that reaction of the dicopper(II)-bis- $\mu$ -thiolate complex shown in **Scheme 1.6.b** with triflic acid (HOTf) in acetonitrile afforded the copper(I)-disulfide complex (**Scheme 1.7**).<sup>30</sup> The reaction was also reported to be reversible using diisopropylethylamine (DIPEA) as a base to deprotonate the pyridinium group, followed by

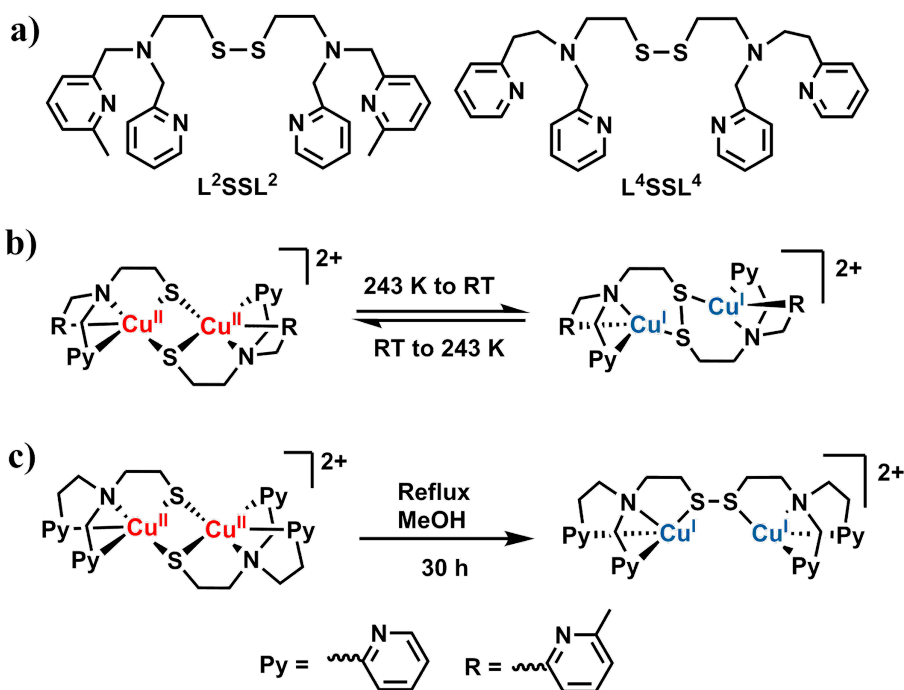


**Scheme 1.7.** Schematic representation of the reversible redox-conversion of copper(I)-disulfide and copper(II)-thiolate complexes induced by the addition of protons or a base.<sup>30, 32</sup>

re-coordination of the pyridine group to the copper(I), promoting the electron transfer to the disulfide group and yields the initial copper(II)-thiolate complex.

At the same time similar studies were also performed in our group. Addition of tetrafluoridoboric acid ( $\text{HBF}_4$ ) to the Cu(II)-thiolate complex (**Scheme 1.7**) was monitored using UV-Visible and  $^1\text{H}$ -NMR spectroscopy.<sup>32</sup> The addition of the acid resulted in sharper proton peaks in  $^1\text{H}$ -NMR spectrum, indicating the formation of Cu(I) species. In contrast to the report of Stack's group, it was observed that the ligand dissociates from the copper centers. DFT studies showed that dissociation of the diprotonated ligand is favored by more than  $100 \text{ kJ mol}^{-1}$  over the formation of a diprotonated Cu(I)-disulfide complex.

Reaction of  $\text{L}^2\text{SSL}^2$  (**Scheme 1.8.a**) with  $[\text{Cu}(\text{MeCN})_4]^+$  in methanol results in formation of an equilibrium mixture of the related copper(II)-thiolate and copper(I)-disulfide compounds. UV-Vis spectroscopy of this mixture showed significant changes in the absorption bands

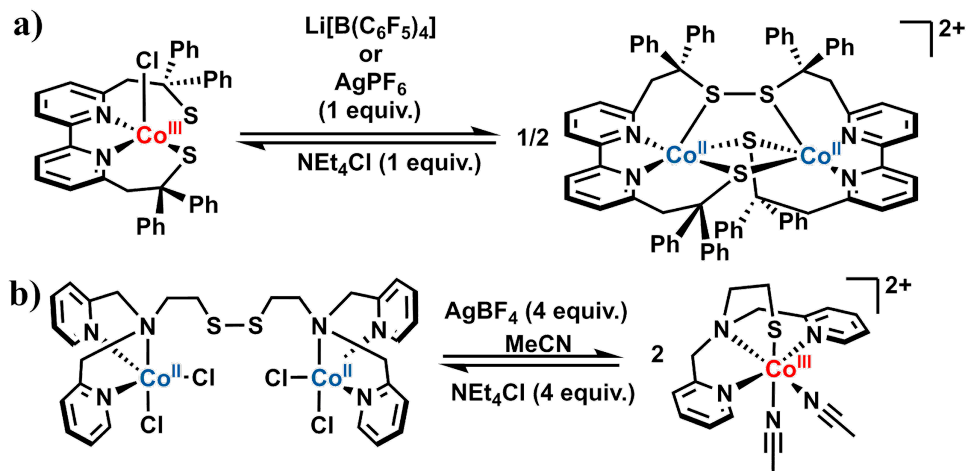


**Scheme 1.8.** a) Structure of the ligand  $\text{L}^2\text{SSL}^2$  and  $\text{L}^4\text{SSL}^4$  used for temperature-induced redox-conversion of copper(I)-disulfide/copper(II)-thiolate; Reaction schemes of temperature-induced redox-conversion of copper(I)-disulfide / copper(II)-thiolate complex of ligand b)  $\text{L}^2\text{SSL}^2$  and c)  $\text{L}^4\text{SSL}^4$ .<sup>31</sup>

upon cooling the solution, indicating a shift in the equilibrium to the Cu(II)-thiolate compound (Reaction **Scheme 1.8.b**).<sup>31</sup> Heating the solution back to room temperature re-established the original spectra, indicating a temperature-induced redox equilibrium. Heating the solution further resulted in the formation of the Cu(I)-disulfide compound. Thus, the Cu(I)-disulfide / Cu(II)-thiolate conversion is reversible in methanol at low temperatures, but irreversible after exposure to higher temperatures. The use of L<sup>4</sup>SSL<sup>4</sup> (**Scheme 1.8.a and Scheme 1.8.c**) resulted in the similar observations, i.e. upon heating the Cu(I)-disulfide compound was irreversibly formed.

### 1.2.2. Cobalt-based Systems

In the last few years, the study of the redox-conversion reaction between metal-thiolate and metal-disulfide complexes has progressed to systems containing other redox-active metal centers. One of the interesting metals to study is cobalt, because of its presence in enzymes such as Co-NHase, as described in Section 1.1.1. The redox-conversion between cobalt(II)-disulfide and cobalt(III)-thiolate compounds was first reported by the group of Duboc in 2014.<sup>33</sup> Via electrochemical methods a mononuclear cobalt(III) complex was obtained of a dianionic N<sub>2</sub>S<sub>2</sub> donor ligand. This five-coordinate cobalt(III) complex is in an unusual high-spin state ( $S = 3/2$ ). Removal of the axial chloride ions using Li[B(C<sub>6</sub>F<sub>5</sub>)<sub>4</sub>] or AgPF<sub>6</sub> generated the (bis-μ-thiolate)-μ-disulfide cobalt(II) complex as shown in

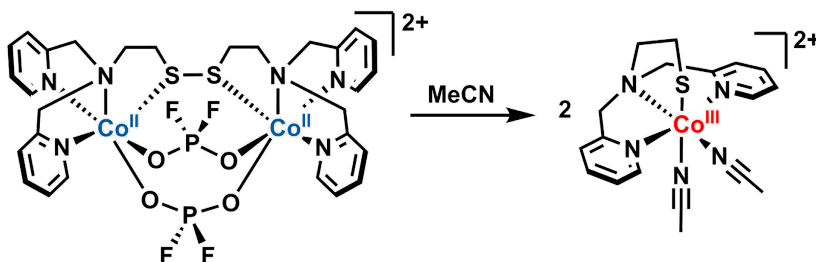


**Scheme 1.9.** Schematic representations of chloride-induced redox-conversion of cobalt complexes from a) Duboc's group,<sup>33</sup> b) Bouwman's group.<sup>34</sup>

**Scheme 1.9.a.** This dinuclear, five-coordinate cobalt(II) complex can also be generated by exhaustive electrolysis at 0 V vs  $\text{Fc}^+/\text{Fc}$  of the mononuclear cobalt(II)-thiolate compound in dichloromethane. The Co(II)-disulfide compound reverts to the Co(III)-thiolate complex upon addition of chloride ions, and the reversibility is maintained up to ten cycles without loss of conversion.

The ligand  $\text{L}^1\text{SSL}^1$ , which was first used in the study of copper-based redox-conversion, in a reaction with cobalt(II) chloride resulted in the formation of the cobalt(II)-disulfide complex  $[\text{Co}_2(\text{L}^1\text{SSL}^1)\text{Cl}_4]$ , in which the cobalt(II) ions are in a trigonal bipyramidal geometry.<sup>34</sup> Removal of the chloride ions using  $\text{AgBF}_4$  in acetonitrile afforded the mononuclear, six-coordinate cobalt(III)-thiolate complex,  $[\text{Co}(\text{L}^1\text{S})(\text{MeCN})_2]^{2+}$  as shown in **Scheme 1.9.b**. This cobalt(III)-thiolate complex can also be generated by the reaction of  $\text{L}^1\text{SSL}^1$  and  $[\text{Co}(\text{MeCN})_6](\text{BF}_4)_2$  in acetonitrile, and can be converted to the cobalt(II)-disulfide complex by addition of  $\text{NEt}_4\text{Cl}$ . The addition or removal of chloride ions thus has an opposite effect compared to that in Duboc's system.

The cobalt(II)-disulfide compound  $[\text{Co}_2(\text{L}^1\text{SSL}^1)(\text{PF}_2\text{O}_2)_2](\text{PF}_6)_2$  containing the unusual bridging  $\text{PF}_2\text{O}_2^-$  anion is stable as such in dichloromethane (nonpolar and non-coordinating solvent) and methanol (polar and weakly coordinating solvent), but converts to the cobalt(III)-thiolate compound  $[\text{Co}(\text{L}^1\text{S})(\text{MeCN})_2]^{2+}$  when dissolved in acetonitrile (polar and coordinating solvent) (**Scheme 1.10**).<sup>35</sup> In contrast, the partially methylated cobalt(II)-disulfide compound  $[\text{Co}_2(\text{L}^2\text{SSL}^2)(\text{PF}_2\text{O}_2)_2](\text{PF}_6)_2$  is stable as such in acetonitrile and does not convert to the corresponding Co(III)-thiolate complex. Similarly, reaction of  $\text{L}^2\text{SSL}^2$  with  $\text{Co}(\text{SCN})_2$  did not result in formation of the expected cobalt(III)-thiolate



**Scheme 1.10.** Schematic representation of the redox-conversion of  $[\text{Co}_2(\text{L}^1\text{SSL}^1)(\text{PF}_2\text{O}_2)_2]^{2+}$  in acetonitrile.<sup>35</sup>

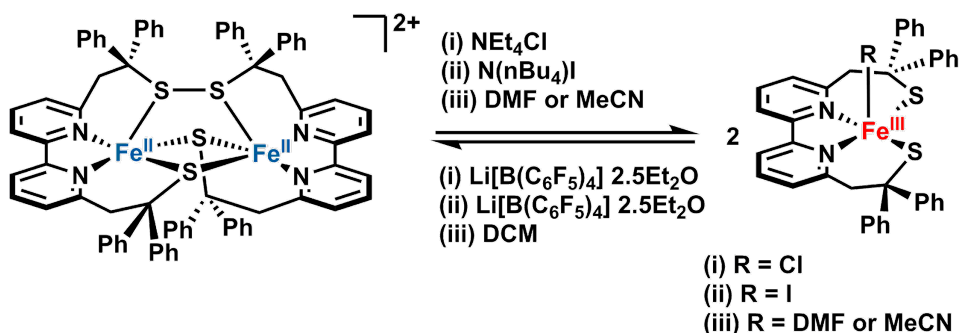


complex whereas the cobalt(III)-thiolate complex  $[\text{Co}(\text{L}^1\text{S})(\text{NCS})_2]$  is formed upon reaction of  $\text{L}^1\text{SSL}^1$  with  $\text{Co}(\text{SCN})_2$  regardless of the solvent used.<sup>34, 35</sup> The compounds  $[\text{Co}_2(\text{L}^1\text{SSL}^1)(\text{NO}_3)_4]$  and  $[\text{Co}_2(\text{L}^2\text{SSL}^2)(\text{NO}_3)_4]$  with the strongly coordinating anion  $\text{NO}_3^-$  are stable as such in both methanol and acetonitrile. Thus, it appears that coordination of acetonitrile to the cobalt(II)-disulfide compounds leads to redox isomerization, but only as long as relatively stronger coordinating ligands are absent.

### 1.2.3. Systems Based on Other Metal Ions

Redox-conversion in manganese and iron systems has been reported by the group of Duboc, using the same ligand as described in Section 1.2.2 for cobalt.<sup>36, 37</sup> The conversion of (bis- $\mu$ -thiolate)- $\mu$ -disulfide dimanganese(II) (isostructural to the cobalt(II) compound shown in **Scheme 1.9.a**) to the mononuclear Mn(III)-dithiolate compound was achieved by addition of halide ions in the non-coordinating solvent dichloromethane; however, the reaction did not go to completion, as approximately 30% of the manganese(III)-thiolate compound was obtained after 16 hours. The ease of the redox-conversion reaction of the manganese system was estimated by computing the Gibbs free energy of the thiolate compounds at 0 K. The Gibbs free energy of the Mn(III)-thiolate compound is significantly higher both in the gas phase (+3.6 kcal/mol) and in  $\text{CH}_2\text{Cl}_2$  solution (+7.9 kcal/mol) than that of the cobalt(III) system (−31.0 kcal/mol and −15.1 kcal/mol, respectively), indicating that the redox-conversion in the manganese system is less favorable compared to the cobalt system.

A redox-conversion system based on iron is interesting as generally iron(II) is more readily oxidized than cobalt(II) or manganese(II). The dinuclear, (bis- $\mu$ -thiolate)- $\mu$ -disulfide diiron(II) complex, isostructural with the cobalt(II) compound in **Scheme 1.9.a**, was shown to convert to the corresponding iron(III)-dithiolate compound upon addition of chloride ions in dimethylformamide in a quantitative yield (**Scheme 1.11**).<sup>37</sup> The reaction was shown to be reversible up to three times without loss of efficiency. Different results were obtained when iodide was employed, as the iodide-coordinated iron(III)-dithiolate is particularly stable and only partially reverts to the initial iron(II) complex in presence of a large excess of lithium salt (**Scheme 1.11**).<sup>37, 38</sup> In addition, a solvent-dependent redox-conversion for the same iron(II) complex was also reported. In non-coordinating and nonpolar solvents such as dichloromethane, the iron(II)-disulfide form is stable, whereas in more polar and



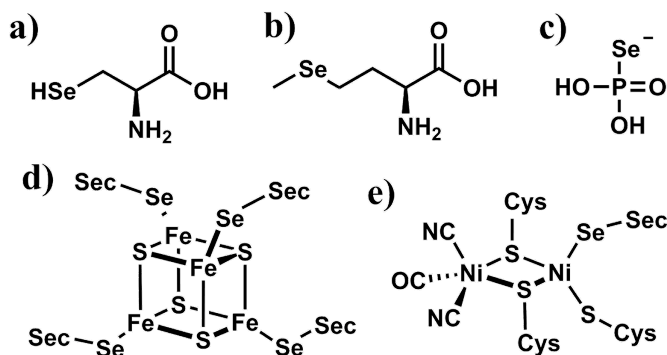
**Scheme 1.11.** Schematic representations of the redox-conversion between iron(II)-disulfide and iron(III)-thiolate compounds induced by chloride ions, iodide ions, or solvent molecules. Reaction conditions for (i) 2 equiv.  $\text{NEt}_4\text{Cl}$  in DMF and 2 equiv.  $\text{Li}[\text{B}(\text{C}_6\text{F}_5)_4] 2.5\text{Et}_2\text{O}$  in DCM; for (ii) 2 equiv.  $\text{N}(\text{nBu}_4)\text{I}$  in DCM and 20 equiv.  $\text{Li}[\text{B}(\text{C}_6\text{F}_5)_4] 2.5\text{Et}_2\text{O}$ .<sup>37, 38</sup>

coordinating solvents such as dimethylformamide (DMF) or acetonitrile the iron(III)-thiolate is formed with a coordinated solvent molecule (**Scheme 1.11**). However, the use of acetonitrile did not result in full conversion, possibly due to a lower affinity of Fe(III) for acetonitrile than for DMF.<sup>37</sup>

To our knowledge, currently other examples of manganese- and iron-based redox-conversion systems have not been reported. It seems that redox-conversion of manganese- and iron-based systems are also ligand-dependent. Utilization of  $\text{L}^1\text{SSL}^1$  (shown to give redox-conversion with copper in **Scheme 1.7**, and with cobalt in **Scheme 1.9**) in combination with iron salts afforded a dinuclear iron(II)-disulfide complex; so far attempts to convert this compound to the corresponding iron(III)-thiolate complex were unsuccessful.<sup>34</sup>

### 1.3. The Analog of Sulfur: Selenium

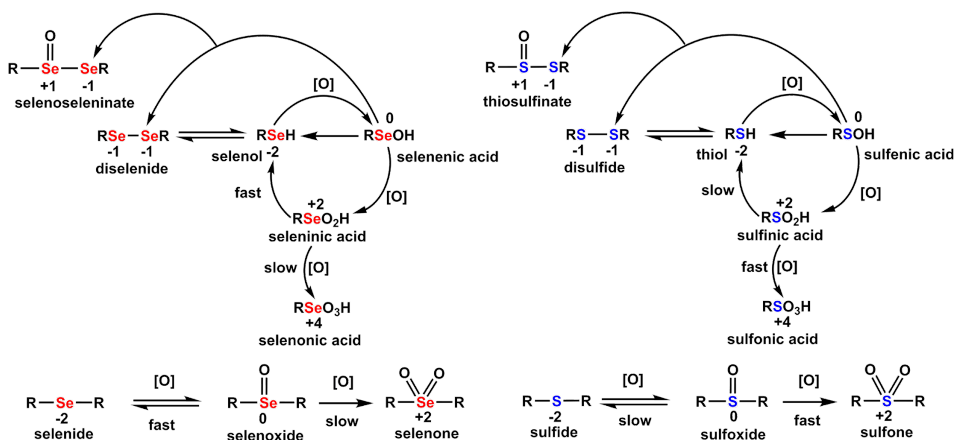
Located below sulfur in the periodic table, selenium is an element that is often described only briefly in chemistry textbooks. Selenium and its compounds, however, are extremely important and selenium is one of the most essential trace elements in the human body.<sup>39</sup> In the 1930s, selenium compounds were found to cause poisoning of livestock.<sup>40</sup> About forty years later, the very same element was discovered to be present in the 21<sup>st</sup> amino acid, selenocysteine.<sup>41–43</sup> Since then, the significance of selenium in biology is the topic of many investigations. Several examples of selenium in biomolecules are depicted in



**Scheme 1.12.** Examples of selenium in biomolecules. a) Selenocysteine (Sec),<sup>41</sup> b) Selenomethionine, c) Monoselenophosphate, a product of selenide and ATP (Adenosine TriPhosphate) catalyzed by SelD (Selenide, water dikinase) enzyme,<sup>45</sup> d) Sec as a ligand in an iron-sulfur cluster in methionine sulfoxide reductase (MsrB) homolog,<sup>46</sup> e) Sec as a ligand in [NiFeSe] hydrogenases.<sup>47</sup>

**Scheme 1.12.** <sup>41, 44-47</sup> Selenium is mostly found in selenocysteine (Sec) and acts as ligand for the metal ion in the active site of several enzymes.

The oxidation states and different oxygenated species that are known for selenium, are similar to those of sulfur (**Scheme 1.13**). However, selenium is a heavier element than sulfur, which causes a number of differences in its properties. For instance, selenium is less basic than



**Scheme 1.13.** Structures of several selenium and sulfur species with different oxidation states. Arrows show chemical transformation between species, and [O] symbolizes two-electron oxidation processes.<sup>49</sup>

sulfur,<sup>48, 49</sup> therefore, at the same pH, selenolates usually are better leaving groups than thiolates.<sup>50</sup> The  $\pi$ -donation of selenium compounds is usually weaker than that of sulfur compounds due to the larger ionic radius of selenium. These properties of selenium imply that its compounds are more reactive than sulfur compounds, for example the rate of the selenolate-diselenide exchange reaction is  $10^7$  times faster than that of the thiol-disulfide exchange reaction.<sup>51</sup>

The enhanced reactivity of selenium in comparison to sulfur compounds does not always make selenium a good choice as an alternative for sulfur in chemical reactions. Although several studies show that selenium compounds have antioxidant activity by scavenging reactive oxygen species (ROS),<sup>49, 52, 53</sup> selenium compounds are known to be more toxic than sulfur compounds, i.e. selenolates can react with dioxygen to produce superoxide radicals.<sup>54</sup> Selenium compounds are also more difficult to handle due to its faster redox reactions, e.g. selenolate (in the form of  $\text{CH}_3\text{Se}^-$ ) is oxidized to the selenenate ion ( $\text{CH}_3\text{SeO}^-$ ) using  $\text{H}_2\text{O}_2$  with a calculated rate constant of  $3.6 \times 10^4 \text{ M}^{-1} \text{ s}^{-1}$ , whereas the rate constant for thiolate oxidation to sulfenate is only  $10.2 \text{ M}^{-1} \text{ s}^{-1}$ .<sup>55</sup> The lower basicity of selenium compounds means that they may not be better ligands than their sulfur analogues, depending on the solvent and the pH.<sup>48, 56</sup>

#### 1.4. Aim and Outline of This Thesis

The goal of the research described in this thesis is to extend the study of redox-conversion reactions in cobalt-based systems, with the aim to provide further understanding of electron transfer in the cobalt-based system and how it acts differently from the copper-based system. In this Chapter, an overview is provided of the redox-conversion reaction, starting from the first report to the state-of-the-art of these reactions. A brief introduction is also provided on selenium and its properties. The challenges and obstacles in this field of research have also been described briefly.

In Chapter 2, the results are described of experimental as well as DFT studies concerning the effectivity of the external ligands 2,2'-bipyridine (bpy) and 1,10-phenanthroline (phen) in inducing a redox-conversion reaction of the cobalt(II)-disulfide complexes  $[\text{Co}_2(\text{L}^1\text{SSL}^1)\text{X}_4]$  ( $\text{X} = \text{Cl}, \text{Br}$ ) to the corresponding cobalt(III)-thiolate compounds. The ligands bpy and phen

were selected based on the hypothesis that redox-conversion of cobalt(II)-disulfide to cobalt(III)-thiolate may be induced by strong-field ligands.

In Chapter 3, the results are described of employment of the anionic ligand 8-quinolinolate ( $\text{quin}^-$ ) as an external ligand, which partially compensates for the dicationic charge of the cobalt(III)-thiolate compounds. The larger estimated ligand-field strength of 8-quinolinolate compared to that of bpy might aid to obtain clean conversion of the cobalt(II)-disulfide compounds  $[\text{Co}_2(\text{L}^x\text{SSL}^x)\text{X}_4]$  ( $x = 1$  or  $2$ ) to the cobalt(III)-thiolate complexes  $[\text{Co}(\text{L}^x\text{S})(\text{quin})]^+$ .

The study of redox-conversion was taken further to the selenolate and diselenide system in order to assess potential differences with the thiolate to disulfide conversion. The synthesis of the diselenide ligand  $\text{L}^1\text{SeSeL}^1$  is described in Chapter 4, as well as the formation of the cobalt(II)-diselenide complex  $[\text{Co}_2(\text{L}^1\text{SeSeL}^1)\text{Cl}_4]$ . The formation of several cobalt(III)-selenolate complexes from the cobalt(II)-diselenide  $[\text{Co}_2(\text{L}^1\text{SeSeL}^1)\text{Cl}_4]$  complex were described.

The synthesis of a new pyridine-containing disulfide ligand with longer bridges between the disulfide and tertiary amines is described in Chapter 5. The reactions of this new ligand as well as two other previously reported ligands with different cobalt(II) salts were investigated. The formation of dinuclear cobalt(II)-disulfide complexes of all the ligands is reported. Combining the knowledge that we obtained from Chapters 2 – 4, the reactivity of the formed cobalt(II)-disulfide complexes was tested using the  $\text{quin}^-$  ligand as an external influence.

Finally, in Chapter 6 a summary of this research is provided, as well as an outlook and suggestions for further research. Parts of this thesis have been published (Chapter 2),<sup>57</sup> submitted (Chapter 3)<sup>58</sup> or are in preparation for publication (Chapters 4 and 5).

## 1.5. References

1. Cramer, J. D. and Jarrett, J. T., *Methods in Enzymology: Radical SAM Enzymes*, 13, **2018**, Vol. 606, 363-388.
2. Brosnan, J. T. and Brosnan, M. E. *J. Nutr.* **2006**, 136 (6), 1636S-1640S.
3. Blackburn, N. J., de Vries, S., Barr, M. E., Houser, R. P., Tolman, W. B., Sanders, D. and Fee, J. A. *J. Am. Chem. Soc.* **1997**, 119 (26), 6135-6143.
4. Iwata, S., Ostermeier, C., Ludwig, B. and Michel, H. *Nature* **1995**, 376 (6542), 660-9.
5. Tsukihara, T., Aoyama, H., Yamashita, E., Tomizaki, T., Yamaguchi, H., Shinzawa-Itoh, K., Nakashima, R., Yaono, R. and Yoshikawa, S. *Science* **1995**, 269 (5227), 1069-74.
6. Lubitz, W., Ogata, H., Ruediger, O. and Reijerse, E. *Chem. Rev.* **2014**, 114 (8), 4081-4148.

7. Schilter, D., Camara, J. M., Huynh, M. T., Hammes-Schiffer, S. and Rauchfuss, T. B. *Chem. Rev.* **2016**, 116 (15), 8693-8749.
8. Angelosante, J. K., Schopp, L. M., Lewis, B. J., Vitalo, A. D., Titus, D. T., Swanson, R. A., Stanley, A. N., Abolins, B. P., Frome, M. J., Cooper, L. E., Tierney, D. L., Moore, C., Rheingold, A. L. and Daley, C. J. *J. Biol. Inorg. Chem.* **2011**, 16 (6), 937-947.
9. Huang, W. J., Jia, J., Cummings, J., Nelson, M., Schneider, G. and Lindqvist, Y. *Structure* **1997**, 5 (5), 691-699.
10. Angelucci, F., Dimastrogiovanni, D., Boumis, G., Brunori, M., Miele, A. E., Saccoccia, F. and Bellelli, A. *J. Biol. Chem.* **2010**, 285 (42), 32557-32567.
11. Berkholz, D. S., Faber, H. R., Savvides, S. N. and Karplus, P. A. *J. Mol. Biol.* **2008**, 382 (2), 371-384.
12. Zong, S., Wu, M., Gu, J., Liu, T., Guo, R. and Yang, M. *Cell Res.* **2018**, 28 (10), 1026-1034.
13. Brennan, B. A., Alms, G., Nelson, M. J., Durney, L. T. and Scarrow, R. C. *J. Am. Chem. Soc.* **1996**, 118 (38), 9194-9195.
14. Payne, M. S., Wu, S. J., Fallon, R. D., Tudor, G., Stieglitz, B., Turner, I. M. and Nelson, M. *J. Biochemistry* **1997**, 36 (18), 5447-5454.
15. Shearer, J., Kung, I. Y., Lovell, S., Kaminsky, W. and Kovacs, J. A. *J. Am. Chem. Soc.* **2001**, 123 (3), 463-468.
16. Xiao, Z., La Fontaine, S., Bush, A. I. and Wedd, A. G. *J. Mol. Biol.* **2019**, 431 (2), 158-177.
17. Hu, C., Yu, Y. and Wang, J. *Chem. Commun.* **2017**, 53 (30), 4173-4186.
18. Schwizer, F., Okamoto, Y., Heinisch, T., Gu, Y., Pellizzoni, M. M., Lebrun, V., Reuter, R., Kohler, V., Lewis, J. C. and Ward, T. R. *Chem. Rev.* **2018**, 118 (1), 142-231.
19. Shearer, J., Jackson, H. L., Schweitzer, D., Rittenberg, D. K., Leavy, T. M., Kaminsky, W., Scarrow, R. C. and Kovacs, J. A. *J. Am. Chem. Soc.* **2002**, 124 (38), 11417-11428.
20. Kennepohl, P., Neese, F., Schweitzer, D., Jackson, H. L., Kovacs, J. A. and Solomon, E. I. *Inorg. Chem.* **2005**, 44 (6), 1826-1836.
21. Camara, J. M. and Rauchfuss, T. B. *Nat. Chem.* **2012**, 4 (1), 26-30.
22. Wang, L., Gennari, M., Barrozo, A., Fize, J., Philouze, C., Demeshko, S., Meyer, F., Orio, M., Artero, V. and Duboc, C. *ACS Catal.* **2019**, 10 (1), 177-186.
23. Wittkamp, F., Senger, M., Stripp, S. T. and Apfel, U. P. *Chem. Commun.* **2018**, 54 (47), 5934-5942.
24. Aoi, N., Takano, Y., Ogino, H., Matsubayashi, G.-e. and Tanaka, T. *J. Chem. Soc., Chem. Commun.* **1985**, (11)
25. Houser, R. P., Young, V. G. and Tolman, W. B. *J. Am. Chem. Soc.* **1996**, 118 (8), 2101-2102.
26. Itoh, S., Nagagawa, M. and Fukuzumi, S. *J. Am. Chem. Soc.* **2001**, 123 (17), 4087-4088.
27. Ueno, Y., Tachi, Y. and Itoh, S. *J. Am. Chem. Soc.* **2002**, 124 (42), 12428-12429.
28. Neuba, A., Haase, R., Meyer-Klaucke, W., Floerke, U. and Henkel, G. *Angew. Chem. Int. Ed.* **2012**, 51 (7), 1714-1718.
29. Osako, T., Ueno, Y., Tachi, Y. and Itoh, S. *Inorg. Chem.* **2004**, 43 (21), 6516-6518.
30. Thomas, A. M., Lin, B.-L., Wasinger, E. C. and Stack, T. D. P. *J. Am. Chem. Soc.* **2013**, 135 (50), 18912-18919.
31. Ording-Wenker, E. C. M., van der Plas, M., Siegler, M. A., Bonnet, S., Bickelhaupt, F. M., Fonseca Guerra, C. and Bouwman, E. *Inorg. Chem.* **2014**, 53 (16), 8494-8504.
32. Ording-Wenker, E. C. M., van der Plas, M., Siegler, M. A., Fonseca Guerra, C. and Bouwman, E. *Chem. Eur. J.* **2014**, 20 (51), 16913-16921.
33. Gennari, M., Gerey, B., Hall, N., Pecaut, J., Collomb, M.-N., Rouzies, M., Clerac, R., Orio, M. and Duboc, C. *Angew. Chem. Int. Ed.* **2014**, 53 (21), 5318-5321.
34. Jiang, F., Siegler, M. A., Sun, X., Jiang, L., Fonseca Guerra, C. and Bouwman, E. *Inorg. Chem.* **2018**, 57 (15), 8796-8805.
35. Jiang, F., Marvelous, C., Verschuur, A. C., Siegler, M. A., Teat, S. J. and Bouwman, E. *Inorg. Chim. Acta* **2022**, 120880.

36. Gennari, M., Brazzolotto, D., Yu, S., Pecaute, J., Philouze, C., Rouzies, M., Clerac, R., Orio, M. and Duboc, C. *Chem. Eur. J.* **2015**, 21 (51), 18770-18778.
37. Wang, L., Reinhard, F. G. C., Philouze, C., Demeshko, S., de Visser, S. P., Meyer, F., Gennari, M. and Duboc, C. *Chem. Eur. J.* **2018**, 24 (46), 11973-11982.
38. Wang, L., Zlatar, M., Vlahovic, F., Demeshko, S., Philouze, C., Molton, F., Gennari, M., Meyer, F., Duboc, C. and Gruden, M. *Chem. Eur. J.* **2018**, 24 (20), 5091-5094.
39. Navarro-Alarcon, M. and Cabrera-Vique, C. *Sci. Total Environ.* **2008**, 400 (1-3), 115-141.
40. Manville, I. A. *Am. J. Public Health* **1939**, 29 (7), 709-19.
41. Bock, A., Forchhammer, K., Heider, J., Leinfelder, W., Sawers, G., Veprek, B. and Zinoni, F. *Mol. Microbiol.* **1991**, 5 (3), 515-520.
42. Cone, J. E., Martindell, R., Davis, J. N. and Stadtman, T. C. *Proc. Natl. Acad. Sci. U.S.A.* **1976**, 73 (8), 2659-2663.
43. Atkins, J. F. and Gesteland, R. F. *Nature* **2000**, 407 (6803), 463-465.
44. Takei, T., Ando, T., Takao, T., Ohnishi, Y., Kurisu, G., Iwaoka, M. and Hojo, H. *Chem. Commun.* **2020**, 56 (91), 14239-14242.
45. Glass, R. S., Singh, W. P., Jung, W., Veres, Z., Scholz, T. D. and Stadtman, T. *Biochemistry* **1993**, 32 (47), 12555-12559.
46. Lee, B. C., Lobanov, A. V., Marino, S. M., Kaya, A., Seravalli, J., Hatfield, D. L. and Gladyshev, V. N. *J. Biol. Chem.* **2011**, 286 (21), 18747-18755.
47. Lee, C. M., Chen, C. H., Ke, S. C., Lee, G. H. and Liaw, W. F. *J. Am. Chem. Soc.* **2004**, 126 (27), 8406-8412.
48. Huber, R. E. and Criddle, R. S. *Arch. Biochem. Biophys.* **1967**, 122 (1), 164-173.
49. Reich, H. J. and Hondal, R. J. *ACS Chem. Biol.* **2016**, 11 (4), 821-841.
50. Stirling, C. J. M. *Acc. Chem. Res.* **1979**, 12 (6), 198-203.
51. Pleasants, J. C., Guo, W. and Rabenstein, D. L. *J. Am. Chem. Soc.* **1989**, 111 (17), 6553-6558.
52. Tapiero, H., Townsend, D. M. and Tew, K. D. *Biomed. Pharmacother.* **2003**, 57 (3-4), 134-144.
53. Nogueira, C. W., Zeni, G. and Rocha, J. B. T. *Chem. Rev.* **2004**, 104 (12), 6255-6285.
54. Chaudiere, J., Courtin, O. and Leclaire, J. *Arch. Biochem. Biophys.* **1992**, 296 (1), 328-336.
55. Cardey, B. and Enescu, M. *ChemPhysChem* **2005**, 6 (6), 1175-1180.
56. Cupp-Sutton, K. and Ashby, M. *Antioxidants* **2016**, 5 (4), 42.
57. Marvelous, C., de Azevedo Santos, L., Siegler, M. A., Fonseca Guerra, C. and Bouwman, E. *Dalton Trans.* **2022**, 51, 8046-8055.
58. Marvelous, C., de Azevedo Santos, L., Siegler, M. A., Fonseca Guerra, C. and Bouwman, E. **2022**, submitted

# Chapter 2

---

## Probing The Redox-conversion of Co(II)-disulfide to Co(III)-thiolate Complexes: The Effect of Ligand-Field Strength

*The redox-conversion reaction of cobalt(II)-disulfide to cobalt(III)-thiolate complexes triggered by addition of the bidentate ligand 2,2'-bipyridine (bpy) has been investigated. Reaction of the cobalt(II)-disulfide complex  $[\text{Co}_2(\text{L}^1\text{SSL}^1)(\text{X})_4]$  ( $\text{L}^1\text{SSL}^1 = \text{di-2-(bis(2-pyridylmethyl)amino)-ethyl-disulfide}$ ;  $\text{X} = \text{Cl}$  or  $\text{Br}$ )  $[\mathbf{1}_\text{X}]$  with 2,2'-bipyridine resulted in the formation of two different products, namely the cobalt(III)-thiolate complex  $[\text{Co}(\text{L}^1\text{S})(\text{bpy})]\text{X}_2$  and the unexpected side product  $[\text{Co}_2(\text{L}^1\text{SSL}^1)(\text{bpy})_2(\text{X})_2]\text{X}_2$ . Crystals of  $[\text{Co}_2(\text{L}^1\text{SSL}^1)(\text{bpy})_2(\text{Cl})_2](\text{BPh}_4)_2$   $[\mathbf{2}\text{Cl}](\text{BPh}_4)_2$  obtained after anion exchange showed the cobalt(II) ions to be in octahedral geometries with the nitrogen donors of the disulfide ligand arranged in a facial conformation and the chloride ion trans to the tertiary amine nitrogen. Remarkably, this side product cannot be converted to the cobalt(III)-thiolate compound  $[\text{Co}(\text{L}^1\text{S})(\text{bpy})](\text{SbF}_6)_2$   $[\mathbf{3}](\text{SbF}_6)_2$  by removal of the chloride ion with use of a silver salt, as this causes scrambling of the ligands, resulting in the formation of  $[\text{Co}(\text{bpy})_3]^{n+}$ .  $[\text{Co}(\text{L}^1\text{S})(\text{bpy})](\text{SbF}_6)_2$  was obtained in a pure form by addition of bpy to a solution in acetonitrile of the compound  $[\text{Co}(\text{L}^1\text{S})(\text{MeCN})_2]^{2+}$   $[\mathbf{4}]^{2+}$ . Addition of  $\text{NEt}_4\text{Cl}$  to  $[\mathbf{3}](\text{SbF}_6)_2$  regenerates the cobalt(II)-disulfide complex  $[\mathbf{1}\text{Cl}]$  as confirmed spectroscopically. DFT studies revealed that the conversion from  $[\mathbf{1}\text{Cl}]$  to  $[\mathbf{3}]^{2+}$  most likely occurs via the hypothetical intermediate species  $[\mathbf{2}\text{Cl}]^{2+}_{\text{mer}}$ , in which the nitrogen atoms of the disulfide ligand are arranged in a meridional conformation. Interestingly, the calculated d-orbital splitting energy of  $[\mathbf{3}]^{2+}$  is lower than that of  $[\mathbf{4}]^{2+}$ , indicating that the ligand-field strength of bpy is lower than anticipated, which hampers clean conversion in the redox-conversion reaction. This study shows that the redox-conversion reaction between cobalt(II)-disulfide and cobalt(III)-thiolate complexes is intricate rather than straightforward.*

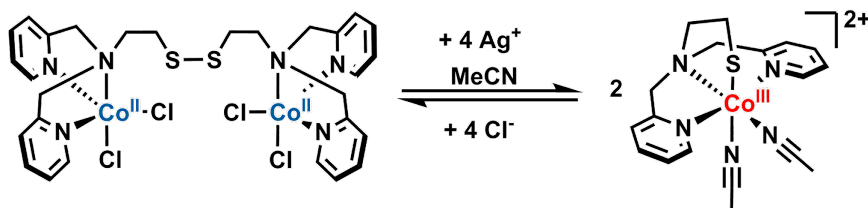
This chapter has been published as a full article: Christian Marvelous, Lucas de Azevedo Santos, Maxime A. Siegler, Célia Fonseca Guerra, and Elisabeth Bouwman, *Dalton Transactions*, 2022, **51**, 8046-8055.



## 2.1. Introduction

Thiol groups are involved in many important aspects of biological systems, notably in proteins as a cysteine amino acid residue, but also in cofactors.<sup>1-3</sup> Thiol groups have rich chemistry, the most known is its oxidation to disulfide species (S–S). The redox reaction of disulfide groups and thiolate ions is also prominent in enzymes, such as in glutathione reductase (glutaredoxin) that catalyzes the reduction of glutathione disulfide (GSSG) into glutathione (GSH).<sup>4, 5</sup> Such redox reactions in enzymes are often accompanied by a redox reaction of a metal center in the active site. However, it is challenging to study the mechanism of the redox-conversion in enzymes, due to the complexity of these systems.

In recent years, a number of studies focused on the thiol/disulfide redox-conversion reaction by making use of biomimetic metal-disulfide and metal-thiolate complexes.<sup>6-14</sup> The observation that the use of disulfide ligands in combination with copper(I) salts could lead to either copper(I)-disulfide or copper(II)-thiolate complexes was first reported by the group of Itoh about two decades ago.<sup>14</sup> Subsequently, it was reported that the redox-conversion reaction between copper(I)-disulfide and copper(II)-thiolate complexes is not only dependent on the ligand structure, but can be triggered by variations in anions, temperature, solvents, and the presence or absence of protons.<sup>6-9</sup> The group of Duboc was the first to report redox-conversion between cobalt(II)-disulfide and cobalt(III)-thiolate compounds, in which the presence or absence of halide ions determine the product of the reaction.<sup>10</sup> They reported a mononuclear, 5-coordinated cobalt(III)-dithiolate complex that upon removal of the chloride anion undergoes redox-conversion to form a dinuclear bis( $\mu$ -thiolato)dicobalt(II)-disulfide complex. Recently, our group reported the reversible redox-conversion between the mononuclear, 6-coordinated cobalt(III)-thiolate complex  $[\text{Co}(\text{L}^1\text{S})(\text{MeCN})_2]^{2+}$  **[4]**<sup>2+</sup> and the dinuclear cobalt(II)-disulfide complex  $[\text{Co}_2(\text{L}^1\text{SSL}^1)\text{Cl}_4]$ , as shown in **Scheme 2.1**.<sup>15</sup> In contrast to the system reported by Duboc's group, in our system *removal* of the chloride ions from the Co(II)-disulfide compound in acetonitrile results in the formation of the related Co(III)-thiolate compound. In order to understand the underlying mechanism in the redox-conversion reactions of Co(II)-disulfide and Co(III)-thiolate complexes these different outcomes have to be rationalized, even though they concern different systems.



**Scheme 2.1.** Schematic representation of the reversible redox-conversion of the cobalt(II)-disulfide complex  $[\text{Co}_2(\text{L}^1\text{SSL}^1)\text{Cl}_4]$  ( $[\mathbf{1Cl}]$ ) and the cobalt(III)-thiolate complex  $[\text{Co}(\text{L}^1\text{S})(\text{MeCN})_2]^{2+}$  ( $[\mathbf{4}]^{2+}$ ) induced by removal or addition of halide ions in MeCN solution.<sup>15</sup>

Our investigation is set out based on the observations described in our previous reports. The redox-conversion between cobalt(II)-disulfide and the corresponding cobalt(III)-thiolate complexes appears to be very sensitive to small changes. In the system that we reported earlier, conversion from the cobalt(II) to the cobalt(III) compound was induced by removing the chloride ions in an acetonitrile solution, or by the use of the thiocyanate anion. It is known that both acetonitrile and thiocyanate induce a stronger ligand-field effect than the  $\pi$ -donating chloride ion. The  $d$ -orbital splitting of the octahedral Co(III) ion is known to be larger than that of the Co(II) ion.<sup>16, 17</sup> Therefore, addition of a ligand that induces a stronger ligand-field effect to a Co(II) complex may yield an intermediate with a larger  $d$ -orbital splitting (**Figure 2.1**). When the ligand-field splitting is large enough to overcome the spin-pairing

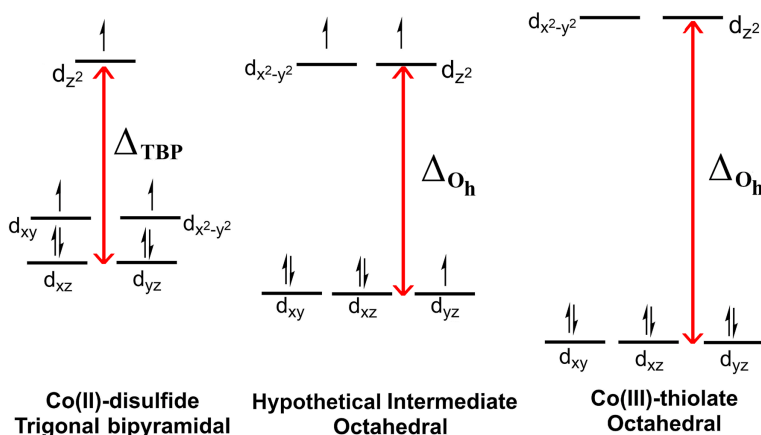


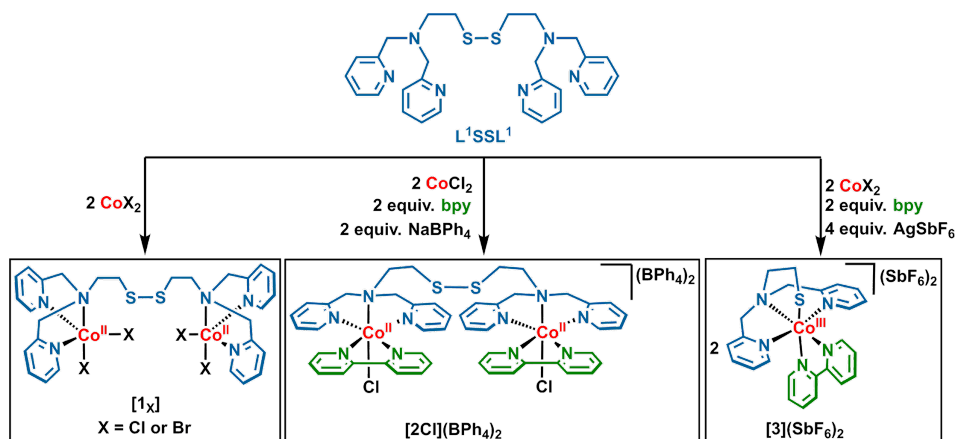
**Figure 2.1.** Energy diagrams of  $d$ -orbital splitting in Co(II)-disulfide and Co(III)-thiolate complexes.

energy, this results in a low-spin (LS) state for the Co(II) center. The instability of the high-energy single electron(s) in the Co(II) center may cause an electron transfer to the disulfide group, driving the reaction to form the cobalt(III)-thiolate species. Based on this theory, we suspect that addition of a ligand with a relatively large ligand-field strength will result in the formation of a Co(III)-thiolate species. Hence, in this study we report our investigation in the utilization of the relatively strong ligand-field, exogenous bidentate ligand 2,2'-bipyridine (bpy) to induce the redox-conversion from cobalt(II)-disulfide to cobalt(III)-thiolate species.

## 2.2. Results

### 2.2.1. Synthesis and Reactivity of the Cobalt Compounds

The cobalt(II)-disulfide compounds  $[\text{Co}_2(\text{L}^1\text{SSL}^1)(\text{X})_4]$  [**1<sub>X</sub>**] ( $\text{X} = \text{Cl}$  or  $\text{Br}$ ) were prepared as depicted in **Scheme 2.2**.<sup>14</sup> Addition of the anhydrous  $\text{CoCl}_2$  or  $\text{CoBr}_2$  salt to a solution of  $\text{L}^1\text{SSL}^1$  in either acetonitrile or methanol afforded solutions of the cobalt(II)-disulfide compounds [**1<sub>Cl</sub>**] and [**1<sub>Br</sub>**], respectively. The compounds were isolated as a purple powder for [**1<sub>Cl</sub>**] in 89% yield and a light purple powder for [**1<sub>Br</sub>**] in 60% yield. The compounds were obtained analytically pure as confirmed with elemental analysis. Unfortunately, the compounds described in this chapter appear to be rather labile; despite the use of analytically pure compounds the MS spectra often show multiple peaks indicating decomposition caused



**Scheme 2.2.** Schematic overview of the synthetic procedures for the cobalt compounds of  $\text{L}^1\text{SSL}^1$  described in the present work.

by the ionization conditions of ESI-MS. ESI-MS spectra of **[1Cl]** dissolved in acetonitrile show peaks at  $m/z$  352.0, 741.0, and 749.0 corresponding to the species  $[\mathbf{1Cl} - 2\text{Cl}^-]^{2+}$ ,  $[\mathbf{1Cl} - \text{Cl}^-]^+$ ,  $[\mathbf{1Cl} - 2\text{Cl}^- + \text{HCOO}^-]^+$  (the formate ion arising from formic acid in the eluting solvent), respectively (Figure AI.1). Similar results were found in the ESI-MS spectra of **[1Br]** (Figure AI.2), with peaks at  $m/z$  398.0, 839.0, and 872.9 corresponding to the species  $[\mathbf{1Br} - 2\text{Br}^-]^{2+}$ ,  $[\mathbf{1Br} - 2\text{Br}^- + \text{HCOO}^-]^+$ , and  $[\mathbf{1Br} - \text{Br}^-]^+$ , respectively. The cobalt(II)-disulfide compounds are paramagnetic, as indicated by the large shifts of the signals in their  $^1\text{H}$ -NMR spectra up to 81 ppm (Figure AI.3–AI.4). The values of the magnetic moments in solution were estimated by Evans' method. The values of the magnetic moment of **[1Cl]** and **[1Br]** dissolved in  $\text{DMSO-d}_6$  are  $4.55 \mu_{\text{B}}$  and  $4.62 \mu_{\text{B}}$ , respectively, calculated per cobalt center. Further characterization with a magnetic-susceptibility balance revealed their magnetic moment values in the solid state to be  $4.38 \mu_{\text{B}}$  and  $4.35 \mu_{\text{B}}$  per cobalt center for **[1Cl]** and **[1Br]**, respectively. The magnetic moments of the compounds **[1x]** are in agreement with the presence of two magnetically non-interacting high-spin Co(II) centers in the dinuclear molecules.

Dissolution of compound **[1x]** in acetonitrile gives purple-colored solutions. Addition of two equivalents of bpy to this solution resulted in a color change to yellow, which was monitored using UV-visible spectroscopy. The UV-visible spectrum of compound **[1Cl]** in acetonitrile is in agreement with the earlier report (**Figure 2.2**).<sup>15</sup> In contrast, the UV-visible spectrum of the yellow solution obtained after addition of bpy does not show clear absorption peaks in the visible region, indicating formation of cobalt(III) species in a low-spin (LS) electron configuration. Attempts at isolation of the anticipated cobalt(III)-thiolate compound  $[\text{Co}(\text{L}^1\text{S})(\text{bpy})_2]\text{Cl}_2$  (**[3]Cl**<sub>2</sub>) from the yellow solution resulted in a mixture of beige and red-colored powders, indicating the formation of at least two different products. Separation of these two products appeared to be difficult, and therefore **[1Br]** was used in reactions with bipyridine with the hope that this would react more cleanly and yield the expected cobalt(III)-thiolate compound **[3]<sup>2+</sup>** in a pure form. Unfortunately, these reactions yielded similar results: workup after the reactions also led to mixtures of beige and red-colored powders, which again could not be separated.

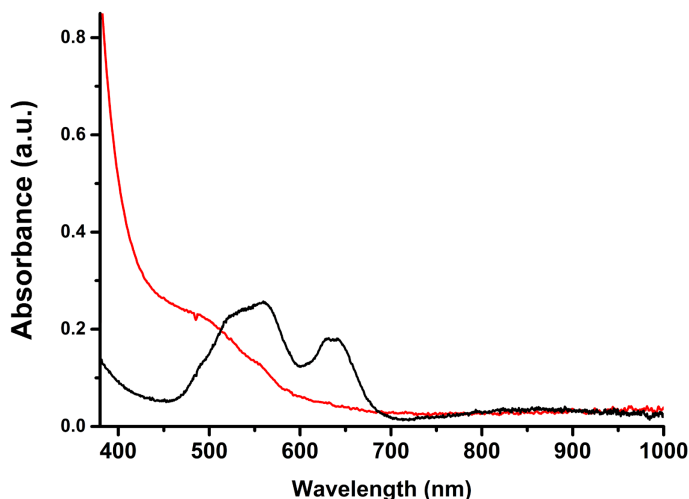


**Figure 2.2.** UV-Visible spectra of a purple solution of 5 mM  $[1\text{Cl}]$  dissolved in acetonitrile (black line) and the yellow solution (red line) obtained after addition of 2 equivalents of 2,2'-bipyridine. UV-visible spectra were recorded using a transmission dip-probe with path length of 4 mm.

In attempts to clarify the composition of the mixtures, we performed different reactions. Reaction of  $[1\text{Cl}]$  in methanol with two equivalents of bpy and with the addition of two equivalents of sodium tetraphenylborate resulted in the formation of the compound  $[\text{Co}_2(\text{L}^1\text{SSL}^1)(\text{bpy})_2(\text{Cl})_2](\text{BPh}_4)_2$  ( $[2\text{Cl}](\text{BPh}_4)_2$ ) as a beige powder after recrystallization in acetone (47% yield). ESI-MS spectra (Figure AI.5) show a peak at  $m/z$  506.5 corresponding to the species  $[2\text{Cl} - \text{Cl}^- + \text{OMe}]^{2+}$  (calculated  $m/z$  506.1) and at 1011.9 corresponding to a partially reduced species  $[2\text{Cl} - \text{Cl}^- + \text{OMe}]^+$  (calculated  $m/z$  1012.2); this reduction possibly occurs during the ionization process. A peak at  $m/z$  157.2 indicates the presence of free bpy. The magnetic susceptibility of  $[2\text{Cl}](\text{BPh}_4)_2$  dissolved in  $\text{DMSO-d}_6$  was measured using Evans' method, yielding a value of  $4.12 \mu_B$  calculated per cobalt center. This value suggests that the two cobalt(II) centers are most likely high-spin. Compound  $[2\text{Cl}](\text{BPh}_4)_2$  was obtained analytically pure as shown by elemental analysis and the structure was determined using X-ray single crystal diffraction.

In another reaction in acetonitrile, the halide ions in  $[1\text{Cl}]$  or  $[1\text{Br}]$  were removed using four equivalents of silver hexafluoroantimonate after which two equivalents of bpy were added. It is known that removal of the halide ions of  $[1\text{Cl}]$  in acetonitrile yields the species  $[4]^{2+}$ , and

subsequent addition of bpy resulted in the formation of  $[3](\text{SbF}_6)_2$ , which was isolated as a dark red powder with variable yield of 68-93%. Elemental analysis of the bulk material demonstrates that  $[3](\text{SbF}_6)_2$  was obtained as an analytically pure compound. Interestingly, dissolution of the dark red powder in either acetonitrile or  $\text{CD}_3\text{CN}$  resulted in a dark red solution which in a few minutes turned light yellow, indicating instability of  $[3](\text{SbF}_6)_2$  in acetonitrile. The  $^1\text{H-NMR}$  spectrum of  $[3](\text{SbF}_6)_2$  in  $\text{CD}_3\text{CN}$  (Figure AI.7) shows signals in the diamagnetic region as expected for low-spin  $\text{Co(III)}$  ions. However, the spectrum also shows that the compound  $[3](\text{SbF}_6)_2$  is not stable in solution; the aromatic peaks can be attributed to originate from  $[3](\text{SbF}_6)_2$ , as well as  $[4]^{2+}$  and free bpy. ESI-MS spectra of  $[3](\text{SbF}_6)_2$  in acetonitrile (Figure AI.8) show the parent peak at  $m/z$  708.0 corresponding to  $[3+\text{SbF}_6]^+$  (calculated  $m/z$  708.0) and a dominant peak is found at 236.6 corresponding to the species  $[3]^{2+}$  (calculated  $m/z$  236.55). In addition, the presence of  $[4]^{2+}$  is confirmed by a peak at  $m/z$  199.6 (calculated  $m/z$  199.55), and a peak at  $m/z$  157.2 indicates the presence of free bpy. The magnetic susceptibility of compound  $[3](\text{SbF}_6)_2$  was measured in the solid state using a magnetic-susceptibility balance and in solution using Evans' method; both methods show that  $[3](\text{SbF}_6)_2$  is diamagnetic. Attempts were undertaken to obtain single crystals of compound  $[3]^{2+}$  using several counter anions, namely with  $\text{SbF}_6^-$ ,  $\text{PF}_6^-$ ,  $\text{NO}_3^-$ ,  $\text{BPh}_4^-$ ,  $\text{BF}_4^-$ ,  $\text{ClO}_4^-$ , and  $\text{CF}_3\text{SO}_3^-$ . Unfortunately, these attempts were not successful or resulted in crystals that did not diffract well, which likely is related to the limited stability of the compound in solution.

After isolation and characterization of the pure compounds  $[2_{\text{Cl}}](\text{BPh}_4)_2$  and  $[3](\text{SbF}_6)_2$  via the synthetic routes described above, we came to the conclusion that the beige and red-colored powders obtained from the reaction of  $[1_{\text{x}}]$  with two equivalents of bpy correspond to the cobalt(II)-disulfide-bipyridine compound  $[2_{\text{x}}]\text{X}_2$  and the cobalt(III)-thiolate-bipyridine complex  $[3]\text{X}_2$ , respectively.

As  $[1_{\text{x}}]$  upon reaction with bpy does not cleanly convert to  $[3]^{2+}$  we also attempted to convert  $[2_{\text{Cl}}](\text{BPh}_4)_2$  to  $[3]^{2+}$  by removal of the chloride ions. The light brown solution of  $[2_{\text{Cl}}](\text{BPh}_4)_2$  in acetonitrile or methanol immediately turned cloudy upon addition of two equivalents of  $\text{AgSbF}_6$ , indicating successful removal of the coordinated chloride anions. Further workup of the reaction mixture afforded a brown-reddish powder. Unexpectedly, ESI-MS of this powder dissolved in acetonitrile showed the presence of the species  $[\text{Co}(\text{bpy})_3]^{2+}$  (calcd.

$m/z$  263.57, found  $m/z$  263.6) instead of the desired  $[3]^{2+}$  (Figure AI.9). The presence of the free ligand  $L^1SSL^1$  is not detected, but several unidentified peaks are also present.

We then conducted a titration experiment to study whether the reverse reaction can be triggered with the addition of chloride ions. A solution of  $[3](SbF_6)_2$  in acetonitrile was titrated with a solution of tetraethylammonium chloride in acetonitrile (**Figure 2.3**). The addition of  $NEt_4Cl$  to the solution of  $[3](SbF_6)_2$  results in a color change of the solution from yellow to darker yellow, and some turbidity is observed. The UV-visible spectra show the decrease in absorbance of the peaks at 394 and 458 nm, and the appearance of new peaks at 565 and 642 nm upon addition of two equivalents of  $NEt_4Cl$  per  $[3]^{2+}$ . The bands at 565 and 642 nm coincide with those of  $[1Cl]$  in acetonitrile, indicating the formation of  $[1Cl]$ . Workup of the reaction mixture indeed resulted in the purple powder of  $[1Cl]$ , in a yield of 26%, as confirmed by the ESI-MS and  $^1H$ -NMR spectra (Figure AI.10 and AI.11).

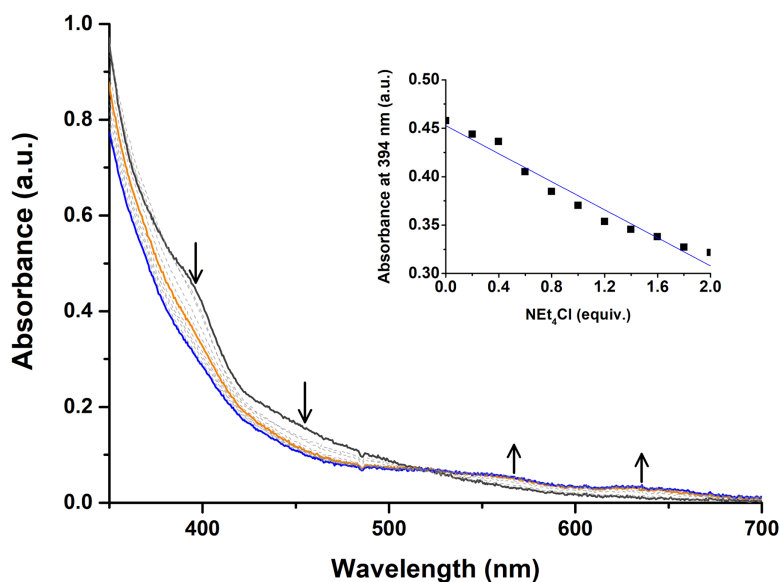


**Figure 2.3.** Changes of the UV-visible spectrum of 5 mM  $[3](SbF_6)_2$  in acetonitrile (black line) upon addition of  $NEt_4Cl$  (orange line = 1 equivalent, blue line = 2 equivalents). Inset shows the change of absorbance at 394 nm as a function of the amount of added  $NEt_4Cl$ . More details and change of absorbance at 458 nm are provided in Figure S12. UV-visible spectra were recorded using a transmission dip probe with 4 mm path length.

With the aim to confirm the assignment of  $[3]^{2+}$  being a cobalt(III)-thiolate compound, additional experiments were performed using 1,10-phenanthroline (phen) instead of bpy, as this ligand is structurally and electronically similar to bpy, but is less likely to dissociate due to its rigidity (See Supporting Information). ESI-MS spectra of an acetonitrile solution containing compound  $[\text{Co}(\text{L}^1\text{S})(\text{phen})](\text{SbF}_6)_2$  (Figure AI.13) show peaks at  $m/z$  732.0 and 248.6, corresponding to the species  $[\text{Co}(\text{L}^1\text{S})(\text{phen})](\text{SbF}_6)^+$  (calculated  $m/z$  732.0) and  $[\text{Co}(\text{L}^1\text{S})(\text{phen})]^{2+}$  (calculated  $m/z$  248.6), respectively. The species  $[\text{Co}(\text{phen})_3]^{2+}$  is also detected in the ESI-MS spectra at  $m/z$  299.9 (calculated  $m/z$  299.6). Crystallization attempts for  $[\text{Co}(\text{L}^1\text{S})(\text{phen})](\text{SbF}_6)_2$  unfortunately resulted in crystals of the oxidized compound  $[\text{Co}(\text{L}^1\text{SO}_2)(\text{phen})](\text{SbF}_6)_2$  containing a sulfinate group (Figure AI.14 and Table AI.1).

### 2.2.2. Description of the Crystal Structures

The crystal structure of  $[1_{\text{Cl}}]$  was previously reported by our group.<sup>15</sup> The crystal data and refinement details for  $[1_{\text{Br}}]$  and  $[2_{\text{Cl}}](\text{BPh}_4)_2$  are provided in Table AI.2. The crystal structure of  $[1_{\text{Br}}]$  is similar to that of  $[1_{\text{Cl}}]$ , but the compounds are not isostructural.  $[1_{\text{Br}}]$  crystallizes in the monoclinic space group  $P2_1/c$ . A projection of the structure of  $[1_{\text{Br}}]$  is depicted in **Figure 2.4.a**. A selection of bond distances and angles is provided in **Table 2.1**. In the asymmetric unit, one molecule of  $[1_{\text{Br}}]$  and one lattice methanol solvent molecule are co-crystallized. The distances and angles around the two independent cobalt centers are very similar. Similar to  $[1_{\text{Cl}}]$ , each cobalt center in  $[1_{\text{Br}}]$  is coordinated to three nitrogen atoms of

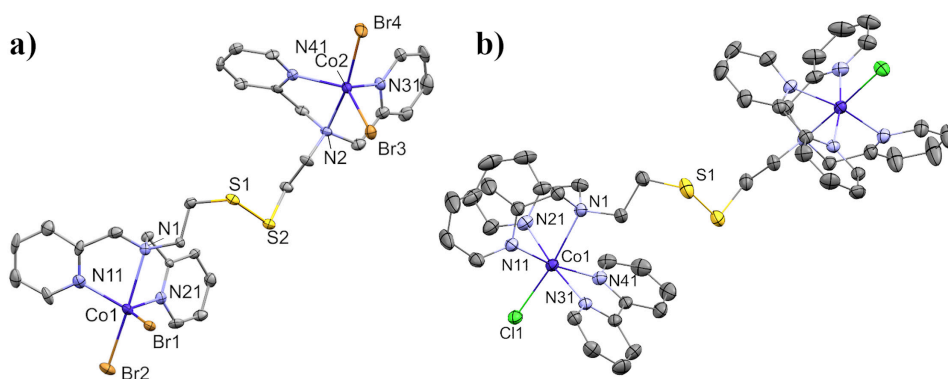


**Figure 2.4.** Displacements ellipsoid plots (50% probability level) of a)  $[\text{Co}_2(\text{L}^1\text{SSL}^1)(\text{Br})_4]$  ( $[1_{\text{Br}}]$ ) and b)  $[\text{Co}_2(\text{L}^1\text{SSL}^1)(\text{bpy})_2(\text{Cl})_2]^{2+}$  ( $[2_{\text{Cl}}]^{2+}$ ) at 110(2) K. Hydrogen atoms, non-coordinated anions, and lattice solvent molecules are omitted for clarity.



**Table 2.1.** Selected bond distances and bond angles in [**1<sub>Br</sub>**].

Atoms	distance (Å)	Atoms	Bond angles (°)
Co1–Br1	2.4589(9)	Br1–Co1–Br2	99.92(3)
Co1–Br2	2.4613(9)	Br1–Co1–N1	90.13(10)
Co1–N1	2.350(4)	Br1–Co1–N11	110.58(13)
Co1–N11	2.074(5)	Br1–Co1–N21	123.75(13)
Co1–N21	2.071(4)	Br2–Co1–N1	169.76(11)
Co1–S1	6.037(1)	N11–Co1–N21	117.99(18)
S1–S2	2.036(2)	N11–Co1–N1	76.11(17)
Co1–Co2	11.671(1)	N21–Co1–N1	76.22(16)

the dinucleating ligand and two halide ions in a distorted trigonal-bipyramidal geometry, with  $\tau_5$  values of the two cobalt centers being 0.77 and 0.66.<sup>18</sup> One intermolecular interaction was found between Br4 and the OH group of the lattice methanol solvent molecule. Even though the structure of [**1<sub>Br</sub>**] is similar to that of [**1<sub>Cl</sub>**], the distance between the two cobalt centers in [**1<sub>Br</sub>**] is significantly larger than in [**1<sub>Cl</sub>**] (11.671 Å vs 8.160 Å).

A projection of the structure of [**2<sub>Cl</sub>**](BPh<sub>4</sub>)<sub>2</sub> is depicted in **Figure 2.4.b**. Selected bond distances and angles are provided in **Table 2.2**. [**2<sub>Cl</sub>**](BPh<sub>4</sub>)<sub>2</sub> crystallizes in the monoclinic space group *C2/c*. The asymmetric unit contains one half of the dinuclear complex found at a site of twofold axial symmetry, one tetraphenylborate anion, one lattice acetone solvent molecule, and one partially occupied lattice water molecule (found at a site of twofold axial symmetry). Both cobalt centers are in a distorted octahedral geometry, coordinated with five nitrogen donor atoms (three from L<sup>1</sup>SSL<sup>1</sup> and two from bpy) as well as one chloride ion. The three nitrogen donor atoms from the ligand L<sup>1</sup>SSL<sup>1</sup> are arranged in a facial fashion, with the

**Table 2.2.** Selected bond distances and angles in [**2<sub>Cl</sub>**](BPh<sub>4</sub>)<sub>2</sub>.

Atoms	Distance (Å)	Atoms	Bond angles (°)
Co1–Cl1	2.3827(6)	N1–Co1–Cl1	171.79(4)
Co1–N1	2.2579(15)	N1–Co1–N11	79.53(6)
Co1–N11	2.1430(16)	N1–Co1–N21	77.32(6)
Co1–N21	2.1394(16)	N1–Co1–N31	97.58(6)
Co1–N31	2.1337(15)	N1–Co1–N41	90.41(6)
Co1–N41	2.1260(16)	Cl1–Co1–N11	97.42(5)
Co1–Co1'	11.6516(9)	Cl1–Co1–N21	94.79(5)
Co1–S1	5.8773(9)	Cl1–Co1–N31	90.46(4)
S1–S1'	2.0298(12)	Cl1–Co1–N41	93.03(5)
		N11–Co1–N21	82.73(6)
		N11–Co1–N31	100.87(6)
		N41–Co1–N21	98.72(6)
		N41–Co1–N31	76.67(6)

tertiary amine nitrogen located *trans* to the chloride ion. The remaining positions are occupied by the two nitrogen donors from bpy.

The average length of the equatorial Co–N bonds is 2.14 Å, in agreement with the presence of high-spin cobalt(II) centers.<sup>19–21</sup> The Co–Cl bond length is slightly larger (2.38 Å) than in [1Cl] (2.32 and 2.27 Å), indicating that the Co–Cl bond in [2Cl](BPh<sub>4</sub>)<sub>2</sub> is slightly weaker. The distance between the cobalt center and the nearest disulfide sulfur atom is slightly smaller (5.88 Å) than those in [1Cl] (5.96 Å and 5.93 Å). The intramolecular distance between two cobalt centers in [2Cl](BPh<sub>4</sub>)<sub>2</sub> is similar to that in [1Br].

### 2.2.3. Density Functional Theory Studies

Density Functional Theory (DFT) computations were performed in order to provide a rationale for the complication when bpy is used in a reaction with [1x] to form [3]<sup>2+</sup>, for which we optimized the geometries of several complexes. The dinuclear cobalt(II)-disulfide compound [1Cl] was simplified to [1\*] in order to make a fair comparison with [3]<sup>2+</sup> as well as [4]<sup>2+</sup>, i.e. the molecule is mononuclear. The molecule [1\*] comprises half of [1Cl] with a methyl group on the tertiary amine nitrogen instead of the disulfide moiety (**Figure 2.5**). The cobalt(III)-thiolate compound [3]<sup>2+</sup> was optimized for two different geometries, differing in

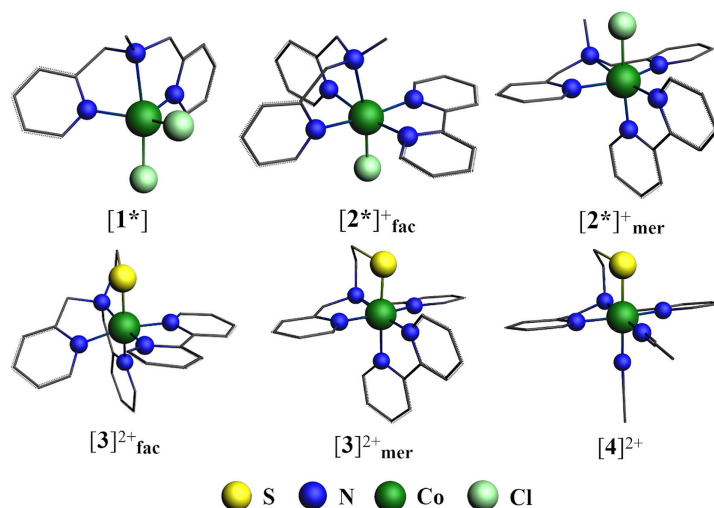


**Figure 2.5.** Optimized geometry structures of all calculated compounds. Carbon atoms are shown in wireframe and hydrogen atoms are omitted for clarity.

the binding mode of the three nitrogen donors of the ligand  $L^1S^-$  (**Figure 2.5**), being facial in  $[3]^{2+}_{\text{fac}}$  or meridional in  $[3]^{2+}_{\text{mer}}$ ; the latter orientation corresponds to the structure reported for  $[4]^{2+}$ ,<sup>15</sup> which was also computed to serve as a comparison for  $[3]^{2+}$ . In addition, we were interested in finding out why the side product  $[2_{\text{Cl}}]$  cannot be converted into  $[3]^{2+}$  and therefore the side product  $[2_{\text{Cl}}]$  was simplified into  $[2^*]^{+}_{\text{fac}}$ , similar to  $[1^*]$ . We also considered the hypothetical isomeric compound  $[2^*]^{+}_{\text{mer}}$ , in which the nitrogen donors of the  $L^1$  fragment are in a meridional conformation, similar to  $[3]^{2+}_{\text{mer}}$ . Based on the experimental data, geometry optimization of  $[1^*]$ ,  $[2^*]^{+}_{\text{fac}}$ ,  $[2^*]^{+}_{\text{mer}}$  was done with  $S = 3/2$  (for high-spin Co(II) complexes), while for  $[3]^{2+}_{\text{fac}}$ ,  $[3]^{2+}_{\text{mer}}$ , and  $[4]^{2+}$  the optimization was done with  $S = 0$  (low-spin Co(III) complexes).

The optimized geometries of the complexes are depicted in **Figure 2.5**. The simplified side product  $[2^*]^{+}_{\text{fac}}$  is more stable by 5 kcal/mol than the hypothetical isomer  $[2^*]^{+}_{\text{mer}}$ . In addition,  $[3]^{2+}_{\text{mer}}$  is more stable than  $[3]^{2+}_{\text{fac}}$  by 8 kcal/mol and therefore  $[3]^{2+}_{\text{mer}}$  was used for further analyses. The likelihood that  $[3]^{2+}_{\text{mer}}$  corresponds with the actual structure of  $[3]^{2+}$  is supported by the crystal structure of  $[\text{Co}(L^1\text{SO}_2)(\text{phen})](\text{SbF}_6)_2$  (**Figure AI.14**) and  $[4](\text{BF}_4)_2$ ,<sup>15</sup> in which the nitrogen donors of  $L^1S^-$  are indeed arranged in a meridional fashion. The results obtained for  $[4]^{2+}$  in a low-spin ( $S=0$ ) state are in agreement with the previous report.<sup>15</sup>

We then studied the energy levels of the molecular orbitals, with a focus on the MO's with large contributions of  $d$ -orbitals of the cobalt centers, with the aim to estimate the ligand-field splitting energies. The levels of the five molecular orbitals with largest contribution of the Co  $d$ -orbitals in  $[1^*]$ ,  $[2^*]^{+}_{\text{fac}}$ ,  $[2^*]^{+}_{\text{mer}}$ ,  $[3]^{2+}_{\text{mer}}$ , and  $[4]^{2+}$  are shown in **Figure 2.6** (see **Figures S15-S19** for detailed description). The MO's comprising large contribution of Co  $d$ -orbitals are not separated into two or three degenerated energy levels as expected for ideal geometries described by the ligand-field theory.<sup>22</sup> Instead, we found the cobalt  $d$ -orbitals to be distributed in five different energy levels, due to the asymmetry of the compounds. However, notably in the octahedral compounds it is clear that the  $d$ -orbitals are distributed into two sets of (nearly degenerate) energy levels, qualitatively corresponding to the  $t_{2g}$  and  $e_g$  levels defined by ligand-field theory.

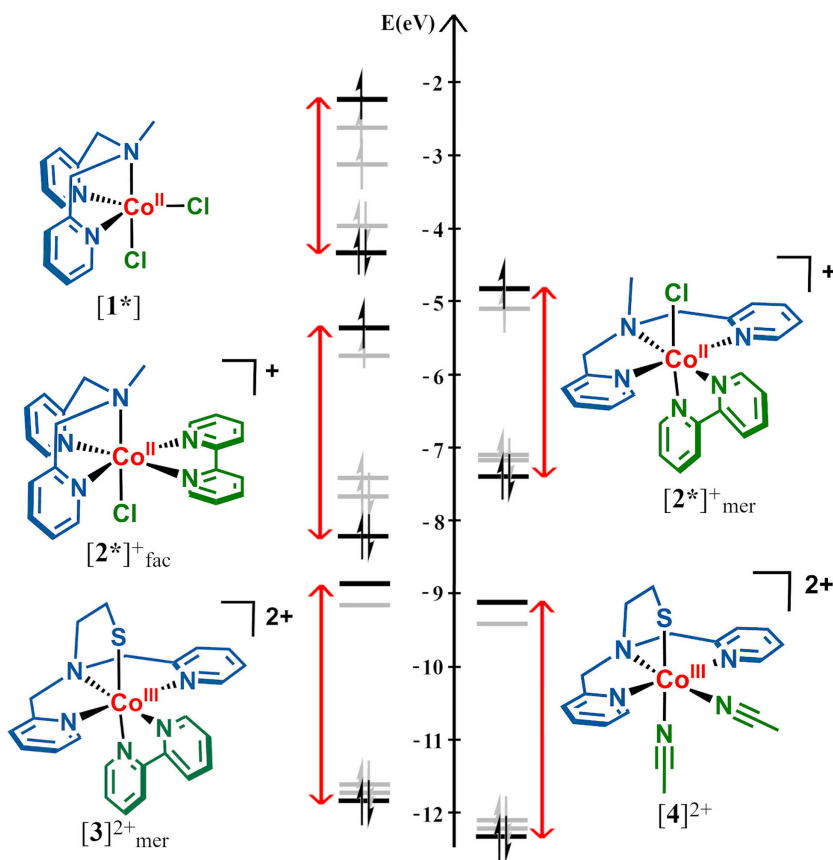


**Figure 2.6.** Simplified energy level diagrams for  $[1^*]$ ,  $[2^*]^+_{\text{fac}}$ ,  $[2^*]^+_{\text{mer}}$ ,  $[3]^{2+}_{\text{mer}}$ , and  $[4]^{2+}$ .

Molecular orbital diagrams show only the five energy levels with the largest Co  $d$ -orbital contributions (highest-lying and lowest-lying energy levels are denoted in black, the remaining energy levels are denoted in grey). The three colors used in the structures indicate the fragments that were used in the DFT computations.

It is not possible to calculate the ligand-field splitting energies from the five molecular orbitals due to the non-degeneracy and the molecular orbitals being a mix of cobalt  $d$ -orbitals and ligand orbitals (see Figures S15-S19). Thus, we can discuss the energy differences in these MO's only in a qualitative way. The energy difference between the highest and lowest MO with large  $d$ -orbital contribution seems to be larger for  $[2^*]^+_{\text{fac}}$  than for the hypothetical isomer  $[2^*]^+_{\text{mer}}$ . Furthermore, the energy difference in  $[4]^{2+}$ , containing two acetonitrile molecules, is slightly larger than that of the bpy-containing compound  $[3]^{2+}_{\text{mer}}$ . Our results thus indicate that for our system, bpy has lower ligand-field strength than acetonitrile, which

is in contradiction with the spectrochemical series.<sup>17, 23-25</sup> It has been reported that bpy might have similar or even larger  $\pi$ -donating than  $\pi$ -accepting properties, suggesting that the large ligand-field strength of bpy may be overestimated.<sup>26</sup>

Upon closer inspection of the distribution of the electron density and energy levels of the SOMOs of  $[2^*]_{\text{fac}}^+$  and  $[2^*]_{\text{mer}}^+$ , we found some interesting differences. In  $[2^*]_{\text{fac}}^+$  the SOMO and the SOMO-1 are at  $-5.1$  eV and  $-5.7$  eV and have respectively mainly cobalt  $d_{x^2-y^2}$  and  $d_{z^2}$  character, whereas in the hypothetical intermediate  $[2^*]_{\text{mer}}^+$  the SOMO and SOMO-1 are at  $-4.8$  eV and  $-5.1$  eV and have mainly cobalt  $d_{z^2}$  and  $d_{x^2-y^2}$  character. Thus, the highest SOMO in  $[2^*]_{\text{mer}}^+$  is more destabilized than in  $[2^*]_{\text{fac}}^+$  and consequently, the single electron from this SOMO will be transferred more readily from the Co(II) center to the disulfide sulfur atom in a redox-conversion reaction. More importantly, if the chloride ion leaves the cobalt in  $[2^*]_{\text{fac}}^+$  and  $[2^*]_{\text{mer}}^+$ , respectively, the SOMO-1 and SOMO with the  $d_{z^2}$  character becomes available to the sulfur atom. From **Figure 2.7**, it is clear that the SOMO in  $[2^*]_{\text{mer}}^+$  can be more readily approached by a sulfur atom of the disulfide group. In contrast, in  $[2^*]_{text{fac}}^+$  extensive rearrangements are necessary to make the  $d_{z^2}$  orbital available to the sulfur atom in order to produce the  $[3]_{\text{fac}}^{2+}$ .

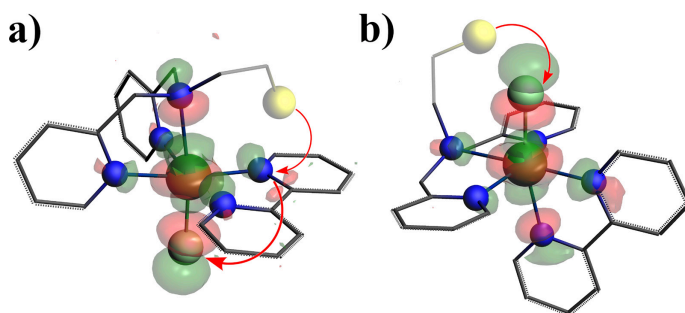


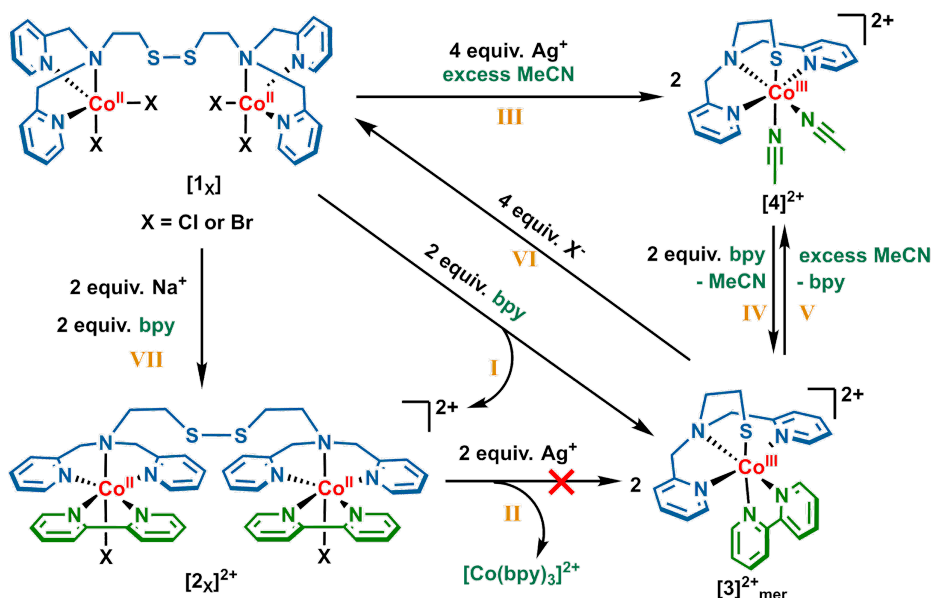
**Figure 2.7.** Schematic drawings of the approach of the sulfur atom to replace chloride in a)  $[2^*]_{\text{fac}}^+$  and b)  $[2^*]_{\text{mer}}^+$ . The  $d_{z^2}$  character of  $[2^*]_{\text{fac}}^+$  and  $[2^*]_{\text{mer}}^+$  (SOMO-1 and SOMO, respectively) is shown as orbital lobes. The sulfur atom was omitted in the calculation of  $[2^*]_{\text{fac}}^+$  and  $[2^*]_{\text{mer}}^+$ , but is included for clarity.

### 2.3. Discussion

It has been reported that redox-conversion reactions of cobalt(II)-disulfide complexes to the corresponding cobalt(III)-thiolate complexes occur under certain conditions.<sup>10, 13, 15</sup> We reported that removal of the chloride ions from [1Cl] in acetonitrile leads to the formation of [4]<sup>2+</sup>, whereas in methanol the compound remains in the cobalt(II)-disulfide state.<sup>15</sup> Furthermore, the reaction of L<sup>1</sup>SSL<sup>1</sup> with Co(NCS)<sub>2</sub> in acetonitrile as well as methanol or dichloromethane leads to the immediate formation of [Co(L<sup>1</sup>S)(NCS)<sub>2</sub>].<sup>15, 27</sup> As both acetonitrile (MeCN) and the thiocyanate anion ([NCS]<sup>-</sup>) are ligands with a stronger ligand-field effect than that of the chloride ion, we hypothesized that the initial formation of a low-spin Co(II)-disulfide intermediate with two degenerate, high-energy MOs containing a single electron facilitates the redox-conversion by electron transfer to the disulfide group.

We assumed that bpy would trigger the redox-conversion reaction of cobalt(II)-disulfide [1x] to the cobalt(III)-thiolate compound [3]<sup>2+</sup>, possibly without the need to remove the halide ions, as bpy is a chelating ligand that is reported to have a relatively strong ligand-field effect. Our initial spectroscopic studies suggested that this redox-conversion reaction indeed occurred, as indicated by the color change of the solution and the change in the UV-Vis spectrum upon addition of two equivalents of bpy to a solution of [1x] (See **Scheme 2.3**, reaction I). However, it appeared that full conversion of [1x] to [3]<sup>2+</sup> does not take place; workup showed that a mixture is formed of [3]<sup>2+</sup> and [2x]<sup>2+</sup>. Unexpectedly, formation of [3]<sup>2+</sup> by halide abstraction of [2x]<sup>2+</sup> (**Scheme 2.3**, reaction II) was unsuccessful, as this reaction led to the formation of [Co(bpy)<sub>3</sub>]<sup>2+</sup>.

Removal of the halides of [1x] in acetonitrile leads to the formation of [4]<sup>2+</sup> (**Scheme 2.3**, reaction III); subsequent addition of bpy results in replacement of the solvent molecules forming [3]<sup>2+mer</sup> (**Scheme 2.3**, reaction IV). In contrast to the reaction of [1x] with bpy (**Scheme 2.3**, reaction I), formation of [4]<sup>2+</sup> via removal of halides in acetonitrile (**Scheme 2.3**, reaction III) is clean;<sup>15</sup> it is most likely driven by the excess of acetonitrile (as solvent) as there is no other ligand present. In addition, [3](SbF<sub>6</sub>)<sub>2</sub> appeared to be unstable when dissolved in acetonitrile, possibly due to bpy having lower ligand-field strength than anticipated (**Scheme 2.3**, reaction V). Finally, we have shown that treatment of a solution of [3](SbF<sub>6</sub>)<sub>2</sub> with the chloride salt NEt<sub>4</sub>Cl in acetonitrile (**Scheme 2.3**, reaction VI) leads to the formation of [1Cl], indicating that the reverse reaction is indeed possible.



**Scheme 2.3.** Overview of all reactions described in this chapter.

The X-ray structure of  $[2_{\text{Cl}}](\text{BPh}_4)_2$  in combination with the molecular orbital analyses of  $[2^*]^+_{\text{fac}}$  and  $[2^*]^+_{\text{mer}}$  provide an explanation for our observations. Due to the facial orientation of the three nitrogen donors of the  $L^1$  fragment in  $[2_{\text{Cl}}]^{2+}$ , approach of the disulfide group to the SOMO-1 based on the  $d_{z^2}$  orbital of the cobalt center necessary for the electron transfer is hampered by the chelating bpy (**Figure 2.7.a**). Several donor atoms need to dissociate and move to other relative positions to allow for the generation of either  $[3]^{2+}_{\text{fac}}$  or  $[3]^{2+}_{\text{mer}}$ . If during this process bpy dissociates, ligand scrambling leads to the formation of  $[Co(bpy)_3]^{2+}$ . The formation of  $[Co(bpy)_3]^{2+}$  is favourable due to its high stability constant ( $\log\beta_3 = 16.1$  in water with 0.1 M ionic strength,  $\log\beta_3 = 36.08$  in 1,2-dichloroethane).<sup>28, 29</sup> We therefore could not use an excess bpy in our reactions to drive reaction I to completion.

In contrast, the coordination mode in the hypothetical intermediate  $[2^*]^+_{\text{mer}}$  allows approach of the disulfide group to the SOMO with high contribution of the cobalt  $d_{z^2}$  orbital, thus replacing the chloride ion (**Figure 2.7.b**). Thus, addition of bpy to  $[1x]$  can lead to two ‘intermediates’: the stable compound  $[2]^{2+}$  that is found as a ‘by product’ and a potentially unstable intermediate with the nitrogen atoms of the  $L^1$  fragment in meridional positions (resembling  $[2^*]^+_{\text{mer}}$ ), which readily converts to  $[3]^{2+}$  and is thus not observed as a product.

## 2.4. Conclusion

The redox-conversion of cobalt(II)-disulfide compound  $[1x]$  to the cobalt(III)-thiolate complex  $[3]^{2+}$  using the bidentate ligand bpy has been investigated using various spectroscopic methods as well as DFT calculations. The formation of species  $[3]^{2+}$  from  $[1x]$  indicates that bpy is indeed able to induce the redox-conversion of a cobalt(II)-disulfide to a cobalt(III)-thiolate complex, even without the addition of silver salts to remove the chloride ions, although the formation of side product  $[2x]^{2+}$  appeared to be inevitable. For the redox-conversion to occur starting from the intermediate  $[2x]^{2+}$ , reorganisation of the donor atoms at cobalt is necessary, and dissociation of bpy during this process results in the formation of highly stable tris-bipyridine cobalt compounds. Furthermore, our DFT studies show that the conversion from  $[1c]$  to  $[3]^{2+}$  most likely proceeds via an intermediate in which the nitrogen atoms of the disulfide ligand are arranged in a meridional fashion, making it possible for the disulfide sulfur atom to approach the high-energy SOMO with predominant cobalt  $d_{x^2}$  contribution for electron transfer.

Our initial hypothesis that the redox-conversion of  $[1x]$  to a cobalt(III) thiolate compound may be induced simply by addition of a strong-field ligand thus has not yet been firmly proven. First of all, it turns out that the ligand-field splitting strength of bpy is lower than anticipated, and additionally, the use of bpy leads to the formation of the highly stable  $[Co(bpy)_3]^{n+}$ . Furthermore, the coordination mode of the ligands appear to be vital, as demonstrated by this study and our previous report. Further studies will be directed to the use of other ligands that are higher in the spectrochemical series, which may further corroborate our findings by inducing cleaner redox-conversion reactions of cobalt(II)-disulfide to the related cobalt(III)-thiolate complexes.

## 2.5. Experimental Section

### 2.5.1. General

All reagents were purchased from commercial sources and used as received unless noted otherwise. Degassed solvents used were obtained by the freeze-pump-thaw method followed by drying the solvents using the appropriate size of molecular sieves. The ligand  $L^1SSL^1$  and cobalt compound  $[Co_2(L^1SSL^1)Cl_4]$   $[1c]$  were prepared according to previously published methods.<sup>14, 15</sup> The synthesis of the cobalt compounds was performed using standard



Schlenk-line techniques under argon atmosphere.  $^1\text{H}$  NMR spectra were recorded on a Bruker 300 DPX spectrometer at room temperature. Mass spectra were recorded on a Thermo Scientific MSQ Plus mass spectrometer with electrospray ionization (ESI) method. Formic acid was added to the eluting solvent in a final concentration of 1% (v/v). Simulated mass spectra were generated using mMass (version 5.5.0) software.<sup>30</sup> IR spectra were obtained using a PerkinElmer Spectrum Two System equipped with Universal ATR module containing diamond crystal for single reflection (scan range 400–4000  $\text{cm}^{-1}$ , resolution 4  $\text{cm}^{-1}$ ). UV-visible spectra were collected using a transmission dip probe with variable path lengths and a reflection probe on an Avantes AvaSpec-2048 spectrometer and using an Avalight-DH-S-Bal light source. Elemental analyses were performed by the Microanalytical Laboratory Kolbe in Germany.

### 2.5.2. Single crystal X-ray crystallography

All reflection intensities were measured at 110(2) K using a SuperNova diffractometer (equipped with Atlas detector) with Mo  $K\alpha$  radiation ( $\lambda = 0.71073$  Å) under the program CrysAlisPro (Version CrysAlisPro 1.171.39.29c, Rigaku OD, 2017). The same program was used to refine the cell dimensions and for data reduction. The structure was solved with the program SHELXS-2018/3 and was refined on  $F^2$  with SHELXL-2018/3.<sup>31</sup> Numerical absorption correction based on Gaussian integration over a multifaceted crystal model was applied using CrysAlisPro. The temperature of the data collection was controlled using the system Cryojet (manufactured by Oxford Instruments). The H atoms were placed at calculated positions using the instructions AFIX 23, AFIX 43, AFIX 137 or AFIX 147 with isotropic displacement parameters having values 1.2 or 1.5  $U_{\text{eq}}$  of the attached C or O atoms.

The structure of compound [**1Br**] is partly disordered. The lattice methanol solvent molecule is found to be disordered over two orientations, with the occupancy factor of the major component of the disorder refining to 0.68(3). The H atoms H1OM and H1O' attached to O1S and O1S' (disordered MeOH lattice solvent molecule) were found from difference Fourier maps, and their coordinates were constrained to be the same using the EXYZ instruction. The O1S–H1OM and O1S'–H1O' bond distances were set to be refined pseudo-freely using the DFIX instruction in order to keep the O–H distance within an acceptable range.

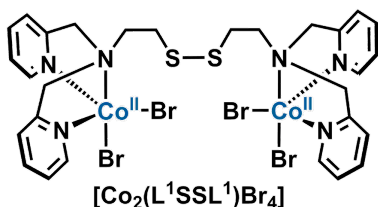
For compound  $[2](\text{BPh}_4)_2$ , the H atom attached to O1W (partially occupied lattice water molecule found at one site of twofold axial symmetry, occupancy factor: 0.419(11)) could not reliably retrieved from the difference Fourier map. The structure is partly disordered. One phenyl group and the lattice acetone solvent molecule are disordered over two orientations, and the occupancy factors of the major components of the disorder refine to 0.874(6) and 0.778(10), respectively. The asymmetric unit also contains another lattice solvent molecule (or a mixture of lattice solvent molecules) that is very disordered. While it might be one partially occupied disordered acetone lattice solvent molecule, it is difficult to assess with certainty the exact nature of the lattice solvent molecule. This contribution has been removed using the SQUEEZE procedure in Platon.<sup>32, 33</sup> The crystal structures of  $[1_{\text{Br}}]$ ,  $[2_{\text{Cl}}](\text{BPh}_4)_2$ , and  $[\text{Co}(\text{L}^1\text{SO}_2)(\text{phen})](\text{SbF}_6)_2$  can be accessed via Cambridge Crystallographic Data Center database, CCDC deposit number: 2093906, 2093907, 2093908.

### 2.5.3. DFT Calculations

All calculations were performed with the Amsterdam Density Functional (ADF) program version 2017.103.<sup>34</sup> Geometries and energies were computed using OPBE functional.<sup>35</sup> Molecular orbitals (MO) were expanded in a large uncontracted TZP Slater type orbital (STO) basis set.<sup>36</sup> Scalar relativistic effects were accounted for using the zeroth order regular approximation (ZORA).<sup>37</sup> The stationary points were checked to be minima at potential energy surface using vibrational analysis. The simplified compound  $[1^*]$ ,  $[2^*]_{\text{fac}}^+$ , and  $[2^*]_{\text{mer}}^+$  were optimized with  $S = 3/2$  (high-spin cobalt(II) center). For the compounds  $[3]^{2+}$  (both facial and meridional conformation) and  $[4]^{2+}$ , calculations were done with  $S = 0$  (low-spin cobalt(III) center).

### 2.5.4. Synthesis of the compounds

#### $[\text{Co}_2(\text{L}^1\text{SSL}^1)\text{Br}_4]$ ( $[1_{\text{Br}}]$ )

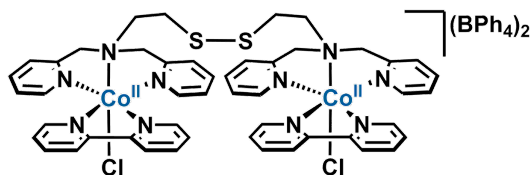


The ligand  $\text{L}^1\text{SSL}^1$  (129 mg, 0.25 mmol) was dissolved in 5 mL dry and degassed acetonitrile. Into the solution of the ligand, anhydrous  $\text{CoBr}_2$  (109 mg, 0.50 mmol, 2 equiv.) was then added. The resulting purple solution was then stirred for 1 hour. The solution was then

concentrated until approximately 1 mL was left in the flask. Into the flask, 12 mL dry and

degassed diethyl ether was added and immediately pale purple precipitates were formed. The precipitates were then washed twice with 10 mL dry and degassed diethyl ether, filtered, and then dried in vacuo. Yield: 144 mg, 0.151 mmol, 60%. Single crystals of **[1<sub>Br</sub>]** were grown after approximately a week using vapor diffusion of diethyl ether into a methanol solution of compound **[1<sub>Br</sub>]**. IR (neat, cm<sup>-1</sup>): 1608s, 1571w, 1480m, 1445s, 1310m, 1291m, 1257w, 1155w, 1092m, 1054m, 1025s, 965w, 862m, 766s, 738m, 650m, 522w, 417m. ESI-MS calcd. for **[1<sub>Br</sub> – Br]<sup>+</sup>**  $m/z$  872.8, found  $m/z$  872.9, calcd. for **[1<sub>Br</sub> – 2Br]<sup>2+</sup>**  $m/z$  398.0, found  $m/z$  398.0. Elemental analysis (%) for **[1<sub>Br</sub>]**·0.6 H<sub>2</sub>O, calcd. C, 34.85; H, 3.47; N, 8.71; found C, 34.89; H, 3.51; N, 8.70.

**[Co<sub>2</sub>(L<sup>1</sup>SSL<sup>1</sup>)(bpy)<sub>2</sub>(Cl)<sub>2</sub>](BPh<sub>4</sub>)<sub>2</sub> (**[2<sub>Cl</sub>](BPh<sub>4</sub>)<sub>2</sub>**)**



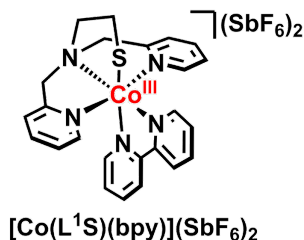
**[Co<sub>2</sub>(L<sup>1</sup>SSL<sup>1</sup>)(bpy)<sub>2</sub>(Cl)<sub>2</sub>](BPh<sub>4</sub>)<sub>2</sub>**

Ligand L<sup>1</sup>SSL<sup>1</sup> (52.01 mg, 0.1 mmol) was dissolved in 5 mL dry and degassed methanol. After all the ligand was dissolved, anhydrous CoCl<sub>2</sub> (26.21 mg, 0.2 mmol, 2 equiv.) was added to the

solution, resulted in dark purple solution. The solution was stirred for 30 minutes, then 2,2'-bipyridine (31.43 mg, 0.2 mmol, 2 equiv.) was added and the solution color immediately turned orange. After stirring the solution for 2 hours, sodium tetraphenylborate (68.90 mg, 0.2 mmol, 2 equiv.) was added to remove 2 equiv. of chloride ligands. The addition of sodium tetraphenylborate quickly resulted in suspension. Into this suspension, 3 mL dry and degassed acetone was added to re-dissolve the complex. The suspension was then turned into solution again with small amount of white precipitates. The solution was filtered into a clean Schlenk flask, and then concentrated under reduced pressure until approximately 1 mL was left in the flask. Into the flask, 12 mL dry and degassed diethyl ether was then added, which afforded beige-colored precipitates. The precipitates were washed twice with 10 mL dry and degassed diethyl ether, filtered, and dried in vacuo. Yield: 78 mg, 47%. Single crystals suitable for X-ray diffraction for this compound were obtained by vapor diffusion of acetone into a methanol solution of **[2](BPh<sub>4</sub>)<sub>2</sub>**. IR (neat, cm<sup>-1</sup>): 3050w, 1603m, 1477m, 1439m, 1314w, 1262w, 1156w, 1058w, 1018m, 766m, 732s, 704s, 611m. ESI-MS calcd. for **[2<sub>Cl</sub> – Cl<sup>-</sup> + OMe<sup>-</sup>]<sup>2+</sup>**  $m/z$  506.1, found  $m/z$  506.5, calcd. for **[2<sub>Cl</sub> – Cl<sup>-</sup> + OMe<sup>-</sup>]<sup>+</sup>**  $m/z$  1012.2,

found  $m/z$  1011.9. Elemental analysis (%) for  $[2\text{Cl}](\text{BPh}_4)_2 \cdot 2 \text{H}_2\text{O}$ , calcd. C, 68.13; H, 5.48; N, 8.28; found C, 68.13; H, 5.41; N, 8.27.

### $[\text{Co}(\text{L}^1\text{S})(\text{bpy})](\text{SbF}_6)_2$ (**[3]**)( $\text{SbF}_6$ )<sub>2</sub>



Ligand  $\text{L}^1\text{SSL}^1$  (52.25 mg, 0.1 mmol) was dissolved in 5 mL dry and degassed acetonitrile. Into the solution of the ligand, anhydrous  $\text{CoBr}_2$  (44.10 mg, 0.2 mmol, 2 equiv.) was added, resulted in a purple solution. The solution was stirred for 1 hour and  $\text{AgSbF}_6$  (153.6 mg, 0.45 mmol, 4.5 equiv) was then added. The addition of silver salt was done in a slight

excess in order to make sure that all the bromide ions were removed. The solution turned into a yellow suspension. The stirring was then stopped and after 1 hour all the solid had settled down, the solution was filtered into a clean Schlenk flask. The remaining solid was washed with 2 mL of dry and degassed acetonitrile and the solution was then filtered into the Schlenk flask containing the previous filtrate. Into this dark brown filtrate, 2,2'-bipyridine (31.04 mg, 0.2 mmol, 2 equiv.) was added. The resulting orange solution was then stirred for another hour, and then concentrated until approximately 1 mL of the solution was left in the flask. Into the solution, 12 mL dry and degassed diethyl ether was then added, resulted in formation of a red oil. The solvent was then removed by filtration using a syringe filter and the resulting red oil was re-dissolved in 1 mL methanol. Dry and degassed diethyl ether (12 mL) was then added into the solution which led to formation of **[3]**( $\text{SbF}_6$ )<sub>2</sub> as a red solid. The solid was washed twice with diethyl ether, filtered and dried in vacuo. Yield: 178 mg, 0.189 mmol, 93%.  $^1\text{H-NMR}$  (300 MHz,  $(\text{CD}_3)_2\text{CO}$ , RT)  $\delta$ (ppm): 1.84 (m, 2H, S- $\text{CH}_2$ ), 2.26 (m, 2H, S- $\text{CH}_2$ - $\text{CH}_2$ -N), 5.07-5.13 (d, 2H, py- $\text{CH}_2$ -N), 6.01-6.15 (d, 1H, py- $\text{CH}_2$ -N), 7.28-10.00 (m, 40H, 16H from **[3]**( $\text{SbF}_6$ )<sub>2</sub>, 24H from  $[\text{Co}(\text{bpy})_3]^{3+}$  species). IR (neat,  $\text{cm}^{-1}$ ): 1700w, 1600m, 1573w, 1485w, 1471w, 1364w, 1318w, 1246w, 1163w, 1088w, 766s, 651vs. ESI-MS calcd. for **[3]**( $\text{SbF}_6$ )<sup>+</sup>  $m/z$  708.0, found  $m/z$  708.0, calcd. for **[3]**<sup>2+</sup>  $m/z$  236.55, found  $m/z$  236.6. Elemental analysis (%) for **[3]**( $\text{SbF}_6$ )<sub>2</sub>·1.5H<sub>2</sub>O, calcd. C, 29.66; H, 2.80; N, 7.21; found C, 29.59; H, 2.66; N, 7.13.

## 2.6. References

1. Paulsen, C. E. and Carroll, K. S. *Chem. Rev.* **2013**, 113 (7), 4633-4679.

2. Cramer, J. D. and Jarrett, J. T., *Methods in Enzymology: Radical SAM Enzymes*, 13, **2018**, Vol. 606, 363-388.
3. Poole, L. B. *Free Radical Biol. Med.* **2015**, 80, 148-157.
4. Sato, I., Shimatani, K., Fujita, K., Abe, T., Shimizu, M., Fujii, T., Hoshino, T. and Takaya, N. *J. Biol. Chem.* **2011**, 286 (23), 20283-20291.
5. Xiao, Z., La Fontaine, S., Bush, A. I. and Wedd, A. G. *J. Mol. Biol.* **2019**, 431 (2), 158-177.
6. Ueno, Y., Tachi, Y. and Itoh, S. *J. Am. Chem. Soc.* **2002**, 124 (42), 12428-12429.
7. Thomas, A. M., Lin, B.-L., Wasinger, E. C. and Stack, T. D. P. *J. Am. Chem. Soc.* **2013**, 135 (50), 18912-18919.
8. Ording-Wenker, E. C. M., van der Plas, M., Siegler, M. A., Bonnet, S., Bickelhaupt, F. M., Fonseca Guerra, C. and Bouwman, E. *Inorg. Chem.* **2014**, 53 (16), 8494-8504.
9. Ording-Wenker, E. C. M., van der Plas, M., Siegler, M. A., Fonseca Guerra, C. and Bouwman, E. *Chem. Eur. J.* **2014**, 20 (51), 16913-16921.
10. Gennari, M., Gerey, B., Hall, N., Pecaut, J., Collomb, M.-N., Rouzies, M., Clerac, R., Orio, M. and Duboc, C. *Angew. Chem. Int. Ed.* **2014**, 53 (21), 5318-5321.
11. Wang, L., Reinhard, F. G. C., Philouze, C., Demeshko, S., de Visser, S. P., Meyer, F., Gennari, M. and Duboc, C. *Chem. Eur. J.* **2018**, 24 (46), 11973-11982.
12. Osako, T., Ueno, Y., Tachi, Y. and Itoh, S. *Inorg. Chem.* **2004**, 43 (21), 6516-6518.
13. Gennari, M., Brazzolotto, D., Yu, S., Pecaut, J., Philouze, C., Rouzies, M., Clerac, R., Orio, M. and Duboc, C. *Chem. Eur. J.* **2015**, 21 (51), 18770-18778.
14. Itoh, S., Nagagawa, M. and Fukuzumi, S. *J. Am. Chem. Soc.* **2001**, 123 (17), 4087-4088.
15. Jiang, F., Siegler, M. A., Sun, X., Jiang, L., Fonseca Guerra, C. and Bouwman, E. *Inorg. Chem.* **2018**, 57 (15), 8796-8805.
16. Miessler, G. L., Fischer, P. J. and Tarr, D. A. *Inorganic Chemistry*. 5th ed.; 2014; p 696.
17. Sharpe, A. G. and Housecroft, C. E. *Inorganic Chemistry*. 4th ed.; Pearson Education Limited: 2012; p 1256.
18. Addison, A. W., Rao, T. N., Reedijk, J., Vanrijn, J. and Verschoor, G. C. *J. Chem. Soc., Dalton Trans.* **1984**, (7), 1349-1356.
19. Cowan, M. G., Olguin, J., Narayanaswamy, S., Tallon, J. L. and Brooker, S. *J. Am. Chem. Soc.* **2012**, 134 (6), 2892-2894.
20. Taylor, R. A., Lough, A. J. and Lemaire, M. T. *J. Mater. Chem.* **2016**, 4 (3), 455-459.
21. Furmeyer, F., Munzberg, D., Carrella, L. M. and Rentschler, E. *Molecules* **2020**, 25 (4)
22. Griffith, J. S. and Orgel, L. E. *Quarterly Reviews, Chemical Society* **1957**, 11 (4), 381.
23. Shimura, Y. and Tsuchida, R. *Bull. Chem. Soc. Jpn.* **1956**, 29 (3), 311-316.
24. Tsuchida, R. *Bull. Chem. Soc. Jpn.* **1938**, 13 (5), 388-400.
25. Tsuchida, R. *Bull. Chem. Soc. Jpn.* **1938**, 13 (6), 436-450.
26. Ashley, D. C. and Jakubikova, E. *Inorg. Chem.* **2018**, 57 (16), 9907-9917.
27. Jiang, F., Marvelous, C., Verschuur, A. C., Siegler, M. A., Teat, S. J. and Bouwman, E. *Inorg. Chim. Acta* **2022**, 120880.
28. Irving, H. and Mellor, D. H. *J. Chem. Soc* **1962**, (DEC), 5237-&.
29. Makrlík, E. and Vaňura, P. *Colloids Surf., A* **1992**, 68 (3), 195-197.
30. Strohm, M., mMass - Open Source Mass Spectrometry Tool. [www.mmass.org](http://www.mmass.org)
31. Sheldrick, G. M. *Acta Crystallogr. Sect. A: Found. Crystallogr.* **2008**, 64, 112-122.
32. Spek, A. L. *Acta Crystallogr. Sect. C: Cryst. Struct. Commun.* **2015**, 71 (Pt 1), 9-18.
33. Spek, A. L. *Acta Crystallogr. Sect. D: Biol. Crystallogr.* **2009**, 65 (2), 148-155.
34. ADF2017.107. SCM Theoretical Chemistry, Vrije Universiteit: Amsterdam, The Netherlands, [www.scm.com](http://www.scm.com)
35. Swart, M., Ehlers, A. W. and Lammertsma, K. *Mol. Phys.* **2004**, 102 (23-24), 2467-2474.
36. Van Lenthe, E. and Baerends, E. J. *J. Comput. Chem.* **2003**, 24 (9), 1142-1156.
37. Van Lenthe, E., Baerends, E. J. and Snijders, J. G. *J. Chem. Phys.* **1994**, 101 (11), 9783-9792.

# Chapter 3

---

## Cleaner and Stronger: How 8-quinolinolate Facilitates Formation of Co(III)-thiolate from Co(II)-disulfide Complexes

*The formation of Co(III)-thiolate complexes from Co(II)-disulfide complexes using the anionic ligand 8-quinolinolate ( $\text{quin}^-$ ) has been studied experimentally and quantum chemically. Two Co(II)-disulfide complexes  $[\text{Co}_2(\text{L}^x\text{SSL}^x)(\text{Cl})_4]$  ( $x=1$  or  $2$ ;  $\text{L}^1\text{SSL}^1 = 2,2'$ -disulfanedylbis( $N,N$ -bis(pyridin-2-ylmethyl)ethan-1-amine;  $\text{L}^2\text{SSL}^2 = 2,2'$ -disulfanedylbis( $N$ -((6-methylpyridin-2-yl)methyl)- $N$ -(pyridin-2-ylmethyl)ethan-1-amine) have been successfully converted with high yield to their corresponding Co(III)-thiolate complexes upon addition of the ligand 8-quinolinolate. The unexpected formation of  $[\text{Co}_2(\text{L}^2\text{SSL}^2)(\text{quin})_2(\text{Cl})_2]$  suggests a potential mechanism for the formation of the Co(III)-thiolate compound. Using density functional theory (DFT) computations the  $d$ -orbital splitting energies of the cobalt-thiolate compounds  $[\text{Co}(\text{L}^1\text{S})(\text{quin})]^+$  and  $[\text{Co}(\text{L}^2\text{S})(\text{quin})]^+$  were estimated to be 3.10 eV and 3.07 eV, confirming that the ligand-field strength of the ligand  $\text{L}^2\text{SSL}^2$  is smaller than that of  $\text{L}^1\text{SSL}^1$ . Furthermore, the orientation of the  $\text{quin}^-$  ligand in the thiolate compounds is imperative, as it determines the strength of the electrostatic interaction between  $\text{quin}^-$  and the thiolate complex. The results suggest that coordination of the oxygen atom of the  $\text{quin}^-$  ligand trans to the sulfur atom of the  $[\text{Co}(\text{L}^1\text{S})]^{2+}$  fragment benefits from more electrostatic attraction between aromatic rings.*

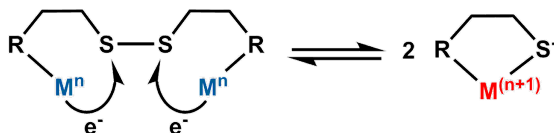
This chapter will be published as a full article: Christian Marvelous, Lucas de Azevedo Santos, Maxime A. Siegler, Célia Fonseca Guerra, and Elisabeth Bouwman, *submitted*

### 3.1. Introduction

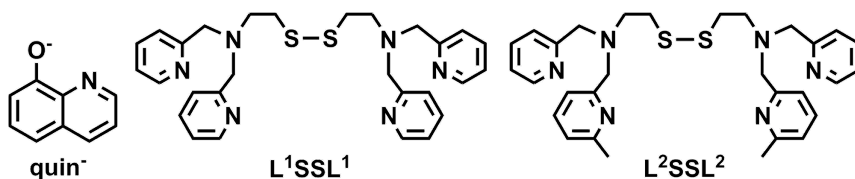
Electron transfer is part of many chemical and important biological processes, some examples including respiration and detoxification.<sup>1-3</sup> Transition-metal ions and sulfur-based ligands engage in such electron-transfer processes, as both species are susceptible to redox changes, leading to the formation and reduction of disulfide bonds of cysteines. One particular reaction that has been studied for two decades concerns the redox-conversion of transition-metal disulfide and thiolate complexes (**Scheme 3.1**).<sup>4</sup> In a typical reaction, two electrons from the two metal centers of a binuclear complex are transferred to the disulfide ligand. Consequently, the disulfide group is reduced into two thiolates, which then bind to the oxidized metal centers.

In recent years, the study of the redox-conversion reaction of disulfide and thiolate compounds has progressed from the copper-based system to other metal ions such as Mn, Fe, and Co.<sup>5-9</sup> The cobalt system in particular is interesting, as cobalt ions are involved in many enzymes and also because the redox-conversion of cobalt-based systems is relatively unexplored. Several reports describe the redox-conversion between cobalt(II)-disulfide and cobalt(III)-thiolate compounds induced chemically by addition or removal of halide ions, or by changing the solvent system.<sup>6, 8, 10</sup> Recently, we reported the redox-conversion of cobalt(II)-disulfide compounds to their corresponding cobalt(III)-thiolate compounds by the addition of the external ligand 2,2'-bipyridine (bpy).<sup>11</sup> It was hypothesized that the ligand-field strength of an added ligand would influence the formation of the cobalt(III)-thiolate complex, although bpy was found to be not suitable to induce this process.

In this Chapter we describe the results of our investigation on the effect of introducing 8-quinolinolate ( $\text{quin}^-$ ) as the exogenous ligand to cobalt(II)-disulfide compounds of the ligands  $\text{L}^1\text{SSL}^1$  (2,2'-disulfanediybis(N,N-bis(pyridin-2-ylmethyl)ethan-1-amine) and  $\text{L}^2\text{SSL}^2$  (2,2'-disulfanediybis(N-((6-methylpyridin-2-yl)methyl)-N-(pyridin-2-ylmethyl)ethan-1-amine) (**Scheme 3.2**). In addition to the expected larger ligand-field strength, we



**Scheme 3.1.** Redox-conversion of metal-disulfide / metal-thiolate complex.



**Scheme 3.2.** Schematic representation of anionic ligand  $\text{quin}^-$  and the ligands  $\text{L}^1\text{SSL}^1$  and  $\text{L}^2\text{SSL}^2$  described in this Chapter.

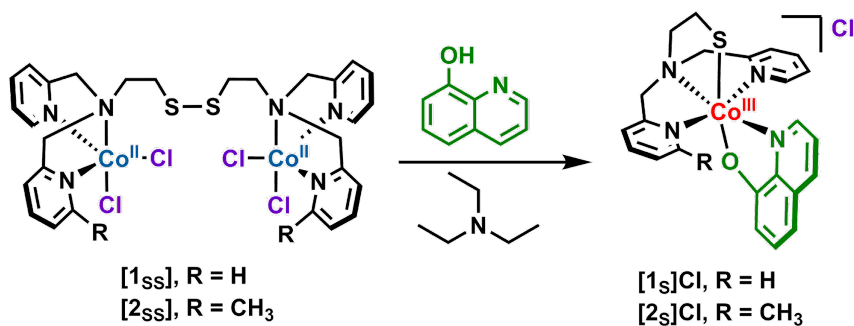
hypothesized that the anionic  $\text{quin}^-$  ligand may compensate for the dicationic charge of the resultant thiolate compound and thus stabilize the relatively electron-poor Co(III) center. Furthermore, the larger aromatic conjugation and electron delocalization of  $\text{quin}^-$  in comparison with bpy might also contribute in some extent to the stabilization of a Co(III)-thiolate complex. Therefore,  $\text{quin}^-$  is expected to trigger a cleaner redox-conversion of cobalt(II)-disulfide compounds to the corresponding cobalt(III)-thiolate complexes than was found for bpy.

## 3.2. Results

### 3.2.1. Synthesis of the compounds

The ligands  $\text{L}^1\text{SSL}^1$  and  $\text{L}^2\text{SSL}^2$  were prepared according to published procedures with slight modifications and were obtained in good yields.<sup>4, 9, 12</sup> The synthesis and characterization of the disulfide compound  $[\text{Co}_2(\text{L}^1\text{SSL}^1)(\text{Cl})_4]$  (**[1ss]**) has been reported earlier.<sup>8</sup> The disulfide compound  $[\text{Co}_2(\text{L}^2\text{SSL}^2)(\text{Cl})_4]$  (**[2ss]**) was isolated as a purple powder in a yield of 72%. The ESI-MS spectrum of **[2ss]** in methanol (Figure AII.1) shows peaks at  $m/z$  777.1 and 376.2 corresponding to the species  $[\text{2ss} - 2\text{Cl}^- + \text{HCOO}^-]^+$  and  $[\text{2ss} - 4\text{Cl}^- + 2\text{HCOO}^-]^{2+}$ , respectively (formic acid was used in the eluting solvent, producing  $\text{HCOO}^-$ ). The  $^1\text{H}$ -NMR spectrum of compound **[2ss]** dissolved in  $\text{CD}_3\text{CN}$  (Figure AII.2) shows the presence of paramagnetic peaks from  $-16$  ppm up to  $44$  ppm, confirming the presence of Co(II) centers. Further characterization using a magnetic susceptibility balance revealed the value of the magnetic moment to be  $3.98 \mu_B$  (calculated for each cobalt ion, spin-only magnetic moment  $3.87 \mu_B$ ), in agreement with the presence of two high-spin Co(II) centers within the binuclear molecule. Finally, elemental analysis shows that the compound **[2ss]** was obtained analytically pure.





**Scheme 3.3.** Schematic representations of the cobalt compounds described in this work.

Addition of the ligand 8-quinolinol (Hquin) and triethylamine to solutions of *in-situ* generated [1<sub>ss</sub>] or [2<sub>ss</sub>] afforded the mononuclear cobalt(III)-thiolate compounds [Co(L<sup>1</sup>S)(quin)]Cl ([1<sub>s</sub>]Cl) and [Co(L<sup>2</sup>S)(quin)]Cl ([2<sub>s</sub>]Cl) (**Scheme 3.3**). Both [1<sub>s</sub>]Cl and [2<sub>s</sub>]Cl were obtained in nearly quantitative yield (96% and 99%, respectively) as brown powders. The ESI-MS spectrum of [1<sub>s</sub>]Cl in methanol (Figure AII.3) shows a signal at  $m/z$  461.1 corresponding to the cationic species [1<sub>s</sub>]<sup>+</sup>. Similarly, the ESI-MS spectrum of [2<sub>s</sub>]Cl in acetonitrile (Figure AII.4) shows a signal at  $m/z$  475.3 corresponding to [2<sub>s</sub>]<sup>+</sup>. The compounds [1<sub>s</sub>]Cl and [2<sub>s</sub>]Cl are diamagnetic both in the solid state as determined with a magnetic susceptibility balance as well as in solution as shown by the <sup>1</sup>H-NMR spectra (Figure AII.5–AII.10), in agreement with the presence of low-spin Co(III) ions. Both [1<sub>s</sub>]Cl and [2<sub>s</sub>]Cl can also be synthesized in the absence of triethylamine, although the <sup>1</sup>H-NMR spectra (Figures AII.11–AII.16) then show the presence of some impurities. Elemental analysis of both [1<sub>s</sub>]Cl and [2<sub>s</sub>]Cl shows that the compounds were obtained analytically pure after recrystallization. Single crystals of [1<sub>s</sub>]Cl were grown using vapor diffusion of dry diethyl ether into a solution of [1<sub>s</sub>]Cl in a 1:1 mixture of dry acetonitrile and dry methanol. Unexpectedly, after some time red single crystals were formed in the NMR tube containing the CD<sub>3</sub>CN solution of [2<sub>s</sub>]Cl, which turned out to be of the disulfide compound [Co<sub>2</sub>(L<sup>2</sup>SSL<sup>2</sup>)(quin)<sub>2</sub>(Cl)<sub>2</sub>] ([2<sub>ss</sub>quin]). Attempts to obtain single crystals of [2<sub>s</sub>]Cl were not successful. However, dark brown single crystals of a compound containing [2<sub>s</sub>]<sup>+</sup> were obtained after anion exchange reaction using vapor diffusion of dry diethyl ether into a dry acetonitrile solution containing [2<sub>s</sub>]Cl and one equivalent of AgSbF<sub>6</sub>. These single crystals

turned out to be of the silver-bridged, dinuclear compound  $[[\text{Co}(\text{L}^2\text{S})(\text{quin})]_2\text{Ag}(\text{MeCN})](\text{SbF}_6)_3$  (**[2s-Ag-2s]**)( $\text{SbF}_6$ )<sub>3</sub>.

### 3.2.2. Description of the crystal structures

Crystallographic data of the structures are provided in Table AII.1. Compound **[1s]**Cl crystallizes in the triclinic space group  $P\bar{1}$ ; the asymmetric unit contains one molecule of **[1s]**Cl and three co-crystallized molecules of methanol. Selected bond distances and angles are provided in **Table 3.1**. The cobalt center in **[1s]**Cl (**Figure 3.1.a**) is coordinated in an octahedral geometry by the sulfur donor and three nitrogen donor atoms of  $\text{L}^1\text{S}^-$ , as well as the oxygen and nitrogen donor atom of the  $\text{quin}^-$  ligand. The octahedral geometry is slightly distorted, i.e. the largest deviation from perfect octahedral bond angles is  $94.98^\circ$  for  $\text{S1-Co1-N31}$ . These small deviations are caused by the 5-membered chelate rings formed

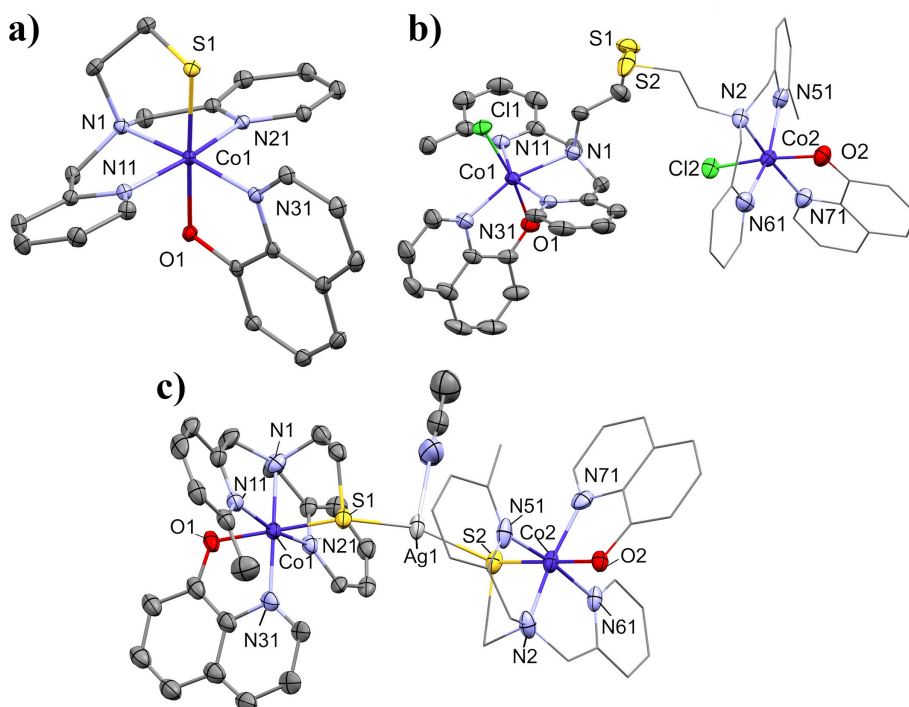


**Figure 3.1.** Displacement ellipsoid plots (50% probability) of a) **[1s]<sup>+</sup>**, b) **[2ssquin]**, and c) **[2s-Ag-2s]<sup>3+</sup>** at 110(2) K. Parts of the binuclear molecule are displayed as wireframe for clarity. Hydrogen atoms, counter ions, disordered molecules, and lattice solvent molecules are omitted for clarity. The methyl groups in **[2ssquin]** at sites of minor occupancy have been removed for clarity.

**Table 3.1.** Selected bond distances and bond angles in [1s]Cl.

Atoms	distance (Å)	Atoms	Bond angles (°)	Atoms	Bond angles (°)
Co1–N1	1.9523(13)	S1–Co1–N2	90.22(4)	O1–Co1–N31	85.29(6)
Co1–N11	1.9333(13)	S1–Co1–N11	93.91(4)	N1–Co1–N11	84.00(5)
Co1–N21	1.9231(13)	S1–Co1–N21	89.47(4)	N1–Co1–N21	85.98(5)
Co1–N31	1.9317(12)	S1–Co1–N31	94.98(4)	N1–Co1–N31	174.78(5)
Co1–O1	1.9638(11)	S1–Co1–O1	176.70(4)	N31–Co1–N11	95.24(5)
Co1–S1	2.2324(4)	O1–Co1–N2	89.53(5)	N31–Co1–N21	94.44(5)
Co1–Cl1	6.3536(5)	O1–Co1–N11	89.33(5)	N21–Co1–N11	169.43(6)
		O1–Co1–N21	87.24(5)		

by the ligand  $L^1S^-$  and  $quin^-$ . The three nitrogen atoms of  $L^1S^-$  are arranged in a meridional fashion, similar to the structure of  $[Co(L^1S)(NCS)_2]$ .<sup>8</sup> The oxygen atom of the  $quin^-$  ligand is located *trans* to the thiolate donor atom, whereas the nitrogen donor of the  $quin^-$  ligand is *trans* to the tertiary amine of  $L^1S$ . The Co–S bond distance is 2.232 Å, in agreement with other reports of low-spin cobalt(III)-thiolate compounds (2.19 – 2.30 Å, average bond distance = 2.252 Å).<sup>8, 13, 14</sup>

The distance between the non-coordinated chloride ion and the cobalt ion is 6.3536 Å. The chloride ion is in close proximity of three lattice methanol solvent molecules, tightly held by hydrogen bond interactions. The closest intermolecular distance between two thiolate sulfur atoms is 6.6478 Å. The distance between two cobalt centers in the unit cell is 9.8510 Å.

Compound [2ssquin] crystallizes in the monoclinic space group  $P2_1/n$ . The structure of [2ssquin] (**Figure 3.1.b**) is partly disordered, as the methyl groups in  $L^2SSL^2$  are located partially on each of the two pyridine rings. The occupancy factors of the major positions of the disorder refine to 0.782(6) and 0.744(6). In the asymmetric unit, one dinuclear molecule and one molecule of acetonitrile are co-crystallized. Each cobalt(II) center is in a distorted octahedral geometry, bound to three nitrogen atoms of the ligand  $L^2S$ , the oxygen and nitrogen donor of one 8-quinolinolate ligand, and one chloride ion. The structure of this dinuclear compound resembles that of  $[Co_2(L^1SSL^1)(bpy)_2(Cl)_2](BPh_4)_2$  reported in our previous study,<sup>11</sup> but in contrast to  $[Co_2(L^1SSL^1)(bpy)_2(Cl)_2](BPh_4)_2$ , the nitrogen donors of  $L^2SSL^2$  are arranged in a meridional fashion, similar to the conformation in [1s]Cl. The chloride ion is coordinated *trans* to the oxygen donor of the  $quin^-$  ligand, and the  $quin^-$  nitrogen atom is *trans* to the tertiary amine of  $L^2SSL^2$ .

Selected bond distances and angles are listed in **Table 3.2**. The bond distances and bond angles related to the Co2 center are very similar to those of Co1. The S–S bond distance in [**2<sub>ssquin</sub>**] is 2.022 Å, comparable to that in [Co<sub>2</sub>(L<sup>1</sup>SSL<sup>1</sup>)(bpy)<sub>2</sub>(Cl)<sub>2</sub>](BPh<sub>4</sub>)<sub>2</sub> (2.029) Å. The Co–Cl bond distance (2.412 Å) is longer than that in [Co<sub>2</sub>(L<sup>1</sup>SSL<sup>1</sup>)(bpy)<sub>2</sub>(Cl)<sub>2</sub>](BPh<sub>4</sub>)<sub>2</sub> (2.38 Å) or the disulfide compound [**1<sub>ss</sub>**] (2.32 and 2.27 Å), indicating that the Co–Cl bond is relatively weaker, possibly due to a *trans* effect of the quin<sup>−</sup> oxygen donor. The Co–N (tertiary amine nitrogen) bond distances are unusually long (2.200 and 2.199 Å) compared to those in other compounds with similar coordination spheres (octahedral Co(II) with four nitrogen donor atoms, one oxygen donor atom and one chloride ion), which are on average 1.952 Å.<sup>15, 16</sup> The distances between the cobalt centers and the nearest disulfide sulfur atom are around 5.8 Å, which is slightly shorter than in [**1<sub>ss</sub>**] (5.96 and 5.93 Å). The structure does not contain hydrogen bonds, but a short intermolecular contact of 3.340 Å between the methylated pyridine ring and the neighboring non-methylated pyridine ring indicates the presence of  $\pi$ – $\pi$  stacking interactions. These  $\pi$ – $\pi$  stacking interactions are in the parallel displaced conformation, most likely due to the different substituents (–CH<sub>3</sub> vs –H) in the interacting moieties.<sup>17</sup>

A displacement ellipsoid plot (50% probability) for [**2<sub>s</sub>-Ag-2<sub>s</sub>**](SbF<sub>6</sub>)<sub>3</sub> is depicted in **Figure 3.1.c** (as the 3+ cation). Bond distances and bond angles are provided in **Table 3.3**. The bond distances and bond angles around the Co2 center are similar to those of Co1. Compound [**2<sub>s</sub>- $\mu$ -Ag-2<sub>s</sub>**](SbF<sub>6</sub>)<sub>3</sub> crystallizes in the monoclinic space group *P*2<sub>1</sub>/*c*. In the asymmetric unit, one cationic molecule [**2<sub>s</sub>-Ag-2<sub>s</sub>**]<sup>3+</sup> is co-crystallized with three SbF<sub>6</sub><sup>−</sup> counter ions and one lattice acetonitrile solvent molecule. The cationic fragment [**2<sub>s</sub>-Ag-2<sub>s</sub>**]<sup>3+</sup> is composed of two [**2<sub>s</sub>**]<sup>+</sup> complexes bridged by a silver ion to which one acetonitrile

**Table 3.2.** Selected bond distances and angles in [**2<sub>ssquin</sub>**].

Atoms	distance (Å)	Atoms	Bond angles (°)	Atoms	Bond angles (°)
Co1–N1	2.200(2)	O1–Co1–Cl1	171.43(6)	Cl1–Co1–N31	93.92(7)
Co1–N11	2.192(2)	O1–Co1–N1	85.64(8)	N1–Co1–N11	78.45(8)
Co1–N21	2.179(2)	O1–Co1–N11	87.30(8)	N1–Co1–N21	77.49(9)
Co1–N31	2.132(2)	O1–Co1–N21	93.15(8)	N1–Co1–N31	161.88(9)
Co1–O1	2.0610(19)	O1–Co1–N31	78.97(8)	N31–Co1–N11	110.02(9)
Co1–Cl1	2.3921(7)	Cl1–Co1–N1	102.14(6)	N31–Co1–N21	93.75(9)
S1–S2	2.0223(19)	Cl1–Co1–N11	90.70(6)	N21–Co1–N11	155.83(9)
Co1–S1	5.848(1)	Cl1–Co1–N21	92.09(6)		

**Table 3.3.** Bond distances and bond angles in [2s-Ag-2s](SbF<sub>6</sub>)<sub>3</sub>.

Atoms	distance (Å)	Atoms	Bond angles (°)	Atoms	Bond angles (°)
Co1-S1	2.2500(19)	S1-Co1-O1	176.4(4)	N1-Co1-N11	84.5(2)
Co1-O1	1.919(7)	S1-Co1-N1	90.23(18)	N1-Co1-N21	83.4(2)
Co1-N1	1.943(6)	S1-Co1-N11	88.73(17)	N1-Co1-N31	170.6(4)
Co1-N11	2.020(5)	S1-Co1-N21	92.49(17)	N31-Co1-N11	103.1(3)
Co1-N21	1.953(5)	S1-Co1-N31	95.4(4)	N31-Co1-N21	88.8(3)
Co1-N31	1.934(7)	O1-Co1-N1	91.1(4)	N21-Co1-N11	167.9(2)
S1-Ag1	2.452(3)	O1-Co1-N11	88.1(5)	S1-Ag1-S2	157.5(2)
S2-Ag1	2.4300(18)	O1-Co1-N21	91.0(5)	S1-Ag1-N91	112.7(2)
Ag1-N91	2.527(10)	O1-Co1-N31	83.7(5)	S2-Ag1-N91	89.3(2)

molecule is coordinated. The cobalt centers in the two [2s]<sup>+</sup> fragments are in slightly distorted octahedral geometries similar to [1s]<sup>+</sup>, coordinated by one oxygen, one sulfur, and four nitrogen atoms. The Co-S bond distances are 2.2500(19) and 2.2612(19) Å, in agreement with the low-spin Co(III)-thiolate compound. The Ag<sup>+</sup> ion is in a T-shaped geometry; the S-Ag bond distances are 2.452(3) and 2.4300(28) Å, the S1-Ag-S2 bond angle is 157.5(2)°. The S-Ag bond distances in [2s-μ-Ag-2s](SbF<sub>6</sub>)<sub>3</sub> are typical, as compared to other structures with similar geometries having an average S-Ag bond distance of 2.413 Å.<sup>18-21</sup>

### 3.2.3. Solution studies of Co(II)-disulfide and Co(III)-thiolate compounds

Addition of 8-quinolinol together with triethylamine into solutions of the disulfide compounds [1ss] or [2ss] results in an immediate color change from purple to dark brown. The UV-visible spectrum of [1ss] in acetonitrile (**Figure 3.2.a**, solid blue line) is in accordance with the literature,<sup>8</sup> and matches the simulated spectrum (details are provided in the Experimental Section) (**Figure 3.2.a**, dashed blue line). The spectrum of [2ss] (**Figure 3.2.b**, solid blue line) is red-shifted compared to that of [1ss]. The two peaks in the spectrum of [2ss] are located at 545 nm ( $1.5 \times 10^3 \text{ M}^{-1} \text{ cm}^{-1}$ ) and 652 nm ( $8.5 \times 10^2 \text{ M}^{-1} \text{ cm}^{-1}$ ), and are ascribed to Co(II) *d-d* transitions reflecting a trigonal-bipyramidal geometry.<sup>22, 23</sup> Another Co(II) *d-d* transition is also visible at around 850–900 nm ( $\epsilon < 100 \text{ M}^{-1} \text{ cm}^{-1}$ ). The simulated spectrum of [2ss] (**Figure 3.2.b**, dashed blue line) has a reasonable match with the experimental spectrum, as the main features of the experimental spectrum are present.

The UV-visible spectra of dark brown solutions of [1s]Cl (**Figure 3.2.a**, black line) and [2s]Cl (**Figure 3.2.b**, black line) show peaks at 412 nm ( $\epsilon = 2.1 \times 10^4 \text{ M}^{-1} \text{ cm}^{-1}$ ) and 424 nm

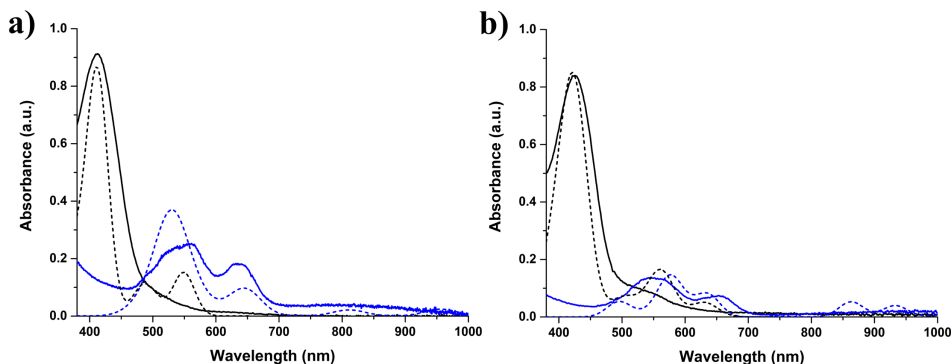


**Figure 3.2.** UV-visible spectra of **a)** 2 mM solution of [1ss] (solid blue line) and 1 mM solution of [1s]Cl (solid black line) in acetonitrile and **b)** 2.5 mM solution of [2ss] (solid blue line) and 1 mM solution of [2s]Cl (solid black line) in acetonitrile. Simulated spectra of the respective compounds are provided as dashed lines; the wavelength of the simulated spectra has been adjusted for clarity. UV-visible spectra were recorded using a transmission dip probe with path length of 0.14 mm. Simulated spectra were generated using TDDFT calculations.

( $\epsilon = 2.0 \times 10^4 \text{ M}^{-1} \text{ cm}^{-1}$ ), respectively, ascribed to a ligand-to-metal charge transfer transition (LMCT), most likely originating from the thiolate sulfur or quin<sup>−</sup> nitrogen donor.<sup>14, 24</sup> The simulated spectra of [1s]Cl (**Figure 3.2.a**, dashed black line) and [2s]Cl (**Figure 3.2.b**, dashed black line) confirm that both absorptions indeed originate from LMCT transitions.

#### 3.2.4. Computational studies

In Chapter 2, we discussed the role of the ligand-field strength of the additional ligand in the redox conversion of the Co(II)-disulfide complex with the LSSL ligand scaffold.<sup>11</sup> In order to further validate the previous findings, we investigated the ligand-field strength of quin<sup>−</sup> using DFT to estimate the *d*-orbital splitting energies of the Co(III)-thiolate complexes. The structures of the cationic compounds [1s]<sup>+</sup> and [2s]<sup>+</sup> were optimized in low-spin singlet states (*S*=0). In addition, we were interested to investigate the influence of ligand orientation on the stability of the cobalt(III)-thiolate complex, as the conformation of the LS ligand scaffold has been shown to affect how the sulfur atom approaches the cobalt center. Therefore, geometry optimizations were also done for both cationic compounds in which the orientation of quin<sup>−</sup> is reversed, so that the nitrogen donor atom is *trans* to the thiolate sulfur, and the oxygen atom *trans* to the tertiary amine nitrogen ([1s,rev]<sup>+</sup> and [2s,rev]<sup>+</sup>). The equilibrium geometries in the gas phase for [1s]<sup>+</sup> and [1s,rev]<sup>+</sup> with selected bond distances are depicted in **Figure 3.3**. Equilibrium geometries for [2s]<sup>+</sup> and [2s,rev]<sup>+</sup> in the gas phase are provided in Figure AII.17.

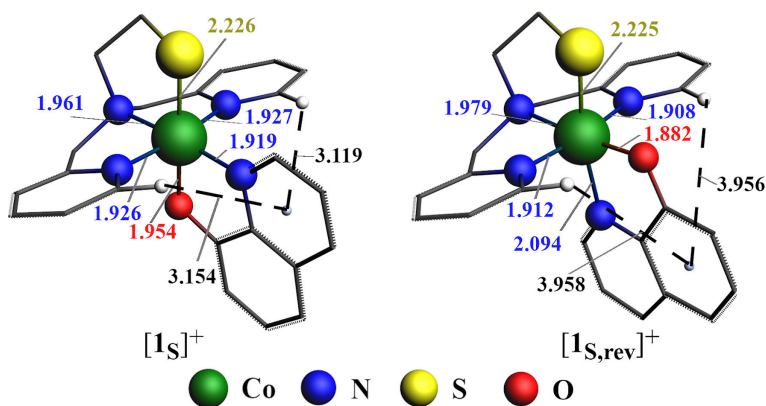


**Figure 3.3.** Equilibrium geometries of  $[1s]^+$  and  $[1s,rev]^+$  in gas phase with selected bond distances (in Å). Hydrogen atoms are omitted for clarity, except for hydrogen atoms of  $[Co(L^1S)]^{2+}$  facing  $quin^-$  ligand. The closest distances between the *ortho*-hydrogen atoms of the pyridine groups and the center of the nearest  $quin^-$  ring are depicted as dashed lines.

The cationic compounds  $[1s]^+$  and  $[2s]^+$  in methanol are about 5 to 6 kcal/mol more stable than  $[1s,rev]^+$  and  $[2s,rev]^+$ , in agreement with the experimental results. The same trend in stability is observed in gas phase. That is, without solvent  $[1s]^+$  and  $[2s]^+$  are about 7 to 9 kcal/mol more stable than  $[1s,rev]^+$  and  $[2s,rev]^+$ . Thus, the preference in orientation of  $quin^-$  is not determined by the media. The gas phase equilibrium geometries of  $[1s]^+$  and  $[2s]^+$  are in good agreement with the geometries found in the crystal structures. The Co-S bond distances in the optimized structures of  $[1s]^+$  or  $[2s]^+$  are 2.225–2.226 Å, and the Co-O and Co-N bond distances are all within error range of those found in the crystal structures.

Attempts were undertaken to estimate *d*-orbital splitting energies of both  $[1s]^+$  and  $[2s]^+$  using the DFT method described in Chapter 2.<sup>11</sup> Similar to the results described in Chapter 2, for both  $[1s]^+$  and  $[2s]^+$ , five non-degenerate molecular orbitals were found with large Co *d*-orbital contributions (Figures AII.18 and AII.19). These five non-degenerate molecular orbitals are distributed in two sets of energy levels roughly corresponding to the expected  $t_{2g}$  and  $e_g$  levels for octahedral ligand-field splitting. The energy difference between the highest and the lowest of these MO levels of  $[1s]^+$  and  $[2s]^+$  are slightly larger (by 0.2 eV) than that of  $[Co(L^1S)(bpy)]^{2+}_{mer}$ , indicative of a larger ligand-field strength of  $quin^-$  compared to bpy. The energy difference of  $[2s]^+$ 's MO sets in a quantitative level is 3.07 eV, which is only slightly smaller than that of  $[1s]^+$  (3.10 eV), indicating weaker ligand-field strength of the

ligand  $L^2SSL^2$  compared to that of  $L^1SSL^1$ . However, care should be taken with such quantitative comparisons, as the five orbitals in the MO sets comprises not only large contributions of the Co  $d$ -orbitals, but also of the donor atoms of the ligands.

In order to explain the stability of  $[1s]^+$  compared to  $[1s_{rev}]^+$ , and analogously of  $[2s]^+$  compared to  $[2s_{rev}]^+$ , we investigated the  $[Co(L^1S)]^{2+} \cdots [quin]^-$  bond formation using activation-strain analysis (see section 3.5.3 for details).<sup>25, 26</sup> We observed that  $\Delta E_{strain}$  (that is the energy to deform) of both  $[1s]^+$  and  $[1s_{rev}]^+$  are very similar (with 0.8 kcal/mol difference), and therefore does not cause the stabilization of  $[1s]^+$  over  $[1s_{rev}]^+$  (see **Table 3.4**). Instead, the interaction energy  $\Delta E_{int}$  of  $[1s]^+$  is more stabilizing by 8.2 kcal/mol than that of  $[1s_{rev}]^+$ . Thus, the interaction between the two fragments  $[Co(L^1S)]^{2+}$  and  $[quin]^-$  defines the stabilization of  $[1s]^+$  over  $[1s_{rev}]^+$ .

Next, we decomposed  $\Delta E_{int}$  into Pauli repulsion energy ( $\Delta E_{Pauli}$ ), electrostatic interaction energy ( $\Delta V_{elstat}$ ), and orbital interaction energy ( $\Delta E_{oi}$ ), using energy-decomposition analysis (see section 3.5.3).<sup>26, 27</sup> The molecular-orbital diagram for the bonding interaction between  $[Co(L^1S)]^{2+}$  and  $[quin]^-$  is provided in Figures AII.20–AII.21. It is apparent from **Table 3.4** that the electrostatic interaction  $\Delta V_{elstat}$  plays the most important role in stabilizing  $[1s]^+$  over  $[1s_{rev}]^+$ , as  $\Delta V_{elstat}$  is about 21 kcal/mol lower for  $[1s]^+$  than for  $[1s_{rev}]^+$ .

The molecular electrostatic potential of both  $[Co(L^1S)]^{2+}$  and  $[quin]^-$  fragments in  $[1s]^+$  and  $[1s_{rev}]^+$  are shown in **Figure 3.4**. It was found that in both  $[1s]^+$  and  $[1s_{rev}]^+$  the positive charges are evenly spread out over the  $[Co(L^1S)]^{2+}$  fragment. In  $[quin]^-$  both the nitrogen and the oxygen atom are more negatively charged but the negative charge is delocalized over the carbon atoms of the aromatic rings. Therefore, the attraction between  $[Co(L^1S)]^{2+}$  and  $[quin]^-$  fragments is not only determined by the electrostatic interaction between the neighboring

**Table 3.4.** Energy terms derived from energy-decomposition analysis of  $[1s]^+$  and  $[1s_{rev}]^+$ .

	Energy (kcal/mol)	
	$[1s]^+$	$[1s_{rev}]^+$
$\Delta E_{bond, methanol}$	-61.7	-55.7
$\Delta E_{bond}$	-238.5	-229.6
$\Delta E_{strain}$	12.4	13.2
$\Delta E_{int}$	-251.0	-242.8
$\Delta V_{elstat}$	-290.2	-269.1
$\Delta E_{Pauli}$	183.6	159.8
$\Delta E_{oi}$	-144.4	-133.4



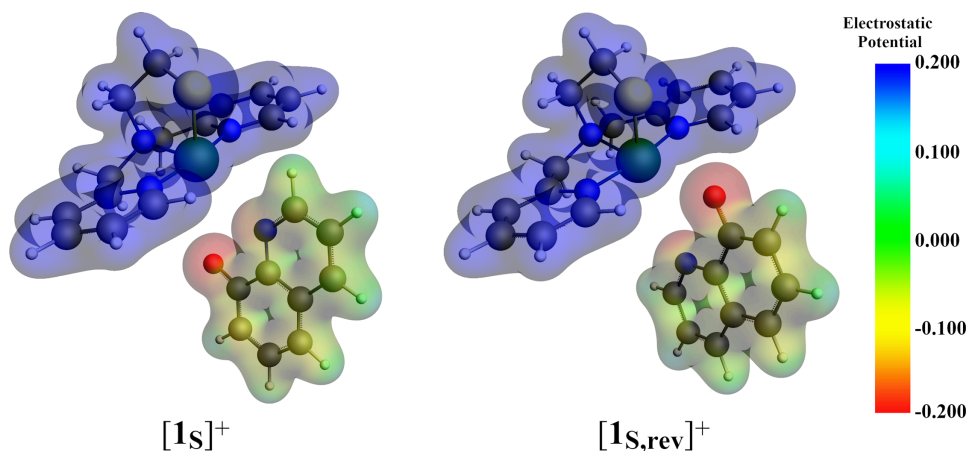


**Figure 3.4.** Electrostatic potential of  $[\text{Co}(\text{L}^1\text{S})]^{2+}$  and  $[\text{quin}]^-$  fragments in  $[\mathbf{1s}]^+$  and  $[\mathbf{1s,rev}]^+$ .

atoms but has a significant contribution from long-range interactions between the  $[\text{Co}(\text{L}^1\text{S})]^{2+}$  and  $[\text{quin}]^-$  fragments. This is demonstrated by the distances of the *ortho*-hydrogen atoms of the pyridine rings to the aromatic ring in the  $\text{quin}^-$  ligand (**Figure 3.3**) which are shorter in  $[\mathbf{1s}]^+$  (3.154 Å and 3.119 Å) than in  $[\mathbf{1s,rev}]^+$  (3.958 Å and 3.956 Å).

### 3.3. Discussion

We try to gain understanding of the influence of the ligand-field strength of the additional ligands on the redox-conversion of cobalt(II) disulfide compounds based on our LSSL scaffold. In Chapter 2 we described our study using the external ligand 2,2'-bipyridine (bpy) in combination with the compound  $[\text{Co}_2(\text{L}^1\text{SSL}^1)(\text{X})_4]$  ( $\text{X} = \text{Cl}, \text{Br}$ ).<sup>11</sup> Unexpectedly, the reaction with bpy turned out to be rather cumbersome, and the ligand-field strength of bpy appeared to be not as large as was anticipated.<sup>11</sup> In the current study we employed a similar strategy, but now using the bidentate ligand 8-quinolinolate. In addition to having a strong ligand-field this ligand is anionic in nature, which might help stabilizing the charge of the Co(III) thiolate fragment.

Indeed, our experimental results show that the addition of  $\text{quin}^-$  to both cobalt(II)-disulfide compounds  $[\mathbf{1ss}]$  and  $[\mathbf{2ss}]$  affords their respective cobalt(III)-thiolate compounds  $[\mathbf{1s}]\text{Cl}$  and  $[\mathbf{2s}]\text{Cl}$  in a clean manner, in contrast to the reactions with bpy. The unexpected formation of single crystals of  $[\mathbf{2ss}_{\text{quin}}]$  provides valuable information about the reactivity of this compound. The crystal structure of  $[\mathbf{2ss}_{\text{quin}}]$  shows that the  $\text{L}^2\text{S}$  fragment binds with the three

nitrogen donor atoms in meridional fashion, whereas in  $[\text{Co}_2(\text{L}^1\text{SSL}^1)(\text{bpy})_2(\text{Cl}_2)](\text{BPh}_4)_2$  the nitrogen donor atoms are in a facial arrangement.<sup>11</sup> In Chapter 2, we showed that formation of the cobalt(III)-thiolate compound with bpy is hampered by the fact that several donor atoms of the chelating ligands in this ‘intermediate’ compound have to dissociate and rearrange before redox-conversion can take place. In addition, DFT calculations showed that the highest singly occupied molecular orbital (SOMO) level of the meridional isomer of the ‘intermediate’ bpy compound is more destabilized than that of facial isomer; thus it is more difficult for electron transfer to occur in the observed ‘intermediate’ with facial arrangement of the nitrogen donor atoms.<sup>11</sup> The meridional orientation of the  $\text{L}^2\text{SSL}^2$  ligand combined with the position of  $\text{quin}^-$  in the structure of  $[\mathbf{2}_{\text{SSquin}}]$  provides space for the disulfide sulfur atom to approach the cobalt(II) center for electron transfer after dissociation of the chloride ions, to ultimately form the cobalt(III)-thiolate species  $[\mathbf{2}_{\text{s}}]^+$ . Thus, the meridional orientation of the ligand  $\text{L}^2\text{SSL}^2$  (and  $\text{L}^1\text{SSL}^1$ ) might be the reason for the more facile conversion of the Co(II)-disulfide to the Co(III)-thiolate compounds when using  $\text{quin}^-$  as the auxiliary ligand.

Using DFT studies, we revealed that the orientation of the asymmetric ligand  $\text{quin}^-$  has a large effect on the stability of the thiolate compounds, as the experimentally obtained  $[\mathbf{1}_{\text{s}}]^+$  is 6 kcal/mol more stable than hypothetical  $[\mathbf{1}_{\text{s,rev}}]^+$  in methanol. This difference in stability is also observed for  $[\mathbf{2}_{\text{s}}]^+$ , which is 5 kcal/mol more stable than  $[\mathbf{2}_{\text{s,rev}}]^+$ . Activation-strain and energy-decomposition analyses show that the higher stability of  $[\mathbf{1}_{\text{s}}]^+$  is caused by more favorable electrostatic interactions between the fragments  $[\text{Co}(\text{L}^1\text{S})]^{2+}$  and  $[\text{quin}]^-$  in  $[\mathbf{1}_{\text{s}}]^+$  compared to  $[\mathbf{1}_{\text{s,rev}}]^+$ . The positively charged  $[\text{Co}(\text{L}^1\text{S})]^{2+}$  fragment and the negatively charged  $[\text{quin}]^-$  fragment are closer in  $[\mathbf{1}_{\text{s}}]^+$  than in  $[\mathbf{1}_{\text{s,rev}}]^+$ , causing stronger electrostatic interactions in  $[\mathbf{1}_{\text{s}}]^+$ .

The ligand  $\text{L}^1\text{SSL}^1$  has been studied extensively for potential redox-conversion reactions using copper(I), cobalt(II), and iron(II) salts, which were successful for copper and cobalt, but not for iron.<sup>4, 8-10, 12, 28</sup> It has been reported that the methylated ligand  $\text{L}^2\text{SSL}^2$  in combination with a copper(I) salt in dichloromethane results in the formation of the corresponding Cu(II) thiolate complex,<sup>9</sup> whereas so far we were unsuccessful to trigger redox-conversion with cobalt(II) salts.<sup>10</sup> The introduction of two methyl groups in the ligand  $\text{L}^2\text{SSL}^2$  has been shown to result in longer Co–N distances,<sup>9, 10, 12</sup> indicating a decrease of the donor ability of the pyridine nitrogen atom, resulting in lower ligand-field strength, thus

decreasing the chances of redox-conversion of its cobalt(II)-disulfide compound to the corresponding cobalt(III)-thiolate complex.<sup>10</sup> The red-shifts of about 10 nm in the UV-visible spectra of [2<sub>ss</sub>] or [2<sub>s</sub>]Cl compared to [1<sub>ss</sub>] or [1<sub>s</sub>]Cl, respectively, indicate that indeed the ligand L<sup>2</sup>SSL<sup>2</sup> has a lower ligand-field strength than L<sup>1</sup>SSL<sup>1</sup>. Our DFT studies further confirm our experimental observations: the smaller energy difference of the highest and lowest MO in the set of orbitals with large cobalt *d*-orbital contribution of [2<sub>s</sub>]<sup>+</sup> compared to that of [1<sub>s</sub>]<sup>+</sup> is in agreement with the ligand-field strength of L<sup>2</sup>SSL<sup>2</sup> being smaller than that of L<sup>1</sup>SSL<sup>1</sup>. Nevertheless, we now have shown that the conversion of the cobalt(II)-disulfide complex of L<sup>2</sup>SSL<sup>2</sup> into cobalt(III)-thiolate compound [2<sub>s</sub>]Cl can be achieved using an external ligand with large ligand-field strength, compensating for the lower ligand-field strength of L<sup>2</sup>SSL<sup>2</sup>.

### 3.4. Conclusion

The cobalt(III)-thiolate complexes [1<sub>s</sub>]Cl and [2<sub>s</sub>]Cl can be formed from a reaction of cobalt(II)-disulfide compound [1<sub>ss</sub>] and [2<sub>ss</sub>] in with the anionic bidentate ligand 8-quinolinolate. Clean conversion was achieved of the disulfide compounds to their respective thiolate compounds in high yields. Our experimental results in combination with DFT calculations show that despite the lower ligand-field strength of the ligand L<sup>2</sup>SSL<sup>2</sup>, conversion of the cobalt(II)-disulfide complex of L<sup>2</sup>SSL<sup>2</sup> to the corresponding cobalt(III)-thiolate complex can be achieved with a strong-field ligand such as 8-quinolinolate. It appeared that the orientation of the asymmetric quin<sup>−</sup> ligand in the thiolate complexes is critical to their stability. The Co(III)-thiolate complexes benefits from more stabilizing electrostatic interactions when the oxygen donor of quin<sup>−</sup> is located *trans* to the thiolate donor. Overall, this study suggests that the redox-conversion of Co(II)-disulfide compounds to Co(III)-thiolate complexes is affected largely by the ligand-field strength of both the disulfide ligand and the additional ligand. However, important parameters to be considered also comprise the charge of the added ligand and the electronic effects caused by its orientation of the auxiliary ligand. Further research will be directed to assess the magnitude of these effects using various ligand systems, and to further expand the investigations with different transition metal ions.

### 3.5. Experimental Section

#### 3.5.1. General

All reagents were purchased from commercial sources and were used as received unless noted otherwise. Degassed solvents used were obtained using the freeze-pump-thaw method followed by drying the solvents using the appropriate size of activated molecular sieves. The ligands  $L^1SSL^1$ ,  $L^2SSL^2$ , and the cobalt compound  $[Co_2(L^1SSL^1)Cl_4]$  [**1ss**] were prepared according to previously published procedures.<sup>8, 12</sup> The ligand  $L^2SSL^2$  was purified similarly to the ligand  $L^1SSL^1$ , by refluxing in petroleum ether followed by cooling instead of using column chromatography as reported. The synthesis of the cobalt compounds was performed using standard Schlenk-line techniques under an argon atmosphere.  $^1H$  NMR spectra were recorded on a Bruker 300 DPX spectrometer at room temperature. Mass spectra were recorded on a Thermo Scientific MSQ Plus and Shimadzu LCMS 2020 mass spectrometer with electrospray ionization (ESI) method. Formic acid was added to the eluting solvent with the final concentration of 1% (v/v). Simulated mass spectra were generated using mMass (version 5.5.0) software.<sup>29</sup> IR spectra were obtained using a PerkinElmer Spectrum Two System equipped with Universal ATR module containing diamond crystal for single reflection (scan range 400-4000  $cm^{-1}$ , resolution 4  $cm^{-1}$ ). Magnetic susceptibility measurements were performed on a Sherwood Scientific Magnetic Susceptibility Balance MK1, and the magnetic moments were calculated according to the literature.<sup>30</sup> Bond distances and angles analysis of the crystal structures were performed using the Mogul module on Mercury (version 4.3.1) software.<sup>31</sup> UV-visible spectra were collected using a transmission dip probe with variable path lengths and a reflection probe on an Avantes AvaSpec-2048 spectrometer and using an Avalight-DH-S-Bal light source. Elemental analyses were performed by the Microanalytical Laboratory Kolbe in Germany.

#### 3.5.2. Single crystal X-ray crystallography

All reflection intensities were measured at 110(2) K using a SuperNova diffractometer (equipped with Atlas detector) with Mo  $K\alpha$  radiation ( $\lambda = 0.71073$  Å) under the program CrysAlisPro (Version CrysAlisPro 1.171.39.29c, Rigaku OD, 2017). The same program was used to refine the cell dimensions and for data reduction. The structure was solved with the program SHELXS-2018/3 and was refined on  $F^2$  with SHELXL-2018/3.<sup>32</sup> Numerical absorption correction based on Gaussian integration over a multifaceted crystal model was

applied using CrysAlisPro. The temperature of the data collection was controlled using the system Cryojet (manufactured by Oxford Instruments). The H atoms were placed at calculated positions using the instructions AFIX 23, AFIX 43 or AFIX 137 with isotropic displacement parameters having values 1.2 or 1.5  $U_{eq}$  of the attached C atoms. The structure of compound [1s]Cl is ordered. The structure of [2ss<sub>quin</sub>] is partly disordered. The asymmetric unit also contains one partially occupied ordered lattice MeCN solvent molecule (occupancy factor: 0.903(7)) and some amount of significantly disordered lattice molecules (MeCN). The structure of [2s-Ag-2s](SbF<sub>6</sub>)<sub>3</sub> is significantly disordered (the Cobalt complex and three SbF<sub>6</sub><sup>-</sup> counterions are mostly disordered). The asymmetric unit also contains one ordered lattice acetonitrile solvent molecule, and some amount of very disordered (and possibly partially occupied) lattice solvent molecules. The contributions of the disordered moiety were removed from the final refinement using the SQUEEZE procedure in Platon.<sup>33, 34</sup>

### 3.5.3. Computational methods

All calculations were performed with the Amsterdam Density Functional (ADF) program version 2017.103 using Zeroth Order Regular Approximation (ZORA) scalar relativistic effect at OPBE functional and TZP basis set for geometry optimizations and energies.<sup>35-38</sup> Solvation of the molecule was simulated using the conductor-like screening model (COSMO) in methanol.<sup>39</sup> The stationary points were checked to be minima at potential energy surface using vibrational analysis. All the compounds were calculated with  $S=0$ , in agreement with our previous study. Time-Dependent Density Functional Theory (TDDFT) calculations for the simulation of the UV-visible spectra were done using Davidson's procedure with ZORA scalar relativistic effect and conductor-like screening model (COSMO) in acetonitrile.<sup>40</sup> The calculations were done for the lowest 10 excitations of the Co(III)-thiolate compounds and lowest 30 excitations of the Co(II)-disulfide compounds. The simulated spectra have been adjusted for clearer comparison with the experimental data, the spectra were red-shifted for [1ss] (22 nm) and [2ss] (20 nm) and blue-shifted for [1s]<sup>+</sup> (66 nm) and [2s]<sup>+</sup> (60 nm). Kohn-Sham molecular orbital (KS-MO) analysis for the determination of *d*-orbital splitting energies of the complex was done according to the published procedure on the optimized geometries of [1s]<sup>+</sup> and [2s]<sup>+</sup> in the gas phase.<sup>11</sup>

The bond energy ( $\Delta E_{\text{bond}}$ ) is given by Equation 3.1 and can be decomposed into the strain energy ( $\Delta E_{\text{strain}}$ ) and interaction energy ( $\Delta E_{\text{int}}$ ) (Equation 3.2). The strain energy is the energy needed to deform the fragments from their equilibrium geometries to their actual geometry in the complex. The interaction energy corresponds to the energy change when the deformed fragments are interacting with each other in the complex and can be further decomposed into electrostatic interaction energy ( $\Delta V_{\text{elstat}}$ ), Pauli repulsion energy ( $\Delta E_{\text{Pauli}}$ ), and orbital interaction energy ( $\Delta E_{\text{oi}}$ ) using energy-decomposition analysis (EDA, Equation 3.3).  $\Delta V_{\text{elstat}}$  represents the Coulomb interaction between the unperturbed charge distributions of the two deformed fragments, which is usually an attractive interaction.  $\Delta E_{\text{Pauli}}$  comprises of the destabilization energy associated with the interaction between occupied orbitals which is responsible for steric repulsion. The stabilizing  $\Delta E_{\text{oi}}$  accounts for the charge-transfer, donor-acceptor interactions, and polarization.

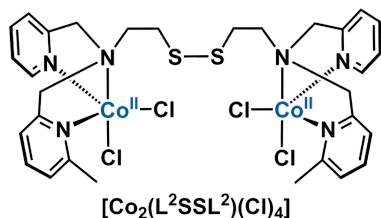
$$\Delta E_{\text{bond}} = E_{\text{optimized complex}} - E_{\text{optimized [Co(L}^1\text{S)]}^{2+}} - E_{\text{optimized [quin]}^-} \text{ Equation 3.1.}$$

$$\Delta E_{\text{bond}} = \Delta E_{\text{strain}} + \Delta E_{\text{int}} \quad \text{Equation 3.2.}$$

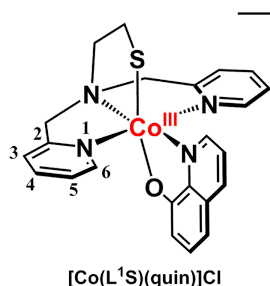
$$\Delta E_{\text{int}} = \Delta V_{\text{elstat}} + \Delta E_{\text{Pauli}} + \Delta E_{\text{oi}} \quad \text{Equation 3.3.}$$

#### 3.5.4. Synthesis of the compounds

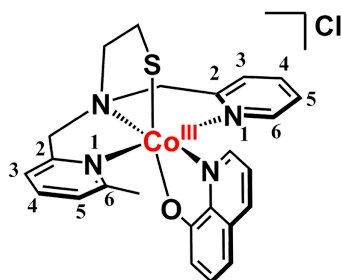
##### [Co<sub>2</sub>(L<sup>2</sup>SSL<sup>2</sup>)(Cl)<sub>4</sub>] ([2ss])



The compound was prepared similarly to compound [1ss],<sup>8</sup> using ligand L<sup>2</sup>SSL<sup>2</sup> instead of L<sup>1</sup>SSL<sup>1</sup>. An intense purple powder was obtained in 72% yield. IR (neat, cm<sup>-1</sup>): 3066w, 2924w, 1668w, 1605s, 1574m, 1442s, 1381m, 1364m, 1298w, 1225w, 1159m, 1090m, 1053m, 1017s, 960m, 860m, 765vs, 730m, 646m, 562w, 536w, 521w, 500w, 417m. UV-Visible spectra in acetonitrile: 545 nm ( $\epsilon = 1.5 \times 10^3 \text{ M}^{-1} \text{ cm}^{-1}$ ), 652 nm ( $\epsilon = 8.5 \times 10^2 \text{ M}^{-1} \text{ cm}^{-1}$ ), 850–950 nm ( $\epsilon < 100 \text{ M}^{-1} \text{ cm}^{-1}$ ). ESI-MS found (calcd.) for [2ss – 4Cl<sup>-</sup> + 2HCOO<sup>-</sup>]<sup>2+</sup> *m/z* 376.2 (376.04) and for [2ss – 2Cl<sup>-</sup> + HCOO<sup>-</sup>]<sup>+</sup> *m/z* 777.1 (777.05). Elemental analysis (%) for compound [2ss] (C<sub>30</sub>H<sub>36</sub>Cl<sub>4</sub>Co<sub>2</sub>N<sub>6</sub>S<sub>2</sub>), calcd. C, 44.79; H, 4.51; N, 10.45; found C, 44.72; H, 4.49; N, 10.43.

**[Co(L<sup>1</sup>S)(8-quinolinolate)]Cl ([1s]Cl)**

The ligand L<sup>1</sup>SSL<sup>1</sup> (52.35 mg, 0.101 mmol) was dissolved in 4 mL dry and deoxygenated methanol. Into the solution of the ligand, anhydrous CoCl<sub>2</sub> (26.25 mg, 0.202 mmol, 2 equiv. to the L<sup>1</sup>SSL<sup>1</sup>) was added. The resulting purple solution was stirred for 1 hour. In a separate flask under argon, 8-quinolinol (45.12 mg, 0.311 mmol) was added along with 44  $\mu$ L of triethylamine (0.316 mmol, 1 equiv. to 8-quinolinol). Dry and deoxygenated methanol (1 mL) was added to dissolve the 8-quinolinol and triethylamine. From this solution, 680  $\mu$ L (=0.202 mmol of 8-quinolinol, 2 equiv. to L<sup>1</sup>SSL<sup>1</sup>) was transferred to the purple solution of [Co<sub>2</sub>(L<sup>1</sup>SSL<sup>1</sup>)Cl<sub>4</sub>]. The color of the solution quickly changed into brown and the solution was stirred for 2 hours. The solution was further concentrated until approximately 1 mL was left in the flask. Into the flask, 10 mL dry and deoxygenated diethyl ether was added, resulting in the formation of a brown precipitate. The precipitate was then washed twice with 10 mL dry and deoxygenated diethyl ether, filtered, and then dried in vacuo. Yield: 96 mg, 0.193 mmol, 96%. Dark brown single crystals of compound [1s]Cl were grown after 2 days using vapor diffusion of dry and deoxygenated diethyl ether into a solution of [1s]Cl in a 1:1 mixture of dry and deoxygenated acetonitrile and methanol. IR (neat, cm<sup>-1</sup>): 2945w, 2602m, 2496m, 1608w, 1570m, 1497s, 1461s, 1444m, 1397m, 1376s, 1321s, 1284m, 1223w, 1172m, 1111m, 1036m, 905w, 851w, 819m, 775m, 748s, 719w, 626m, 516s, 462m, 448m, 424m. ESI-MS calcd. for [1s]<sup>+</sup> *m/z* 461.08, found *m/z* 461.1. <sup>1</sup>H-NMR (300 MHz, CD<sub>3</sub>CN, RT)  $\delta$ (ppm): 1.29–1.33 (t, triethylamine.HCl), 1.84–1.87 (t, 2 H, N-CH<sub>2</sub>-CH<sub>2</sub>-S), 3.01–3.08 (q, triethylamine.HCl), 3.34–3.38 (t, 2H, N-CH<sub>2</sub>-CH<sub>2</sub>-S), 4.57–4.62 and 5.45–5.50 (d, 4H, py-CH<sub>2</sub>-N), 6.87–6.90 (dd, 1H, ortho-CH-O(quin<sup>-</sup>)), 7.06–7.09 (dd, 1H, para-CH-O(quin<sup>-</sup>)), 7.13–7.17 (t, 2H, 2H<sub>4</sub>(py)), 7.25–7.27 (dd, 2H, 2H<sub>3</sub>(py)), 7.37–7.42 (t, 1H, meta-CH-O(quin<sup>-</sup>)), 7.46–7.48 (d, 2H, 2H<sub>6</sub>(py)), 7.85–7.88 (3H, m, meta-CH-N(quin<sup>-</sup>) and 2H<sub>5</sub>(py)), 8.50–8.53 (dd, 1H, para-CH-N(quin<sup>-</sup>)), 9.04–9.06 (dd, 1H, ortho-CH-N(quin<sup>-</sup>)). Elemental analysis (%) for compound [1s]Cl·1.5 H<sub>2</sub>O (C<sub>23</sub>H<sub>22</sub>ClCoN<sub>4</sub>OS·1.5 H<sub>2</sub>O), calcd. C, 52.73; H, 4.81; N, 10.69; found C, 52.86; H, 4.67; N, 10.58.

**[Co(L<sup>2</sup>S)(8-quinolinolate)]Cl ([2s]Cl)****[Co(L<sup>2</sup>S)(quin)]Cl**

Compound [2s]Cl was obtained using a similar procedure as for compound [1s]Cl but using L<sup>2</sup>SSL<sup>2</sup> instead of L<sup>1</sup>SSL<sup>1</sup>. Yield: 102 mg, 0.2 mmol, 99%. Dark brown single crystals of compound [2s-Ag-2s](SbF<sub>6</sub>)<sub>3</sub> were grown after two days using vapor diffusion of diethyl ether into an acetonitrile solution containing [2s]Cl and one equivalent of AgSbF<sub>6</sub>. IR (neat, cm<sup>-1</sup>): 3391br, 2978w, 2603w, 2497w, 1608w, 1568m, 1497s, 1462s, 1447m, 1381s, 1322s, 1289w, 1225w, 1173w, 1111m, 1067w, 1037m, 960w, 902w, 830m, 807m, 776m, 748s, 726w, 650m, 624m, 517s, 462w, 436w, 413w. ESI-MS calcd. for [2s]<sup>+</sup> *m/z* 475.1, found *m/z* 475.3. <sup>1</sup>H-NMR (300 MHz, CD<sub>3</sub>CN, RT): 1.26–1.31 (t, triethylamine.HCl), 1.78 (s, 3H, py-CH<sub>3</sub>), 2.98–3.05 (q, triethylamine.HCl), 3.18–3.50 (m, 2H, N-CH<sub>2</sub>-CH<sub>2</sub>-S and N-CH<sub>2</sub>-CH<sub>2</sub>-S, the other two protons overlaps with the solvent peaks at around 1.9 ppm), 4.50–4.62, 5.43–5.48, and 5.75–5.80 (d, d, t, 4H, N-CH<sub>2</sub>-py and N-CH<sub>2</sub>-pyMe), 6.89–6.92 (d, 1H, ortho-CH-O(quin<sup>-</sup>)), 6.92–6.95 (dd, 1H, H<sub>5</sub>(pyMe)), 7.01–7.07 (td, 2H, 2H<sub>3</sub>(py and pyMe)), 7.08–7.12 (t, 1H, para-CH-N(quin<sup>-</sup>)), 7.27–7.29 (d, 1H, para-CH-O(quin<sup>-</sup>)), 7.36–7.41 (t, 2H, meta-CH-N(quin<sup>-</sup>) and meta-CH-O(quin<sup>-</sup>)), 7.66–7.72 (t, 1H, H<sub>5</sub>(py)), 7.75–7.82 (m, 2H, 2H<sub>4</sub>(py and pyMe)), 8.47–8.50 (dd, 1H, H<sub>6</sub>(py)), 9.26–9.29 (dd, 1H, ortho-CH-N(quin<sup>-</sup>)). Elemental analysis (%) for compound [2s]Cl·H<sub>2</sub>O (C<sub>24</sub>H<sub>25</sub>ClCoN<sub>4</sub>OS·H<sub>2</sub>O), calcd. C, 54.50; H, 4.95; N, 10.59; found C, 54.26; H, 4.79; N, 10.49.

**3.6. References**

1. Martin, D. R. and Matyushov, D. V. *Sci. Rep.* **2017**, 7, 1-11.
2. Li, Y., Park, J.-S., Deng, J.-H. and Bai, Y. *J. Bioenerg. Biomembr.* **2006**, 38 (5-6), 283-291.
3. Riebe, O., Fischer, R. J., Wampler, D. A., Kurtz, D. M. and Bahl, H. *Microbiology (Reading)* **2009**, 155 (Pt 1), 16-24.
4. Ueno, Y., Tachi, Y. and Itoh, S. *J. Am. Chem. Soc.* **2002**, 124 (42), 12428-12429.
5. Gennari, M., Brazzolotto, D., Yu, S., Pecaut, J., Philouze, C., Rouzies, M., Clerac, R., Orio, M. and Duboc, C. *Chem. Eur. J.* **2015**, 21 (51), 18770-18778.
6. Gennari, M., Gerey, B., Hall, N., Pecaut, J., Collomb, M.-N., Rouzies, M., Clerac, R., Orio, M. and Duboc, C. *Angew. Chem. Int. Ed.* **2014**, 53 (21), 5318-5321.
7. Wang, L., Reinhard, F. G. C., Philouze, C., Demeshko, S., de Visser, S. P., Meyer, F., Gennari, M. and Duboc, C. *Chem. Eur. J.* **2018**, 24 (46), 11973-11982.
8. Jiang, F., Siegler, M. A., Sun, X., Jiang, L., Fonseca Guerra, C. and Bouwman, E. *Inorg. Chem.* **2018**, 57 (15), 8796-8805.



9. Ording-Wenker, E. C. M., van der Plas, M., Siegler, M. A., Bonnet, S., Bickelhaupt, F. M., Fonseca Guerra, C. and Bouwman, E. *Inorg. Chem.* **2014**, 53 (16), 8494-8504.
10. Jiang, F., Marvelous, C., Verschuur, A. C., Siegler, M. A., Teat, S. J. and Bouwman, E. *Inorg. Chim. Acta* **2022**, 120880.
11. Marvelous, C., de Azevedo Santos, L., Siegler, M. A., Fonseca Guerra, C. and Bouwman, E. *Dalton Trans.* **2022**, 51, 8046-8055.
12. Itoh, S., Nagagawa, M. and Fukuzumi, S. *J. Am. Chem. Soc.* **2001**, 123 (17), 4087-4088.
13. Franz, K. J., Doerr, L. H., Spingler, B. and Lippard, S. J. *Inorg. Chem.* **2001**, 40 (15), 3774-3780.
14. Dey, S., Todorova, T. K., Fontecave, M. and Mougél, V. *Angew. Chem. Int. Ed.* **2020**, 59 (36), 15726-15733.
15. Lonnon, D. G., Craig, D. C. and Colbran, S. B. *Inorg. Chem. Commun.* **2003**, 6 (11), 1351-1353.
16. Zhu, C.-Y., Zhang, Y.-Q., Liao, R.-Z., Xia, W., Hu, J.-C., Wu, J., Liu, H. and Wang, F. *Dalton Trans.* **2018**, 47 (37), 13142-13150.
17. Janiak, C. *J. Chem. Soc., Dalton Trans.* **2000**, (21), 3885-3896.
18. Konno, T., Kawamoto, T., Kuwabara, R., Yoshimura, T. and Hirotsu, M. *Chem. Lett.* **2002**, (3), 304-305.
19. Tamura, M., Yoshinari, N., Igashira-Kamiyama, A. and Konno, T. *Acta Crystallogr. Sect. E: Struct. Rep. Online* **2007**, 63, M1641-U629.
20. Yoshinari, N., Chikamoto, Y., Iwata, M., Kawamoto, T. and Konno, T. *Bull. Chem. Soc. Jpn.* **2006**, 79 (7), 1066-1068.
21. Yoshinari, N., Igashira-Kamiyama, A. and Konno, T. *Acta Crystallogr. Sect. E: Struct. Rep. Online* **2006**, 62, M1229-M1231.
22. Chan, S. L.-F., Lam, T. L., Yang, C., Lai, J., Cao, B., Zhou, Z. and Zhu, Q. *Polyhedron* **2017**, 125, 156-163.
23. Massoud, S. S., Broussard, K. T., Mautner, F. A., Vicente, R., Saha, M. K. and Bernal, I. *Inorg. Chim. Acta* **2008**, 361 (1), 123-131.
24. Pal, A. K., Li, C., Hanan, G. S. and Zysman-Colman, E. *Angew. Chem. Int. Ed.* **2018**, 57 (27), 8027-8031.
25. Bickelhaupt, F. M. and Houk, K. N. *Angew. Chem. Int. Ed.* **2017**, 56 (34), 10070-10086.
26. Vermeeren, P., Van Der Lubbe, S. C. C., Fonseca Guerra, C., Bickelhaupt, F. M. and Hamlin, T. A. *Nature Protocols* **2020**, 15 (2), 649-667.
27. Bickelhaupt, F. M. and Baerends, E. J., *Reviews in Computational Chemistry: Reviews in Computational Chemistry, Vol 15*, **2000**, Vol. 15, 1-86.
28. Jiang, F., Siegler, M. A. and Bouwman, E. *Inorg. Chem. Commun.* **2018**, 94, 53-56.
29. Strohm, M., mMass - Open Source Mass Spectrometry Tool. [www.mmass.org](http://www.mmass.org)
30. Bain, G. A. and Berry, J. F. *J. Chem. Educ.* **2008**, 85 (4), 532-536.
31. Macrae, C. F., Sovago, I., Cottrell, S. J., Galek, P. T. A., McCabe, P., Pidcock, E., Platings, M., Shields, G. P., Stevens, J. S., Towler, M. and Wood, P. A. *J. Appl. Crystallogr.* **2020**, 53, 226-235.
32. Sheldrick, G. M. *Acta Crystallogr. Sect. A: Found. Crystallogr.* **2008**, 64, 112-122.
33. Spek, A. L. *Acta Crystallogr. Sect. C: Cryst. Struct. Commun.* **2015**, 71 (Pt 1), 9-18.
34. Spek, A. L. *Acta Crystallogr. Sect. D: Biol. Crystallogr.* **2009**, 65 (2), 148-155.
35. ADF2017.107. SCM Theoretical Chemistry, Vrije Universiteit: Amsterdam, The Netherlands, [www.scm.com](http://www.scm.com)
36. Swart, M., Ehlers, A. W. and Lammertsma, K. *Mol. Phys.* **2004**, 102 (23-24), 2467-2474.
37. Van Lenthe, E. and Baerends, E. J. *J. Comput. Chem.* **2003**, 24 (9), 1142-1156.
38. Van Lenthe, E., Baerends, E. J. and Snijders, J. G. *J. Chem. Phys.* **1994**, 101 (11), 9783-9792.
39. Klamt, A. and Schuurmann, G. *J. Chem. Soc., Perkin Trans. 2* **1993**, (5), 799-805.
40. Rosa, A., Baerends, E. J., van Gisbergen, S. J. A., van Lenthe, E., Groeneveld, J. A. and Snijders, J. G. *J. Am. Chem. Soc.* **1999**, 121 (44), 10356-10365.

# Chapter 4

---

## Redox-conversion Reactivity of The Chalcogen Family: Selenium vs Sulfur

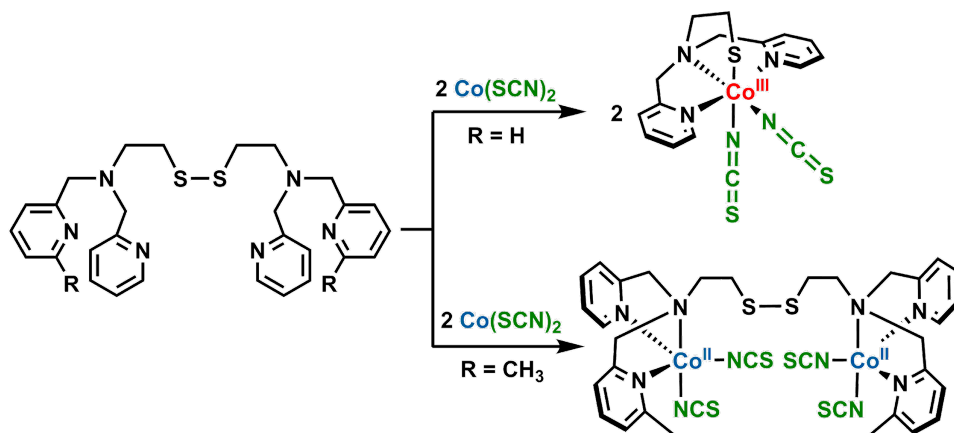
*The synthesis is described of the selenium-based ligand  $L^1\text{SeSeL}^1$  (2,2'-diselanediybis( $N,N$ -bis(pyridin-2-ylmethyl)ethan-1-amine) along with its reactivity with cobalt(II) salts. The cobalt(II)-diselenide complex  $[\text{Co}_2(\text{L}^1\text{SeSeL}^1)\text{Cl}_4]$  was obtained in good yield, and its spectroscopic properties closely resemble that of its sulfur analog. Reaction of  $\text{L}^1\text{SeSeL}^1$  with Co(II) thiocyanate results in the formation of the cobalt(III) compound  $[\text{Co}(\text{L}^1\text{Se})(\text{NCS})_2]$ , similar to reaction of  $\text{L}^1\text{SSL}^1$ . The redox-conversion reactions from the Co(II)-diselenide compound  $[\text{Co}(\text{L}^1\text{SeSeL}^1)\text{Cl}_4]$  to Co(III)-selenolate complexes  $[\text{Co}(\text{L}^1\text{Se})(\text{MeCN})_2](\text{SbF}_6)_2$  and  $[\text{Co}(\text{L}^1\text{Se})(\text{quin})]\text{Cl}$  were achieved in a good yield using external triggers such as removal of the halide ions or the addition of the strong-field ligand 8-quinolinolate. Our computational studies show that the ligand-field strength of selenium compounds is smaller than their sulfur analogs, indicating that redox-conversion of cobalt(II)-diselenide into cobalt(III)-selenolate complexes may be more arduous than for the related sulfur compounds.*

This chapter will be submitted for publication: Christian Marvelous, Maxime A. Siegler, Célia Fonseca Guerra, and Elisabeth Bouwman, *manuscript in preparation*

### 4.1. Introduction

Electron-transfer reactions frequently occur in biological systems, usually involving transition-metal ions in metalloenzymes.<sup>1-3</sup> Selenium is used in biomimetic studies as an analog for sulfur, as selenium is present in nature in the amino acid selenocysteine, often resulting in enhanced reaction rates compared to cysteine-containing enzymes.<sup>4-7</sup> The redox chemistry of selenium compounds is known to be similar to their sulfur analogues, for example the reduction of the diselenide bond into selenolate ions. Additionally, selenium compounds can participate in faster thiol/disulfide-like exchange reactions,<sup>8</sup> which is an indirect consequence of the more nucleophilic properties of these selenium compounds under neutral conditions.<sup>9</sup>

In the past decade, the redox-conversion reaction of metal-thiolate and metal-disulfide compounds has gathered a lot of interest. The study of the redox-conversion reaction of thiolate and disulfide compounds may provide mechanistic understanding on electron-transfer reactions catalyzed by metalloenzymes. Some reported examples concern the redox-conversion of copper(I)-disulfide vs copper(II)-thiolate complexes and cobalt(II)-disulfide vs cobalt(III)-thiolate complexes.<sup>10, 11</sup> The redox-conversion of cobalt(II)-disulfide to cobalt(III)-thiolate is particularly interesting for several reasons. First of all only few examples have been reported on this matter and expansion of the scope will be helpful to gain more understanding. Additionally, the reactivity of specific disulfide ligands is a point of interest as slightly different ligands may result in a different outcomes. For example, it has been reported that the ligand  $L^1SSL^1$  upon reaction with  $Co(SCN)_2$  results in formation of a cobalt(III)-thiolate complex, whereas the same reaction with the dimethylated ligand  $L^2SSL^2$  does not lead to a cobalt(III)-thiolate complex (**Scheme 4.1**).<sup>12</sup> Finally, the redox-conversion reaction mechanism seems to be different for the cobalt-based system than for the copper-based system, as sulfur is often not coordinated in the cobalt(II)-disulfide system, preventing direct electron transfer. In Chapter 2 and Chapter 3, the reactivity is described of the cobalt-based systems with both of these ligands.<sup>13, 14</sup> It was found that the ligand-field strength of the exogenous ligand affects the formation of cobalt(III)-thiolate complexes. In addition, it was found that the mechanism of the redox-conversion reaction depends on the different coordination modes of the disulfide ligand as well as the exogenous bidentate ligand.<sup>13, 14</sup>



**Scheme 4.1.** Different reactivity of ligand  $L^1SSL^1$  ( $R=H$ ) and  $L^2SSL^2$  ( $R=CH_3$ ) with  $Co(SCN)_2$ .<sup>10,11</sup>

To the best of our knowledge, the redox-conversion reaction using selenium-based ligands has not yet been reported. It is of importance to know whether the redox-conversion can also occur with selenolate/diselenide species, as it may give rise to a new perspective on the importance of selenium compared to sulfur in electron-transfer reactions in biology. Yet, the use of selenium as a replacement for sulfur in the redox-conversion reaction of  $Co(II)$ -diselenide to the corresponding  $Co(III)$ -selenolate complex may be challenging. The biggest challenge is that the diselenide bond has been reported to be more stable towards reduction than the disulfide bond,<sup>15</sup> and thus would make the redox-conversion reaction more complicated. Therefore, it is our interest to investigate the redox-conversion reaction of the selenium-based ligand  $L^1SeSeL^1$  by the reaction with different cobalt(II) salts or adjusting the ligand-field strength with use of external ligands.

## 4.2. Results

### 4.2.1. Synthesis of the compounds

The precursor of the ligand, selenocystamine dihydrochloride was obtained in 37% yield as a light yellow powder and characterized using ESI-MS and NMR (Figure AIII.1 and AIII.2). The ligand 2,2'-diselanediybis( $N,N$ -bis(pyridin-2-ylmethyl)ethan-1-amine) ( $L^1SeSeL^1$ ) was prepared via the reductive amination of selenocystamine dihydrochloride with 2-pyridinecarboxaldehyde using sodium cyanoborohydride as reducing agent (**Scheme 4.2**). The ligand  $L^1SeSeL^1$  was obtained as a pale red solid in 26% yield after recrystallization.

The ESI-MS spectrum (Figure AIII.3) shows peaks at  $m/z$  612.9 and 306.8 corresponding to the species  $[\text{L}^1\text{SeSeL}^1 + \text{H}]^+$  and  $[\text{L}^1\text{SeSeL}^1 + 2\text{H}]^{2+}$ , respectively. Both  $^1\text{H}$ -NMR spectroscopy (Figure AIII.4) and elemental analysis showed that the ligand  $\text{L}^1\text{SeSeL}^1$  was obtained analytically pure.

The reaction scheme illustrates the synthesis of cobalt(II) complexes [1] and [2] from a cobalt(III) precursor. The precursor is a cobalt(III) complex with a Se-containing ligand and two cyanide groups. It reacts with 2 equivalents of  $\text{CoCl}_2$  in the presence of  $\text{AgSbF}_6$  and acetonitrile to form the cobalt(II) complex [1], which features a Se-Se bridge and two cobalt(II) centers coordinated by cyanide and chloride ligands. Alternatively, the precursor reacts with 2 equivalents of  $\text{Co}(\text{SCN})_2$  to form the cobalt(II) complex [2], which features a Se-containing ligand and two cobalt(II) centers coordinated by cyanide and thiocyanate ligands.

70

pure by elemental analysis and its structure was further elucidated using single crystal X-ray diffraction.

The cobalt(III)-selenolate compound  $[\text{Co}(\text{L}^1\text{Se})(\text{NCS})_2]$  (**[2]**) was obtained from a reaction of the ligand  $\text{L}^1\text{SeSeL}^1$  with two equivalents of  $\text{Co}(\text{SCN})_2$ , while the compounds  $[\text{Co}(\text{L}^1\text{Se})(\text{MeCN})_2](\text{SbF}_6)_2$  (**[3]**)( $\text{SbF}_6$ )<sub>2</sub> and  $[\text{Co}(\text{L}^1\text{Se})(\text{quin})]\text{Cl}$  (**[4]**)Cl were prepared via *in situ* formation of compound **[1]** and subsequent addition of silver hexafluoroantimonate (for **[3]**)( $\text{SbF}_6$ )<sub>2</sub> or 8-quinolinol (Hquin, for **[4]**)Cl (**Scheme 4.3**). All cobalt(III)-selenolate compounds were obtained in good yields (76%, 91%, 78%, for **[2]**, **[3]**)( $\text{SbF}_6$ )<sub>2</sub>, and **[4]**)Cl, respectively), and appeared to be hygroscopic. The ESI-MS spectrum of an acetonitrile solution of **[2]** (Figure AIII.7) shows peaks at  $m/z$  464.0 and 889.0 attributed to the species  $[\text{Co}(\text{L}^1\text{Se})(\text{NCS})(\text{MeCN})]^+$  and  $[2 \times 2 - 2\text{SCN}^- + \text{HCOO}^-]^+$ , respectively. The ESI-MS spectrum of an acetonitrile solution of **[3]**)( $\text{SbF}_6$ )<sub>2</sub> (Figure AIII.8) shows peaks at  $m/z$  223.6, 410.1, 863.0, and 1054.9, corresponding to the species  $[\mathbf{3}]^{2+}$ ,  $[\mathbf{3} - 2\text{MeCN} + \text{HCOO}^-]^+$ ,  $[2 \times \mathbf{3} - 4\text{MeCN} + 3\text{HCOO}^-]^+$ , and  $[2 \times \mathbf{3} - 4\text{MeCN} + 2\text{HCOO}^- + (\text{SbF}_6)]^+$ , respectively. The ESI-MS spectrum of an acetonitrile solution of compound **[4]**)Cl (Figure AIII.9) shows a major peak at  $m/z$  509.1 which can be assigned to  $[\mathbf{4}]^+$ . All cobalt(III)-selenolate compounds were found to be diamagnetic based on  $^1\text{H}$ -NMR spectroscopy (Figure AIII.10–AIII.16) and the determination of their magnetic moments using a magnetic susceptibility balance. Elemental analysis of the cobalt(III)-selenolate compounds show that the compounds were analytically pure (further details in Experimental Section).

#### 4.2.2. Single Crystal X-Ray Crystallography

Single crystals of **[1]**, **[2]**, and **[4]**)Cl were obtained using vapor diffusion of diethyl ether into solutions of each compound (See Experimental Section). Unfortunately, single crystals of compound **[3]**)( $\text{SbF}_6$ )<sub>2</sub> could not be obtained as all crystallization attempts resulted in the formation of oils. Projections of the crystal structures are depicted in **Figure 4.1**. Full crystallographic parameters are provided in Table AIII.1. The structure of **[1]** crystallizes in the triclinic space group  $P\bar{1}$  and the asymmetric unit contains one molecule of **[1]** and one lattice diethyl ether solvent molecule. Both cobalt(II) centers are found to be in a distorted trigonal-bipyramidal geometry ( $\tau_5 = 0.72$  for Co1 and  $\tau_5 = 0.62$  for Co2,  $\tau_5 = 1$  is calculated

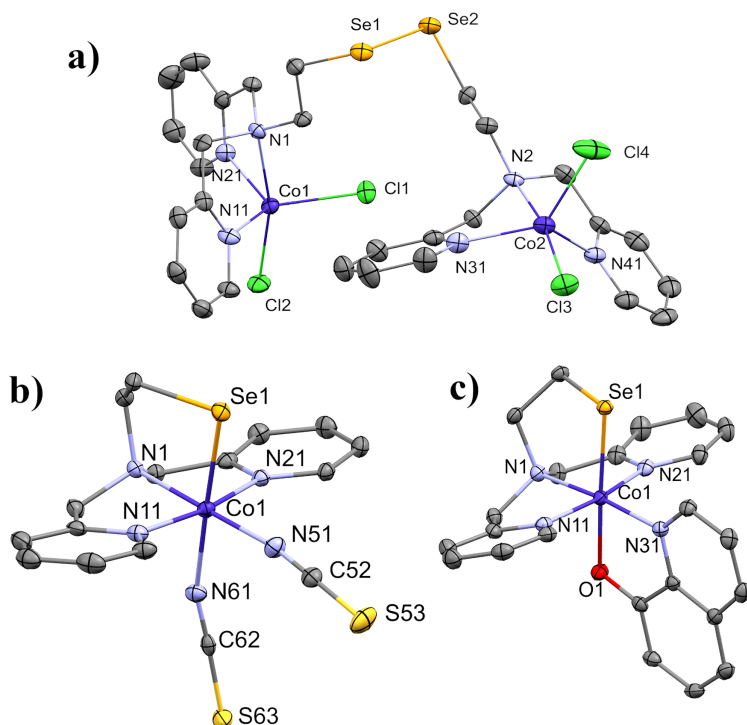


**Figure 4.1.** Displacement ellipsoid plots (50% probability level) of a)  $[\text{Co}_2(\text{L}^1\text{SeSeL}^1)\text{Cl}_4]$  ([1]), b)  $[\text{Co}(\text{L}^1\text{Se})(\text{NCS})_2]$  ([2]), and c)  $[\text{Co}(\text{L}^1\text{Se})(\text{quin})]^+$  ([4]<sup>+</sup>) at 110(2) K. Hydrogen atoms, non-coordinated anions, and lattice solvent molecules are omitted for clarity.

for a perfect trigonal-bipyramidal geometry and  $\tau_5 = 0$  for perfect square pyramidal geometry).<sup>16</sup> Each of the cobalt(II) centers is coordinated by three nitrogen atoms from the ligand  $\text{L}^1\text{SeSeL}^1$  and two chloride anions. The apical positions are occupied by one of the chloride ions and the tertiary amine nitrogen atom. The diselenide group is not coordinated to the Co metal centers, as observed with the disulfide group in the structure of the related compound  $[\text{Co}_2(\text{L}^1\text{SSL}^1)\text{Cl}_4]$ . Selected bond distances and angles are provided in **Table 4.1**. The bond distances and angles related to Co2 are similar to those of Co1. The Se1–Se2 bond distance (2.3208(7) Å) is on par with the average Se–Se bond in the reported structures (2.305 Å).<sup>17, 18</sup> All other bond distances and angles are also found within the expected values.

The structure of [2] crystallizes in the orthorhombic space group *Pbca*, and one molecule of [2] is found in the asymmetric unit without co-crystallized lattice solvent molecules. The cobalt center is found in a near perfect octahedral geometry, formed by the coordination of

**Table 4.1.** Selected bond distances and bond angles in[1].

Atoms	Distance (Å)	Atoms	Bond angle (°)
Se1–Se2	2.3208(7)	N1–Co1–Cl2	165.89(10)
Co1–N1	2.303(3)	N1–Co1–Cl1	91.71(10)
Co1–N11	2.074(4)	N1–Co1–N11	75.99(13)
Co1–N21	2.079(4)	N1–Co1–N21	76.95(14)
Co1–Cl1	2.2848(13)	Cl2–Co1–Cl1	102.39(5)
Co1–Cl2	2.3290(12)	Cl2–Co1–N11	95.82(10)
		Cl2–Co1–N21	97.52(11)
		N11–Co1–Cl1	122.63(12)
		N11–Co1–N21	118.18(15)
		N21–Co1–Cl1	112.65(11)

five nitrogen atoms (two from  $\text{NCS}^-$  ions and three from the ligand  $\text{L}^1\text{Se}^-$ ) and one selenolate ion. The three nitrogen donors of the ligand  $\text{L}^1\text{Se}^-$  are coordinated to the cobalt center in a meridional fashion, similar to the ligand  $\text{L}^1\text{S}^-$  in previous reports.<sup>10, 13</sup> As a consequence, one of the  $\text{NCS}^-$  ions is coordinated to *trans* to the selenolate ion and the other  $\text{NCS}^-$  ion is coordinated *trans* to the tertiary amine nitrogen. The structure is very similar to the structure of the previously reported compound  $[\text{Co}(\text{L}^1\text{S})(\text{NCS})_2]$ .<sup>10</sup>  $\pi$ -Stacking interactions are present between pyridines of two neighboring molecules, the distances ranging from 3.337 Å to 3.351 Å. Short contacts of 3.693 Å are present in the unit cell between the selenolate ion and a sulfur atom of an  $\text{NCS}^-$  group of a neighboring molecule. A selection of bond distances and angles in [2] is provided in **Table 4.2**.

The structure of [4]Cl crystallizes in the monoclinic space group  $P2_1/n$ , and the asymmetric unit contains one molecule of [4]Cl and two disordered lattice chloroform solvent molecules. The cobalt center is found in a slightly distorted octahedral geometry, similar to [2]. Four nitrogen donor atoms (three from the ligand  $\text{L}^1\text{Se}^-$ , one from the ligand  $\text{quin}^-$ ), one oxygen, and one selenolate donor atom are coordinated to the cobalt center. The structure of [4]Cl is very similar to the reported structure of its sulfur analog  $[\text{Co}(\text{L}^1\text{S})(\text{quin})]\text{Cl}$ .<sup>14</sup> The bond distances and bond angles are similar to the structure  $[\text{Co}(\text{L}^1\text{S})(\text{quin})]\text{Cl}$ , except for the Co1–Se1 bond distance, which is larger due to larger ionic radius of selenium compared to sulfur. Unlike [2],  $\pi$ -stacking interactions are not present in the structure of [4]Cl. A selection of bond distances and angles is provided in **Table 4.3**.



**Table 4.2.** Bond distances and bond angles in [2].

Atoms	Distance (Å)	Atoms	Bond angle (°)	Atoms	Bond angle (°)
Co1–Se1	2.3608(4)	Se1–Co1–N61	178.00(6)	N61–Co1–N51	89.65(8)
Co1–N1	1.9601(18)	Se1–Co1–N1	90.91(5)	N1–Co1–N11	84.87(7)
Co1–N11	1.9353(18)	Se1–Co1–N11	88.29(6)	N1–Co1–N21	84.20(7)
Co1–N21	1.9229(18)	Se1–Co1–N21	91.95(5)	N1–Co1–N51	179.27(8)
Co1–N51	1.8999(19)	Se1–Co1–N51	88.36(6)	N51–Co1–N11	95.14(8)
Co1–N61	1.9976(19)	N61–Co1–N1	91.08(7)	N51–Co1–N21	95.79(8)
		N61–Co1–N11	91.78(8)	N11–Co1–N21	169.07(8)
		N61–Co1–N21	88.35(7)		

**Table 4.3.** Bond distances and bond angles in [4]Cl.

Atoms	Distance (Å)	Atoms	Bond angle (°)	Atoms	Bond angle (°)
Co1–Se1	2.3552(3)	Se1–Co1–O1	176.94(5)	O1–Co1–N31	85.47(7)
Co1–N1	1.9527(18)	Se1–Co1–N1	90.72(5)	N1–Co1–N11	83.81(8)
Co1–N11	1.9389(18)	Se1–Co1–N11	92.80(5)	N1–Co1–N21	85.48(8)
Co1–N21	1.9333(19)	Se1–Co1–N21	88.21(5)	N1–Co1–N31	174.67(7)
Co1–N31	1.9307(18)	Se1–Co1–N31	94.37(5)	N31–Co1–N11	94.37(8)
Co1–O1	1.9770(14)	O1–Co1–N1	89.53(7)	N31–Co1–N21	96.22(8)
		O1–Co1–N11	90.26(7)	N11–Co1–N21	169.26(8)
		O1–Co1–N21	88.77(7)		

#### 4.2.3. Solution Studies of the Cobalt(II)-Diselenide and Cobalt(III)-Selenolate Compounds

The cobalt compounds described in this Chapter are soluble in acetonitrile, except for [2] which is only slightly soluble in acetonitrile but fully soluble in dimethylsulfoxide. The UV-visible spectrum of each compound is depicted in **Figure 4.2**. A solution of [1] in acetonitrile has an intense purple color and the UV-visible spectrum shows two peaks at 558 nm ( $\epsilon = 3.15 \times 10^2 \text{ M}^{-1} \text{ cm}^{-1}$ ) and 635 nm ( $\epsilon = 2.22 \times 10^2 \text{ M}^{-1} \text{ cm}^{-1}$ ) as well as a small peak at around 850 nm, corresponding to the Co(II) *d-d* transitions in a trigonal-bipyramidal geometry.<sup>19, 20</sup> The UV-visible spectrum of [1] is very similar to that of the disulfide compound  $[\text{Co}_2(\text{L}^1\text{SSL}^1)\text{Cl}_4]$  reported earlier, with no apparent shift in the absorption wavelengths.<sup>10</sup>

Compound [2] was dissolved in a mixture of acetonitrile : dimethylsulfoxide ( $v : v = 19 : 1$ ), resulting in a maroon-colored solution, whereas solutions of [3](SbF<sub>6</sub>)<sub>2</sub> and [4]Cl in acetonitrile are yellow. The color of the solution of [4]Cl is rather intense compared to those of the two other cobalt(III)-selenolate compounds. The UV-visible spectra of

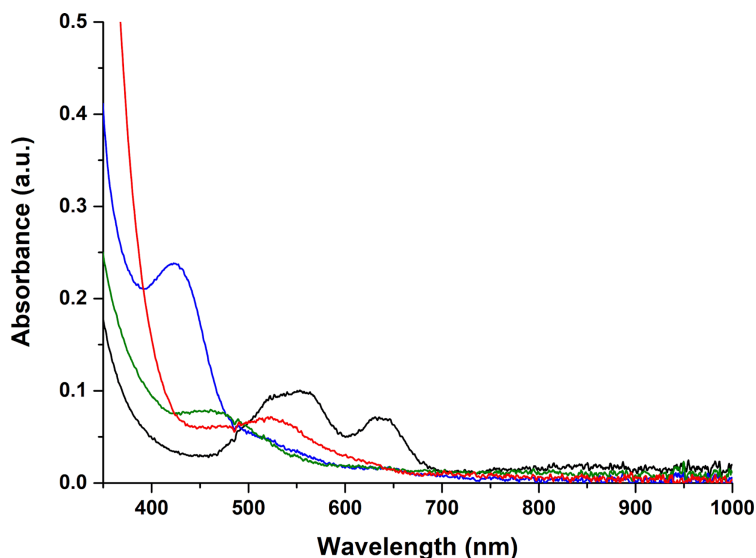


**Figure 4.2.** UV-visible spectra of acetonitrile solutions of [1] (2.5 mM concentration, black trace), [3](SbF<sub>6</sub>)<sub>2</sub> (2 mM, green trace), [4]Cl (1 mM, blue trace), and a solution of [2] (2.5 mM, red trace) in 19 : 1 acetonitrile : dimethylsulfoxide. UV-visible spectra were taken using a transmission dip probe with path length of 1.4 mm.

cobalt(III)-selenolate compounds [2], [3](SbF<sub>6</sub>)<sub>2</sub>, and [4]Cl generally show one absorption peak. The UV-visible spectrum of [2] shows a weak absorption peak at 523 nm ( $\epsilon = 2.10 \times 10^2 \text{ M}^{-1} \text{ cm}^{-1}$ ), whereas [3](SbF<sub>6</sub>)<sub>2</sub> shows similar weak absorption peak at 465 nm ( $\epsilon = 3.39 \times 10^2 \text{ M}^{-1} \text{ cm}^{-1}$ ). Such absorptions in UV-Vis spectra have been ascribed to Co(III) *d-d* transitions in an octahedral geometry.<sup>21, 22</sup> The spectrum of [4]Cl shows one strong absorption peak at 422 nm ( $\epsilon = 1.70 \times 10^3 \text{ M}^{-1} \text{ cm}^{-1}$ ) tentatively ascribed to a ligand-to-metal charge transfer from the quin<sup>-</sup> ligand to the cobalt center, similar to the spectrum of [Co(L<sup>1</sup>S)quin]Cl described in Chapter 3.<sup>14</sup>

#### 4.2.4. The Ligand-Field Splitting Energy of Selenolate Compounds

In Chapters 2 and 3, the ligand-field strength of exogenous ligands has been shown to affect the conversion of cobalt(II)-disulfide to cobalt(III)-thiolate species; the ligand-field strength was estimated from the MO energy levels using DFT computations.<sup>13, 14</sup> In this Chapter, a similar approach was taken to approximate the ligand-field strength of the ligand L<sup>1</sup>SeSeL<sup>1</sup>. The structures of [2], [3]<sup>2+</sup>, as well as [4]<sup>+</sup> were optimized using ZORA-OPBE/TZP all-electron basis set. The equilibrium geometries show satisfactory results, as shown by

similarities of the bond lengths of [2] and [4]<sup>+</sup> with the experimental values from the crystal structures (**Table 4.4**). The largest bond length deviation of 0.024 Å is found in the calculated Co1–N11 bond in [2]<sup>+</sup>. Other calculated bond lengths deviate by about 0.002 Å to 0.024 Å.

The *d*-orbital splitting energy was estimated using the method described in Chapter 2.<sup>13</sup> Again we found the five non-degenerate molecular orbitals with the highest contribution from Co *d*-orbitals (Figure AIII.17–AIII.19). These five orbitals approximately form two sets of orbitals in agreement with an octahedral splitting according to ligand-field theory. As the two sets of orbitals also contain contributions from the ligands in varying amounts, the *d*-orbital splitting energy can only be estimated in a rather qualitative way from the energy difference of the highest and the lowest orbital of this set. The results are compared to the sulfur analogs of [2], [3]<sup>2+</sup>, and [4]<sup>+</sup> in **Figure 4.3**. The energy differences between the highest and lowest MO with large *d*-orbital contributions in compounds [2], [3]<sup>2+</sup>, and [4]<sup>+</sup> are qualitatively smaller than those of their corresponding sulfur analogs. Therefore, replacement of sulfur with selenium apparently resulted in a slightly weaker ligand-field strength of the L<sup>1</sup>Se ligand. The differences between the *d*-orbital energies of the selenolate compounds with those of the sulfur analogs seems to follow a trend, i.e. the difference in energy of the highest and lowest MO comprising major *d*-orbital contribution between the Se and S compounds becomes smaller from [2] via [3]<sup>2+</sup> to [4]<sup>+</sup>. This apparent trend seems to be related to the ligand-field strength of the auxiliary ligands, from the weakest to the strongest in the order of NCS<sup>−</sup> < CH<sub>3</sub>CN < quin<sup>−</sup>, indicating that the contribution of the auxiliary ligand in the overall ligand-field splitting energy becomes dominant.<sup>23, 24</sup>

**Table 4.4.** Comparison between experimental and DFT bond distances in [2] and in [4]<sup>+</sup>.

Atoms	Bond Distance in [2] (Å)		Atoms	Bond Distance in [4] <sup>+</sup> (Å)	
	XRD	DFT		XRD	DFT
Co1–Se1	2.3608(4)	2.358	Co1–Se1	2.3552(3)	2.361
Co1–N1	1.9601(18)	1.966	Co1–N1	1.9527(18)	1.967
Co1–N11	1.9353(18)	1.911	Co1–N11	1.9389(18)	1.925
Co1–N21	1.9229(18)	1.906	Co1–N21	1.9333(19)	1.925
Co1–N51	1.8999(19)	1.846	Co1–N31	1.9307(18)	1.921
Co1–N61	1.9976(19)	1.962	Co1–O1	1.9770(14)	1.958

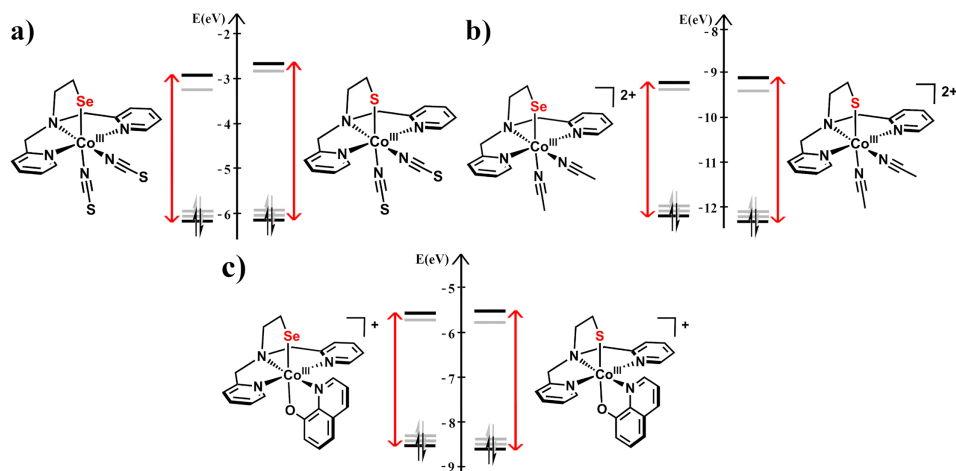


**Figure 4.3.** Comparison of the estimated *d*-orbital splitting energies of a) [2], b) [3]<sup>2+</sup>, and c) [4]<sup>+</sup> with its corresponding sulfur analog.

### 4.3. Discussion

The disulfide ligand L<sup>1</sup>SSL<sup>1</sup> in copper(I) or cobalt(II) complexes has been reported to facilitate intramolecular electron transfer with the metal center, in a so-called redox-conversion reaction.<sup>10, 25, 26</sup> To the best of our knowledge, this redox-conversion reaction has never been reported for a selenium-based ligand. Therefore, our study of the potential redox-conversion cobalt(II)-diselenide compounds started with the preparation of the new ligand L<sup>1</sup>SeSeL<sup>1</sup>, which structurally resembles the sulfur analog L<sup>1</sup>SSL<sup>1</sup>. Our results show that indeed redox-conversion reactions can also take place using a diselenide ligand.

The reaction of L<sup>1</sup>SeSeL<sup>1</sup> with cobalt(II) chloride in acetonitrile afforded the cobalt(II)-diselenide compound [1], which resembles the reported compound [Co<sub>2</sub>(L<sup>1</sup>SSL<sup>1</sup>)Cl<sub>4</sub>], having very similar spectroscopic properties.<sup>10</sup> The reaction with cobalt(II) thiocyanate resulted in the cobalt(III)-selenolate complex [2], similar to [Co(L<sup>1</sup>S)(NCS)<sub>2</sub>]. However, the ESI-MS spectrum of a solution of [2] (Figure AIII.7) shows signals attributed to the apparent formation of the diselenide dimer of the compound. Other spectroscopic techniques that were used to characterize [2] showed that in the solid state compound [2] is pure, but indicate that in solution [2] easily reverts to a diselenide-cobalt(II) compound.

Like its sulfur analog, [1] undergoes a redox-conversion reaction upon the addition of an external trigger, as shown by the formation of [3](SbF<sub>6</sub>)<sub>2</sub> and [4]Cl after treatment of *in situ* formed [1] with a silver salt or quinolinol. Full conversion of [1] to [3](SbF<sub>6</sub>)<sub>2</sub> was achieved successfully. In principle, this reactivity is similar to the formation of [Co(L<sup>1</sup>S)(MeCN)<sub>2</sub>]<sup>2+</sup> from the reaction of L<sup>1</sup>SSL<sup>1</sup> with [Co(MeCN)<sub>6</sub>](BF<sub>4</sub>)<sub>2</sub>,<sup>10</sup> or from the dissolution of [Co<sub>2</sub>(L<sup>1</sup>SSL<sup>1</sup>)(PF<sub>2</sub>O<sub>2</sub>)<sub>2</sub>](PF<sub>6</sub>)<sub>2</sub> in acetonitrile.<sup>12</sup> Acetonitrile will coordinate to the cobalt center and has sufficiently strong ligand-field effect to trigger the conversion, as long as there is no strongly coordinating ligand or anion. Despite the observed formation of [3](SbF<sub>6</sub>)<sub>2</sub>, this compound likely is unstable in solution. In the <sup>1</sup>H-NMR spectrum of [3](SbF<sub>6</sub>)<sub>2</sub>, partial decomposition of the cobalt(III)-selenolate complex is indicated by the presence of several peaks in the aromatic region (6.60–7.25 ppm) as well as at 2.75 ppm, which possibly arise from degradation of the ligand. The instability of the cobalt(III)-selenolate compounds can be explained by the more negative reduction potential of the diselenide bond than that of the disulfide bond;<sup>27</sup> re-oxidation of selenolate to the diselenide (dimer) appears to be relatively easy of as indicated by the presence of peaks assigned to dimeric compounds in the ESI-MS spectra of [2] and [3](SbF<sub>6</sub>)<sub>2</sub>. Nevertheless, full conversion of [1] to [4]Cl was achieved in a clean manner with the strong-field ligand quinolinolate.

Based on the experimental results it seems that the presence of selenium in the ligand causes a smaller ligand-field splitting than sulfur. Although the ligand-field splitting energy of the selenium-based ligand may be smaller than that of the sulfur analog, it appears that this can be counteracted by the auxiliary ligand. This assumption is supported by our DFT computations, with the results shown in **Figure 4.3**: the difference in energy of the highest and lowest MO orbital with major *d*-orbital contribution of the selenolate compounds compared to the thiolate analogs becomes smaller in the order of NCS<sup>−</sup>, CH<sub>3</sub>CN, and quin<sup>−</sup>. These results indicate that indeed the ligand-field strength contribution of these auxiliary ligand overcomes the smaller ligand-field splitting energy of the selenium donor atom. The clean formation of [4]Cl shows that with the strong-field ligand quin<sup>−</sup> full conversion can be achieved. Generally, our results show the similarities and differences in redox-conversion reactivity of the diselenide ligand L<sup>1</sup>SeSeL<sup>1</sup> compared to L<sup>1</sup>SSL<sup>1</sup>.

#### 4.4. Conclusion

The diselenide  $L^1SeSeL^1$  analog of the disulfide ligand  $L^1SSL^1$  was successfully synthesized. Reaction of the ligand  $L^1SeSeL^1$  with cobalt(II) salts resulted in the formation of either cobalt(II)-diselenide compound [1] with chloride ions or the cobalt(III)-selenolate compound [2] with thiocyanate ions. The redox-conversion of cobalt(II)-diselenide compound [1] to cobalt(III)-selenolate compounds [3]( $SbF_6$ )<sub>2</sub> or [4] has been proven to be successful, using the strategies employed in previous reports for  $L^1SSL^1$ . The cobalt(III)-selenolate compounds [2] and [3]( $SbF_6$ )<sub>2</sub> appear to be relatively unstable in solution, the compounds partially revert to a diselenide compound or decompose. However, formation of [4] is clean, showing that the ligand-field strength of the auxiliary ligand can overpower the weaker ligand-field exerted by the selenium-based ligand. Overall, our results indicate that cobalt compounds with the ligand  $L^1SeSeL^1$  show reactivity that is very similar to the sulfur analogs. The selenium-based ligand appears to exert a slightly lower ligand-field strength, which is not unexpected due to the stronger pi-donating effects of the larger lone pairs on selenium. These studies can be directed to investigate the kinetics of the reaction, or derivatization of the ligand  $L^1SeSeL^1$ , which may give insights not only in the diselenide to selenolate conversion, but also their efficiency in natural systems.

#### 4.5. Experimental Section

##### 4.5.1. General

All reagents were purchased from commercial sources and used as received unless noted otherwise. Deoxygenated solvents used were obtained by the freeze-pump-thaw method followed by drying the solvents using appropriate size of molecular sieves. The synthesis of the cobalt compounds was performed using standard Schlenk-line techniques under argon atmosphere.  $^1H$  NMR spectra were recorded on a Bruker 300 DPX spectrometer at room temperature. Mass spectra were recorded on a Thermo Scientific MSQ Plus or Shimadzu LCMS 2020 mass spectrometer with electrospray ionization (ESI) method, formic acid was added to the eluting solvent with 1% final concentration. Simulated mass spectra were generated using the mMass (version 5.5.0) software.<sup>28</sup> IR spectra were obtained using a PerkinElmer Spectrum Two System equipped with Universal ATR module containing diamond crystal for single reflection (scan range 400–4000  $cm^{-1}$ , resolution 4  $cm^{-1}$ ). Analyses of bond distances and angles of the structures were performed using the Mogul

module in Mercury (version 4.3.1) software.<sup>29</sup> UV-visible spectra were collected using a transmission dip probe with variable path lengths and reflection probe on an Avantes AvaSpec-2048 spectrometer and using an AVALIGHT-DH-S-Bal light source. Elemental analyses were performed by the Microanalytical Laboratory Kolbe in Germany.

#### 4.5.2. *Single crystal X-ray crystallography*

All reflection intensities were measured at 110(2) K using a SuperNova diffractometer (equipped with Atlas detector) with Mo  $K\alpha$  radiation ( $\lambda = 0.71073$  Å) under the program CrysAlisPro (Version CrysAlisPro 1.171.39.29c, Rigaku OD, 2017). The same program was used to refine the cell dimensions and for data reduction. The structure was solved with the program SHELXS-2018/3 and was refined on  $F^2$  with SHELXL-2018/3.<sup>30</sup> Numerical absorption correction based on Gaussian integration over a multifaceted crystal model was applied using CrysAlisPro. The temperature of the data collection was controlled using the system Cryojet (manufactured by Oxford Instruments). The H atoms were placed at calculated positions using the instructions AFIX 23, AFIX 43 or AFIX 137 with isotropic displacement parameters having values 1.2 or 1.5  $U_{eq}$  of the attached C atoms. The crystal structures of [1] and [2] are ordered. For compound [4]Cl, the two lattice chloroform molecules were found to be disordered over either two or three orientations, and the occupancy factors for the major / minor components of the disorder can be retrieved from the .cif file.

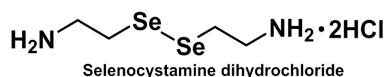
#### 4.5.3. *Computational methods*

All calculations were performed with density functional theory using the Amsterdam Density Functional (ADF) program version 2017.103.<sup>31</sup> Geometries and energies were computed using OPBE functional.<sup>32</sup> Molecular orbitals (MO) were expanded in a large uncontracted TZP Slater type orbital (STO) basis set.<sup>33</sup> Scalar relativistic effects were accounted for using the zeroth order regular approximation (ZORA).<sup>34</sup> The stationary points were checked to be minima at potential energy surface using vibrational analysis. The calculations for all cobalt(III)-selenolate compounds were done with  $S = 0$  (low-spin cobalt(III) center). The  $d$ -orbital splitting energies were estimated using similar method described in Chapter 2.<sup>13</sup>

#### 4.5.4. Synthesis of the compounds

##### Selenocystamine dihydrochloride ( $C_4H_{12}N_2Se_2 \cdot 2HCl$ )

*Caution: Selenium and its derivative listed here are extremely toxic and exudes foul smell, one should ensure proper ventilation and personal protective equipment at all times.*



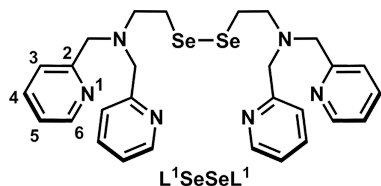
A 3-necked round-bottomed flask was purged with argon before the reaction was started. Into the 3-necked round-bottomed flask, selenium powder (4.75 g, 60 mmol) was added, followed by 25 mL of demineralized water (previously bubbled with argon). The flask was then fitted with a gas outlet and an addition funnel. In another flask, 15.0 grams of lead(II) acetate trihydrate was dissolved in 300 mL demineralized water. The solution of lead(II) acetate was added to a gas washing bottle, keeping the solution level above the bubbler to detect any gas formation. The gas outlet of the reaction flask was connected to the inlet of the gas washing bottle. In a separate flask, 4.54 grams of  $NaBH_4$  (120 mmol, 2 equiv.) was dissolved in 25 mL demineralized water, bubbled with argon for 20 minutes, and the solution was quickly transferred to the addition funnel. The colloidal selenium mixture was stirred and  $NaBH_4$  was added slowly to keep the bubbling at a moderate pace. During the addition of  $NaBH_4$ , the solution in the gas-trap apparatus changed color from colorless to black, indicating the formation of  $PbSe$  species. The grey colloidal selenium mixture changed to a clear red solution during the addition of  $NaBH_4$  and ultimately to a light yellow solution after full addition of  $NaBH_4$ . The solution was stirred for 10 minutes, followed by addition of selenium powder (4.75 g, 60 mmol) in four portions over the course of 30 minutes. The resulting dark red-colored solution was stirred for another 20 minutes. While stirring, 2-chloroethylamine hydrochloride (13.9 g, 120 mmol, 2 equiv.) was dissolved in 30 mL  $NaOH$  5 M, which was deoxygenated by bubbling with argon for 20 minutes. This solution was transferred to the addition funnel, then added dropwise to the reaction mixture. The gas outlet and the addition funnel was removed after the addition, and the resulting solution was stirred overnight at room temperature under an argon atmosphere.

The reaction mixture was transferred into a separating funnel, then extracted with  $5 \times 100$  mL  $CHCl_3$ . The organic layer was collected and subsequently dried over  $MgSO_4$ . The organic layer was filtered and concentrated using a rotary evaporator. The resulting oil (15.34 g) was



dissolved in 100 mL methanol and 100 mL ethyl acetate. Anhydrous HCl in diethyl ether (65 mL) was added slowly to the solution, and the reaction mixture was stirred for an hour. After an hour, the mixture was concentrated using a rotary evaporator. The resulting solid (12.13 g) was dissolved in the minimum amount of methanol, and ethyl acetate was added slowly until the formation of precipitates occurred. Filtration of the light yellow solid and subsequent washing with diethyl ether followed by drying in air gave a light yellow powder as the product. Yield = 7.05 g, (37%). ESI-MS found (calcd.) for  $[M+H]^+$   $m/z$  248.9 (248.94).  $^1\text{H-NMR}$  (300 MHz,  $(\text{CD}_3)_2\text{SO}$ , RT),  $\delta(\text{ppm})$ : 8.24 (s, 4H, amine  $\text{NH}_2$ ), 3.35 (s, 8H,  $\text{NH}_2\text{-CH}_2\text{-CH}_2\text{-Se-}$ ).

### 2,2'-Diselanediyibis(N,N-bis(pyridin-2-ylmethyl)ethan-1-amine) ( $\text{L}^1\text{SeSeL}^1$ )

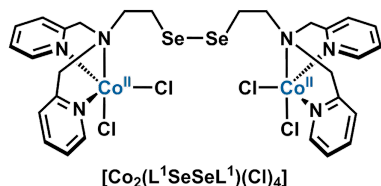


In a 500 mL round-bottom flask, selenocystamine dihydrochloride (3.22 grams, 10.1 mmol) was dissolved in 150 mL methanol, resulting in a red-colored solution. Into the solution, 2-pyridinecarboxaldehyde (4 mL, 42 mmol, 4 equiv.)

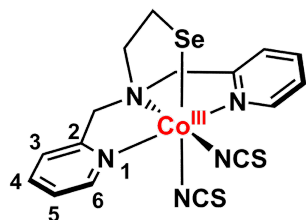
was added and the reaction mixture was stirred for one hour. Then, sodium cyanoborohydride (2.95 g, 47 mmol, 4.7 equiv.) was added in four portions, the first two portions were added over the course of 15 minutes. The remaining portions were added after stirring the solution for 12 hours, over the course of 15 minutes. The color of the solution turned yellow-green, and the solution was stirred for another three days. The reaction was quenched after three days by addition of 37% HCl until pH = 1. The solvent was removed using a rotary evaporator, resulting in a yellow oil, which was dissolved in 50 mL NaOH (10 M). The solution was transferred into a separatory funnel and extracted with  $3 \times 100$  mL  $\text{CHCl}_3$ . The organic layer was collected, dried over  $\text{MgSO}_4$ . Filtration of the solids and removal of the solvent using a rotary evaporator resulted in a red-orange oil, which was carefully treated with 10 mL 70%  $\text{HClO}_4$ . Absolute ethanol (400 mL) was added to the mixture, the initially formed turbid solution turned clear orange after 3 hours of stirring. The orange-colored solution was then removed, resulting in a dark red sticky oil, which was converted back to the free base using 50 mL NaOH (10 M). The solution was transferred to a separatory funnel and extracted again with  $3 \times 100$  mL  $\text{CHCl}_3$ . The organic layer was collected, dried over  $\text{MgSO}_4$ , filtered, and then the solvent was removed using a rotary evaporator. The resulting crude product (red oil) was

crystallized using 300 mL petroleum ether under overnight reflux condition. After reflux, the petroleum ether solution was transferred to an erlenmeyer flask and stored in a refrigerator for several days until a pale red precipitate formed. The solids were collected by filtration, dried in air and weighed. Yield = 1.6 g (26%). ESI-MS found (calcd.) for  $[L^1SeSeL^1 + H]^+$   $m/z$  612.9 (613.1)  $[L^1SeSeL^1 + 2H]^{2+}$   $m/z$  306.8 (307.06).  $^1H$ -NMR (300 MHz,  $CD_3CN$ , RT),  $\delta$ (ppm): 2.79-2.84 (t, 4H, N-CH<sub>2</sub>-CH<sub>2</sub>-Se), 3.04-3.08 (t, 4H, N-CH<sub>2</sub>-CH<sub>2</sub>-Se), 3.78 (s, 8H, N-CH<sub>2</sub>-Py), 7.17-7.22 (ddd, 4H, Py-H<sub>5</sub>), 7.54-7.56 (d, 4H, Py-H<sub>3</sub>), 7.68-7.74 (td, 4H, Py-H<sub>4</sub>), 8.46-8.49 (m, 4H, Py-H<sub>6</sub>). Elemental analysis (%) for  $L^1SeSeL^1$  ( $C_{28}H_{32}N_6Se_2$ ) calcd. C, 55.09; H, 5.28; N, 13.77; found C, 54.96; H, 5.31; N, 13.60.

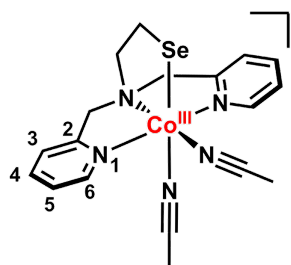
**$[Co_2(L^1SeSeL^1)(Cl)_4]$  (**[1]**)**



The ligand  $L^1SeSeL^1$  (65.8 mg, 0.108 mmol) was dissolved in 5 mL dry and deoxygenated acetonitrile. Anhydrous  $CoCl_2$  (28.0 mg, 0.216 mmol, 2 equiv.) was added into the solution of  $L^1SeSeL^1$  and the color immediately turned dark purple. The solution was stirred for three hours and then concentrated *in vacuo* until approximately 1 mL was left in the flask. Diethyl ether (12 mL) was subsequently added into the flask, affording a purple precipitate. The precipitate was filtered, washed twice with diethyl ether, then dried *in vacuo*. The dried purple powder was collected and weighed. The purple powder is air stable. Yield = 46.6 mg (50%). Purple platelike single crystals of **[1]** were grown using vapor diffusion of diethyl ether into an acetonitrile solution of **[1]**. IR (neat,  $cm^{-1}$ ): 3065vw, 3029vw, 2964vw, 2916w, 2848vw, 1606vs, 1571m, 1480s, 1442vs, 1380w, 1367w, 1308m, 1292m, 1260m, 1226vw, 1156m, 1099m, 1083m, 1053s, 1023vs, 981w, 961m, 900w, 862w, 844w, 766vs, 736m, 683w, 649m, 513w, 477m, 417s. ESI-MS found (calcd.) for  $[1 - 2Cl^-]^{2+}$   $m/z$  400.0 (399.95), for  $[1 - 2Cl^- + HCOO^-]^+$   $m/z$  845.1 (844.90). Elemental analysis (%) for **[1]** ( $C_{28}H_{32}Co_2N_6Se_2Cl_4$ ) calcd. C, 38.65; H, 3.71; N, 9.66; found C, 38.49; H, 3.69; N, 9.46.

**[Co(L<sup>1</sup>Se)(NCS)<sub>2</sub>] ([2])****[Co(L<sup>1</sup>Se)(NCS)<sub>2</sub>]**

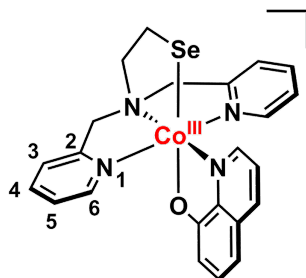
Preparation of [2] was similar to compound [1], using Co(SCN)<sub>2</sub> instead of CoCl<sub>2</sub>. Ligand L<sup>1</sup>SeSeL<sup>1</sup> (68.0 mg, 0.111 mmol) in dry and deoxygenated acetone was mixed with Co(SCN)<sub>2</sub> (39.0 mg, 0.222 mmol, 2 equiv.). A purple powder was obtained. Yield = 81.0 mg (76%). Dark red single crystals of [2] were grown using vapor diffusion of diethyl ether into a 1:1 acetonitrile:methanol solution of [2] over the course of three days. IR (neat, cm<sup>-1</sup>): 2969w, 2900w, 2057vs, 1692w, 1606s, 1572m, 1482m, 1443s, 1366m, 1307m, 1291m, 1250m, 1225w, 1155m, 1100m, 1079m, 1054s, 1024s, 973m, 957m, 901w, 862w, 841w, 763vs, 734m, 722m, 650m, 512w, 475s, 446w, 418s. <sup>1</sup>H-NMR (300 MHz, CD<sub>3</sub>CN, RT), δ(ppm): 3.22-3.30 (m, 2H, N-CH<sub>2</sub>-CH<sub>2</sub>-Se), 4.18-4.24 (d, 2H, N-CH<sub>2</sub>-py), 4.92-4.97 (d, 2H, N-CH<sub>2</sub>-py), 7.44-7.47 (d, 2H, Py-H<sub>3</sub>), 7.54-7.59 (t, 2H, Py-H<sub>5</sub>), 7.96-8.01 (t, 2H, Py-H<sub>4</sub>), 8.47-8.49 (d, 2H, Py-H<sub>6</sub>), the proton signal of N-CH<sub>2</sub>-CH<sub>2</sub>-Se is obscured by the solvent peak at around 2.12-2.25 ppm, but was assigned using <sup>1</sup>H-COSY spectrum. ESI-MS found (calcd.) for [2 - SCN<sup>-</sup> + MeCN]<sup>+</sup> *m/z* 463.9 (463.99), for [2×2 - 2SCN<sup>-</sup> + HCOO<sup>-</sup>]<sup>+</sup> *m/z* 889.0 (888.92). Elemental analysis (%) for [2] (C<sub>16</sub>H<sub>16</sub>CoN<sub>5</sub>S<sub>2</sub>Se) + 0.3H<sub>2</sub>O calcd. C, 39.56; H, 3.44; N, 14.42; found C, 39.46; H, 3.31; N, 14.31.

**[Co(L<sup>1</sup>Se)(MeCN)<sub>2</sub>](SbF<sub>6</sub>)<sub>2</sub> ([3])(SbF<sub>6</sub>)<sub>2</sub>****[Co(L<sup>1</sup>Se)(MeCN)<sub>2</sub>](SbF<sub>6</sub>)<sub>2</sub>**

The ligand L<sup>1</sup>SeSeL<sup>1</sup> (61.0 mg, 0.1 mmol) was dissolved in 5 mL dry and deoxygenated acetonitrile. Anhydrous CoCl<sub>2</sub> (26.0 mg, 0.2 mmol, 2 equiv.) was added and the resulting purple-colored solution was stirred for 30 minutes. Silver hexafluoroantimonate (143.7 mg, 0.42 mmol, 4.2 equiv.) was added and the resulting solution turned brown with some white precipitate, presumably AgCl. The resulting suspension was stirred for 2 hours, followed by filtration into a clean schlenk flask. The brown filtrate was concentrated until approximately 1 mL. Diethyl ether (12 mL) was added into the flask resulting in the formation of a dark

brown oil. The oil was separated by careful removal of the diethyl ether using a syringe, then the oil was washed twice with diethyl ether, and dried *in vacuo*. The oil quickly solidified and turned into a semi-crystalline powder. Yield = 166.8 mg (91%). IR (neat,  $\text{cm}^{-1}$ ): 3516s, 3466s, 3262m, 3201m, 3122m, 2988m, 2972m, 2901m, 1624m, 1612m, 1573w, 1538w, 1471m, 1446m, 1411w, 1394w, 1378w, 1290w, 1249w, 1231w, 1165w, 1056m, 1026m, 973w, 896vw, 880vw, 838w, 821vw, 765s, 727s, 655vs, 624vs, 480m, 452m, 421m. ESI-MS found (calcd.) for  $[\mathbf{3}]^{2+}$   $m/z$  223.6 (223.52), for  $[\mathbf{3} - 2\text{MeCN} + \text{HCOO}^-]^+$   $m/z$  410.1 (410.98), for a dimer  $[2 \times \mathbf{3} - 4\text{MeCN} + 3\text{HCOO}^-]^+$   $m/z$  863.0 (862.96), and for  $[2 \times \mathbf{3} - 4\text{MeCN} + 2\text{HCOO}^- + \text{SbF}_6^-]^+$   $m/z$  1054.9 (1054.86).  $^1\text{H-NMR}$  (300 MHz,  $\text{CD}_3\text{OD}$ , RT),  $\delta(\text{ppm})$ : 2.83-2.86 (m, 2H, N- $\text{CH}_2$ - $\text{CH}_2$ -Se), 3.07-3.11 (m, 2H, N- $\text{CH}_2$ - $\text{CH}_2$ -Se), 3.81 (s, 4H, N- $\text{CH}_2$ -py), 7.42-7.47 (t, 4H, Py- $\text{H}_3$  and Py- $\text{H}_5$ ), 7.85-7.91 (t, 2H, Py- $\text{H}_4$ ), 8.62-8.64 (d, 2H, Py- $\text{H}_6$ ). The compound is not stable in solution, as is apparent from impurities detected at 2.75 (s, 1H), 6.38-6.44 (t, 0.5H), 6.72-6.75 (d, 0.5H), 6.89-6.91 (d, 0.5H), 7.19-7.24 (t, 0.5H). Elemental analysis (%) for  $[\mathbf{3}](\text{SbF}_6)_2$  ( $\text{C}_{18}\text{H}_{22}\text{CoF}_{12}\text{N}_5\text{Sb}_2\text{Se}$ ) calcd. C, 55.09; H, 5.28; N, 13.77; found C, 54.96; H, 5.31; N, 13.60.

#### $[\text{Co}(\text{L}^1\text{Se})(\text{quin})]\text{Cl}$ ( $[\mathbf{4}]\text{Cl}$ )



$[\text{Co}(\text{L}^1\text{Se})(\text{quin})]\text{Cl}$

The ligand  $\text{L}^1\text{SeSeL}^1$  (61.19 mg, 0.1 mmol) and anhydrous  $\text{CoCl}_2$  (26.0 mg, 0.2 mmol, 2 equiv.) were dissolved in 5 mL dry and deoxygenated methanol, affording a solution of  $[\mathbf{1}]$  as described above. Into this solution, 8-quinolinol (28.88 mg, 0.2 mmol, 2 equiv.) was added. The solution turned from purple into brown and the solution was stirred for another three hours. The solution was concentrated until approximately 1 mL, diethyl ether

(12 mL) was added to the concentrated solution, which resulted in the formation of a brown precipitate. The brown precipitate was filtered, washed twice with diethyl ether, then dried *in vacuo*, and weighed. Yield = 85.19 mg (78%). Dark brown single crystals of  $[\mathbf{4}]\text{Cl}$  were grown using vapor diffusion of diethyl ether into a chloroform solution of  $[\mathbf{4}]\text{Cl}$ . IR (neat,  $\text{cm}^{-1}$ ): 3361b, 2984w, 2969w, 2050vw, 1657s, 1632s, 1571m, 1498s, 1463s, 1408s, 1374s, 1321s, 1284m, 1222w, 1173w, 1156w, 1110m, 1053w, 1008m, 980w, 876w, 831s, 803w, 749s, 703s, 663w, 643w, 552w, 531m, 516w 501w, 454w, 420w. ESI-MS found (calcd.) for

[4]<sup>+</sup> *m/z* 509.1 (509.03) and its isotopic pattern. <sup>1</sup>H-NMR (300 MHz, CD<sub>3</sub>CN, RT), δ(ppm): 3.61-3.63 (t, 2H, N-CH<sub>2</sub>-CH<sub>2</sub>-Se), 4.54-4.59 and 5.45-5.50 (d, d, total 4H, N-CH<sub>2</sub>-Py), 6.86-6.89 (dd, 1H, ortho-CH-O(quin)), 7.02-7.05 (dd, 1H, para-CH-O(quin)), 7.10-7.15 (t, 2H, Py-H<sub>5</sub>), 7.34-7.39 (m, 3H, Py-H<sub>3</sub> and meta-CH-O(quin)), 7.46-7.49 (d, 2H, Py-H<sub>4</sub>), 7.74 (dd, 1H, meta-CH-N(quin)), 7.79-7.85 (td, 2H, Py-H<sub>6</sub>), 8.45-8.48 (d, 1H, para-CH-N(quin)), 9.02-9.04 (d, 1H, ortho-CH-N(quin)), the proton signal of N-CH<sub>2</sub>-CH<sub>2</sub>-Se is obscured by the solvent peak at around 2.15-2.25 ppm, but was assigned using <sup>1</sup>H-COSY spectrum. Elemental analysis (%) for [4]Cl (C<sub>23</sub>H<sub>22</sub>CoN<sub>4</sub>OSeCl) + H<sub>2</sub>O calcd. C, 49.17; H, 4.31; N, 9.97; found C, 48.77; H, 3.97; N, 9.89.

#### 4.6. References

- Gennari, M. and Duboc, C. *Acc. Chem. Res.* **2020**, 53 (11), 2753-2761.
- Hu, C., Yu, Y. and Wang, J. *Chem. Commun.* **2017**, 53 (30), 4173-4186.
- Martin, D. R. and Matyushov, D. V. *Sci. Rep.* **2017**, 7, 1-11.
- Bock, A., Forchhammer, K., Heider, J., Leinfelder, W., Sawers, G., Veprek, B. and Zinoni, F. *Mol. Microbiol.* **1991**, 5 (3), 515-520.
- Cone, J. E., Martindell, R., Davis, J. N. and Stadtman, T. C. *Proc. Natl. Acad. Sci. U.S.A.* **1976**, 73 (8), 2659-2663.
- Reich, H. J. and Hondal, R. J. *ACS Chem. Biol.* **2016**, 11 (4), 821-841.
- Takei, T., Ando, T., Takao, T., Ohnishi, Y., Kurisu, G., Iwaoka, M. and Hojo, H. *Chem. Commun.* **2020**, 56 (91), 14239-14242.
- Steinmann, D., Nauser, T. and Koppenol, W. H. *J. Org. Chem.* **2010**, 75 (19), 6696-6699.
- Huber, R. E. and Criddle, R. S. *Arch. Biochem. Biophys.* **1967**, 122 (1), 164-173.
- Jiang, F., Siegler, M. A., Sun, X., Jiang, L., Fonseca Guerra, C. and Bouwman, E. *Inorg. Chem.* **2018**, 57 (15), 8796-8805.
- Ording-Wenker, E. C. M., van der Plas, M., Siegler, M. A., Bonnet, S., Bickelhaupt, F. M., Fonseca Guerra, C. and Bouwman, E. *Inorg. Chem.* **2014**, 53 (16), 8494-8504.
- Jiang, F., Marvelous, C., Verschuur, A. C., Siegler, M. A., Teat, S. J. and Bouwman, E. *Inorg. Chim. Acta* **2022**, 120880.
- Marvelous, C., de Azevedo Santos, L., Siegler, M. A., Fonseca Guerra, C. and Bouwman, E. *Dalton Trans.* **2022**, 51, 8046-8055.
- Marvelous, C., de Azevedo Santos, L., Siegler, M. A., Fonseca Guerra, C. and Bouwman, E. **2022**, submitted
- Yue, D., Cheng, G., He, Y., Nie, Y., Jiang, Q., Cai, X. and Gu, Z. *J. Mater. Chem. B* **2014**, 2 (41), 7210-7221.
- Addison, A. W., Rao, T. N., Reedijk, J., Vanrijn, J. and Verschoor, G. C. *J. Chem. Soc., Dalton Trans.* **1984**, (7), 1349-1356.
- Singh, P., Singh, H. B. and Butcher, R. J. *J. Organomet. Chem.* **2018**, 876, 1-9.
- Sureshkumar, D., Gunasundari, T., Saravanan, V. and Chandrasekaran, S. *Tetrahedron Lett.* **2007**, 48 (4), 623-626.
- Chan, S. L.-F., Lam, T. L., Yang, C., Lai, J., Cao, B., Zhou, Z. and Zhu, Q. *Polyhedron* **2017**, 125, 156-163.
- Massoud, S. S., Broussard, K. T., Mautner, F. A., Vicente, R., Saha, M. K. and Bernal, I. *Inorg. Chim. Acta* **2008**, 361 (1), 123-131.
- Basolo, F. *J. Am. Chem. Soc.* **1950**, 72 (10), 4393-4397.
- Matsuoka, N. *Bull. Chem. Soc. Jpn.* **1986**, 59 (7), 2151-2155.

- 
23. Shimura, Y. and Tsuchida, R. *Bull. Chem. Soc. Jpn.* **1956**, 29 (3), 311-316.
  24. Ishii, T., Tsuboi, S., Sakane, G., Yamashita, M. and Breedlove, B. K. *Dalton Trans.* **2009**, (4), 680-7.
  25. Itoh, S., Nagagawa, M. and Fukuzumi, S. *J. Am. Chem. Soc.* **2001**, 123 (17), 4087-4088.
  26. Ueno, Y., Tachi, Y. and Itoh, S. *J. Am. Chem. Soc.* **2002**, 124 (42), 12428-12429.
  27. Besse, D., Siedler, F., Diercks, T., Kessler, H. and Moroder, L. *Angew. Chem. Int. Ed.* **1997**, 36 (8), 883-885.
  28. Strohm, M., mMass - Open Source Mass Spectrometry Tool. [www.mmass.org](http://www.mmass.org)
  29. Macrae, C. F., Sovago, I., Cottrell, S. J., Galek, P. T. A., McCabe, P., Pidcock, E., Platings, M., Shields, G. P., Stevens, J. S., Towler, M. and Wood, P. A. *J. Appl. Crystallogr.* **2020**, 53, 226-235.
  30. Sheldrick, G. M. *Acta Crystallogr. Sect. A: Found. Crystallogr.* **2008**, 64, 112-122.
  31. ADF2017.107. SCM Theoretical Chemistry, Vrije Universiteit: Amsterdam, The Netherlands, [www.scm.com](http://www.scm.com)
  32. Swart, M., Ehlers, A. W. and Lammertsma, K. *Mol. Phys.* **2004**, 102 (23-24), 2467-2474.
  33. Van Lenthe, E. and Baerends, E. J. *J. Comput. Chem.* **2003**, 24 (9), 1142-1156.
  34. Van Lenthe, E., Baerends, E. J. and Snijders, J. G. *J. Chem. Phys.* **1994**, 101 (11), 9783-9792.



# Chapter 5

---

## Structural Investigations and Reactivity of Cobalt(II)-Disulfide Complexes

*Controlling the bio-inspired redox interconversion of Co(II)-disulfide compounds and their related Co(III)-thiolate complexes is a perplexing task as the factors triggering this reaction are not fully understood. Three disulfide ligands 2,2'-disulfanediyldis(N,N-bis((3,5-dimethyl-1H-pyrazol-1-yl)methyl)ethan-1-amine) ( $L^{mpz}SSL^{mpz}$ ), 3,3'-disulfanediyldis(N,N-bis(pyridin-2-ylmethyl)propan-1-amine) ( $L^pSSL^p$ ), and 2,2'-disulfanediyldis(N,N-bis(6-methylpyridin-2-ylmethyl)ethan-1-amine) ( $L^3SSL^3$ ) with different chain lengths and pyrazole or pyridine groups were reacted with cobalt(II) salts and the resulting complexes were studied for their potential to form Co(III)-thiolate complexes. Crystal structures of  $[Co_2(L^{mpz}SSL^{mpz})(Br)_4]$  [**1<sub>Br</sub>**],  $[Co_2(L^{mpz}SSL^{mpz})(NCS)_4]$  [**1<sub>NCS</sub>**],  $[Co_2(L^pSSL^p)(NCS)_4]$  [**2<sub>NCS</sub>**], and  $[Co_2(L^3SSL^3)(Cl)_4]$  [**3<sub>Cl</sub>**] show that generally the disulfide sulfur donors do not coordinate to the cobalt(II) centers, resulting in dinuclear structures containing two 5-coordinate cobalt centers. However, a unique asymmetric dinuclear complex is found in [**1<sub>Br</sub>**] in which one of the sulfur atoms coordinates to one of the cobalt ions. Thiocyanate-induced Co(III)-thiolate formation in the presence of either ligand  $L^{mpz}SSL^{mpz}$  or  $L^pSSL^p$  is evidently unsuccessful, as Co(II)-disulfide complexes were obtained. The reaction of all Co(II)-disulfide complexes with 8-quinolinol suggest that redox conversion to Co(III)-thiolate complexes may take place, but the reactions are not clean.*

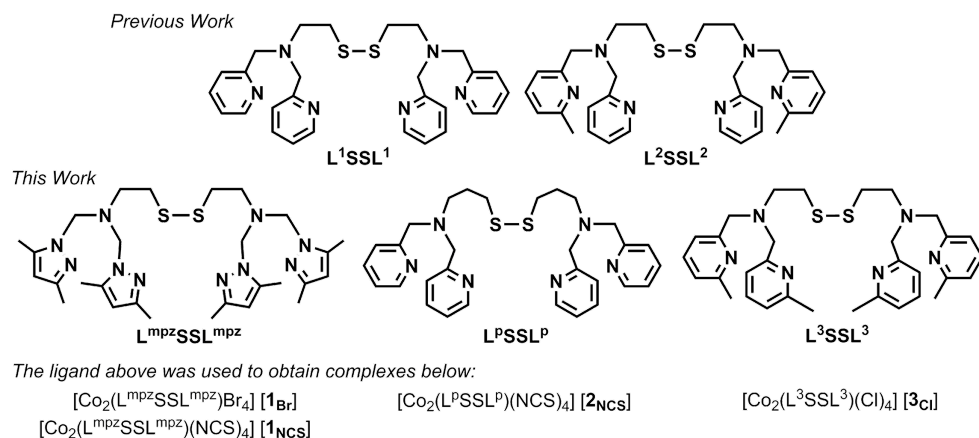
This chapter will be submitted for publication: Christian Marvelous, Maxime A. Siegler, and Elisabeth Bouwman, *manuscript in preparation*



## 5.1. Introduction

The conversion of specific metal<sup>(n)</sup>-disulfide complexes into the corresponding redox-interconverted metal<sup>(n+1)</sup>-thiolate complexes has emerged recently as an interesting field of study. The study of this redox-conversion reaction is inspired by the natural enzymes, in which the thiol/disulfide conversion and redox reactions are important in for example glutaredoxins, thioredoxins, or in the heme binding of the heme oxygenase enzyme.<sup>1-4</sup> In the past two decades, several examples of the redox conversion of copper(I)-disulfide complexes into the corresponding copper(II)-thiolate complexes have been reported. The ligand structures were shown to have a large influence on the formation of either a dinuclear *transoid*-Cu(I)-disulfide, *cisoid*-Cu(I)-disulfide, or Cu(II)-μ-thiolate complex.<sup>5, 6</sup>

Recently, the study of redox interconversion reactions has progressed from copper to cobalt complexes. The ligand L<sup>1</sup>SSL<sup>1</sup> (**Scheme 5.1**) used in the formation of Cu(II)-μ-thiolate complex was shown to form dinuclear Co(II)-disulfide complexes when reacted with cobalt(II) halides; however, the reaction with cobalt(II) thiocyanate resulted in the corresponding Co(III)-thiolate compound.<sup>7</sup> On the other hand, the slightly different ligand L<sup>2</sup>SSL<sup>2</sup> (**Scheme 5.1**) in combination with cobalt(II) thiocyanate affords the dinuclear Co(II)-disulfide complex instead of a Co(III)-thiolate complex.<sup>8</sup> These studies show that the changes in the disulfide ligand structure have a large effect on the formation of either Co(II)-disulfide complex or Co(III)-thiolate complex. However, the delicate balance between



**Scheme 5.1.** Various ligand structures reported in previous work and in the present work, along with the formula of the complexes obtained using the ligand in the present work.

Co(II)-disulfide and Co(III)-thiolate complexes has been shown to be also sensitive to alteration of the coordination environment such as addition or removal of halides, change in solvents, or the addition of external ligands.<sup>7-10</sup>

The occurrence of finite examples of Co(II)-disulfide to Co(III)-thiolate redox conversion limits our current understanding of the factors triggering these reactions. Thus, the difference in reactivity of various disulfide ligands with Co(II) salts is a point of interest for additional studies. Therefore, in the research described in this Chapter, the three ligands depicted in **Scheme 5.1** were reacted with different Co(II) salts to see whether Co(III)-thiolate complexes could be formed. The ligand  $L^{\text{mpz}}\text{SSL}^{\text{mpz}}$  was previously used in reactions with Cu(I) and Cu(II) salts and resulted in the formation of Cu(I)-disulfide and Cu(II)-disulfide complexes.<sup>11</sup> Also for  $L^3\text{SSL}^3$ , reaction with a Cu(I) salt resulted in formation of the Cu(I)-disulfide.<sup>5</sup> The ligand  $L^{\text{p}}\text{SSL}^{\text{p}}$  is new; its structure is similar to that of  $L^1\text{SSL}^1$ , the only difference being propylene instead of an ethylene bridges between the disulfide moiety and the tertiary amines on the structure. Therefore, the change in the electronic effect of the ligand  $L^{\text{p}}\text{SSL}^{\text{p}}$  compared to the ligand  $L^1\text{SSL}^1$  is minimal and its reactivity to form a Co(III)-thiolate complex is expected to be similar.

## 5.2. Results

### 5.2.1. Synthesis and Characterization of the Compounds

The ligands  $L^{\text{mpz}}\text{SSL}^{\text{mpz}}$  and  $L^3\text{SSL}^3$  were prepared following reported procedures.<sup>5, 11</sup> For the ligand  $L^{\text{p}}\text{SSL}^{\text{p}}$ , the precursor bis(3-aminopropyl)disulfide was prepared following a literature procedure,<sup>12</sup> and was obtained as slightly yellow oil in 90% yield. The oil was pure enough for further reaction as characterized with ESI-MS and <sup>1</sup>H-NMR spectroscopy (Figure AIV.1–AIV.2). The oil was used for the preparation of  $L^{\text{p}}\text{SSL}^{\text{p}}$ , which was obtained as a dark brown oil in 65% yield, was characterized with ESI-MS, <sup>1</sup>H-NMR, and <sup>13</sup>C-NMR spectroscopy (Figure AIV.3–AIV.5), and was determined to be pure enough for use in complex synthesis. The oil is stable in air for several months, although the color darkens overtime.

Addition of one equivalent of a disulfide ligand to two equivalents of a cobalt salt resulted in 69–94% yields of the cobalt(II)-disulfide complexes  $[\text{Co}_2(L^{\text{mpz}}\text{SSL}^{\text{mpz}})(\text{Br})_4]$  [**1Br**],  $[\text{Co}_2(L^{\text{mpz}}\text{SSL}^{\text{mpz}})(\text{NCS})_4]$  [**1Ncs**],  $[\text{Co}_2(L^{\text{p}}\text{SSL}^{\text{p}})(\text{NCS})_4]$  [**2Ncs**], and  $[\text{Co}_2(L^3\text{SSL}^3)\text{Cl}_4]$  [**3Cl**].

The ESI-MS spectrum of an acetonitrile solution of  $[1_{Br}]$  (Figure AIV.6), shows peaks that can be assigned to the species  $[1_{Br} - 2Br^- + HCOO^-]^+$  at  $m/z$  907.0 and  $[1_{Br} - 3Br^- + HCOO^-]^{2+}$  at  $m/z$  414.1. The ESI-MS spectrum of  $[1_{NCS}]$  dissolved in acetonitrile (Figure AIV.7) shows peaks at  $m/z$  922.1, 760.1, and 351.2 assigned to the species  $[1_{NCS} - NCS^- + HCOO^- + H^+]^+$ , and both partially reduced species  $[1_{NCS} - 3NCS^-]^+$  and  $[1_{NCS} - 4SCN^-]^{2+}$ . The ESI-MS spectrum of an acetonitrile solution of  $[2_{NCS}]$  (Figure AIV.9) show peaks corresponding to the species  $[2_{NCS} - NCS^-]^+$  at  $m/z$  836.0, and  $[2_{NCS} - 2NCS^-]^{2+}$  at  $m/z$  389.1. In the ESI-MS spectrum of an acetonitrile solution of  $[3_{Cl}]$  (Figure AIV.11) peaks are present for  $[3_{Cl} - 2Cl^- + HCOO^-]^+$ ,  $[3_{Cl} - 3Cl^- + HCOO^-]^{2+}$ , and  $[3_{Cl} - 2Cl^-]^{2+}$  at  $m/z$  805.1, 385.1, and 380.1, respectively. Solid-state magnetic susceptibility measurements for all compounds were determined using a magnetic susceptibility balance. The values of the magnetic moment calculated for two cobalt centers in  $[1_{Br}]$ ,  $[1_{NCS}]$ ,  $[2_{NCS}]$ , and  $[3_{Cl}]$  are  $5.93 \mu_B$ ,  $5.29 \mu_B$ ,  $5.43 \mu_B$ , and  $6.19 \mu_B$ , respectively, in agreement with the presence of two high-spin cobalt(II) centers in each of the compounds.<sup>13-15</sup> Furthermore,  $^1H$ -NMR spectra of  $[1_{NCS}]$ ,  $[2_{NCS}]$ , and  $[3_{Cl}]$  (Figure AIV.8, AIV.10, and AIV.12) show large upfield and downfield shifts of the peaks, ranging from  $-57$  ppm up to  $83$  ppm. All compounds were found to be analytically pure based on elemental analysis.

Compound  $[1_{Br}]$  has very limited solubility in various organic solvents, its  $^1H$ -NMR spectrum and absorption spectrum in solution could not be obtained. In DMSO the compound is moderately soluble, however, over a short period of time the blue solution turned into pink, indicating degradation of the complex. Therefore, solid-state reflectance spectrum of the blue powder of  $[1_{Br}]$  (Figure AIV.13) was obtained. It shows two relatively strong peaks at  $441$  and  $738$  nm, assigned to  $d-d$  transitions of the cobalt(II) centers. The UV-visible absorption spectra of a dark purple solution of  $[1_{NCS}]$  in acetone (Figure AIV.14), bright blue-purple acetone solution of  $[2_{NCS}]$  (Figure AIV.15), as well as pale purple acetonitrile solution of  $[3_{Cl}]$  (Figure AIV.16) generally show two peaks (**Table 5.1**), that are ascribed to the  $d-d$  transitions of Co(II) ions in a trigonal-bipyramidal geometry.<sup>16, 17</sup>

**Table 5.1.** UV-visible absorption of the cobalt complexes described in this work.

Compound	Absorption $\lambda_{\text{max}}$ in nm ( $\epsilon$ in $\text{M}^{-1} \text{cm}^{-1}$ )
[1Br]	441 (*), 738 (*)
[1NCS]	588 ( $7.4 \times 10^2$ ) 824 ( $< 100$ )
[2NCS]	520 ( $3.5 \times 10^2$ ) 615 ( $4.3 \times 10^2$ )
[3Cl]	545 ( $1.5 \times 10^2$ ) 588 ( $1.4 \times 10^2$ )

\* Solid state spectrum

### 5.2.2. Description of the Crystal Structures

Projections of the crystal structures are shown in **Figure 5.1**, selected bond distances are provided in **Table 5.2**. The crystallographic data and the complete list of bond distances and bond angles are provided in Table AIV.1–AIV.6. Compound [1Br] crystallizes in the triclinic space group *P*-1. The asymmetric unit contains one molecule of [1Br]. One of two cobalt centers in [1Br] is in a distorted trigonal-bipyramidal geometry (Co2,  $\tau_5 = 0.74$ ),<sup>18</sup> and the other in a slightly distorted octahedral geometry (Co1). Two bromide ions and three nitrogen atoms from the ligand  $\text{L}^{\text{mpz}}\text{SSL}^{\text{mpz}}$  are coordinated to each of the cobalt centers. One of the

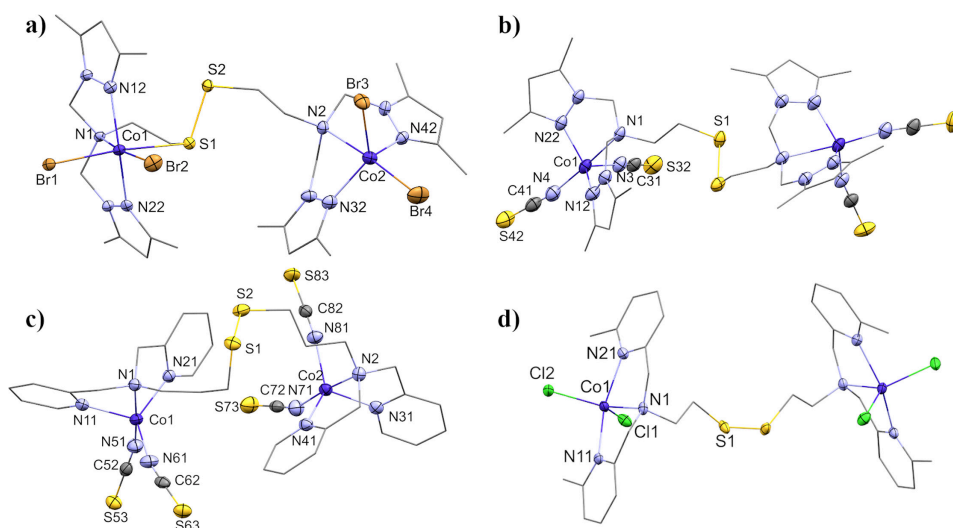


**Figure 5.1.** Projections of the structures of a) [1Br], b) [1NCS], c) [2NCS], d) [3Cl]. Displacement ellipsoids (50% probability) for all non-carbon atoms. Carbon atoms except those in  $\text{NCS}^-$  are shown as wireframe, and disordered moieties, hydrogen atoms and lattice solvent molecules are omitted for clarity.

**Table 5.2.** Selected bond distances in [1NCS], [1Br], [2NCS], and [3Cl].

Atoms	Bond distances (Å)		Atoms	Bond distances (Å)	
	[1Br]	[1NCS]		[2NCS]	[3Cl]
S1–S2	2.0454(14)	2.0396(10)	S1–S2	2.0272(9)	2.0311(12)
Co1–N1	2.264(3)	2.3701(17)	Co1–N1	2.2785(19)	2.1406(14)
Co2–N2	2.378(4)		Co2–N2	2.2337(19)	
Co1–N12	2.129(3)	2.0444(17)	Co1–N11	2.0661(19)	2.1631(14)
Co1–N22	2.060(4)	2.0400(17)	Co1–N21	2.0530(19)	2.1918(15)
Co2–N32	2.072(4)		Co2–N31	2.032(2)	
Co2–N42	2.060(4)		Co2–N41	2.0509(19)	
Co1–S1	2.6084(12)	6.0600(7)	Co1–S1	6.2951(7)	4.8457(9)
Co2–S2	6.090(1)		Co2–S2	5.6117(8)	

sulfur atoms of  $L^{mpz}SSL^{mpz}$  (S1) is coordinated to Co1, completing the octahedral geometry, with the three nitrogen donor atoms bound in a meridional fashion. The asymmetric structure of [1Br] is similar to the structures of  $[Fe_2(L^1SSL^1)Cl_4]$  and  $[Cu_2(L^{mpz}SSL^{mpz})(CH_3CN)_2(BF_4)_2]_n(BF_4)_{2n}$ .<sup>7, 11</sup> The distance between the coordinated sulfur donor to the cobalt(II) center is 2.6084(12) Å, which is slightly shorter than the Fe–S bond in  $[Fe_2(L^1SSL^1)Cl_4]$  (2.6925(8) Å) or the Cu–S bond in  $[Cu_2(L^{mpz}SSL^{mpz})(CH_3CN)_2(BF_4)_2]_n(BF_4)_{2n}$  (2.7761(8) Å).<sup>7, 11</sup> As a consequence of the binding of the sulfur donor atom to Co1, the Co1–N<sub>(pyrazole)</sub> bonds are longer than the Co2–N<sub>(pyrazole)</sub> bonds.

Compound [1NCS] crystallizes in the monoclinic space group  $C2/c$ . The asymmetric unit contains one half a molecule of [1NCS] (the other half of the dinuclear compound is generated by a two-fold rotation axis perpendicular to the S–S bond and one co-crystallized lattice acetonitrile molecule. The cobalt centers are in slightly distorted trigonal-bipyramidal geometries ( $\tau_5 = 0.91$ ),<sup>18</sup> coordinated with five nitrogen atoms, two of which are from the  $NCS^-$  ions and three from the  $L^{mpz}SSL^{mpz}$  ligand. As the disulfide atoms are not coordinated to the metal centers, the S1–S2 bond is slightly shorter in [1NCS] than in [1Br].

The asymmetric unit of [2NCS] (monoclinic space group  $P2_1/c$ ) contains one molecule of the dinuclear compound. Both cobalt centers are in a distorted trigonal-bipyramidal geometry ( $\tau_5 = 0.73$  and  $0.78$ ).<sup>18</sup> The coordination sphere of the cobalt centers is similar to those in [1NCS], comprising two nitrogen atoms from  $NCS^-$  ions and three nitrogen atoms from the ligand  $L^pSSL^p$ . Interestingly, the S1–S2 bond distance in [2NCS] is the shortest among all reported compounds in this manuscript. All other bond distances are similar to those in

reported cobalt(II)-disulfide complexes.<sup>7-9</sup> Short contacts and stacking interactions are present between pyridine moieties of neighboring molecules, with distances ranging from 3.392 Å to 3.681 Å. The  $\pi$ - $\pi$ -stacking interactions are in the parallel displaced conformation, as usually found for interactions between pyridine rings.<sup>19</sup>

Compound [3Cl] crystallizes in the monoclinic space group *I2/a*. The asymmetric unit contains one half of the dinuclear molecule (the other half is symmetrically generated *via* a twofold axis perpendicular to the S–S bond) and one lattice acetonitrile solvent molecule. The  $-(\text{CH}_2)_2\text{--S--S--}(\text{CH}_2)_2-$  is found to be disordered over three orientations, and the occupancy factors for each component of the disorder refines to 0.7596(18), 0.110(2) and 0.131(3). Two chloride ions and three nitrogen atoms of the ligand  $\text{L}^3\text{SSL}^3$  are coordinated to a cobalt center in a geometry that is in between trigonal bipyramid and a square pyramid. ( $\tau_5 = 0.56$ ).<sup>18</sup> In contrast to the other structures, where the apical positions of the trigonal bipyramid are occupied by the tertiary amine and a  $\text{Br}^-$  or  $\text{NCS}^-$  anion, in [3Cl] the apical positions are occupied by the pyridine nitrogen atoms. As a consequence, the bond distance of Co–N (tertiary amine) is shorter (2.1406(14) Å) in compound [3Cl] than in the unmethylated compound  $[\text{Co}_2(\text{L}^1\text{SSL}^1)(\text{X})_4]$ .<sup>7, 10</sup> The presence of the methyl groups on the pyridine rings causes longer Co–N(py) distances (2.1631(14) Å and 2.1918(15) Å). Longer Co–N(py) bond distances are also observed in compounds with the ligand  $\text{L}^2\text{SSL}^2$  (asymmetric methylated ligand) described in Chapter 3.<sup>20</sup> The presence of the methyl groups also causes the ligand  $\text{L}^3\text{SSL}^3$  to bind in meridional fashion. The N(py)–Co–N(py) angle is  $157.28^\circ$ , which is significantly larger than those found on non-methylated pyridine compounds  $[\text{Co}_2(\text{L}^1\text{SSL}^1)(\text{X})_4]$  (about  $116^\circ$ – $118^\circ$ ).

### 5.2.3. Reactivity of Disulfide Complexes with Exogenous Ligand 8-quinolinolate

As described in Chapters 2 and 3, several attempts have been undertaken to generate cobalt(III)-thiolate complexes by using various exogenous ligands.<sup>10, 20</sup> It was found that the anionic ligand 8-quinolinolate ( $\text{quin}^-$ ) is superior in this reaction than 2,2'-bipyridine or 1,10-phenanthroline, as the use of  $\text{quin}^-$  generally leads to much cleaner reactions.<sup>20</sup> For that reason,  $\text{quin}^-$  was utilized in attempts to convert cobalt(II)-disulfide complexes of the ligands  $\text{L}^{\text{mpz}}\text{SSL}^{\text{mpz}}$ ,  $\text{L}^{\text{p}}\text{SSL}^{\text{p}}$ , and  $\text{L}^3\text{SSL}^3$  into their corresponding cobalt(III)-thiolate complexes.

The addition of 8-quinolinol (Hquin) and  $K_2CO_3$ , to solutions containing *in situ* formed disulfide complexes of  $L^{mpz}SSL^{mpz}$ ,  $L^pSSL^p$ , and  $L^3SSL^3$  resulted in distinct color changes of the solutions. Isolation of the products resulted in three different brown solids, which initially were assumed to be the compounds  $[Co(L^{mpz}S)(quin)]Br$ ,  $[Co(L^pS)(quin)]Cl$ , and  $[Co(L^3S)(quin)]Cl$ . While the ESI-MS spectra show that the cobalt(III)-thiolate species  $[Co(L^{mpz}S)(quin)]^+$  (found  $m/z$  495.0, Figure AIV.17),  $[Co(L^pS)(quin)]^+$  (found  $m/z$  475.0, Figure AIV.18), and  $[Co(L^3S)(quin)]^+$  (found  $m/z$  489.0, Figure AIV.19) were formed, the formation of these cobalt(III)-thiolate species is not clean. In all attempts formation of at least one side product is apparent, presumably the compound  $[Co(quin)_2(CH_3CN)]^+$  (found  $m/z$  387.9). In the reaction using ligand  $L^3SSL^3$ , the cobalt(II)-disulfide species as well as free ligand are detected in the MS (See Figure AIV.19 for more details).

Other characterization techniques, such as  $^1H$ -NMR spectroscopy in methanol- $d_4$  (Figure AIV.20 – AIV.22) and determination of magnetic moments with a magnetic susceptibility balance also show that the solid compounds are not pure. The calculated magnetic moments (between 3.60 and  $2.76 \mu_B$ ) are not in agreement with low-spin cobalt(III)-thiolate complexes and confirm the presence of starting material and/or other type of cobalt(II) compounds.

### 5.3. Discussion

The different reactivity of various Co(II)-disulfide compounds is of importance, as understanding of their reactivity may provide a rationale on redox conversion reactions occurring in biology. In this Chapter it is shown that reactions of the ligands  $L^{mpz}SSL^{mpz}$  and  $L^3SSL^3$  with cobalt(II) bromide or chloride afford the expected cobalt(II)-disulfide complexes  $[1Br]$  and  $[3Cl]$ . The structure of  $[1Br]$  is unusual, as in contrast to the expected 5-coordinate geometry of the cobalt(II) ions, one of the cobalt(II) centers is in an octahedral geometry due to coordination of one of the disulfide sulfur atoms. Similar asymmetric structures were reported for  $[Fe_2(L^1SSL^1)Cl_4]$  and for the polymeric compound  $[Cu_2(L^{mpz}SSL^{mpz})(CH_3CN)_2(BF_4)_2]_n(BF_4)_{2n}$ .<sup>7, 11</sup> So far, there are only two reports on similar asymmetric compounds with cobalt(II) centers (coordination of one of disulfide sulfur atom to one cobalt, the other sulfur atom is not coordinated to any metal), in which the Co–S bond distances are 2.262 Å and 2.272 Å.<sup>21, 22</sup> Compared to those, the Co–S bond distance in compound  $[1Br]$  is the longest at 2.6084(12) Å and can be considered semi-coordinating.

Coordination of one of the disulfide sulfur atoms to cobalt in [**1<sub>Br</sub>**] causes the S–S bond as well as Co–N(pyrazole) bonds to be slightly elongated. The geometry of the cobalt(II) ions in [**3<sub>Cl</sub>**] is intermediate to the trigonal bipyramidal and square pyramidal geometries, featuring unusual meridional binding of the three nitrogen donors of the ligand possibly due to the steric repulsion of methylated pyridine groups of L<sup>3</sup>SSL<sup>3</sup>.<sup>23, 24</sup>

Reaction of cobalt(II) thiocyanate with the ligand L<sup>1</sup>SSL<sup>1</sup> has been reported to result in the formation of the corresponding Co(III)-thiolate compound [Co(L<sup>1</sup>S)(NCS)<sub>2</sub>].<sup>7</sup> However, with the ligands L<sup>mpz</sup>SSL<sup>mpz</sup> and L<sup>P</sup>SSL<sup>P</sup> the use of cobalt(II) thiocyanate does not afford the expected Co(III)-thiolate compounds but instead the dinuclear Co(II)-disulfide compounds [**1<sub>NCS</sub>**] and [**2<sub>NCS</sub>**] were formed, similar to the reactions with the ligand L<sup>2</sup>SSL<sup>2</sup>.<sup>8</sup> Based on electrochemical data, it has been suggested that the ligand L<sup>mpz</sup>SSL<sup>mpz</sup> has a stabilizing effect on the Cu(I)-disulfide system.<sup>11</sup> The stabilization of low oxidation states by the ligand L<sup>mpz</sup>SSL<sup>mpz</sup> seems to hamper formation of the Co(III)-thiolate complex starting from L<sup>mpz</sup>SSL<sup>mpz</sup>, even with the use of the strong ligand-field NCS<sup>−</sup> ion. We anticipated that the reaction of the ligand L<sup>P</sup>SSL<sup>P</sup> with Co(SCN)<sub>2</sub> would produce a cobalt(III)-thiolate complex, as the ligand L<sup>P</sup>SSL<sup>P</sup> is structurally similar to ligand L<sup>1</sup>SSL<sup>1</sup>. Possibly, the longer chain between the disulfide and tertiary amine on L<sup>P</sup>SSL<sup>P</sup> disfavors coordination of the sulfur to the cobalt center due to the formation of a six-membered chelate ring. Another explanation might be that the longer Co–S distance hampers efficient electron transfer.

Finally, we investigated the reactivity of the cobalt(II)-disulfide complexes of the ligands L<sup>mpz</sup>SSL<sup>mpz</sup>, L<sup>P</sup>SSL<sup>P</sup>, and L<sup>3</sup>SSL<sup>3</sup> with the anionic ligand 8-quinolinol (Hquin). The strong-field ligand Hquin has been described in Chapter 3 to induce conversion of Co(II)-disulfide into Co(III)-thiolate compounds with the ligands L<sup>1</sup>SSL<sup>1</sup> and L<sup>2</sup>SSL<sup>2</sup>.<sup>20</sup> It was found that quin<sup>−</sup> is able to generate a Co(III)-thiolate complex with L<sup>2</sup>SSL<sup>2</sup>, although L<sup>2</sup>SSL<sup>2</sup> structurally and electronically hampers formation of the Co(III)-thiolate complex (compared to L<sup>1</sup>SSL<sup>1</sup>). The initial results seemed to indicate that Co(III)-thiolate complexes were formed of the ligands L<sup>mpz</sup>S, L<sup>P</sup>S, and L<sup>3</sup>S. However, whereas ESI-MS of the products indeed showed the presence of the desired Co(III)-thiolate compounds, further analysis showed the presence of side products, presumably the complex [Co(quin)<sub>2</sub>(MeCN)]<sup>+</sup>. The formation of [Co(quin)<sub>2</sub>(MeCN)]<sup>+</sup> is unanticipated as stoichiometric amounts of Hquin were used. Our overall results indicate that the ligands L<sup>mpz</sup>SSL<sup>mpz</sup>, L<sup>P</sup>SSL<sup>P</sup>, and L<sup>3</sup>SSL<sup>3</sup> in



combination with Co(II) salts are less prone than  $L^1SSL^1$  or  $L^2SSL^2$  to result in Co(III)-thiolate complexes in our reaction conditions.

## 5.4. Conclusion

Four new Co(II)-disulfide complexes with the ligands  $L^{mpz}SSL^{mpz}$ ,  $L^pSSL^p$ , and  $L^3SSL^3$  were synthesized and characterized using various spectroscopic methods. The compound [**1Br**] has a rare asymmetric structure, which can be potentially explored further as it hints on the formation of Co–S bond. The structure of compound [**3Cl**] demonstrates how changes of ligand structure causes steric repulsion and consequently changes the binding mode of the ligand as well as the geometry of the complex. Furthermore, the ligand  $L^{mpz}SSL^{mpz}$  and the new ligand  $L^pSSL^p$  in combination with Co(II) thiocyanate did not result in formation of Co(III)-thiolate compounds. Reactions of cobalt(II)-disulfide complexes of the ligands  $L^{mpz}SSL^{mpz}$ ,  $L^pSSL^p$ , and  $L^3SSL^3$  with the ligand 8-quinolinol were not successful. The reactions were not clean, as indicated by the formation of one or more side products. Nevertheless, as the ESI-MS of the reactions indicated the presence of the desired Co(III)-thiolate compounds, these new Co(II)-disulfide complexes may be subjected to further study towards the formation of Co(III)-thiolate complexes by inducing a larger ligand field strength with external ligands, or by manipulating the temperature / pH of the solution.

## 5.5. Experimental section

### 5.5.1. General

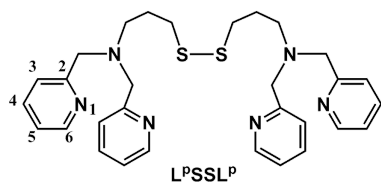
All reagents were purchased from commercial sources and used as received unless noted otherwise. Deoxygenated solvents used were obtained by the freeze-pump-thaw method followed by drying the solvents using the appropriate size of activated molecular sieves. The ligands  $L^{mpz}SSL^{mpz}$  and  $L^3SSL^3$  as well as the bis(3-aminopropyl)disulfide precursor for the ligand  $L^pSSL^p$  were prepared according to previously published procedures.<sup>5, 11, 12</sup> The synthesis of the cobalt compounds was performed using standard Schlenk-line techniques under an argon atmosphere.  $^1H$  NMR spectra were recorded on a Bruker 300 DPX spectrometer at room temperature. Mass spectra were recorded on a Thermo Scientific MSQ Plus mass spectrometer with electrospray ionization (ESI) method. Formic acid was added to the eluting solvent with the final concentration of 1% (v/v). Simulated mass spectra were generated using mMass (version 5.5.0) software.<sup>25</sup> IR spectra were obtained using a PerkinElmer Spectrum Two System equipped with Universal ATR module containing

diamond crystal for single reflection (scan range 400–4000  $\text{cm}^{-1}$ , resolution 4  $\text{cm}^{-1}$ ). Magnetic moment values were measured using a magnetic susceptibility balance (Sherwood Scientific MSB MK1) at room temperature, and the calculation of the magnetic moment follows the published procedure.<sup>26</sup> Bond distances and angles analysis of the crystal structures were performed using Mogul module on Mercury (version 4.3.1) software.<sup>27</sup> UV-visible spectra were collected using a transmission dip probe with variable path lengths and reflection probe on an Avantes AvaSpec-2048 spectrometer and using an Avalight-DH-S-Bal light source. Elemental analyses were performed by the Microanalytical Laboratory Kolbe in Germany.

### 5.5.2. Single crystal X-ray crystallography

All reflection intensities were measured at 110(2) K using a SuperNova diffractometer (equipped with Atlas detector) with either Mo  $K\alpha$  radiation ( $\lambda = 0.71073$  Å) for [**1Br**], [**2Ncs**] and [**3Cl**] or Cu  $K\alpha$  radiation ( $\lambda = 1.54178$  Å) for [**1Ncs**] under the program CrysAlisPro (Version CrysAlisPro 1.171.39.29c, Rigaku OD, 2017). The same program was used to refine the cell dimensions and for data reduction. The structure was solved with the program SHELXS-2018/3 and was refined on  $F^2$  with SHELXL-2018/3.<sup>28</sup> Numerical absorption correction based on Gaussian integration over a multifaceted crystal model was applied using CrysAlisPro for the data of [**1Br**], [**2Ncs**] and [**3Cl**]. Analytical numeric absorption correction based using a multifaceted crystal was applied using CrysAlisPro for the data of [**1Ncs**]. The temperature of the data collection was controlled using the system Cryojet (manufactured by Oxford Instruments). The H atoms were placed at calculated positions using the instructions AFIX 23, AFIX 43 or AFIX 137 with isotropic displacement parameters having values 1.2 or 1.5  $U_{\text{eq}}$  of the attached C atoms. The structures of [**1Br**] and [**2Ncs**] are ordered. The structures of [**1Ncs**] and [**3Cl**] are partly disordered. In the asymmetric unit [**1Ncs**], one site probably contains a mixture of disordered lattice solvent molecules (MeCN and Et<sub>2</sub>O), and that contribution has been removed from the final refinement using the SQUEEZE procedure in Platon.<sup>29, 30</sup>

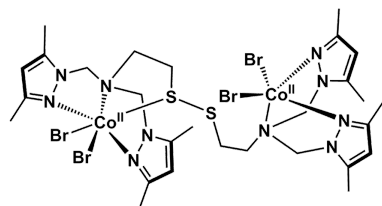
## 5.5.3. Synthesis of the compounds

**3,3'-disulfanedylbis(*N,N*-bis(pyridin-2-ylmethyl)propan-1-amine) (L<sup>p</sup>SSL<sup>p</sup>)**

Bis(3-aminopropyl)disulfide (1.8 grams, 10 mmol) was weighed into a clean round-bottom flask. The oil was dissolved in 150 mL methanol, after which 2-pyridinecarboxaldehyde (2.2 grams, 20 mmol, 2 equiv.) was added. The color of the solution quickly turned yellow. The pH of the solution was then adjusted to 5 by adding 37% HCl solution, and the solution was stirred overnight. Afterwards, NaCNBH<sub>3</sub> (1.5 grams, 23.8 mmol, 2.38 equiv.) was added in two portions. The color of the solution initially turned orange, then turned turbid to lighter yellow. The solution was stirred for another two days, then quenched by adding 37% HCl until pH 1. Methanol was removed by rotary evaporator, resulting in a yellow solution. This yellow solution was mixed with 75 mL 10 M NaOH, stirred for 30 minutes, resulting in a pale yellow solution with orange oil. The solution and oil were extracted with 3x100 mL CHCl<sub>3</sub>. The organic layer was collected and dried over MgSO<sub>4</sub>. The mixture was filtered and the solution was concentrated under reduced pressure to give a yellow oil. The yellow oil was redissolved in 75 mL methanol, followed by addition of 2-pyridinecarboxaldehyde (2.2 grams, 20 mmol, 2 equiv.). The pH of the solution was adjusted to 5 and the color of the solution changed to dark red. The solution was stirred for one hour. Subsequently, NaCNBH<sub>3</sub> (1.5 grams, 23.8 mmol, 2.38 equiv.) was added in two portions over the course of 30 minutes. The solution was stirred overnight, and subsequently quenched with 37% HCl until pH 1. The solution was then concentrated using a rotary evaporator, resulting in the formation of a red oil. The oil was treated with 75 mL NaOH 10 M and extracted with CHCl<sub>3</sub> (3x100mL). The organic layer was collected, dried over MgSO<sub>4</sub>, and filtered. The solution was concentrated and a red oil was formed. The red oil was cooled in an ice bath, and dropwise addition of 10 mL 70% HClO<sub>4</sub> resulted in a dark brown oil. Absolute ethanol (300 mL) was added to the oil, and the mixture was stirred for 3 hours. The ethanol was decanted and the remaining oil was converted to the free base form by addition of 50 mL NaOH 10 M. The solution was again extracted with CHCl<sub>3</sub> (3x100mL). The organic layer was collected, dried, and filtered. Removal of the CHCl<sub>3</sub> under reduced pressure yielded the final product as a dark brown oil (3.5 g, 64% yield). ESI-MS found (calcd.) for [L<sup>p</sup>SSL<sup>p</sup> + H]<sup>+</sup> *m/z* 545.2 (545.2), for

$[\text{L}^{\text{P}}\text{SSL}^{\text{P}} + 2\text{H}]^{2+}$   $m/z$  273.2 (273.1).  $^1\text{H}$ -NMR (300 MHz,  $\text{CD}_3\text{CN}$ , RT)  $\delta(\text{ppm})$ : 1.75-1.84 (qu, 4H, N-CH<sub>2</sub>-CH<sub>2</sub>-CH<sub>2</sub>-S), 2.52-2.62 (dt, 8H, N-CH<sub>2</sub>-CH<sub>2</sub>-CH<sub>2</sub>-S), 3.73 (s, 8H, N-CH<sub>2</sub>-Py), 7.15-7.19 (ddd, 4H, Py-H<sub>3</sub>), 7.49-7.51 (d, 4H, Py-H<sub>5</sub>), 7.65-7.71 (td, 4H, Py-H<sub>4</sub>), 8.44-8.47 (m, 4H, Py-H<sub>6</sub>).  $^{13}\text{C}$ -NMR (75 MHz,  $\text{CD}_3\text{CN}$ , RT)  $\delta(\text{ppm})$ : 26.62 (N-CH<sub>2</sub>-CH<sub>2</sub>-CH<sub>2</sub>-S), 35.63 (N-CH<sub>2</sub>-CH<sub>2</sub>-CH<sub>2</sub>-S), 51.93 (N-CH<sub>2</sub>-CH<sub>2</sub>-CH<sub>2</sub>-S), 59.71 (N-CH<sub>2</sub>-Py), 120.36 (Py-C<sub>5</sub>), 124.02 (Py-C<sub>3</sub>), 136.29 (Py-C<sub>4</sub>), 148.81 (Py-C<sub>6</sub>), 161.28 (Py-C<sub>2</sub> (quarternary carbon)).

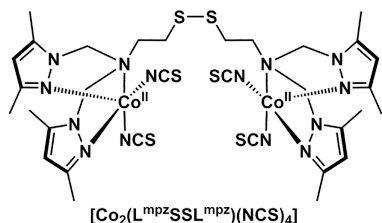
**$[\text{Co}_2(\text{L}^{\text{mpz}}\text{SSL}^{\text{mpz}})(\text{Br})_4]$  (**1<sub>Br</sub>**)**



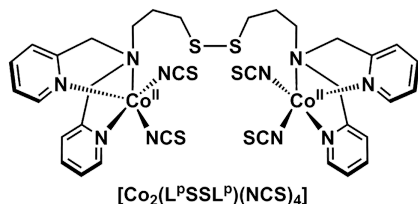
**$[\text{Co}_2(\text{L}^{\text{mpz}}\text{SSL}^{\text{mpz}})(\text{Br})_4]$**

Ligand  $\text{L}^{\text{mpz}}\text{SSL}^{\text{mpz}}$  (330.0 mg, 0.564 mmol) was dissolved in 5 mL dry and deoxygenated acetonitrile, resulting in a clear solution. Into the solution, solid  $\text{CoBr}_2$  (249.6 mg, 1.129 mmol) was added. An intense blue solution and some blue precipitates were immediately formed, but the mixture was stirred

further for one hour. After one hour, the mixture was concentrated until approximately 1 mL was left in the flask. Into this mixture, diethyl ether was added, resulting in the formation of a blue precipitate. The precipitate was collected by filtration, washed twice with diethyl ether, dried *in vacuo*, then collected and weighed. Yield = 508.3 mg (88%) of an intense blue powder. Blue needle-shaped single crystals suitable for X-Ray diffraction were obtained using vapor diffusion of diethyl ether into a solution of **1<sub>Br</sub>** in methanol (although it is very poorly soluble in methanol). IR (neat,  $\text{cm}^{-1}$ ): 2955w, 2921w, 1551s, 1467s, 1419s, 1386s, 1372s, 1337m, 1320m, 1300m, 1279s, 1243m, 1176w, 1147m, 1133m, 1106s, 1043s, 1015m, 982m, 948m, 905w, 863m, 825m, 812m, 800m, 783s, 762m, 717w, 688w, 662w, 633w, 626m, 613m, 597w, 581w, 555w, 521w, 491w, 471w, 451m, 406m. ESI-MS found / calcd. for  $[\text{1Br} - 2\text{Br}^- + \text{HCOO}^-]^+$   $m/z$  907.0 (907.02), for  $[\text{1Br} - 3\text{Br}^- + \text{HCOO}^-]^{2+}$   $m/z$  414.1 (413.5). Elemental analysis (%) for **1<sub>Br</sub>** ( $\text{C}_{28}\text{H}_{44}\text{Co}_2\text{S}_2\text{N}_{10}\text{Br}_4$ ) + 0.7 $\text{H}_2\text{O}$ , calcd. C, 32.50; H, 4.42; N, 13.53; found C, 32.50; H, 4.42; N, 13.50.

**[Co<sub>2</sub>(L<sup>mpz</sup>SSL<sup>mpz</sup>)(NCS)<sub>4</sub>] ([1<sub>NCS</sub>])**

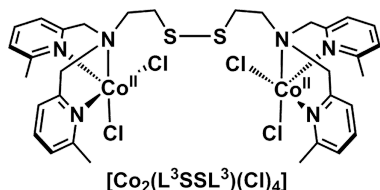
The synthesis procedure of [1<sub>NCS</sub>] is similar to that of [1<sub>Br</sub>], using Co(SCN)<sub>2</sub> instead of CoBr<sub>2</sub>. The solution of ligand L<sup>mpz</sup>SSL<sup>mpz</sup> (320.0 mg, 0.547 mmol) was mixed with Co(SCN)<sub>2</sub> (191.6 mg, 1.094 mmol, 2 equiv.). Yield = 481.4 mg (94%). Purple single crystals suitable for X-Ray diffraction were obtained using vapor diffusion of diethyl ether into a concentrated solution of [1<sub>NCS</sub>] in acetonitrile. IR (neat, cm<sup>-1</sup>): 2922vw, 2059vs, 1615vw, 1550s, 1466s, 1418s, 1387s, 1335m, 1299s, 1279m, 1259m, 1242m, 1230m, 1171w, 1130m, 1104s, 1053s, 1038s, 987m, 855m, 814s, 692w, 660w, 627w, 597w, 559w, 516w, 496vw, 476m, 449w, 407vw. ESI-MS found (calcd.) for [1<sub>NCS</sub> – NCS<sup>-</sup> + HCOOH]<sup>+</sup> *m/z* 922.1 (922.1), for [1<sub>NCS</sub> – 3NCS<sup>-</sup>]<sup>+</sup> (partial reduction from the ESI-MS) *m/z* 760.1 (760.16), and for [1<sub>NCS</sub> – 4SCN<sup>-</sup>]<sup>2+</sup> (partial reduction from the ESI-MS) *m/z* 351.09 (351.1). Elemental analysis (%) for [1<sub>NCS</sub>] (C<sub>32</sub>H<sub>44</sub>Co<sub>2</sub>S<sub>6</sub>N<sub>14</sub>) + 1.3H<sub>2</sub>O, calcd. C, 40.10; H, 4.90; N, 20.46; found C, 40.05; H, 4.86; N, 20.46.

**[Co<sub>2</sub>(L<sup>p</sup>SSL<sup>p</sup>)(NCS)<sub>4</sub>] ([2<sub>NCS</sub>])**

The dark brown oil of L<sup>p</sup>SSL<sup>p</sup> (54.5 mg, 0.1 mmol) was added to a Schlenk flask, followed by 5 mL dry and deoxygenated methanol to dissolve the oil. Solid Co(SCN)<sub>2</sub> (35.0 mg, 0.2 mmol, 2 equiv.) was added to the resulting brown solution, affording a blue-colored solution. The blue-colored solution was stirred for two hours. After two hours, the solution was concentrated until approximately 1 mL was left in the flask. Diethyl ether was added into the flask upon which a blue-purple precipitate was formed. The precipitate was filtered, washed twice with diethyl ether, followed by drying under vacuum, and weighed. Yield = 65.5 mg (73%). Dark purple single crystals suitable for X-Ray diffraction were grown using vapor diffusion of diethyl ether into the solution of [2<sub>NCS</sub>] in acetonitrile. IR (neat, cm<sup>-1</sup>): 2597vw, 2070vs, 2043s, 1607m, 1570w, 1479m, 1462w, 1443m, 1361w, 1286m, 1246w, 1222w, 1181w, 1156m, 1098m, 1054m, 1027m, 970w, 954m, 903w, 839w, 825w, 769s, 732m, 651m, 550w, 477m, 417m. ESI-MS found / calcd. for [2<sub>NCS</sub> – NCS<sup>-</sup>]<sup>+</sup>

$m/z$  836.0 (836.0), for  $[\mathbf{2NCS} - 2\text{NCS}]^{2+}$   $m/z$  389.1 (389.0). Elemental analysis (%) for  $[\mathbf{2NCS}]$  ( $\text{C}_{34}\text{H}_{36}\text{Co}_2\text{S}_6\text{N}_{10}$ ) + 0.5 $\text{C}_4\text{H}_{10}\text{O}$  (diethyl ether), calcd. C, 46.39; H, 4.43; N, 15.03; found C, 46.58; H, 4.09; N, 15.02.

#### $[\text{Co}_2(\text{L}^3\text{SSL}^3)(\text{Cl})_4]$ ( $[\mathbf{3Cl}]$ )



In a Schlenk flask, the ligand  $\text{L}^3\text{SSL}^3$  (57.3 mg, 0.1 mmol) was dissolved in 3 mL dry and deoxygenated methanol, after which solid anhydrous  $\text{CoCl}_2$  (25.9 mg, 0.2 mmol, 2 equiv.) was added. The purple solution was initially clear, but overtime a

precipitate formed. The solution was stirred for one hour. Concentration of the solution followed by addition of diethyl ether afforded a purple precipitate. The precipitate was filtered, washed twice with diethyl ether, then dried in vacuo and weighed. Yield = 57.1 mg (69%). Purple single crystals suitable for X-Ray diffraction were obtained using vapor diffusion of diethyl ether into the solution of  $[\mathbf{3Cl}]$  in acetonitrile. IR (neat,  $\text{cm}^{-1}$ ): 3674vw, 3543w, 3477w, 2987m, 2903m, 1636w, 1605s, 1575m, 1456s, 1393w, 1377m, 1346m, 1294w, 1269w, 1241w, 1221w, 1162m, 1093s, 1049m, 1011s, 963w, 909w, 896w, 874m, 792vs, 758m, 718w, 653vw, 562w, 550w, 531w, 476m, 450w, 435w, 413w. ESI-MS found (calcd.) for  $[\mathbf{3Cl} - 2\text{Cl}^- + \text{HCOO}^-]^{+}$   $m/z$  805.1 (805.08), for  $[\mathbf{3Cl} - 3\text{Cl}^- + \text{HCOO}^-]^{2+}$   $m/z$  385.1 (385.1), and for  $[\mathbf{3Cl} - 2\text{Cl}^-]^{2+}$   $m/z$  380.1 (380.04). Elemental analysis (%) for  $[\mathbf{3Cl}]$  ( $\text{C}_{32}\text{H}_{40}\text{Co}_2\text{S}_2\text{N}_6\text{Cl}_4$ ) + 0.5 $\text{H}_2\text{O}$ , calcd. C, 45.67; H, 4.91; N, 9.99; found C, 45.61; H, 4.78; N, 9.99.

#### 5.5.4. Reactivity of Co(II)-disulfide complexes with 8-quinolinol

In a typical reaction in a Schlenk flask under argon atmosphere, 0.2 mmol of ligand ( $\text{L}^{\text{mpz}}\text{SSL}^{\text{mpz}}$ ,  $\text{L}^{\text{p}}\text{SSL}^{\text{p}}$ , or  $\text{L}^3\text{SSL}^3$ ) was dissolved in 5 mL dry and deoxygenated methanol. To the solution, 0.4 mmol (2 equiv.) of anhydrous  $\text{CoX}_2$  ( $\text{X}=\text{Br}$  for  $\text{L}^{\text{mpz}}\text{SSL}^{\text{mpz}}$ ,  $\text{X}=\text{Cl}$  for  $\text{L}^{\text{p}}\text{SSL}^{\text{p}}$  and  $\text{L}^3\text{SSL}^3$ ) was added to generate the Co(II)-disulfide complexes  $[\text{Co}_2(\text{L}^{\text{mpz}}\text{SSL}^{\text{mpz}})(\text{Br})_4]$  ( $[\mathbf{1Br}]$ ),  $[\text{Co}_2(\text{L}^{\text{p}}\text{SSL}^{\text{p}})(\text{Cl})_4]$  ( $[\mathbf{2Cl}]$ ) or  $[\text{Co}_2(\text{L}^3\text{SSL}^3)(\text{Cl})_4]$  ( $[\mathbf{3Cl}]$ ). The solution was stirred for an hour at room temperature, after which 8-quinolinol (Hquin, 0.4 mmol, 2 equiv. to the ligand) was added along with 0.4 mmol of anhydrous  $\text{K}_2\text{CO}_3$ . In all attempts the solution turned dark brown immediately. The solution was stirred overnight under argon atmosphere,

resulting in a formation of white precipitates (presumably KX salt or unreacted  $K_2CO_3$ ). The solution was filtered into a Schlenk flask under argon using a syringe filter. The filtrate was concentrated under vacuum until approximately 1 mL of solvent was left in the flask. Into this concentrated solution, 12 mL of diethyl ether was added to precipitate the complex as a brown powder. The excess of diethyl ether in the solution was removed by filtration, and the powder was washed with diethyl ether twice or until the color of the solution remained transparent. Subsequent drying of the product in vacuo afforded brown powders, which were presumed to be  $[Co(L^{mpzS})(quin)]Br$ ,  $[Co(L^PS)(quin)]Cl$ , or  $[Co(L^3S)(quin)]Cl$  with the yield of 159 mg, 113 mg, and 83 mg, respectively. The products were further characterized with ESI-MS,  $^1H$ -NMR spectroscopy, and with a magnetic susceptibility balance. The ESI-MS spectra and  $^1H$ -NMR spectra can be found on Appendix AIV.17 – AIV.22.

## 5.6. References

1. Nakamura, H., Nakamura, K. and Yodoi, J. *Annu. Rev. Immunol.* **1997**, 15, 351-369.
2. Ragsdale, S. W. and Yi, L. *Antioxid. Redox Signal.* **2011**, 14 (6), 1039-1047.
3. Wouters, M. A., Fan, S. W. and Haworth, N. L. *Antioxid. Redox Signal.* **2010**, 12 (1), 53-91.
4. Xiao, Z., La Fontaine, S., Bush, A. I. and Wedd, A. G. *J. Mol. Biol.* **2019**, 431 (2), 158-177.
5. Itoh, S., Nagagawa, M. and Fukuzumi, S. *J. Am. Chem. Soc.* **2001**, 123 (17), 4087-4088.
6. Ueno, Y., Tachi, Y. and Itoh, S. *J. Am. Chem. Soc.* **2002**, 124 (42), 12428-12429.
7. Jiang, F., Siegler, M. A., Sun, X., Jiang, L., Fonseca Guerra, C. and Bouwman, E. *Inorg. Chem.* **2018**, 57 (15), 8796-8805.
8. Jiang, F., Marvelous, C., Verschuur, A. C., Siegler, M. A., Teat, S. J. and Bouwman, E. *Inorg. Chim. Acta* **2022**, 120880.
9. Gennari, M., Gerey, B., Hall, N., Pecaut, J., Collomb, M.-N., Rouzies, M., Clerac, R., Orio, M. and Duboc, C. *Angew. Chem. Int. Ed.* **2014**, 53 (21), 5318-5321.
10. Marvelous, C., de Azevedo Santos, L., Siegler, M. A., Fonseca Guerra, C. and Bouwman, E. *Dalton Trans.* **2022**, 51, 8046-8055.
11. Ording-Wenker, E. C. M., Siegler, M. A. and Bouwman, E. *Inorg. Chim. Acta* **2015**, 428, 193-202.
12. Doi, J. T. and Musker, W. K. *J. Org. Chem.* **2002**, 50 (1), 1-4.
13. Dori, Z. and Gray, H. B. *Inorg. Chem.* **1968**, 7 (5), 889-&.
14. Mulyana, Y., Alley, K. G., Davies, K. M., Abrahams, B. F., Moubaraki, B., Murray, K. S. and Boskovic, C. *Dalton Trans.* **2014**, 43 (6), 2499-2511.
15. Suzuki, M., Kanatomi, H. and Murase, I. *Bull. Chem. Soc. Jpn.* **1984**, 57 (1), 36-42.
16. Chan, S. L.-F., Lam, T. L., Yang, C., Lai, J., Cao, B., Zhou, Z. and Zhu, Q. *Polyhedron* **2017**, 125, 156-163.
17. Massoud, S. S., Broussard, K. T., Mautner, F. A., Vicente, R., Saha, M. K. and Bernal, I. *Inorg. Chim. Acta* **2008**, 361 (1), 123-131.
18. Addison, A. W., Rao, T. N., Reedijk, J., Vanrijn, J. and Verschoor, G. C. *J. Chem. Soc., Dalton Trans.* **1984**, (7), 1349-1356.
19. Janiak, C. *J. Chem. Soc., Dalton Trans.* **2000**, (21), 3885-3896.
20. Marvelous, C., de Azevedo Santos, L., Siegler, M. A., Fonseca Guerra, C. and Bouwman, E. **2022**, submitted
21. Lydon, J. D., Elder, R. C. and Deutsch, E. *Inorg. Chem.* **2002**, 21 (8), 3186-3197.
22. Nosco, D. L., Elder, R. C. and Deutsch, E. *Inorg. Chem.* **1980**, 19 (9), 2545-2551.

- 
23. Graddon, D. P., Watton, E. C., Schulz, R. and Weeden, D. G. *Nature* **1963**, 198 (4887), 1299-&.
  24. Nagao, H., Komeda, N., Mukaida, M., Suzuki, M. and Tanaka, K. *Inorg. Chem.* **1996**, 35 (23), 6809-6815.
  25. Strohalm, M., mMass - Open Source Mass Spectrometry Tool. [www.mmass.org](http://www.mmass.org)
  26. Bain, G. A. and Berry, J. F. *J. Chem. Educ.* **2008**, 85 (4), 532-536.
  27. Macrae, C. F., Sovago, I., Cottrell, S. J., Galek, P. T. A., McCabe, P., Pidcock, E., Platings, M., Shields, G. P., Stevens, J. S., Towler, M. and Wood, P. A. *J. Appl. Crystallogr.* **2020**, 53, 226-235.
  28. Sheldrick, G. M. *Acta Crystallogr. Sect. A: Found. Crystallogr.* **2008**, 64, 112-122.
  29. Spek, A. L. *Acta Crystallogr. Sect. C: Cryst. Struct. Commun.* **2015**, 71 (Pt 1), 9-18.
  30. Spek, A. L. *Acta Crystallogr. Sect. D. Biol. Crystallogr.* **2009**, 65 (2), 148-155.





# Chapter 6

---

Summary, Conclusions, and Outlook

## 6.1. Summary

### 6.1.1. Introduction

Investigations of synthetic models of active sites of enzymes have provided a great deal of understanding in chemical processes occurring in enzymes, such as the catalytic mechanisms or the role of a specific moiety in these active sites.<sup>1-8</sup> During such investigations, some new and unprecedented reactivity of synthetic models are often discovered. One of the many interesting types of reactivity encountered in the last two decades concerns the redox interaction of a disulfide ligand with transition metal ions. The redox interaction can be fine-tuned to change the redox state of the sulfur ligand as well as the transition metal ions, in what is now known as a redox-conversion reaction.<sup>9, 10</sup> These redox-conversion reactions are important as they may shed light on electron-transfer reactions that often occur in Nature.

Despite their importance, so far only a handful of studies have been reported on the redox-conversion reaction of metal-disulfide and metal-thiolate complexes. The majority of these studies were focused on copper-based disulfide/thiolate conversion.<sup>9-16</sup> Recently, several examples of the redox-conversion reaction have emerged concerning cobalt(II)-disulfide and cobalt(III)-thiolate complexes.<sup>17-19</sup> Much like copper-based systems, the cobalt-based disulfide/thiolate conversion is governed by small changes in the coordination environment, though more examples are needed in order to understand the reaction mechanism. In Chapter 1, an extensive discussion concerning the state-of-the-art in redox-conversion reactions is given.

### 6.1.2. The Importance of Ligand-Field Strength and Ligand Orientation on Redox-conversion of Co(II)-disulfide to Co(III)-thiolate Complexes

In spite of a number of recent examples of cobalt(II)-disulfide to cobalt(III)-thiolate redox-conversion reactions,<sup>17-19</sup> there is limited understanding on how the coordination environment of the metal ion affects this reaction. In Chapters 2 and 3, results are described of our pursuit of understanding the reaction by focusing on the ligand-field strength of the auxiliary ligands used. For this purpose the ligands 2,2'-bipyridine (bpy) and 8-quinolinolate (quin<sup>-</sup>) were used, both being considered to be strong-field ligands. In addition, the negative charge on the ligand quin<sup>-</sup> may help stabilizing the positive charge on the cobalt(III)-thiolate complex.

In Chapter 2 is described how addition of bpy to the cobalt(II)-disulfide compound  $[\text{Co}_2(\text{L}^1\text{SSL}^1)(\text{Cl})_4]$  led to the formation of the cobalt(III)-thiolate species  $[\text{Co}(\text{L}^1\text{S})(\text{bpy})]^{2+}$ . However, formation of the side products  $[\text{Co}_2(\text{L}^1\text{SSL}^1)(\text{bpy})_2(\text{Cl})_2](\text{Cl})_2$  and  $[\text{Co}(\text{bpy})_3]^{n+}$  was also observed, which was not expected.<sup>20</sup> In Chapter 3 it is shown that a reaction with  $\text{quin}^-$  leads to the product  $[\text{Co}(\text{L}^1\text{S})(\text{quin})]^+$  in almost quantitative yield without having to remove the chloride ligands.<sup>21</sup> Furthermore, use of the ligand  $\text{quin}^-$  resulted in the successful conversion of the cobalt(II)-disulfide complex  $[\text{Co}_2(\text{L}^2\text{SSL}^2)(\text{Cl})_4]$ . Several attempts of using the ligand  $\text{L}^2\text{SSL}^2$  with cobalt(II) in the redox-conversion reaction have been reported, but so far formation of its Co(III)-thiolate complex was elusive. However, in this case also a side product was unexpectedly found, namely  $[\text{Co}_2(\text{L}^2\text{SSL}^2)(\text{quin})_2(\text{Cl})_2]$ .

Nevertheless, the formation and the crystal structure of these side products convey valuable insight on how the conversion of the cobalt(II)-disulfide to a cobalt(III)-thiolate compound proceeds. In the structure of the side product  $[\text{Co}_2(\text{L}^1\text{SSL}^1)(\text{bpy})_2(\text{Cl})_2]^{2+}$  the nitrogen donors of  $\text{L}^1\text{SSL}^1$  are in a facial arrangement, hampering the approach of the disulfide group to the cobalt center. In contrast, in the structure of  $[\text{Co}_2(\text{L}^2\text{SSL}^2)(\text{quin})_2(\text{Cl})_2]$  the nitrogen donor atoms of  $\text{L}^2\text{SSL}^2$  are in a meridional orientation, which allows for the disulfide to approach the cobalt center for an efficient electron transfer.

DFT calculations were employed to estimate ligand-field strength of the ligands in the compounds. Molecular orbital analyses show that the estimated  $d$ -orbital splitting energy of a simplified Co(II)-disulfide species is definitively smaller than those of the Co(III)-thiolate complexes. The estimated  $d$ -orbital splitting energy of  $[\text{Co}(\text{L}^1\text{S})(\text{bpy})]^{2+}$  appears to be smaller than that of  $[\text{Co}(\text{L}^1\text{S})(\text{MeCN})_2]^{2+}$ , suggesting that bpy exerts a smaller ligand-field splitting than acetonitrile.<sup>20</sup> Apart from the fact that an excess of acetonitrile is present in the reaction, this result may account for the formation of side products when bpy is employed. The estimated  $d$ -orbital splitting energy for the complex  $[\text{Co}(\text{L}^1\text{S})(\text{quin})]^+$  appears to be slightly larger than that of  $[\text{Co}(\text{L}^1\text{S})(\text{bpy})]^{2+}$ , in agreement with the experimental results. Comparison of the estimated  $d$ -orbital splitting of  $[\text{Co}(\text{L}^1\text{S})(\text{quin})]^+$  and  $[\text{Co}(\text{L}^2\text{S})(\text{quin})]^+$  indicated that the ligand  $\text{L}^2\text{SSL}^2$  exerts a weaker ligand field than  $\text{L}^1\text{SSL}^1$ . Despite the electron-donating effect, *ortho*-methylation of pyridine groups on  $\text{L}^2\text{SSL}^2$  has been reported to reduce the donor ability of the pyridine nitrogen, mostly because of steric hindrance, causing larger metal-nitrogen distances, and thus smaller ligand-field splitting.<sup>9, 18, 20</sup>

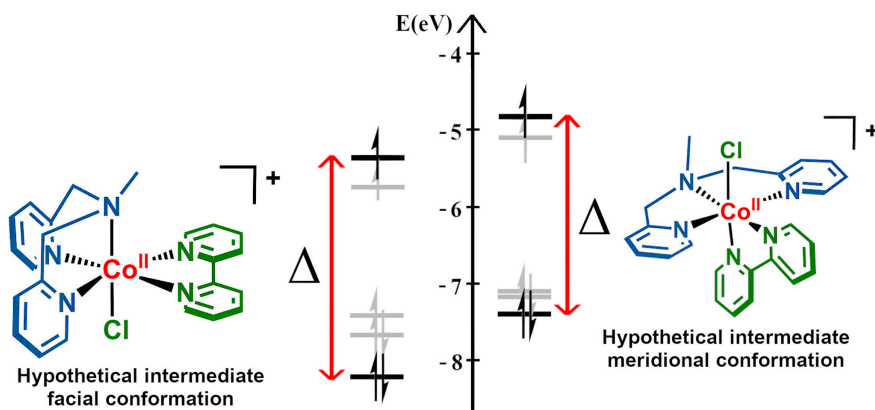


**Figure 6.1.** Simplified energy diagrams showing the destabilization of the highest SOMO level of the hypothetical intermediate in meridional geometry compared to facial geometry.

The results described in Chapters 2 and 3 reveal that the orientation of the disulfide ligand and the auxiliary ligand also affect the redox conversion.<sup>20, 21</sup> In Chapter 2, the auxiliary ligand bpy is a symmetrical bidentate ligand and thus only the binding mode of the disulfide ligand was investigated using computational methods. It was found that the highest SOMO level of the hypothetical intermediate compound with the nitrogen donor atoms of the disulfide ligand in meridional conformation is more destabilized than that of the facial isomer that was found in the crystal structure (**Figure 6.1**). This indicates that electron transfer from Co to S should be more facile when the nitrogen donor atoms of the ligand  $L^1S$  are in meridional arrangement. In contrast, the ligand  $quin^-$  used in Chapter 3 is asymmetric and therefore its binding mode to cobalt was investigated. The complex  $[Co(L^1S)(quin)]^+$  is more stable energetically when the negatively charged oxygen is *trans* to the sulfur donor than when it is *trans* to the tertiary amine nitrogen. Quantum chemical analyses showed that the coordination of the oxygen of  $quin^-$  opposite to sulfur atom of ligand  $L^1S$  benefits from more electrostatic interaction between the aromatic rings of  $quin^-$  and the positively charged  $[Co(L^1S)]^{2+}$  fragment.

### 6.1.3. Resemblance of Selenium and Sulfur in The Redox-conversion Reaction

We expanded the scope of our study to selenium, which is known to have similar properties to sulfur, especially in its redox reactions.<sup>22, 23</sup> The first redox-conversion reaction for a Co(II)-diselenide to Co(III)-selenolate compounds is described in Chapter 4. The

Co(II)-diselenide compound  $[\text{Co}_2(\text{L}^1\text{SeSeL}^1)(\text{Cl})_4]$  was obtained using the ligand  $\text{L}^1\text{SeSeL}^1$ , a new ligand analogous with the ligand  $\text{L}^1\text{SSL}^1$  described in Chapters 2 and 3. The spectroscopic properties of the Co(II)-diselenide compound  $[\text{Co}_2(\text{L}^1\text{SeSeL}^1)(\text{Cl})_4]$  resemble those of the disulfide analog  $[\text{Co}_2(\text{L}^1\text{SSL}^1)(\text{Cl})_4]$ . Formation of Co(III)-selenolate compounds was achieved from the reaction of  $\text{L}^1\text{SeSeL}^1$  with  $\text{Co}(\text{SCN})_2$  yielding  $[\text{Co}(\text{L}^1\text{Se})(\text{NCS})_2]$ , by removal of chloride ions from  $[\text{Co}_2(\text{L}^1\text{SeSeL}^1)(\text{Cl})_4]$  in an acetonitrile solution resulting in  $[\text{Co}(\text{L}^1\text{Se})(\text{MeCN})_2]^{2+}$ , or upon addition of  $\text{quin}^-$  to  $[\text{Co}_2(\text{L}^1\text{SeSeL}^1)(\text{Cl})_4]$  giving  $[\text{Co}(\text{L}^1\text{Se})(\text{quin})]^+$ ; these products resemble the thiolate analogs described in Chapters 2 and 3. However, it appeared that the cobalt(III)-selenolate compounds are rather unstable in solution. DFT calculations indicate that the selenolate donor atom exerts a smaller ligand-field splitting than the thiolate donor atom. In combination with the knowledge acquired in Chapters 2 and 3, the results indicate that the conversion of Co(II)-diselenide to Co(III)-selenolate is not much more difficult to achieve than for the sulfur analogs, but that the selenolate products are less stable in solution. These results show how selenium and sulfur resemble each other in the redox-conversion reaction, but also highlights the differences, which may be relevant to consider for further studies regarding the kinetics of the reaction.

#### 6.1.4. Ligand Modification and Stabilization of Co(III)-thiolate Complexes

In Chapter 5 the results are described of the use of three different disulfide ligands in attempts to obtain Co(III)-thiolate compounds. In the ligand  $\text{L}^3\text{SSL}^3$  all four pyridine groups of the parent ligand  $\text{L}^1\text{SSL}^1$  are methylated, while the ligand  $\text{L}^p\text{SSL}^p$  resembles  $\text{L}^1\text{SSL}^1$  but has two propylene groups between the tertiary amines and the disulfide groups. The ligand  $\text{L}^{\text{mpz}}\text{SSL}^{\text{mpz}}$  is significantly different from  $\text{L}^1\text{SSL}^1$ , as it contains dimethylpyrazole instead of pyridine groups.

A number of Co(II)-disulfide compounds with these three different ligands were isolated and characterized. The compound  $[\text{Co}_2(\text{L}^{\text{mpz}}\text{SSL}^{\text{mpz}})(\text{Br})_4]$  surprisingly revealed asymmetric coordination of the ligand; one of the disulfide sulfur donor atoms is coordinated to one of the cobalt centers, while the other sulfur donor atom does not coordinate. Reaction of the ligand  $\text{L}^{\text{mpz}}\text{SSL}^{\text{mpz}}$  with  $\text{Co}(\text{SCN})_2$  affords cobalt(II)-disulfide compound  $[\text{Co}_2(\text{L}^{\text{mpz}}\text{SSL}^{\text{mpz}})(\text{NCS})_4]$ , indicating that the ligand-field strength of the pyrazole ligand is

too low to be overcome with the relatively strong-field anions. Unexpectedly, also the reaction of  $L^pSSL^p$  with  $Co(SCN)_2$  resulted in a cobalt(II)-disulfide compound.

Using the knowledge gained from the previous Chapters, attempts were undertaken to form Co(III)-thiolate complexes of the ligand  $L^{mpz}SSL^{mpz}$ ,  $L^pSSL^p$ , and  $L^3SSL^3$  by the addition of  $quin^-$ . The formation of Co(III)-thiolate complexes seemed to be successful as in ESI-MS spectra peaks were present that could be assigned to the expected products. However, in almost all attempts at least one side product was formed, and it appeared not possible to isolate the expected thiolate compounds. Overall, the results indicate that the ligand-field strength of  $L^{mpz}SSL^{mpz}$ ,  $L^pSSL^p$ , and  $L^3SSL^3$  is not large enough to be able to convert the Co(II)-disulfide compounds to the corresponding Co(III)-thiolate redox isomers.

## 6.2. Conclusions and Outlook

Up until now, to the best of our knowledge only three reports describe the redox-conversion of Co(II)-disulfide to Co(III)-thiolate complexes.<sup>17-19</sup> The research field is extended further by some examples that are described in this thesis. From the Co(II)-disulfide and Co(III)-thiolate as well as the Co(II)-diselenide and Co(III)-selenolate complexes that we have investigated, several conclusions can be drawn.

1. The disulfide ligand is the foremost factor in regulating the redox conversion of Co(II)-disulfide and Co(III)-thiolate complexes. Small changes in the disulfide ligand structure have an immense effect on the reactivity of the corresponding Co(II)-disulfide complexes due to steric and ligand-field effects.
2. Inducing an increase in the ligand-field strength of the disulfide ligand most likely will enable the conversion to corresponding Co(III)-thiolate complexes. A smaller ligand-field effect can be counterbalanced by the use of auxiliary ligands that exert strong ligand field.
3. The cleanliness of the redox conversion of Co(II)-disulfide to Co(III)-thiolate complexes is determined by the magnitude of the overall ligand-field splitting energy of the complex, the charge of the exogenous ligand, the arrangement of the ligands in the first coordination sphere of the complex, and the formation constant of side products relative to that of the Co(III)-thiolate complex.

In the research described in this thesis we have employed computational methods in order to estimate the ligand-field strength of the various ligands in a qualitative manner. The DFT computations revealed that the molecular orbitals are a mixture of metal *d*-orbitals and ligand orbitals. Our qualitative picture of the estimated ligand-field splitting has been valuable for understanding the experimental findings.

So far, examples are not known on the effect of addition or removal of protons on the redox conversion of Co(II)-disulfide and Co(III)-thiolate compounds, nor on the influence of temperature in these reactions. Using our current knowledge, it is expected that addition of protons will change the coordinating ability of the ligands, with direct consequences for the ligand-field stabilization of the complex. Lower reaction temperatures most likely will result in stabilization of the low-spin state of the cobalt compounds and might thereby facilitate the formation of cobalt(III)-thiolate compounds. Therefore, in the near future, both experimental and theoretical studies can be directed towards understanding the role of protons, as well as detailed thermodynamic studies of the reaction. Furthermore, additional systematic studies to the design of the disulfide ligand need to be conducted. It was shown that *ortho*-methylation of pyridine rings in the ligands L<sup>2</sup>SSL<sup>2</sup> and L<sup>3</sup>SSL<sup>3</sup> results in weaker donating ability of these pyridine nitrogen atoms due to steric effects.<sup>9</sup> Thus, it might be interesting to examine functionalization on the *para* position of the pyridine rings to eliminate steric effects and enable a stronger donating ability of the pyridine nitrogens, which may induce the redox-conversion of Co(II)-disulfide to Co(III)-thiolate compounds.

Currently the redox conversion of other metal-disulfide to metal-thiolate complexes is underexplored. Further investigations of redox-conversion reactions based on other transition metals may reveal interesting applications of this redox-conversion, such as for molecular magnetic switches, sensing materials for halide ions, protons, or temperatures. In addition, cobalt(III) complexes with a ligand containing pyridine and thiolate moieties have recently emerged as promising catalysts for electrochemical CO<sub>2</sub> reduction.<sup>24, 25</sup> In this light, the catalytic activity of the Co(III)-thiolate complexes described in this thesis for CO<sub>2</sub> reduction may be worthy of investigation.



### 6.3. References

1. Koval, I. A., Gamez, P., Belle, C., Selmecezi, K. and Reedijk, J. *Chem. Soc. Rev.* **2006**, 35 (9), 814.
2. Brazzolotto, D., Gennari, M., Queyriaux, N., Simmons, T. R., Pécaut, J., Demeshko, S., Meyer, F., Orio, M., Artero, V. and Duboc, C. *Nat. Chem.* **2016**, 8 (11), 1054-1060.
3. Ghosh, A. C., Duboc, C. and Gennari, M. *Coord. Chem. Rev.* **2021**, 428
4. Wang, L., Gennari, M., Barrozo, A., Fize, J., Philouze, C., Demeshko, S., Meyer, F., Orio, M., Artero, V. and Duboc, C. *ACS Catal.* **2019**, 10 (1), 177-186.
5. Leipzig, B. K., Rees, J. A., Kowalska, J. K., Theisen, R. M., Kavcic, M., Poon, P. C. Y., Kaminsky, W., DeBeer, S., Bill, E. and Kovacs, J. A. *Inorg. Chem.* **2018**, 57 (4), 1935-1949.
6. Lugo-Mas, P., Dey, A., Xu, L., Davin, S. D., Benedict, J., Kaminsky, W., Hodgson, K. O., Hedman, B., Solomon, E. I. and Kovacs, J. A. *J. Am. Chem. Soc.* **2006**, 128 (34), 11211-11221.
7. Shearer, J., Kung, I. Y., Lovell, S., Kaminsky, W. and Kovacs, J. A. *J. Am. Chem. Soc.* **2001**, 123 (3), 463-468.
8. Carroll, M. E., Barton, B. E., Rauchfuss, T. B. and Carroll, P. J. *J. Am. Chem. Soc.* **2012**, 134 (45), 18843-18852.
9. Itoh, S., Nagagawa, M. and Fukuzumi, S. *J. Am. Chem. Soc.* **2001**, 123 (17), 4087-4088.
10. Ueno, Y., Tachi, Y. and Itoh, S. *J. Am. Chem. Soc.* **2002**, 124 (42), 12428-12429.
11. Houser, R. P., Young, V. G. and Tolman, W. B. *J. Am. Chem. Soc.* **1996**, 118 (8), 2101-2102.
12. Neuba, A., Haase, R., Meyer-Klaucke, W., Floerke, U. and Henkel, G. *Angew. Chem. Int. Ed.* **2012**, 51 (7), 1714-1718.
13. Thomas, A. M., Lin, B.-L., Wasinger, E. C. and Stack, T. D. P. *J. Am. Chem. Soc.* **2013**, 135 (50), 18912-18919.
14. Ording-Wenker, E. C. M., Siegler, M. A., Lutz, M. and Bouwman, E. *Inorg. Chem.* **2013**, 52 (22), 13113-13122.
15. Ording-Wenker, E. C. M., van der Plas, M., Siegler, M. A., Bonnet, S., Bickelhaupt, F. M., Fonseca Guerra, C. and Bouwman, E. *Inorg. Chem.* **2014**, 53 (16), 8494-8504.
16. Ording-Wenker, E. C. M., van der Plas, M., Siegler, M. A., Fonseca Guerra, C. and Bouwman, E. *Chem. Eur. J.* **2014**, 20 (51), 16913-16921.
17. Gennari, M., Gerey, B., Hall, N., Pécaut, J., Collomb, M.-N., Rouzies, M., Clerac, R., Orio, M. and Duboc, C. *Angew. Chem. Int. Ed.* **2014**, 53 (21), 5318-5321.
18. Jiang, F., Marvelous, C., Verschuur, A. C., Siegler, M. A., Teat, S. J. and Bouwman, E. *Inorg. Chim. Acta* **2022**, 120880.
19. Jiang, F., Siegler, M. A., Sun, X., Jiang, L., Fonseca Guerra, C. and Bouwman, E. *Inorg. Chem.* **2018**, 57 (15), 8796-8805.
20. Marvelous, C., de Azevedo Santos, L., Siegler, M. A., Fonseca Guerra, C. and Bouwman, E. *Dalton Trans.* **2022**, 51, 8046-8055.
21. Marvelous, C., de Azevedo Santos, L., Siegler, M. A., Fonseca Guerra, C. and Bouwman, E. **2022**, submitted
22. Reich, H. J. and Hondal, R. J. *ACS Chem. Biol.* **2016**, 11 (4), 821-841.
23. Steinmann, D., Nauser, T. and Koppenol, W. H. *J. Org. Chem.* **2010**, 75 (19), 6696-6699.
24. Ahmed, M. E., Rana, A., Saha, R., Dey, S. and Dey, A. *Inorg. Chem.* **2020**, 59 (8), 5292-5302.
25. Dey, S., Todorova, T. K., Fontecave, M. and Mougél, V. *Angew. Chem. Int. Ed.* **2020**, 59 (36), 15726-15733.

# Appendix I

## Supplementary Information for Chapter 2

### Synthesis of Compound $[\text{Co}(\text{L}^1\text{S})(\text{phen})](\text{SbF}_6)_2$

The compound  $[\text{Co}(\text{L}^1\text{S})(\text{phen})](\text{SbF}_6)_2$  was prepared in a similar manner as compound **[3]** $(\text{SbF}_6)_2$ , using 1,10-phenanthroline (phen) instead of bpy. A red powder was obtained in 85% yield. IR (neat,  $\text{cm}^{-1}$ ): 1608s, 1518m, 1485w, 1426s, 1376w, 1344w, 1298w, 1247w, 1225w, 1149w, 1105m, 1091m, 1058m, 1022m, 979w, 955w, 909w, 869w, 847s, 769s, 726s, 649vs, 569m, 526m, 448m, 421s. ESI-MS in acetonitrile calcd. for  $[\text{Co}(\text{L}^1\text{S})(\text{phen})](\text{SbF}_6)^+ m/z$  732.0, found  $m/z$  732.0; calcd. for  $[\text{Co}(\text{L}^1\text{S})(\text{phen})]^{2+} m/z$  248.55, found  $m/z$  248.6; calcd. for  $[\text{Co}(\text{phen})_3]^{2+} m/z$  299.6, found  $m/z$  299.9. Elemental analysis (%) for  $[\text{Co}(\text{L}^1\text{S})(\text{phen})](\text{SbF}_6)_2$ , calcd. C, 32.23; H, 2.50; N, 7.23; found C, 33.03; H, 2.48; N, 7.18. Single crystals were obtained by vapor diffusion of dry and deoxygenated diethyl ether into the dry and deoxygenated acetonitrile solution of compound  $[\text{Co}(\text{L}^1\text{S})(\text{phen})](\text{SbF}_6)_2$ .

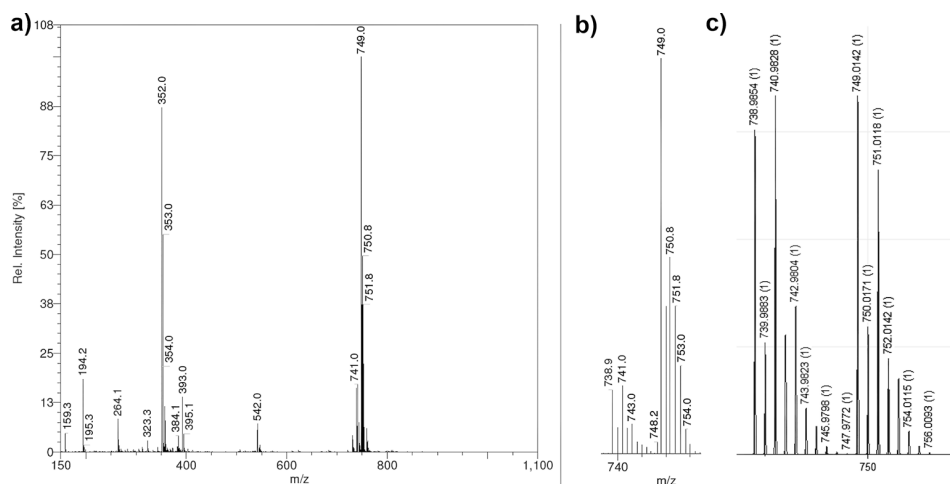


**Figure AL.1.** ESI-MS spectrum of a) **[1Cl]** dissolved in acetonitrile; b) the experimental isotopic distribution of the main signals; c) simulated isotopic distribution of the main signals. ESI-MS found (calcd.) for  $[\text{1Cl} - 2\text{Cl}^-]^{2+} m/z$  352.0 (352.0), for  $[\text{1Cl} - \text{Cl}^-]^+ m/z$  741.0 (741.0), and for  $[\text{1Cl} - 2\text{Cl}^- + \text{HCOO}^-]^+ m/z$  749.0 (749.0).

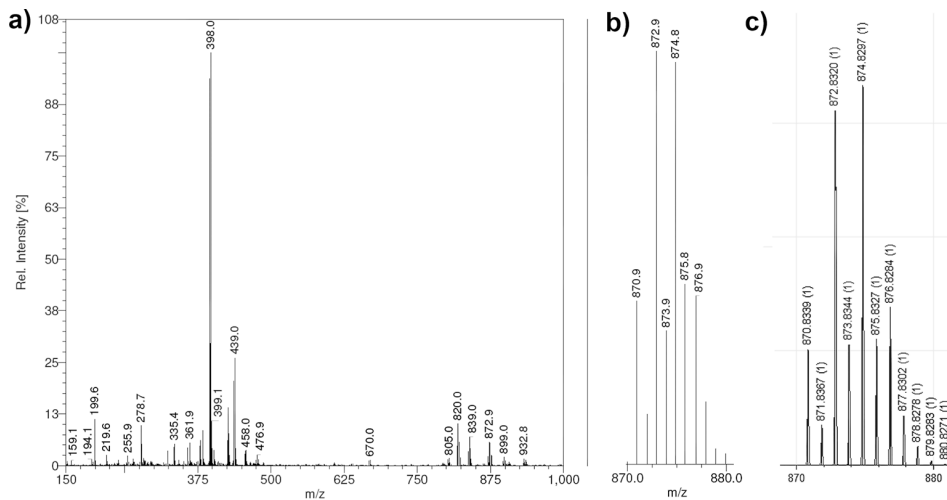


**Figure AI.2.** ESI-MS spectrum of a)  $[1_{Br}]$  dissolved in acetonitrile; b) the experimental isotopic distribution; c) simulated isotopic distribution. ESI-MS found (calcd.) for  $[1_{Br} - 2Br^-]^{2+}$   $m/z$  398.0 (397.9), for  $[1_{Br} - 2Br^- + HCOO^-]^+$   $m/z$  839.0 (838.9), and for  $[1_{Br} - Br^-]^+$   $m/z$  872.9 (872.8).

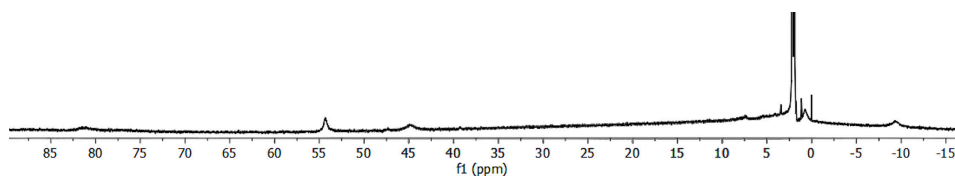


**Figure AI.3.**  $^1H$ -NMR spectrum of compound  $[1_{Cl1}]$  dissolved in  $CD_3CN$ .

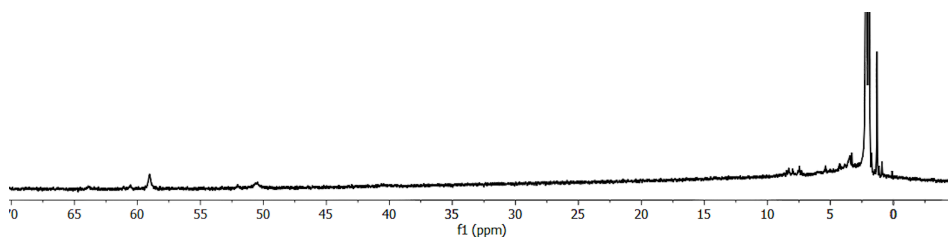


**Figure AI.4.**  $^1H$ -NMR spectrum of compound  $[1_{Br}]$  dissolved in  $CD_3CN$ .

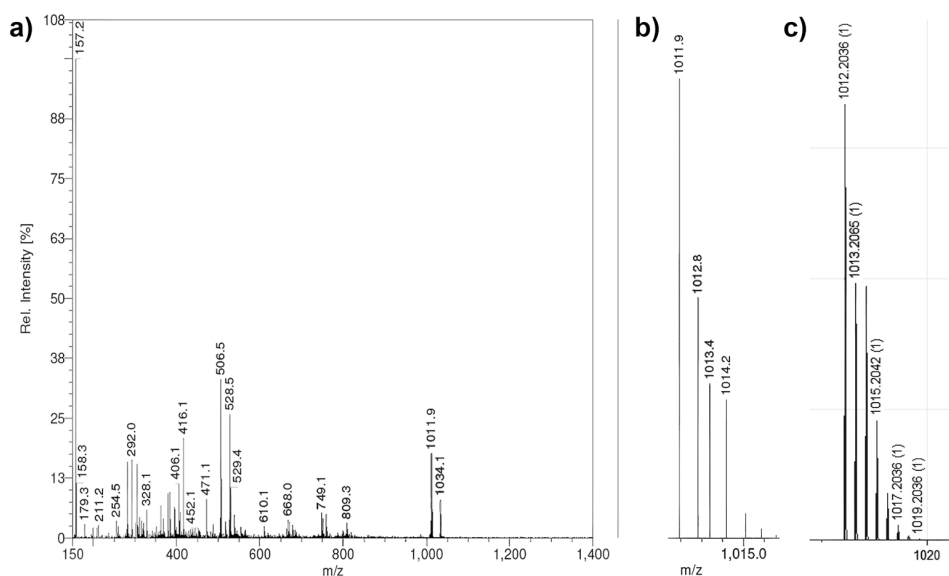


**Figure AI.5.** ESI-MS spectrum of a)  $[2\text{Cl}](\text{BPh}_4)_2$  dissolved in methanol; b) the experimental isotopic distribution; c) simulated isotopic distribution. ESI-MS found (calcd.) for  $[2\text{Cl} - \text{Cl}^- + \text{OMe}]^{2+}$   $m/z$  506.5 (506.1), for partially reduced species  $[2\text{Cl} - \text{Cl}^- + \text{OMe}]^+$   $m/z$  1011.9 (1012.2).

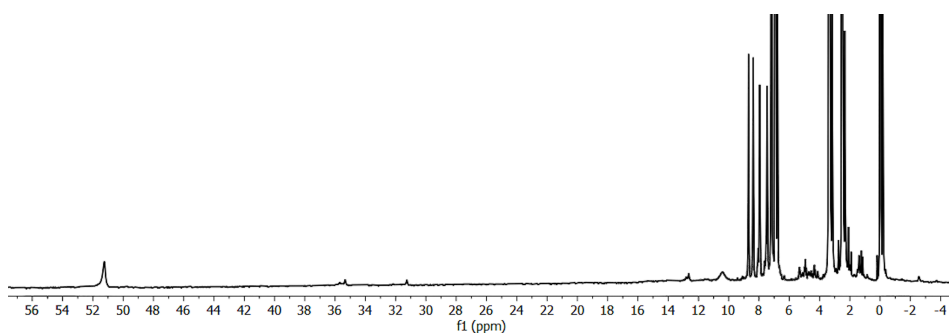


**Figure AI.6.**  $^1\text{H}$ -NMR spectrum of compound  $[2\text{Cl}](\text{BPh}_4)_2$  dissolved in  $\text{DMSO-d}_6$ . The diamagnetic region contains peaks that corresponds to the ligand  $\text{L}^1\text{SSL}^1$  and bipyridine, indicating dissociation of the ligand upon dissolution of the compound.

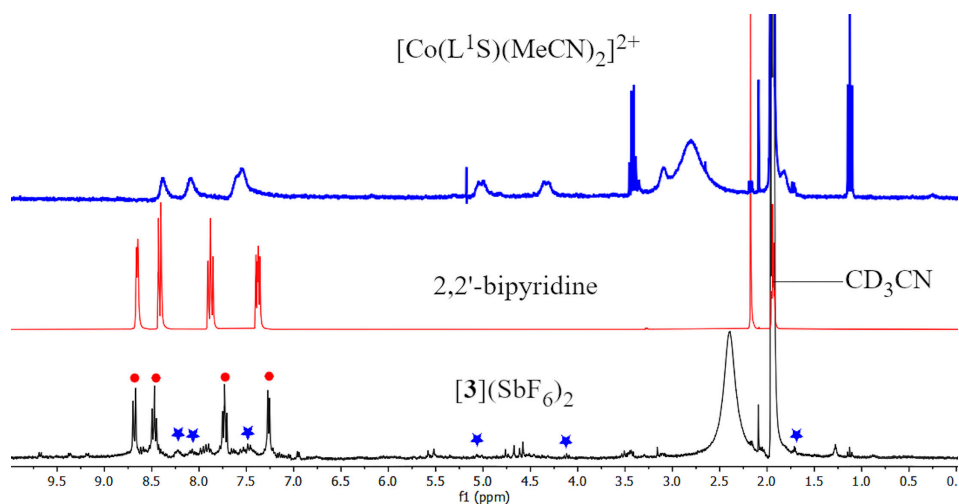


**Figure AI.7.**  $^1\text{H}$ -NMR spectrum of compound  $[3](\text{SbF}_6)_2$  (black trace) dissolved in  $\text{CD}_3\text{CN}$ .  $^1\text{H}$ -NMR spectrum of  $[\text{Co}(\text{L}^1\text{S})(\text{MeCN})_2]^{2+}$  (blue trace) and 2,2'-bipyridine (red trace) dissolved in  $\text{CD}_3\text{CN}$  are provided. The red dots and blue stars indicated the presence of 2,2'-bipyridine and  $[\text{Co}(\text{L}^1\text{S})(\text{MeCN})_2]^{2+}$ , respectively.

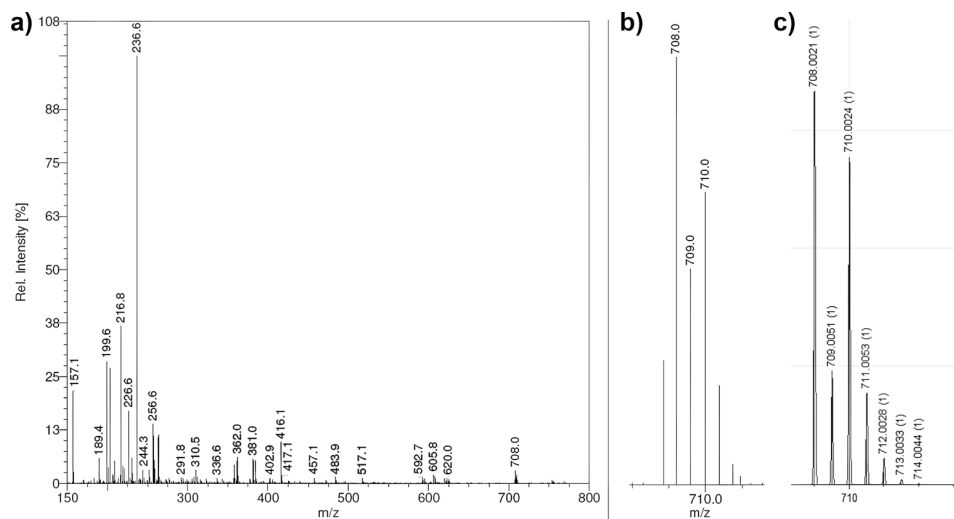


**Figure AI.8.** ESI-MS spectrum of a)  $[3](\text{SbF}_6)_2$  dissolved in acetonitrile; b) the experimental isotopic distribution; c) simulated isotopic distribution. ESI-MS found (calcd.) for  $[3]^{2+}$   $m/z$  236.6 (236.55), for  $[3](\text{SbF}_6)^+$   $m/z$  708.0 (708.0). Species  $[\text{Co}(\text{L}^1\text{S})(\text{MeCN})_2]^{2+}$  ( $m/z$  199.6 (199.55)) and  $[2,2'\text{-bipyridine} + \text{H}]^+$  ( $m/z$  157.1 (157.0)) are present.

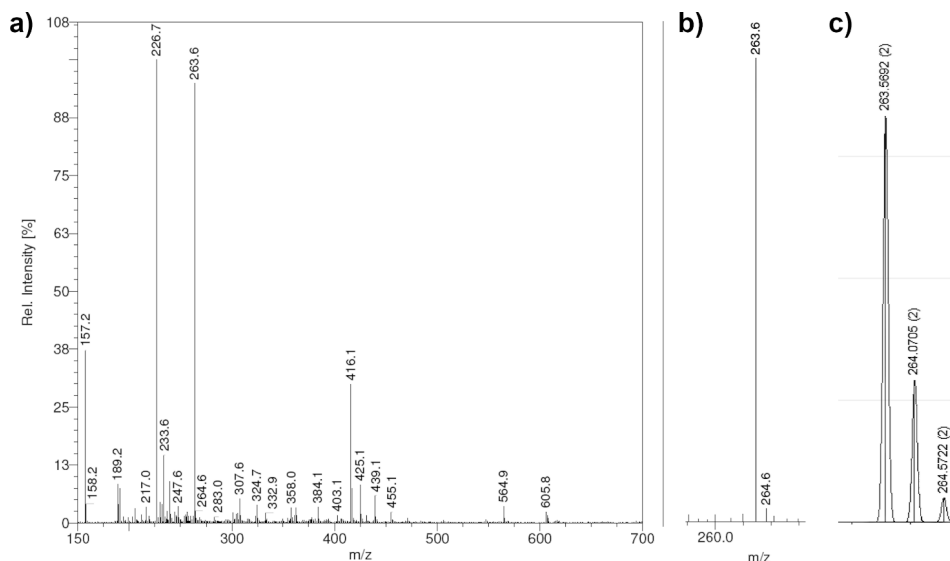


**Figure AL9.** ESI-MS spectrum of a) the isolated brown-reddish powder from the reaction between  $[2\text{Cl}](\text{BPh}_4)_2$  with  $\text{AgSbF}_6$ , the powder was dissolved in acetonitrile; b) the experimental isotopic distribution; c) simulated isotopic distribution. ESI-MS found (calcd.) for  $[(\text{Co}(\text{bpy})_3)_2]^+$   $m/z$  263.6 (263.6).

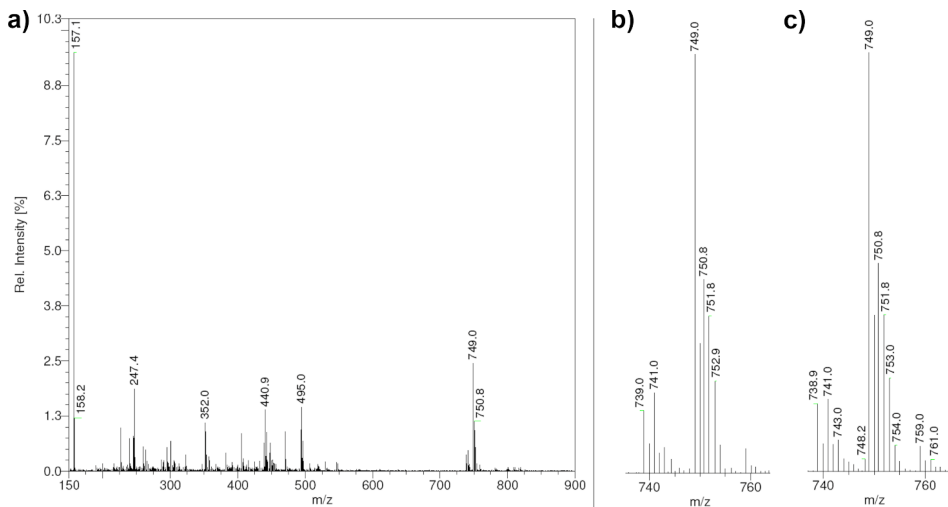


**Figure AL10.** ESI-MS spectrum of a) the isolated purple powder from the reaction between  $[3](\text{SbF}_6)_2$  with  $\text{NEt}_4\text{Cl}$ , the powder was dissolved in acetonitrile; b) the experimental isotopic distribution; c) the experimental isotopic distribution for compound  $[1\text{Cl}]$ . ESI-MS found (calcd.) for  $[1\text{Cl} - 2\text{Cl}]^{2+}$   $m/z$  352.0 (352.0), for  $[1\text{Cl} - \text{Cl}]^+$   $m/z$  741.0 (741.0), and for  $[1\text{Cl} - 2\text{Cl} + \text{HCOO}]^+$   $m/z$  749.0 (749.0).

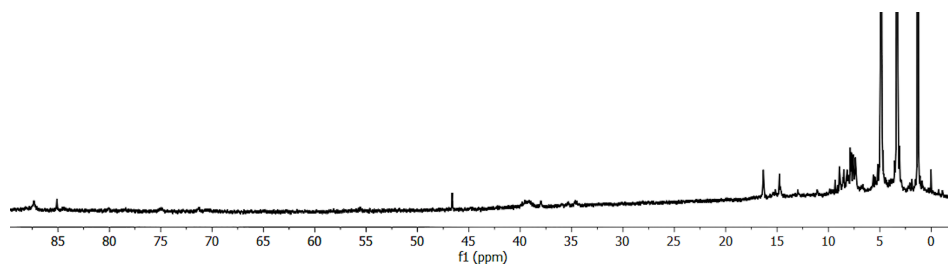


**Figure AI.11.**  $^1\text{H}$ -NMR spectrum of the isolated purple powder from the reaction between  $[\mathbf{3}](\text{SbF}_6)_2$  with  $\text{NEt}_4\text{Cl}$ , the powder was dissolved in  $\text{CD}_3\text{CN}$ .

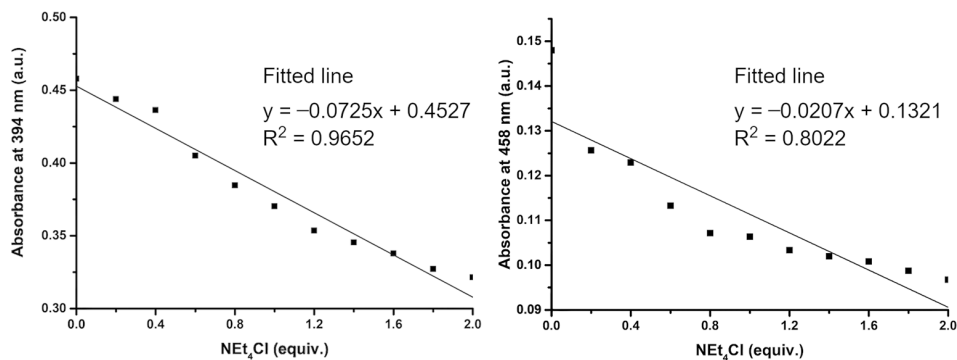


**Figure AI.12.** Changes of absorbance at 394 nm and 458 nm as a function of the amount of added  $\text{NEt}_4\text{Cl}$  to 5 mM solution of  $[\mathbf{3}](\text{SbF}_6)_2$ . Linear fitting details are provided.

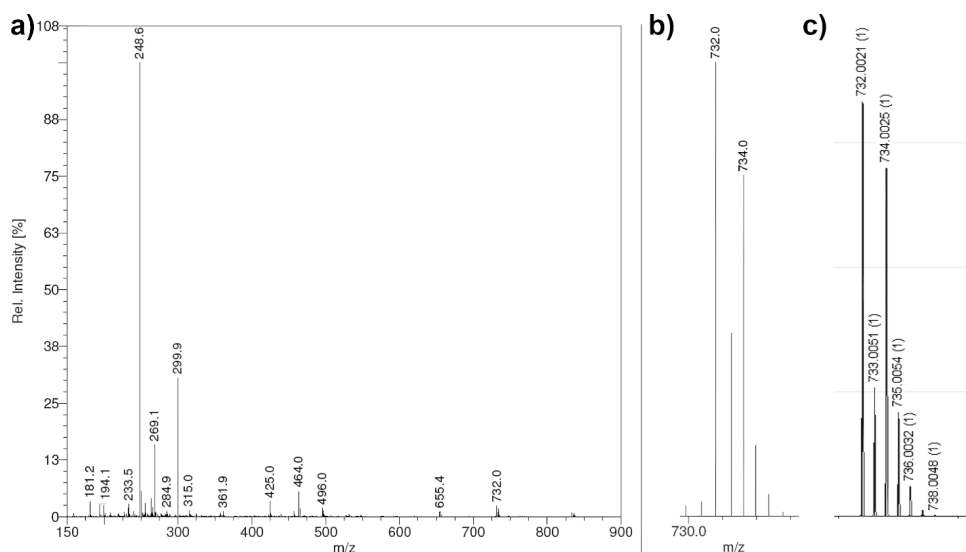


**Figure AI.13.** ESI-MS spectrum of a)  $[\text{Co}(\text{L}^1\text{S})(\text{phen})](\text{SbF}_6)_2$ , the powder was dissolved in acetonitrile; b) the experimental isotopic distribution; c) simulated isotopic distribution. ESI-MS found (calcd.) for  $[\text{Co}(\text{L}^1\text{S})(\text{phen})]^{2+}$   $m/z$  248.6 (248.55) and for  $[\text{Co}(\text{L}^1\text{S})(\text{phen})](\text{SbF}_6)^+$   $m/z$  732.0 (732.0). The species  $[\text{Co}(\text{phen})_3]^{2+}$  is also found (calcd.) at  $m/z$  299.9 (299.6).

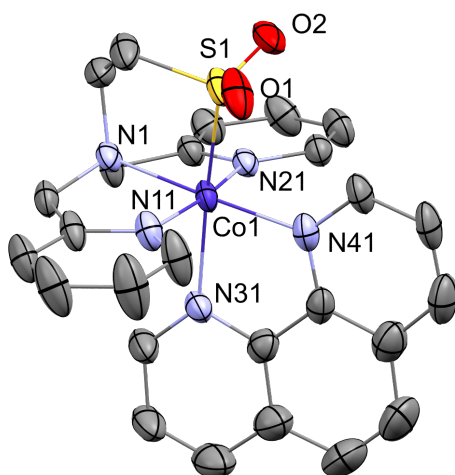


**Figure AI.14.** Displacements ellipsoid plot (50% probability level) of the oxidized compound  $[\text{Co}(\text{L}^1\text{SO}_2)(\text{phen})](\text{SbF}_6)_2$  at 110(2) K. Hydrogen atoms, non-coordinated anions, and lattice solvent molecules are omitted for clarity.



**Table AI.1.** Selected bond distances and bond angles in [Co(L<sup>1</sup>SO<sub>2</sub>)(phen)](SbF<sub>6</sub>)<sub>2</sub>.

Atoms	distance (Å)	Atoms	Bond angles (°)
Co1–N1	1.976(4)	S1–Co1–N1	86.78(11)
Co1–N11	1.921(4)	S1–Co1–N11	88.59(13)
Co1–N21	1.929(4)	S1–Co1–N21	95.64(11)
Co1–N31	2.084(4)	S1–Co1–N31	172.01(12)
Co1–N41	1.969(4)	S1–Co1–N41	92.32(12)
Co1–S1	2.1866(13)	N31–Co1–N41	82.36(16)
S1–O1	1.460(4)	N31–Co1–N1	98.77(15)
S1–O2	1.456(4)	N21–Co1–N1	84.00(16)

**Table AI.2.** Crystallographic Data for the crystal structures in the present work.

	[1Br]	[2Cl](BPh <sub>4</sub> ) <sub>2</sub>	[Co(L <sup>1</sup> SO <sub>2</sub> )(phen)](SbF <sub>6</sub> ) <sub>2</sub>
Chemical formula	C <sub>28</sub> H <sub>32</sub> Br <sub>4</sub> Co <sub>2</sub> N <sub>6</sub> S <sub>2</sub> , CH <sub>4</sub> O	C <sub>48</sub> H <sub>48</sub> Cl <sub>2</sub> Co <sub>2</sub> N <sub>10</sub> S <sub>2</sub> , 2(C <sub>24</sub> H <sub>20</sub> B), 2(C <sub>3</sub> H <sub>6</sub> O), 0.42(O)	C <sub>26</sub> H <sub>24</sub> CoN <sub>5</sub> O <sub>2</sub> S, 2(F <sub>6</sub> Sb), 0.566(C <sub>4</sub> H <sub>10</sub> O), 1.434(C <sub>2</sub> H <sub>3</sub> N)
<i>M<sub>r</sub></i>	986.26	1779.17	1101.82
Crystal system	Monoclinic	Monoclinic	Monoclinic
Space group	<i>P</i> 2 <sub>1</sub> / <i>c</i>	<i>C</i> 2/ <i>c</i>	<i>P</i> 2 <sub>1</sub> / <i>c</i>
Cell lengths ( <i>a</i> , <i>b</i> , <i>c</i> ) (Å)	15.7651(7), 11.9665(5), 19.6343(8)	19.0139(7), 20.1121(7), 27.0156(13)	21.5627 (5), 13.6523 (4), 14.0315 (4)
Cell angles (α, β, γ) (°)	90, 103.345(4), 90	90, 108.171(4), 90	90, 103.059 (3), 90
Cell volume (Å <sup>3</sup> )	3604.1 (3)	9815.8 (7)	4023.8 (2)
<i>Z</i>	4	4	4
μ (mm <sup>-1</sup> )	5.50	0.49	1.89
Crystal size (mm)	0.11 × 0.08 × 0.02	0.26 × 0.19 × 0.10	0.29 × 0.09 × 0.05
Temperature (K)	110(2)	110(2)	110(2)
Diffractionmeter	SuperNova, Dual, Cu at zero, Atlas detector	SuperNova, Dual, Cu at zero, Atlas detector	SuperNova, Dual, Cu at zero, Atlas detector
Radiation type	Mo <i>K</i> α	Mo <i>K</i> α	Mo <i>K</i> α
<i>T</i> <sub>min</sub> , <i>T</i> <sub>max</sub>	0.734, 0.982	0.520, 1.000	0.439, 1.000
No. of measured, independent and observed [ <i>I</i> > 2σ( <i>I</i> )] reflections	28658, 6355, 4720	38544, 11261, 8613	50549, 7091, 5615
<i>R</i> <sub>int</sub>	0.065	0.038	0.049
(sin θ/λ) <sub>max</sub> (Å <sup>-1</sup> )	0.595	0.650	0.595
<i>R</i> [ <i>F</i> <sup>2</sup> > 2σ( <i>F</i> <sup>2</sup> )], <i>wR</i> ( <i>F</i> <sup>2</sup> ), <i>S</i>	0.047, 0.114, 1.05	0.043, 0.105, 1.02	0.039, 0.102, 1.04
No. of reflections	6355	11261	7091
No. of parameters	398	652	661
No. of restraints		309	404
H-atom treatment	H-atom parameters constrained	H-atom parameters constrained	H-atom parameters constrained
Δρ <sub>max</sub> , Δρ <sub>min</sub> (e Å <sup>-3</sup> )	1.94, -0.82	0.56, -0.31	0.79, -0.77

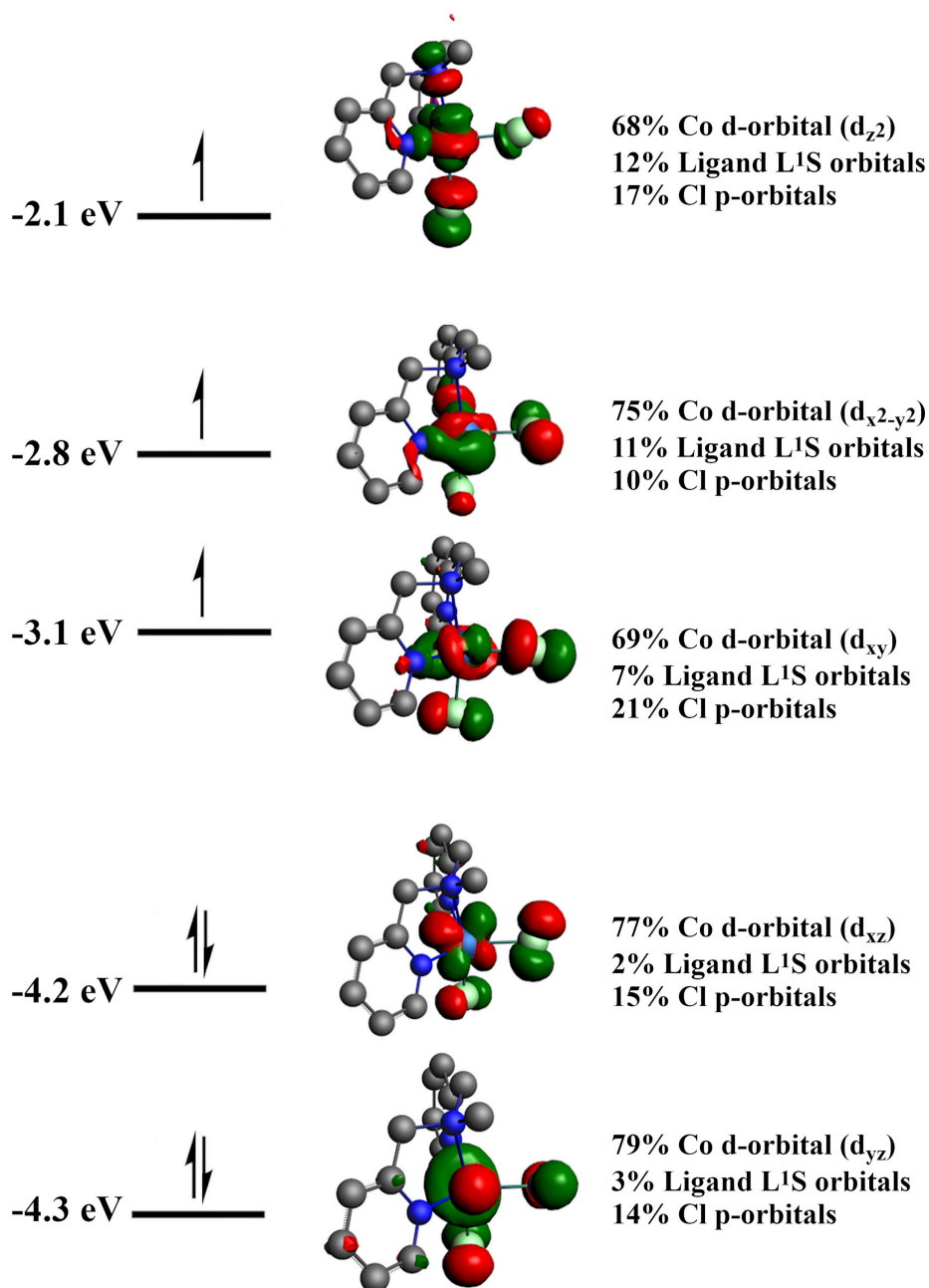


**Figure AI.15.** Several frontier orbitals of [1\*] associated with Co *d*-orbitals along with their energies, orbital visualization, and orbital composition.

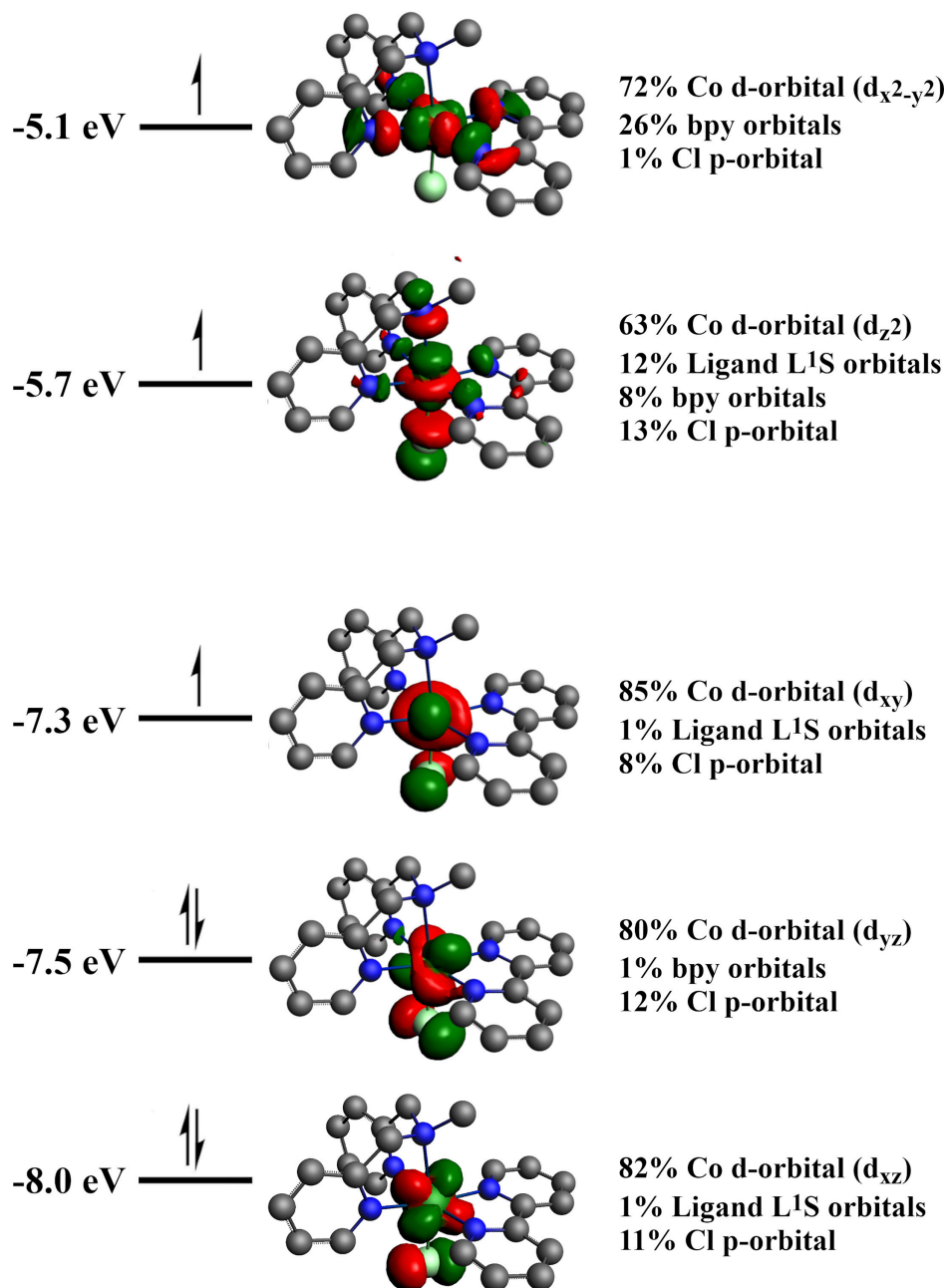


**Figure AI.16.** Several frontier orbitals of  $[2^*]^+_{\text{fac}}$  associated with Co  $d$ -orbitals along with their energies, orbital visualization, and orbital composition.

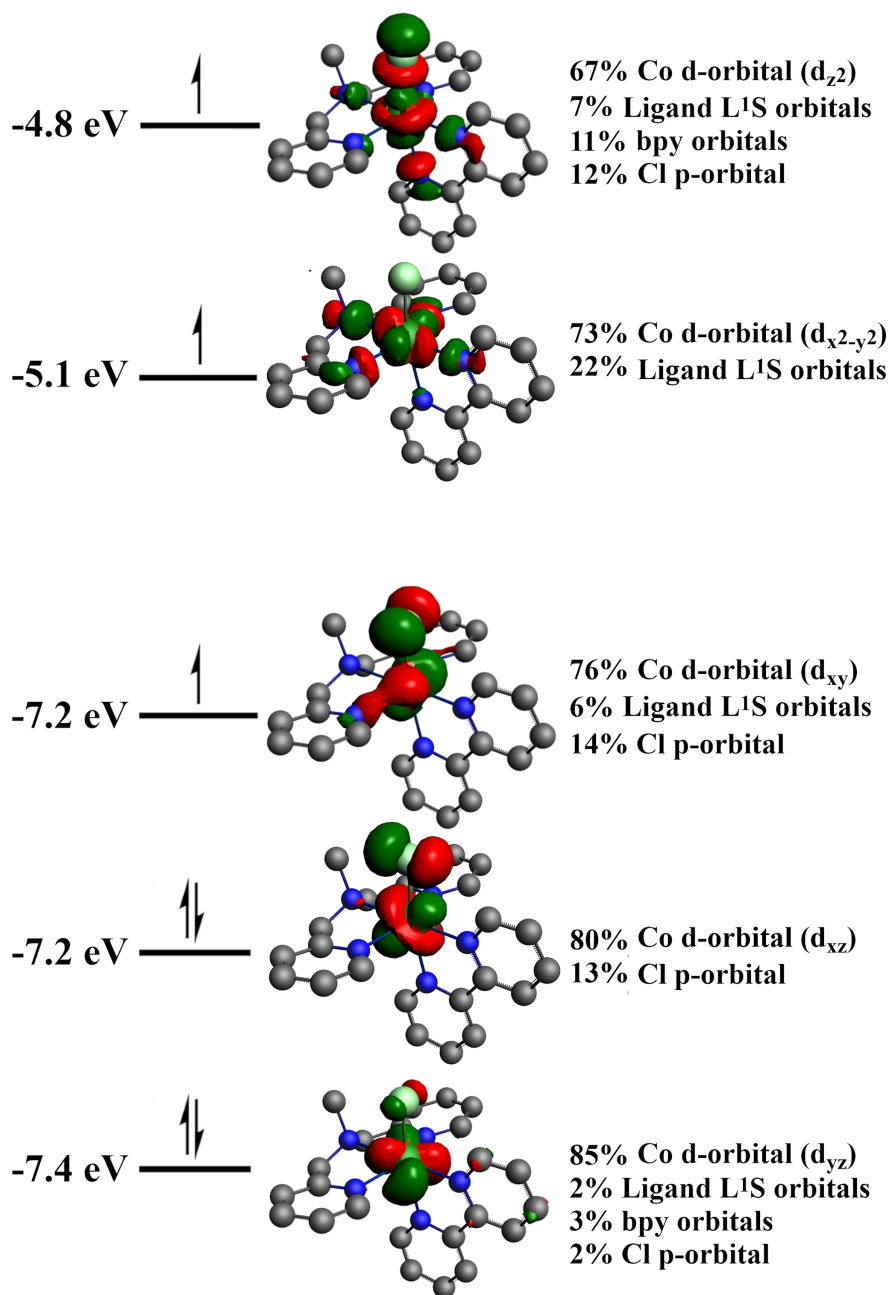


**Figure AI.17.** Several frontier orbitals of  $[2^*]^+_{\text{mer}}$  associated with Co *d*-orbitals along with their energies, orbital visualization, and orbital composition.

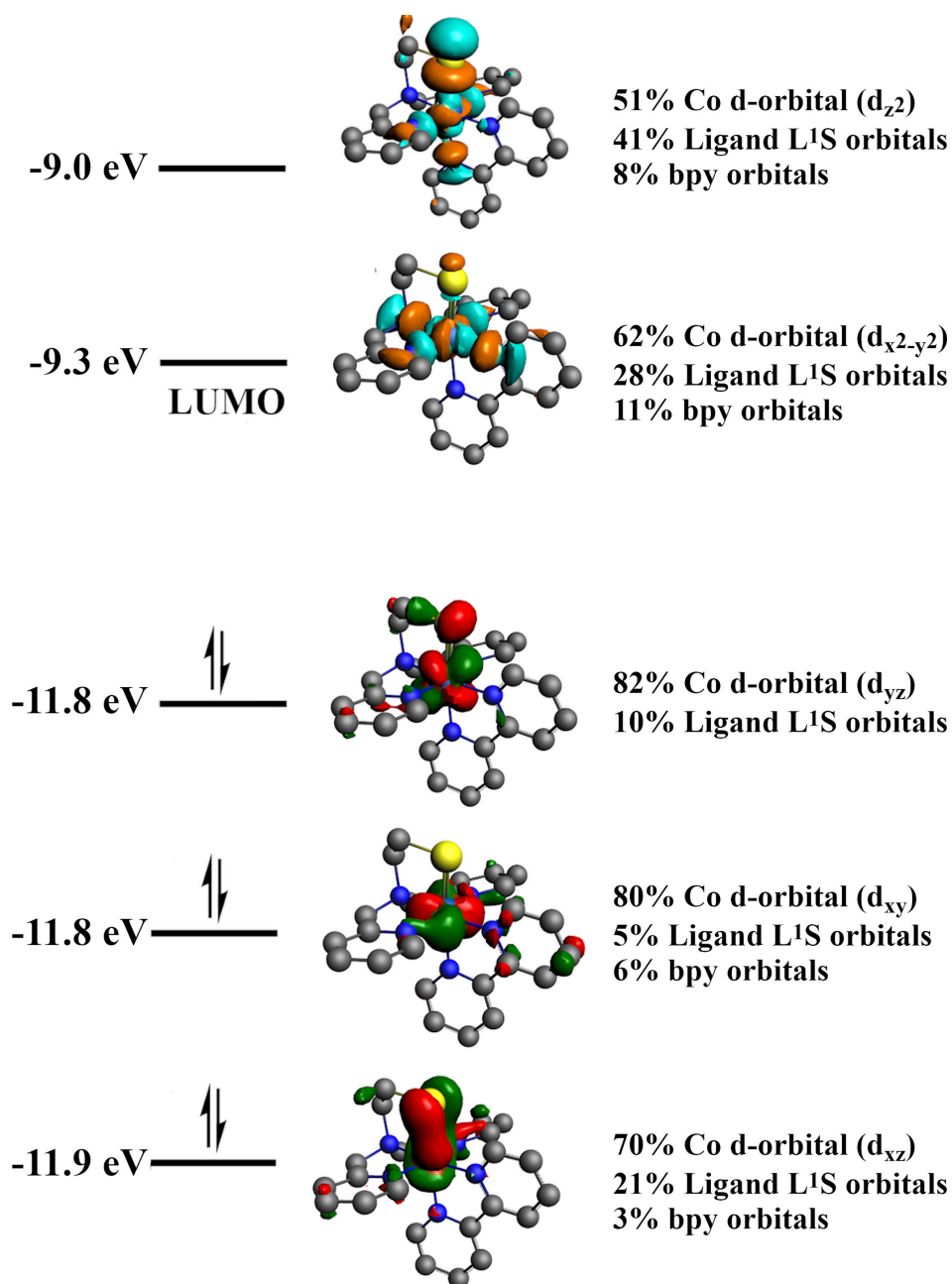


**Figure AI.18.** Several frontier orbitals of  $[3]^{2+}_{\text{mer}}$  associated with Co  $d$ -orbitals along with their energies, orbital visualization, and orbital composition.

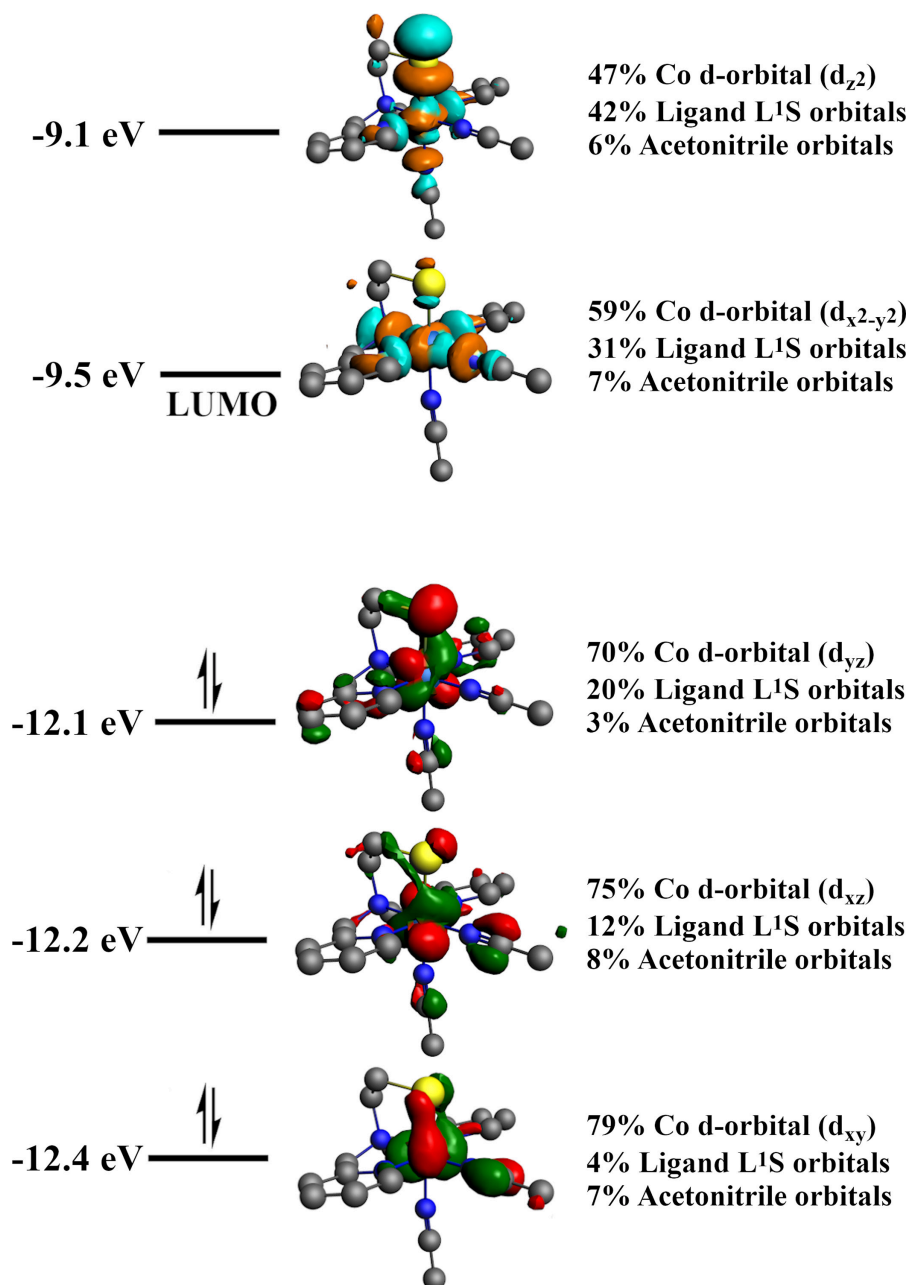


**Figure AI.19.** Several frontier orbitals of  $[4]^{2+}$  associated with Co  $d$ -orbitals along with their energies, orbital visualization, and orbital composition.



# Appendix II

## Supplementary Information for Chapter 3

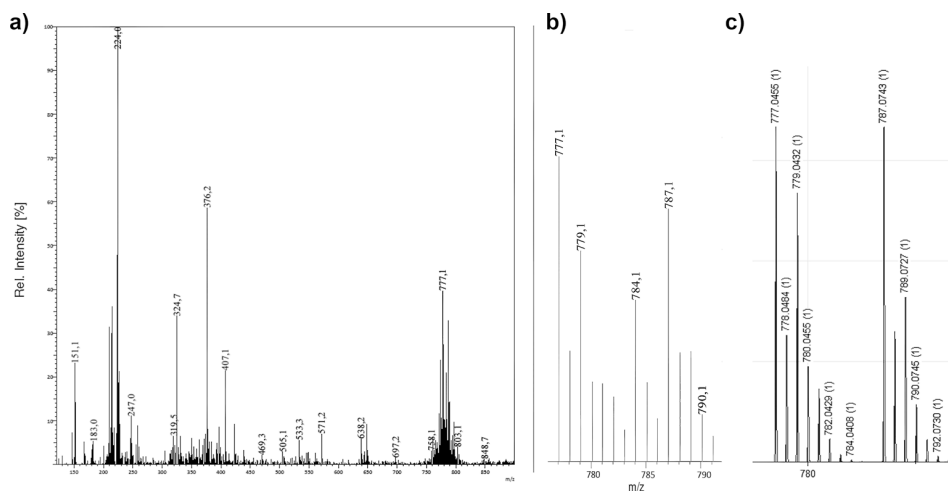


**Figure AII.1.** ESI-MS spectrum of compound [2ss] dissolved in methanol. ESI-MS found (calcd.) for  $[2_{ss} - 4Cl^- + 2HCOO^-]^{2+}$   $m/z$  376.2 (376.04), for  $[2_{ss} - 2Cl^- + HCOO^-]^+$   $m/z$  777.1 (777.05), and for  $[2_{ss} - 3Cl^- + 2HCOO^-]^+$   $m/z$  787.1 (787.07).

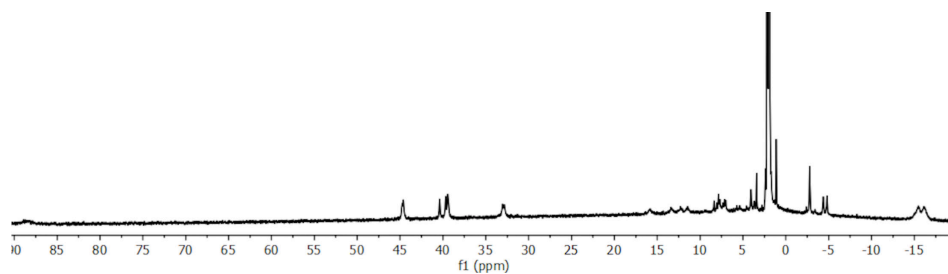


**Figure AII.2.**  $^1H$ -NMR spectrum of compound [2ss] dissolved in  $CD_3CN$ .



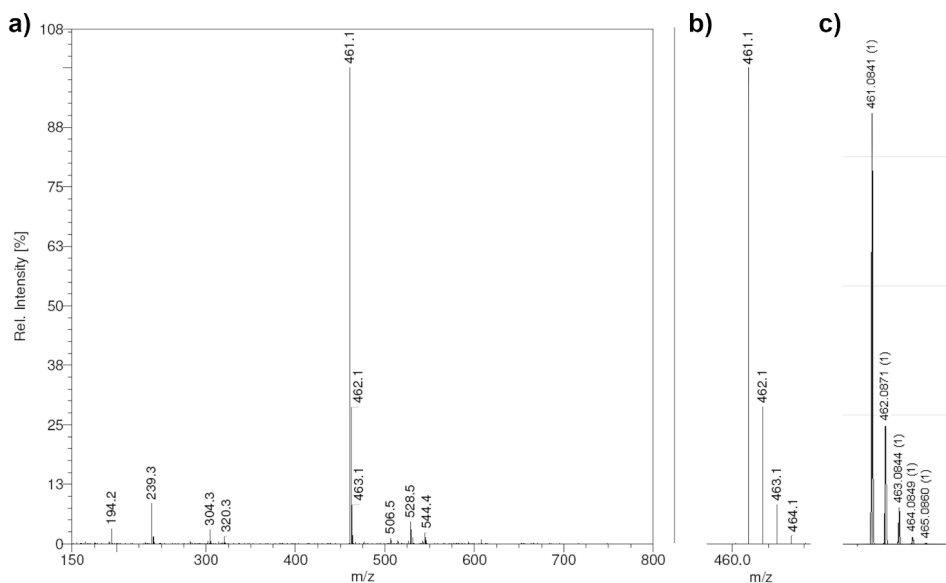


**Figure AII.3.** ESI-MS spectrum of a)  $[1s]Cl$  dissolved in methanol; b) the experimental isotopic distribution of the main signal; c) simulated isotopic distribution. ESI-MS found (calcd.) for  $[1s]^+$   $m/z$  461.1 (461.08).

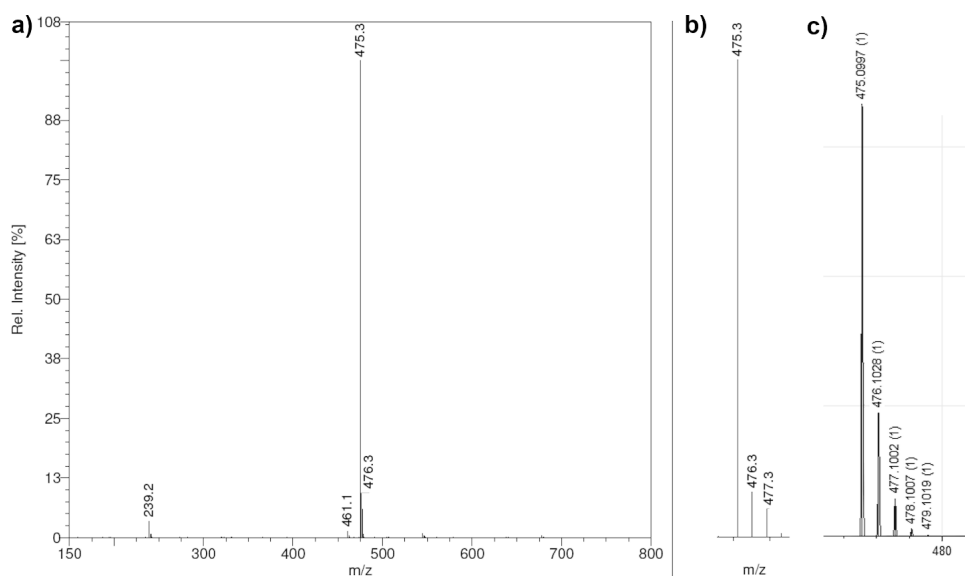


**Figure AII.4.** ESI-MS spectrum of a)  $[2s]Cl$  dissolved in acetonitrile; b) the experimental isotopic distribution of the main signal; c) simulated isotopic distribution. ESI-MS found (calcd.) for  $[2s]^+$   $m/z$  475.3 (475.1).

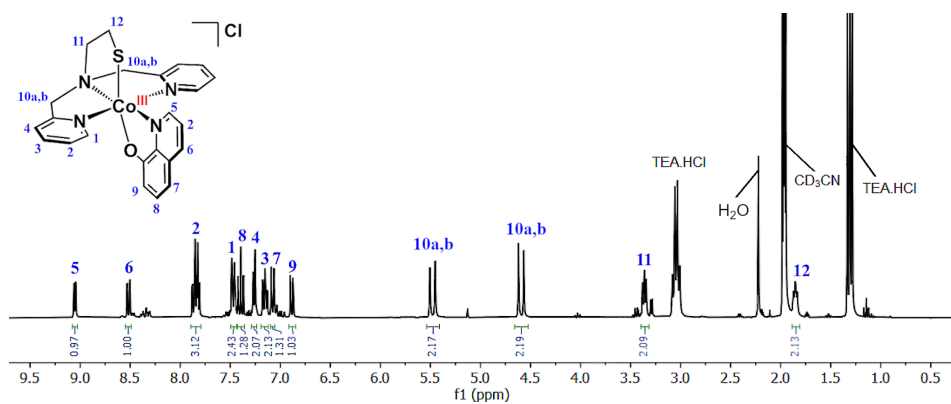


Figure AII.5.  $^1\text{H}$ -NMR spectrum of  $[\mathbf{1s}]\text{Cl}$  dissolved in  $\text{CD}_3\text{CN}$ .

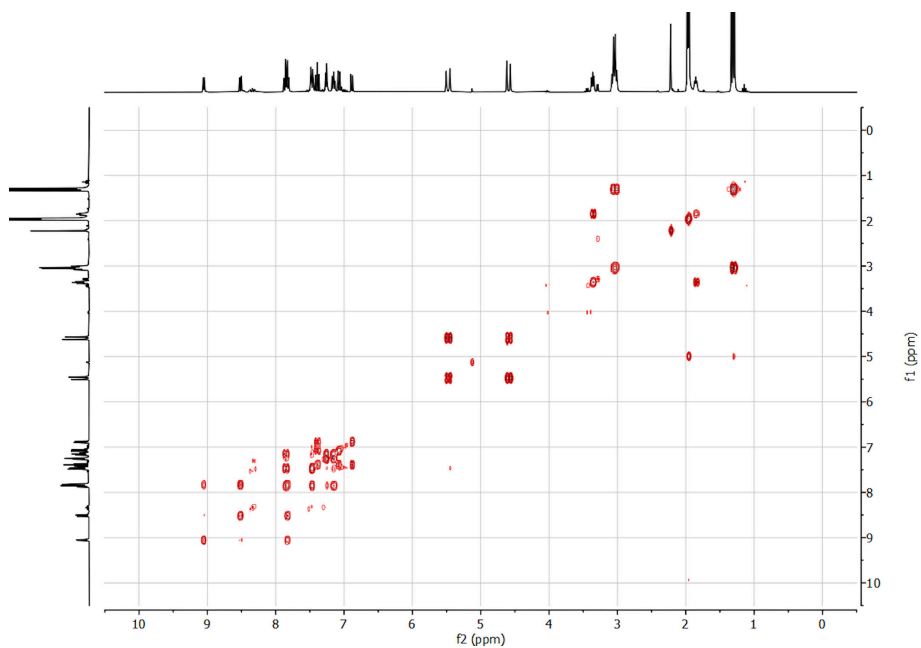
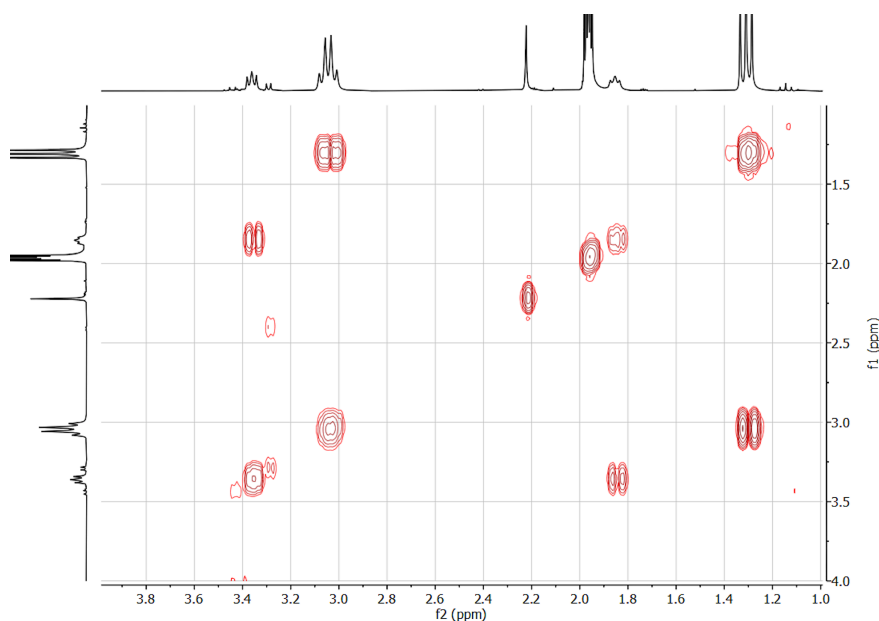
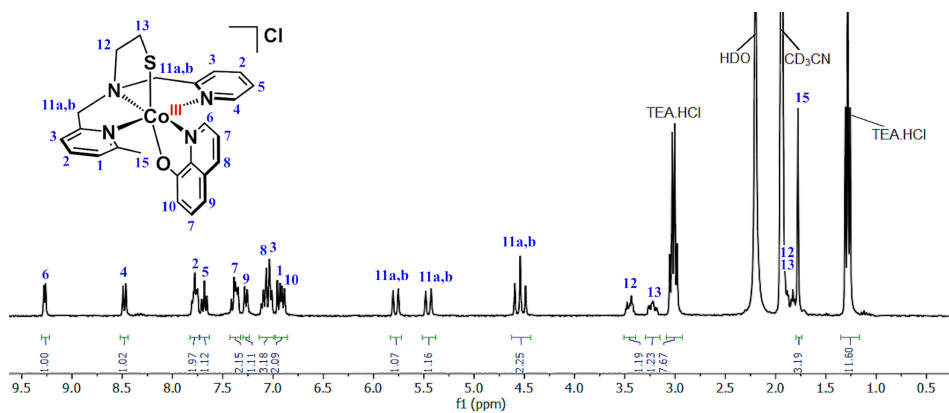


Figure AII.6.  $^1\text{H}$ - $^1\text{H}$ -COSY NMR spectrum of  $[\mathbf{1s}]\text{Cl}$  dissolved in  $\text{CD}_3\text{CN}$ .



**Figure AII.7.**  $^1\text{H}$ - $^1\text{H}$ -COSY NMR spectrum of  $[1\text{s}]\text{Cl}$  dissolved in  $\text{CD}_3\text{CN}$ . The spectrum shows the correlation of protons in  $\text{N-CH}_2\text{-CH}_2\text{-S}$  (3.2–3.5 ppm and 1.84–1.87 ppm).



**Figure AII.8.**  $^1\text{H}$ -NMR spectrum of  $[2\text{s}]\text{Cl}$  dissolved in  $\text{CD}_3\text{CN}$ .

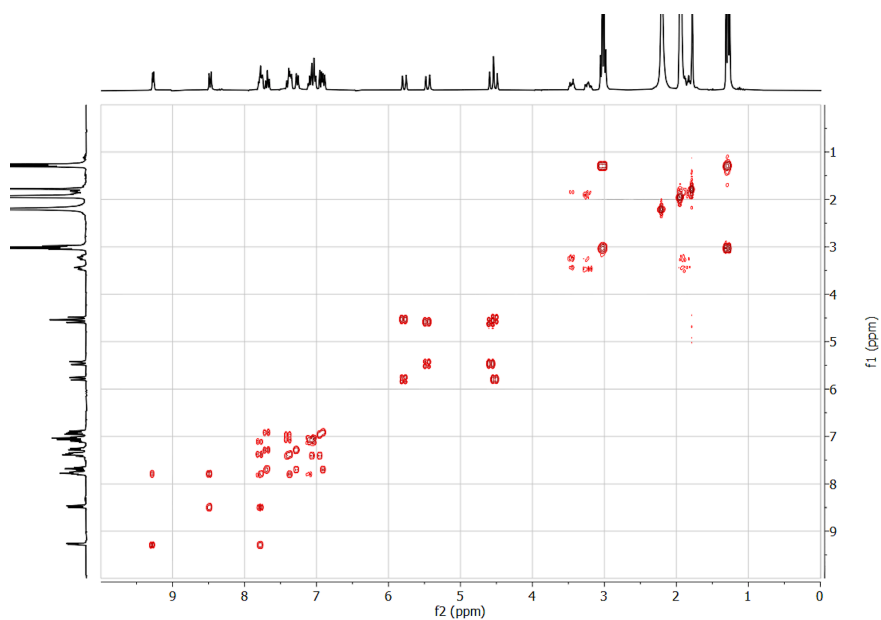


**Figure AII.9.**  $^1\text{H}$ - $^1\text{H}$ -COSY NMR spectrum of  $[2\text{s}]\text{Cl}$  dissolved in  $\text{CD}_3\text{CN}$ .

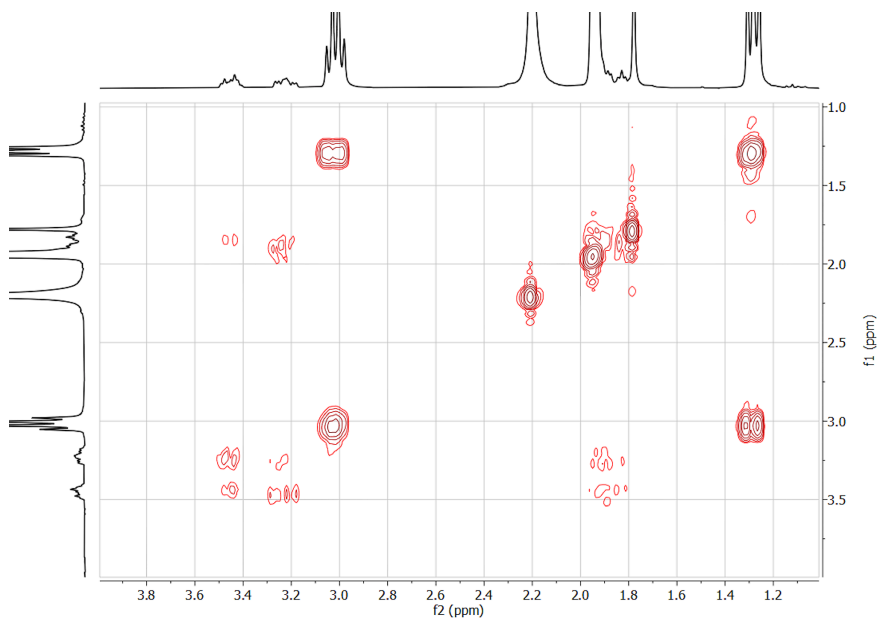


**Figure AII.10.**  $^1\text{H}$ - $^1\text{H}$ -COSY NMR spectrum of  $[2\text{s}]\text{Cl}$  dissolved in  $\text{CD}_3\text{CN}$ . The spectrum shows the correlation of protons in  $\text{N-CH}_2\text{-CH}_2\text{-S}$  (3.18–3.50 ppm) with the solvent peak (1.9 ppm), indicating that the solvent peak obscures the proton peak of interest.

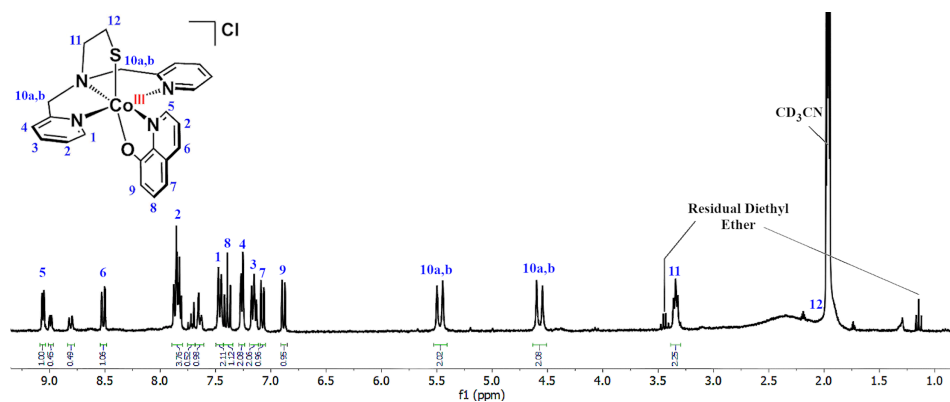


**Figure AII.11.**  $^1\text{H}$ -NMR spectrum of  $[1s]\text{Cl}$  dissolved in  $\text{CD}_3\text{CN}$ . The synthesis was done in absence of triethylamine. Impurities (as unlabeled peaks) are present mostly in the aromatic region.

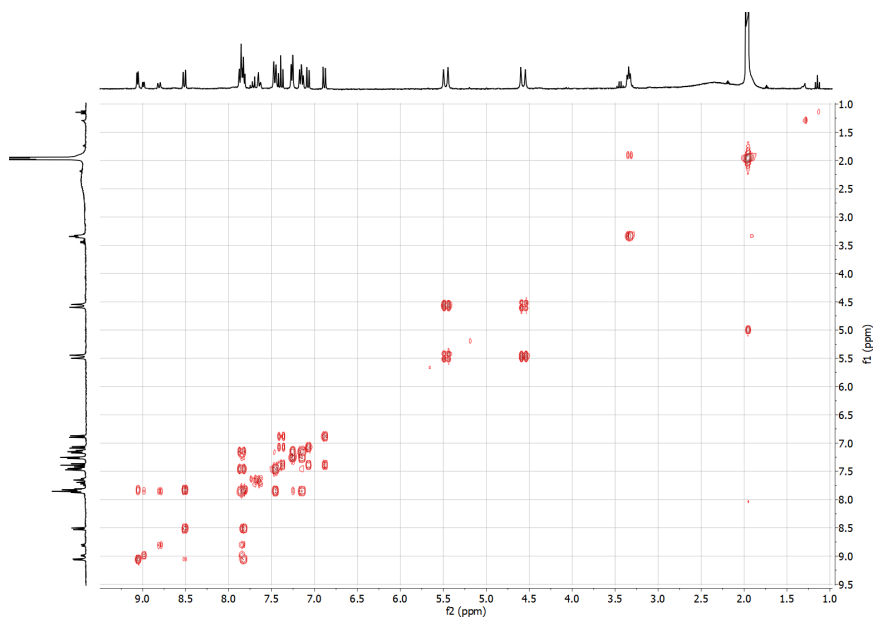


**Figure AII.12.**  $^1\text{H}$ - $^1\text{H}$ -COSY NMR spectrum of  $[1s]\text{Cl}$  dissolved in  $\text{CD}_3\text{CN}$ . The synthesis was done in absence of triethylamine.

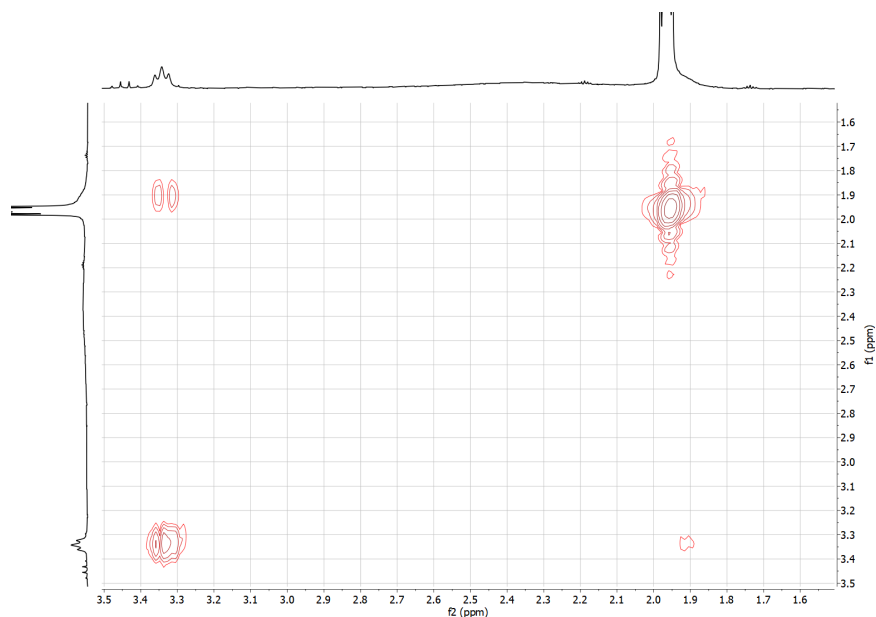


**Figure AII.13.**  $^1\text{H}$ - $^1\text{H}$ -COSY NMR spectrum of  $[\mathbf{1s}]\text{Cl}$  dissolved in  $\text{CD}_3\text{CN}$ . The synthesis was done in absence of triethylamine. The spectrum shows the correlation of protons in  $\text{N-CH}_2\text{-CH}_2\text{-S}$  (3.2–3.4 ppm and 1.84–1.87 ppm).

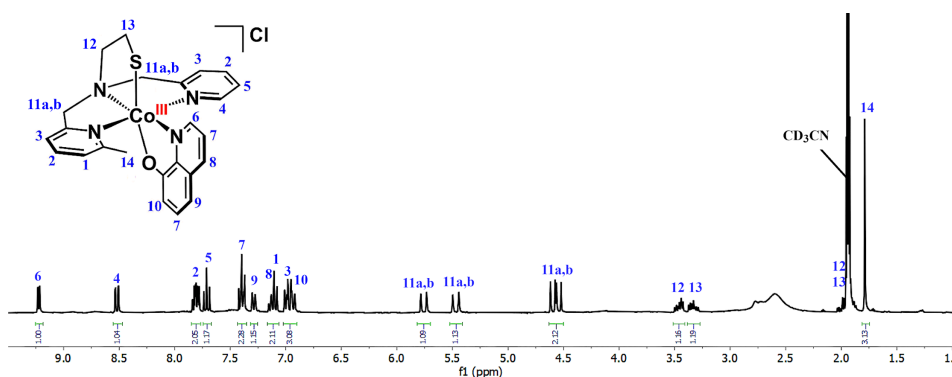


**Figure AII.14.**  $^1\text{H}$ -NMR spectrum of  $[\mathbf{2s}]\text{Cl}$  dissolved in  $\text{CD}_3\text{CN}$ . The synthesis was done in absence of triethylamine.

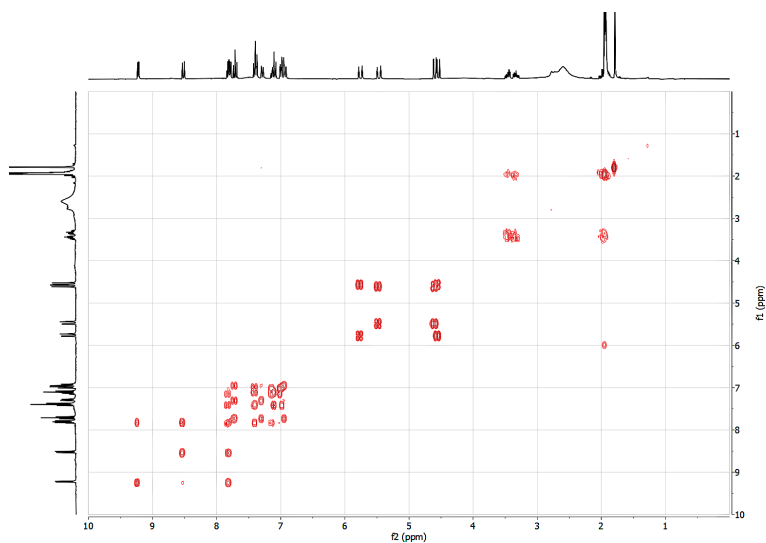


**Figure AII.15.**  $^1\text{H}$ - $^1\text{H}$ -COSY NMR spectrum of  $[2_s]\text{Cl}$  dissolved in  $\text{CD}_3\text{CN}$ . The synthesis was done in absence of triethylamine.

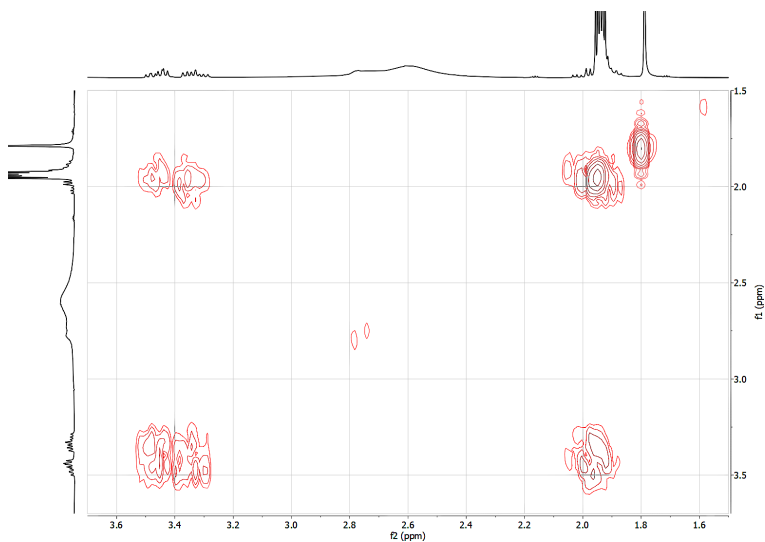


**Figure AII.16.**  $^1\text{H}$ - $^1\text{H}$ -COSY NMR spectrum of  $[2_s]\text{Cl}$  dissolved in  $\text{CD}_3\text{CN}$ . The synthesis was done in absence of triethylamine. The spectrum shows the correlation of protons in  $\text{N-CH}_2\text{-CH}_2\text{-S}$  (3.18–3.50 ppm) with the solvent peak (1.9 ppm), indicating that the solvent peak obscures the proton peak of interest.

**Table AII.1.** Crystallographic data for all crystals in the present work.

	[1s]Cl	[2s-Ag-2s](SbF <sub>6</sub> ) <sub>3</sub>	[2ssquin]
Chemical formula	C <sub>23</sub> H <sub>22</sub> CoN <sub>4</sub> OS· 3(CH <sub>4</sub> O)·Cl	C <sub>50</sub> H <sub>51</sub> AgCo <sub>2</sub> N <sub>9</sub> O <sub>2</sub> S <sub>2</sub> · 3(F <sub>6</sub> Sb)·0.969(C <sub>2</sub> H <sub>3</sub> N)	C <sub>48</sub> H <sub>48</sub> Cl <sub>2</sub> Co <sub>2</sub> N <sub>8</sub> O <sub>2</sub> S <sub>2</sub> · 0.903(C <sub>2</sub> H <sub>3</sub> N)
<i>M<sub>r</sub></i>	593.01	1846.88	1058.87
Crystal system	Triclinic	Monoclinic	Monoclinic
Space group	<i>P</i> -1	<i>P</i> 2 <sub>1</sub> / <i>c</i>	<i>P</i> 2 <sub>1</sub> / <i>n</i>
Cell lengths ( <i>a</i> , <i>b</i> , <i>c</i> ) (Å)	8.8184(3), 13.0506(5), 13.3362(5)	15.7072(5), 27.0793(6), 19.3101(6)	18.4673(4), 14.9350(4), 19.1135(4)
Cell angles (α, β, γ) (°)	63.783(4), 73.530(3), 84.488(3)	90, 112.171(3), 90	90, 97.898(2), 90
Cell volume (Å <sup>3</sup> )	1319.66(10)	7606.1 (4)	5221.7(2)
<i>Z</i>	2	4	4
μ (mm <sup>-1</sup> )	7.11	1.87	0.86
Crystal size (mm)	0.41 × 0.33 × 0.18	0.52 × 0.37 × 0.22	0.35 × 0.22 × 0.20
Temperature (K)	110(2)	110(2)	110(2)
Diffractometer	SuperNova, Dual, Cu at zero, Atlas detector	SuperNova, Dual, Cu at zero, Atlas detector	SuperNova, Dual, Cu at zero, Atlas detector
Radiation type	Cu <i>K</i> α	Mo <i>K</i> α	Mo <i>K</i> α
<i>T</i> <sub>min</sub> , <i>T</i> <sub>max</sub>	0.161, 0.410	0.295, 1.000	0.425, 1.000
No. of measured, independent and observed [ <i>I</i> > 2σ( <i>I</i> )] reflections	16974, 5155, 5078	61799, 21893, 14227	62110, 11982, 9923
<i>R</i> <sub>int</sub>	0.025	0.048	0.045
(sin θ/λ) <sub>max</sub> (Å <sup>-1</sup> )	0.616	0.650	0.650
<i>R</i> [ <i>F</i> <sup>2</sup> > 2σ( <i>F</i> <sup>2</sup> )], <i>wR</i> ( <i>F</i> <sup>2</sup> ), <i>S</i>	0.028, 0.071, 1.05	0.072, 0.231, 1.07	0.048, 0.128, 1.03
No. of reflections	5155	21893	11982
No. of parameters	340	1385	618
No. of restraints	-	2501	2
H-atom treatment	H-atom parameters constrained	H-atom parameters constrained	H-atom parameters constrained
Δρ <sub>max</sub> , Δρ <sub>min</sub> (e Å <sup>-3</sup> )	0.28, -0.46	1.75, -1.28	0.69, -0.59



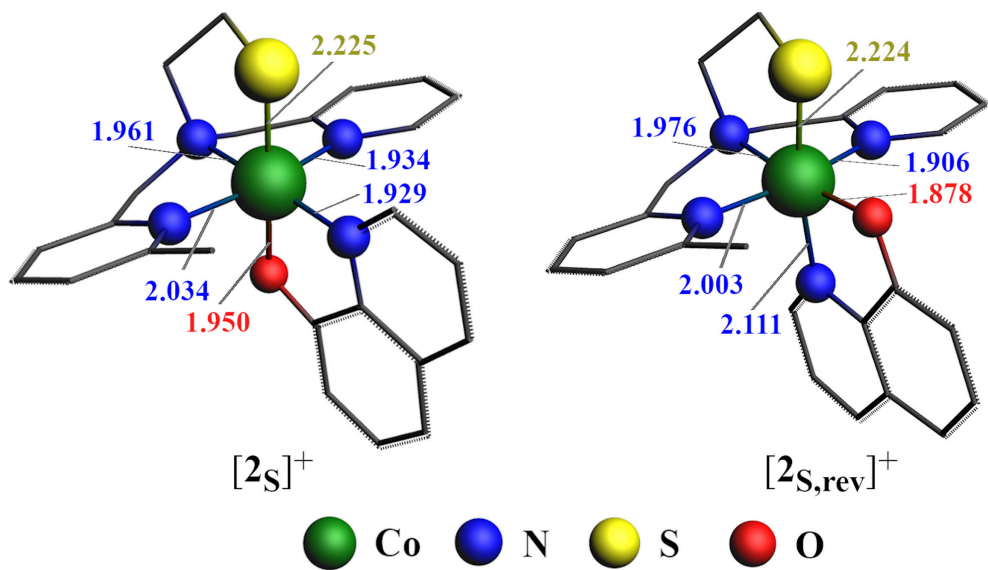


**Figure AII.17.** Optimized geometries of  $[2_S]^+$  and  $[2_{S,rev}]^+$  with selected bond distances (Å).

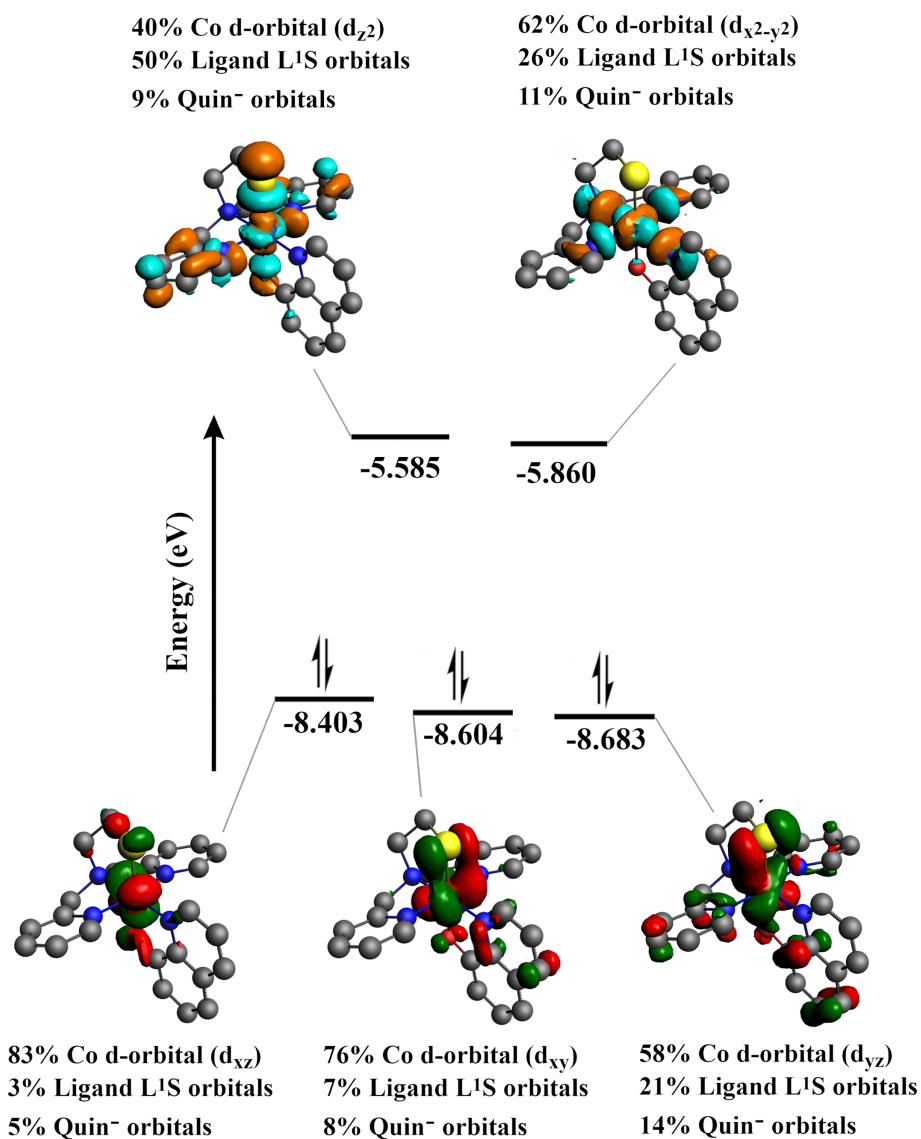


**Figure AII.18.** Several frontier orbitals of  $[1s]^+$  associated with Co  $d$ -orbitals along with their energies, orbital visualization, and orbital composition.

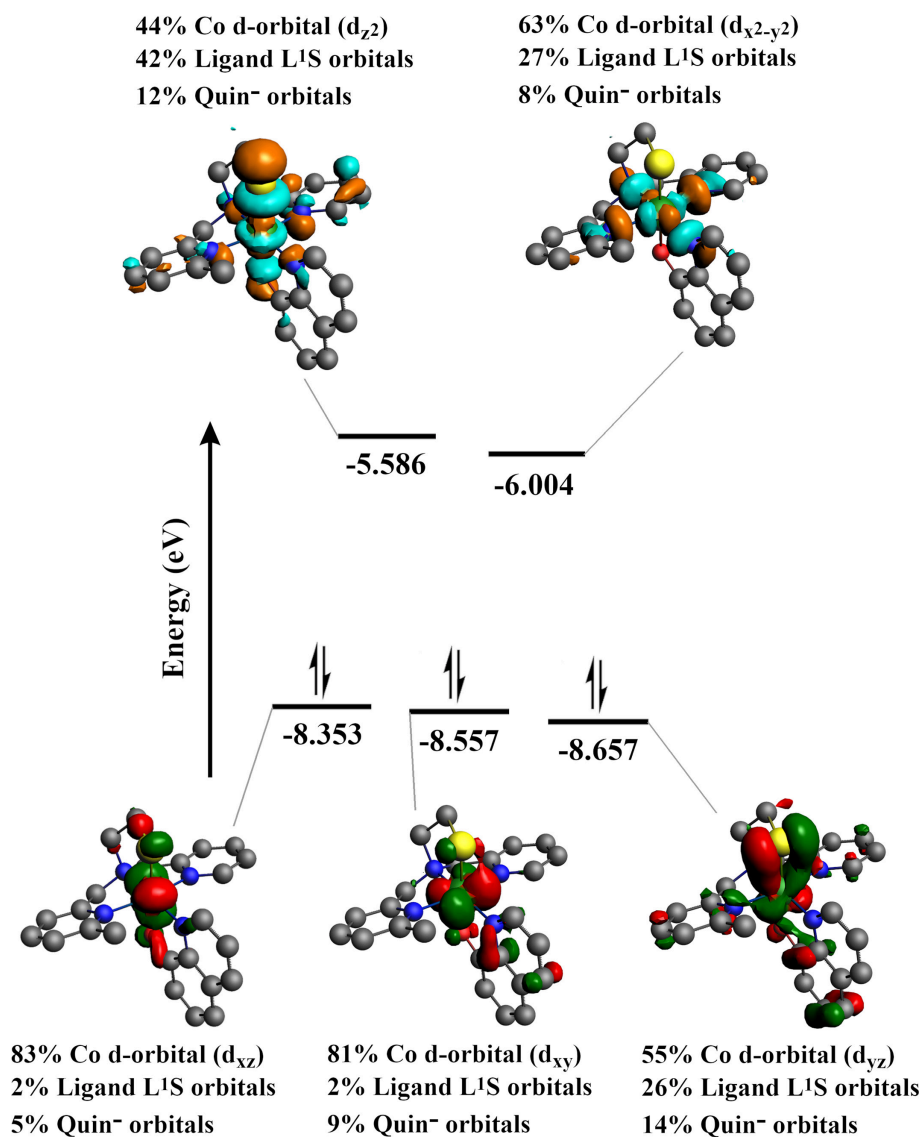


**Figure AII.19.** Several frontier orbitals of  $[2s]^+$  associated with Co  $d$ -orbitals along with their energies, orbital visualization, and orbital composition.

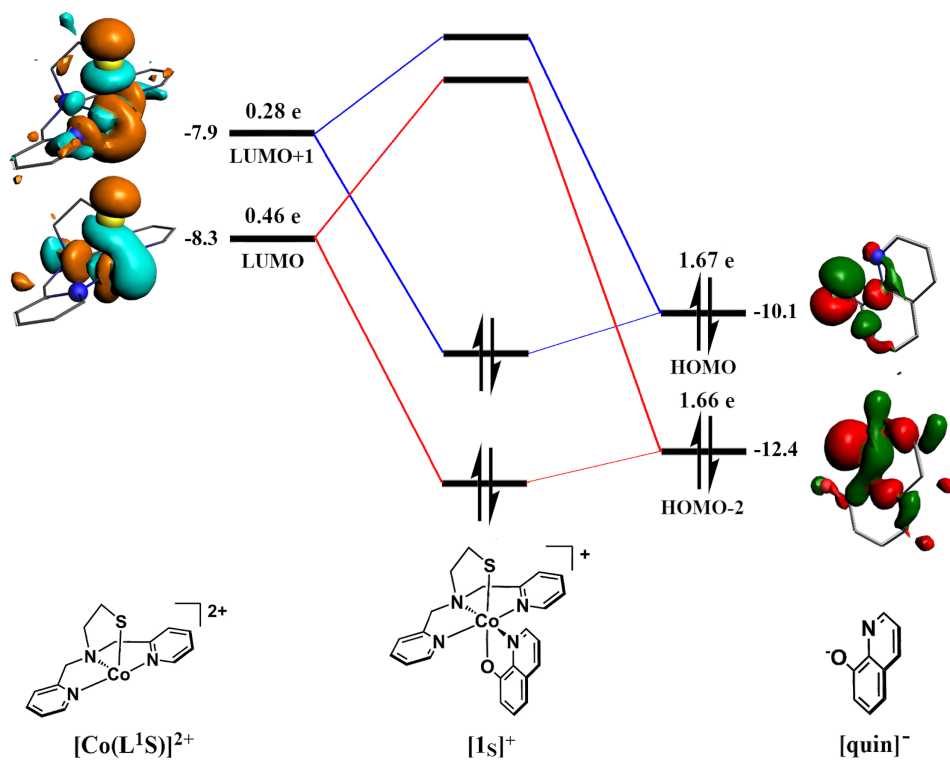


**Figure AII.20.** Molecular orbital diagram for the interaction between the fragments  $[\text{Co}(\text{L}^1\text{S})]^{2+}$  and  $[\text{quin}]^-$  in  $[1\text{s}]^+$ . Fragment molecular orbital energies (in eV) obtained from the Kohn-Sham Fock matrix diagonal elements (see references <sup>1-3</sup> for details).

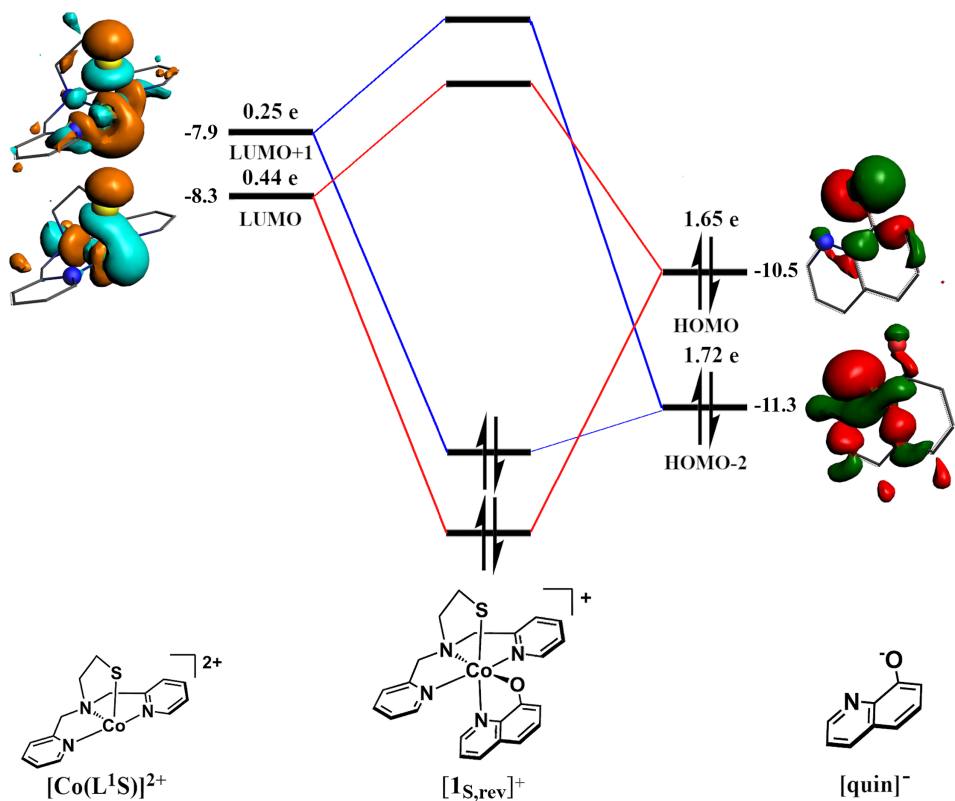


**Figure AII.21.** Molecular orbital diagram for the interaction between the fragments  $[\text{Co}(\text{L}^1\text{S})]^{2+}$  and  $[\text{quin}]^-$  in  $[\mathbf{1}_{\text{s,rev}}]^+$ . Fragment molecular orbital energies (in eV) obtained from the Kohn-Sham Fock matrix diagonal elements (see references <sup>1-3</sup> for details).

## References

1. Bickelhaupt, F. M., Solà, M. and Fonseca Guerra, C. *J. Mol. Model.* **2006**, 12 (5), 563-568.
2. Bickelhaupt, F. M., Solà, M. and Fonseca Guerra, C. *Inorg. Chem.* **2007**, 46 (13), 5411-5418.
3. Bickelhaupt, F. M., Solà, M. and Guerra, C. F. *J. Comput. Chem.* **2007**, 28 (1), 238-250.

# Appendix III

## Supplementary Information for Chapter 4

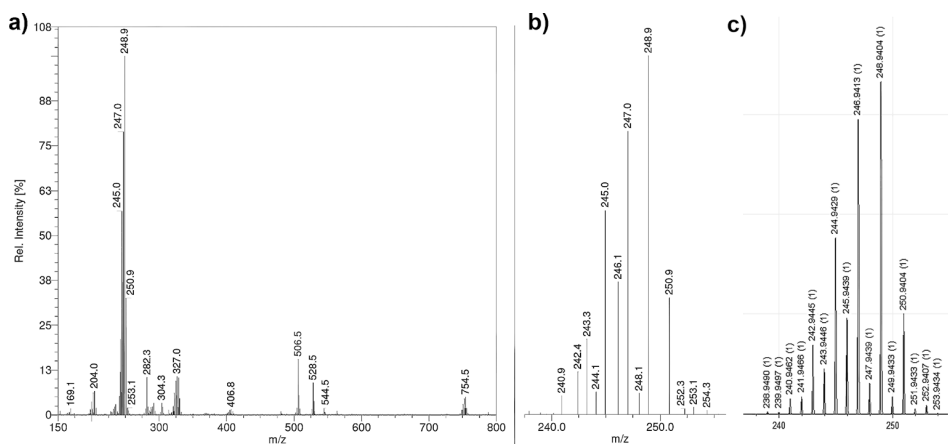


**Figure AIII.1.** ESI-MS spectrum of a) selenocystamine hydrochloride; b) the experimental isotopic distribution of the main signal; c) simulated isotopic distribution. ESI-MS found (calcd.) for  $[(\text{NH}_2\text{C}_2\text{H}_4\text{Se})_2 + \text{H}]^+$   $m/z$  248.9 (248.94).

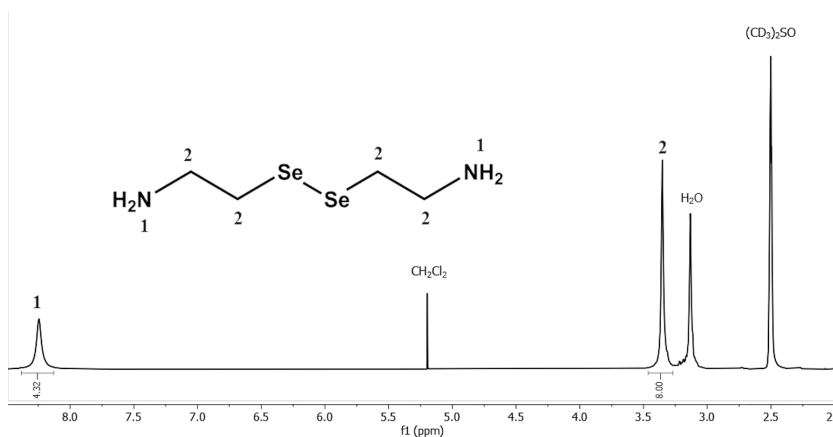


**Figure AIII.2.**  $^1\text{H}$ -NMR spectrum of selenocystamine hydrochloride in  $(\text{CD}_3)_2\text{SO}$ .

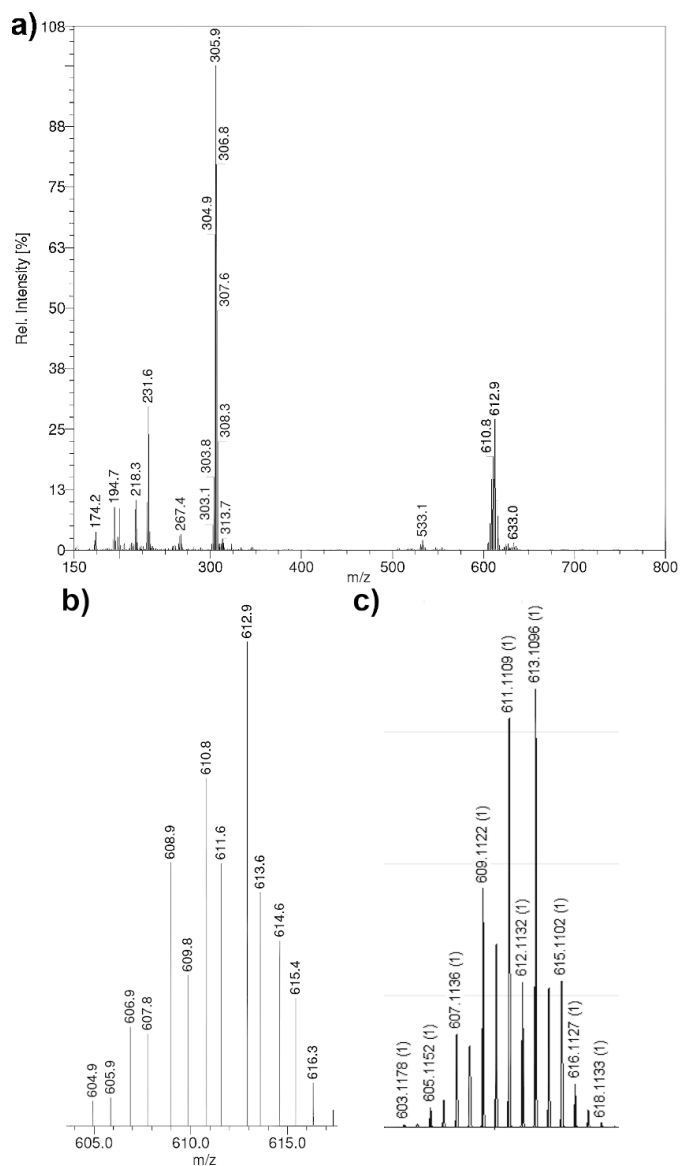


**Figure AIII.3.** ESI-MS spectrum of a)  $L^1\text{SeSeL}^1$ ; b) the experimental isotopic distribution of the main signal; c) simulated isotopic distribution. ESI-MS found (calcd.) for  $[L^1\text{SeSeL}^1 + \text{H}]^+$   $m/z$  612.9 (613.1) and for  $[L^1\text{SeSeL}^1 + 2\text{H}]^{2+}$   $m/z$  306.8 (307.06).

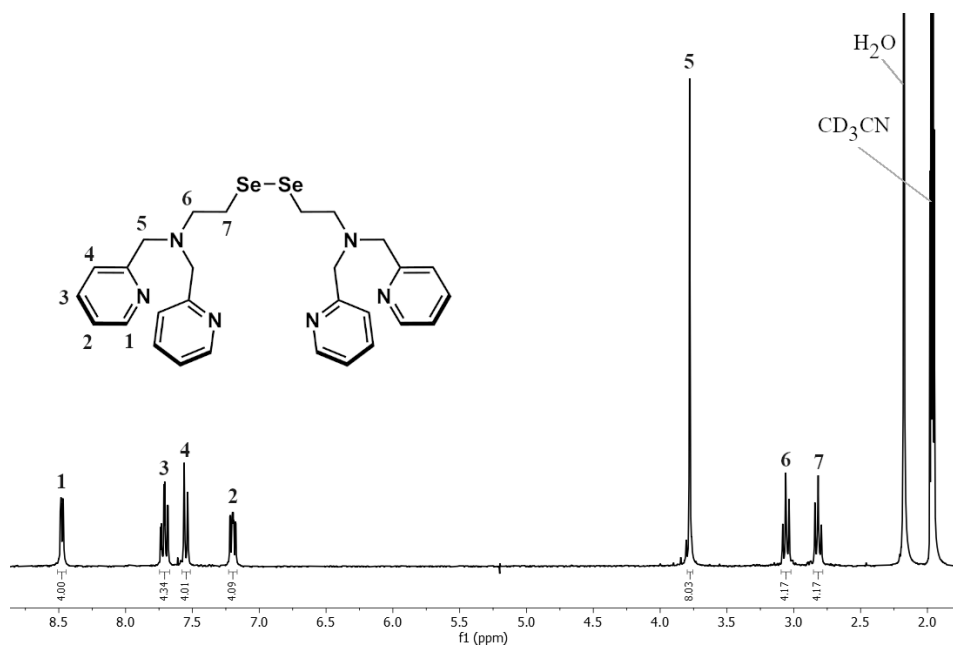


**Figure AIII.4.**  $^1H$ -NMR spectrum of  $L^1SeSeL^1$  in  $CD_3CN$ .



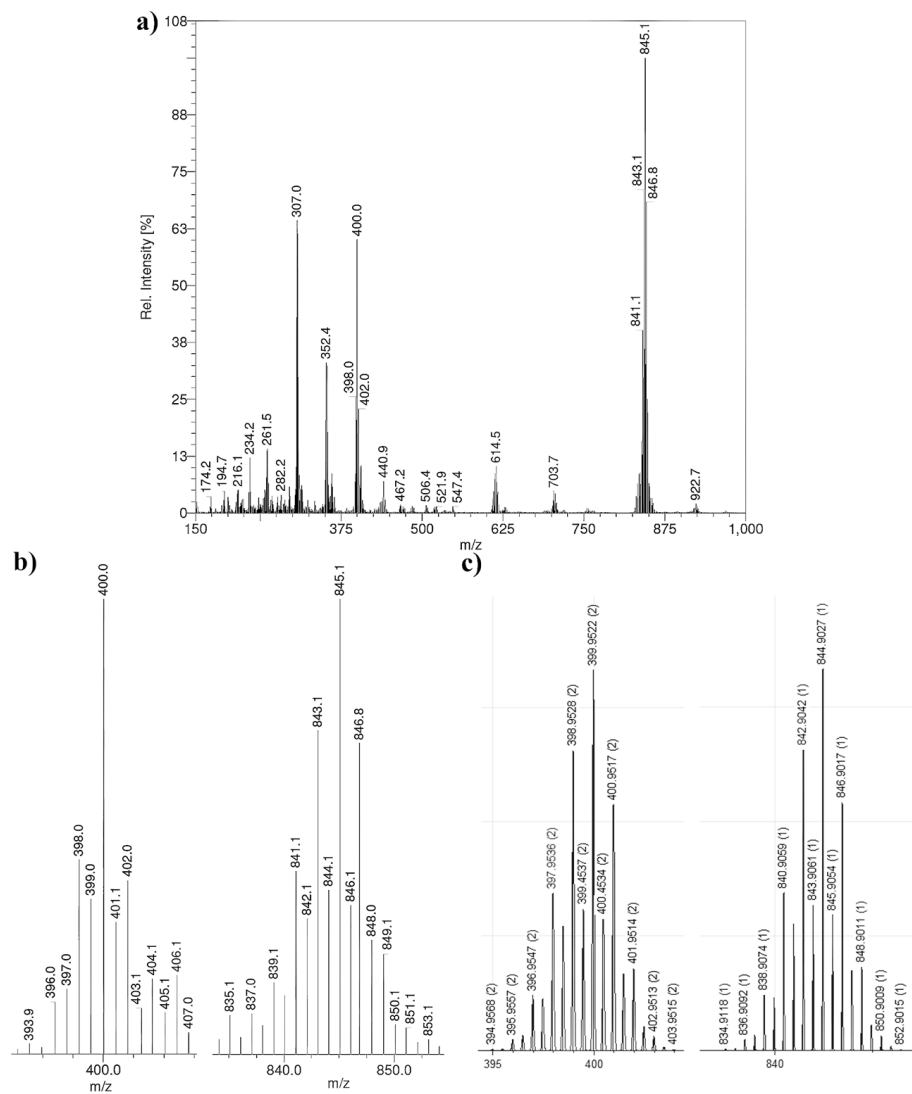


**Figure AIII.5.** ESI-MS spectrum of a)  $[\text{Co}_2(\text{L}^1\text{SeSeL}^1)(\text{Cl})_4]$  (**1**); b) the experimental isotopic distribution of the main peaks; c) simulated isotopic distribution. ESI-MS found (calcd.) for  $[\mathbf{1} - 2\text{Cl}]^{2+}$   $m/z$  400.0 (399.95) and for  $[\mathbf{1} - 2\text{Cl} + \text{HCOO}]^+$   $m/z$  845.1 (844.90).

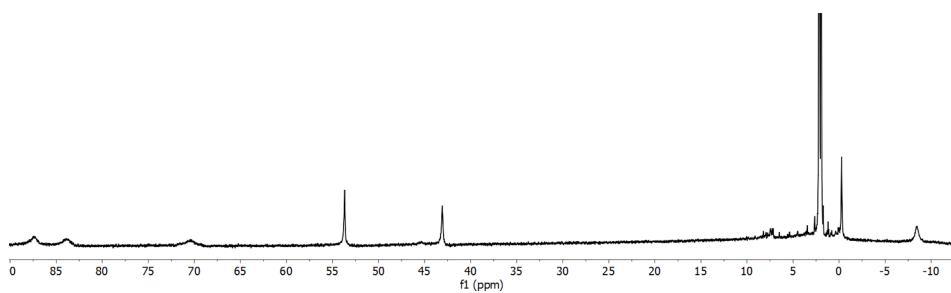


**Figure AIII.6.**  $^1\text{H}$ -NMR spectrum of compound [1] in  $\text{CD}_3\text{CN}$ .

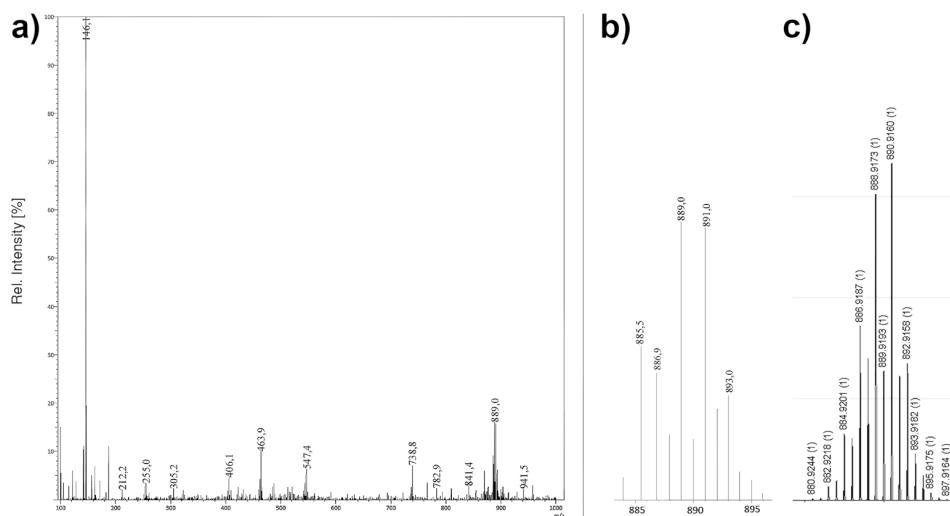


**Figure AIII.7.** ESI-MS spectrum of a)  $[\text{Co}(\text{L}^1\text{Se})(\text{NCS})_2]$  ([2]); b) the experimental isotopic distribution of the main signal; c) simulated isotopic distribution. ESI-MS found (calcd.) for  $[2 - \text{SCN}^- + \text{MeCN}]^+ m/z$  463.9 (463.99), for  $[2 \times 2 - 2\text{SCN}^- + \text{HCOO}^-]^+ m/z$  889.0 (888.92).

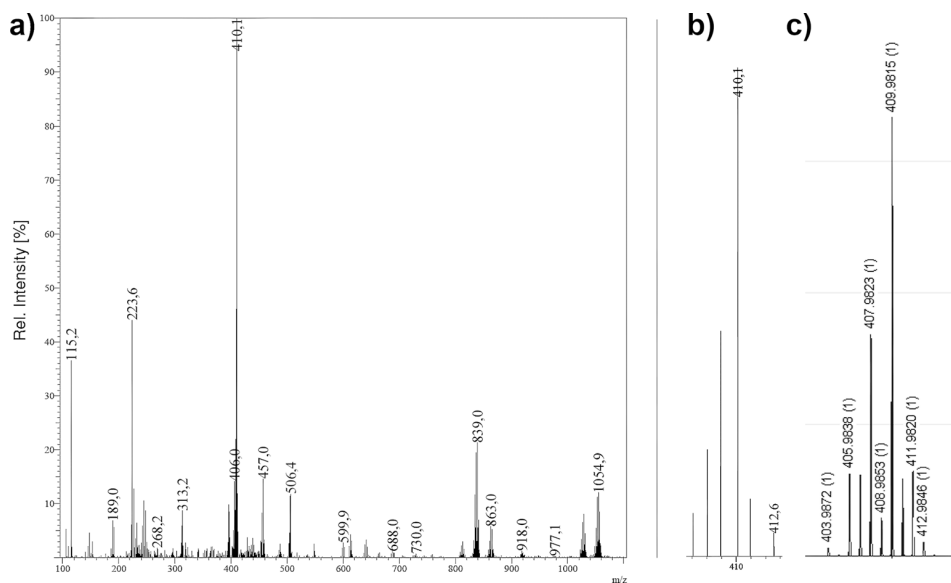


**Figure AIII.8.** ESI-MS spectrum of a)  $[\text{Co}(\text{L}^1\text{Se})(\text{MeCN})_2](\text{SbF}_6)_2$  (**[3]**); b) the experimental isotopic distribution of the main signal; c) simulated isotopic distribution. ESI-MS found (calcd.) for  $[\mathbf{3}]^{2+}$   $m/z$  223.6 (223.52), for  $[\mathbf{3} - 2\text{MeCN} + \text{HCOO}]^+ m/z$  410.1 (409.98), for the dimer  $[2 \times \mathbf{3} - 4\text{MeCN} + 3\text{HCOO}]^+ m/z$  863.0 (862.96), and  $[2 \times \mathbf{3} - 4\text{MeCN} + 2\text{HCOO}^- + \text{SbF}_6]^- m/z$  1054.9 (1054.86).

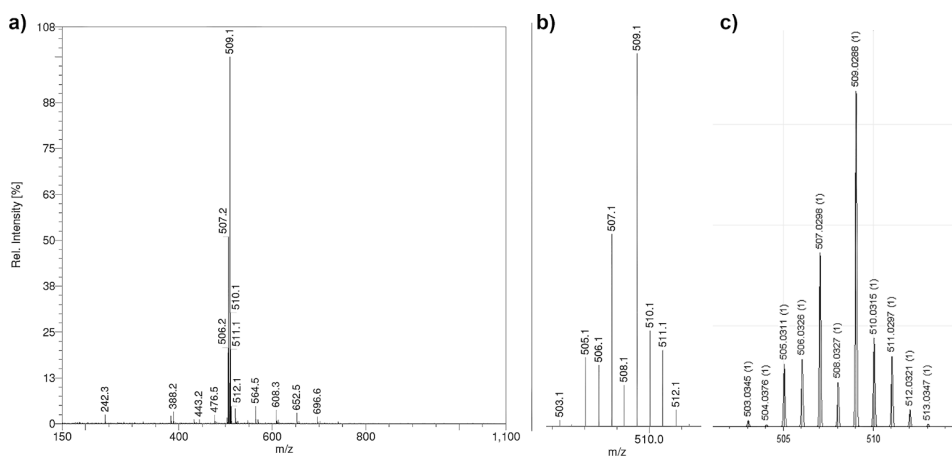


**Figure AIII.9.** ESI-MS spectrum of a) compound  $[\text{Co}(\text{L}^1\text{Se})(\text{quin})]\text{Cl}$  (**[4]Cl**); b) the experimental isotopic distribution of the main signal; c) simulated isotopic distribution. ESI-MS found (calcd.) for  $[\mathbf{4}]^+ m/z$  509.1 (509.03).

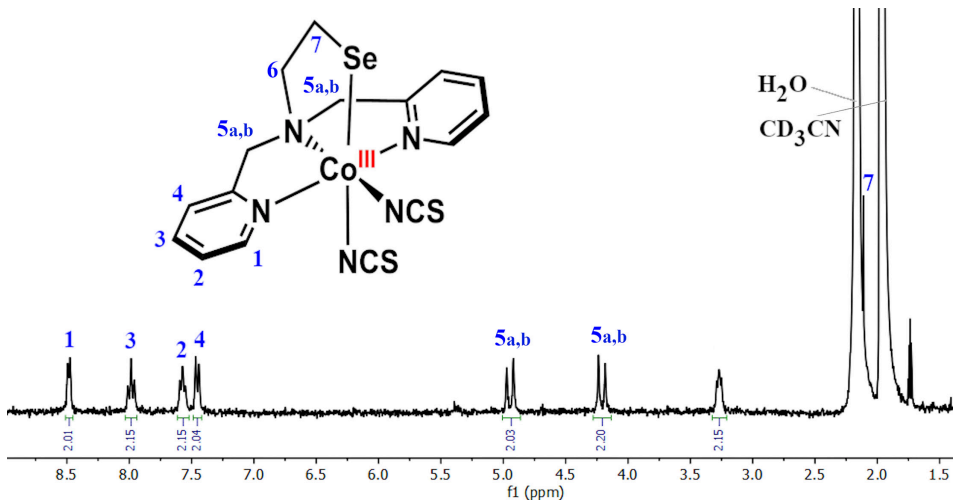


**Figure AIII.10.**  $^1\text{H}$ -NMR spectrum of compound [2] dissolved in  $\text{CD}_3\text{CN}$ .

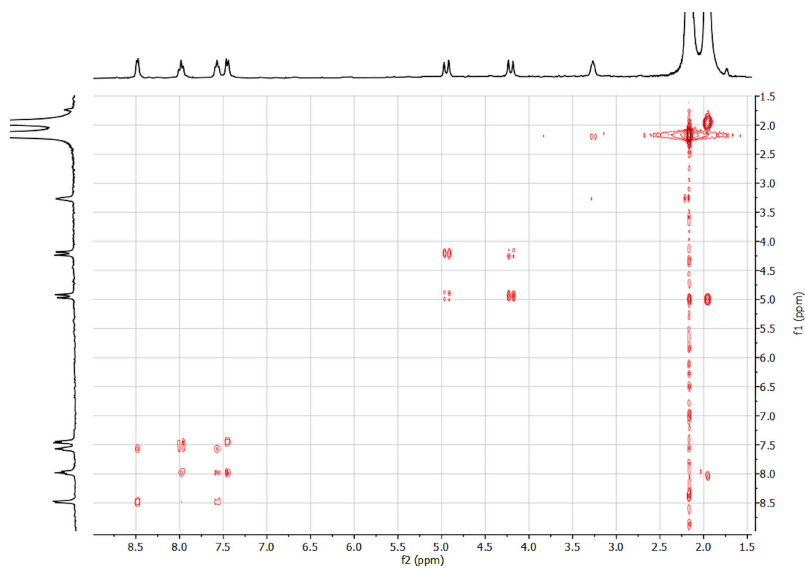


**Figure AIII.11.**  $^1\text{H}$ - $^1\text{H}$  COSY NMR spectrum of compound [2] dissolved in  $\text{CD}_3\text{CN}$ .

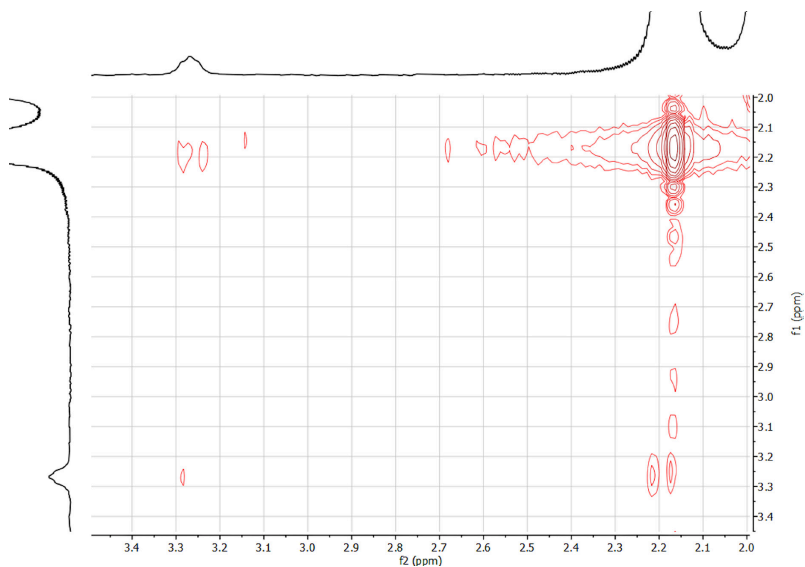


**Figure AIII.12.**  $^1\text{H}$ - $^1\text{H}$  COSY NMR spectrum at 2.0-3.5 ppm of compound [2] dissolved in  $\text{CD}_3\text{CN}$ . The correlation of the  $\text{H}_2\text{N}-\text{CH}_2-\text{CH}_2-\text{Se}$  (about 3.3 ppm) with  $\text{H}_2\text{N}-\text{CH}_2-\text{CH}_2-\text{Se}$  (about 2.1-2.2 ppm) is shown.

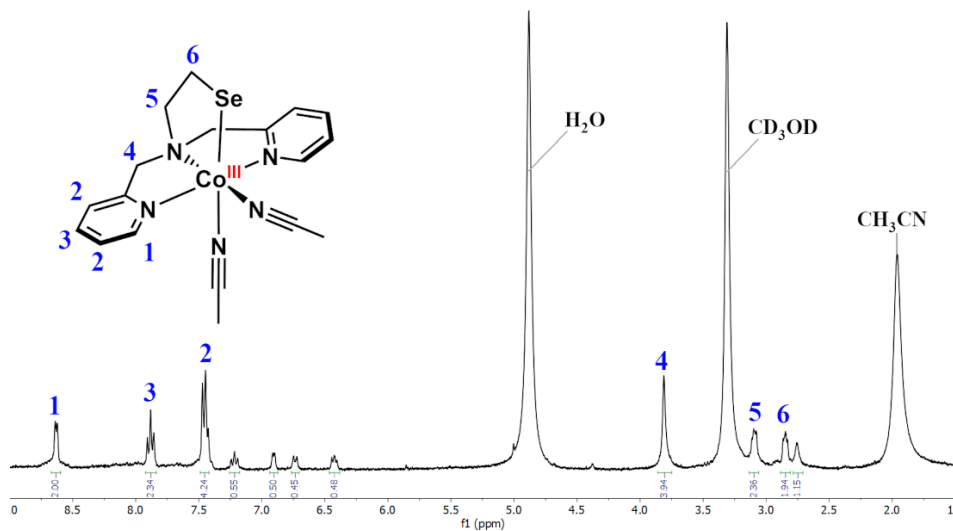


**Figure AIII.13.**  $^1\text{H}$ -NMR spectrum [3]( $\text{SbF}_6$ ) $_2$  dissolved in  $\text{CD}_3\text{OD}$ . The spectrum shows unassigned aromatic peaks at 6.4-7.25 ppm and an aliphatic peak at 2.75 ppm, most likely arises from the degradation of the ligand.

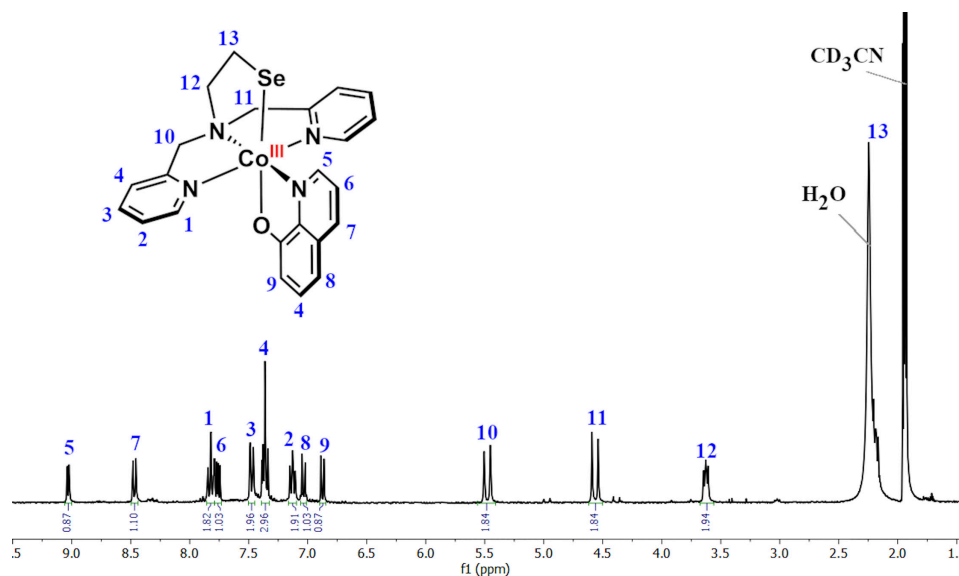


Figure AIII.14.  $^1\text{H}$ -NMR spectrum of compound [4]Cl dissolved in  $\text{CD}_3\text{CN}$ .

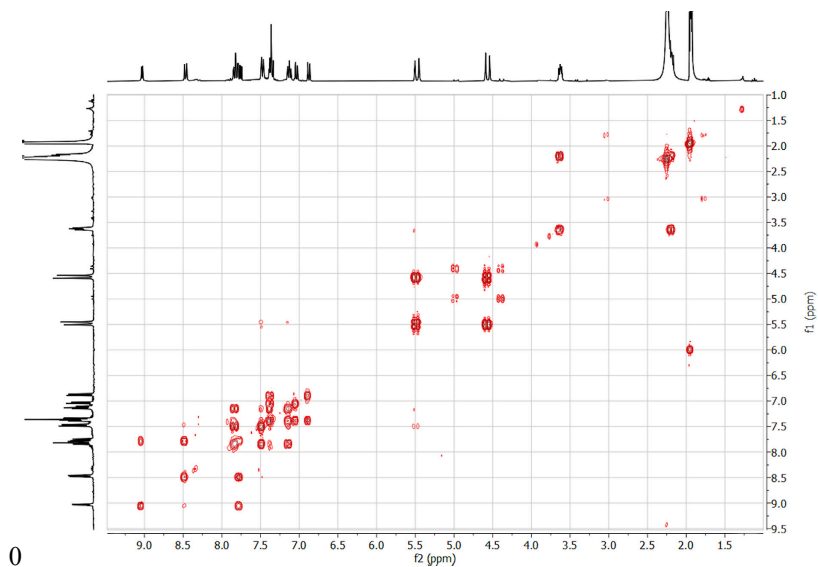
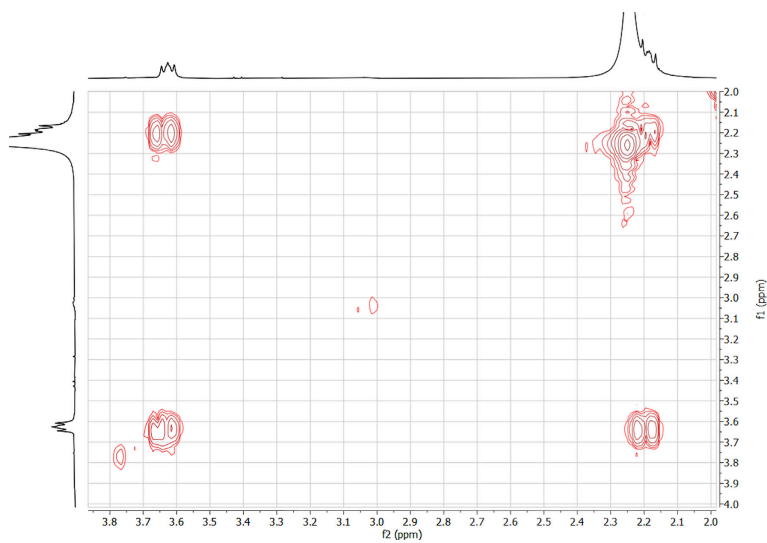


Figure AIII.15.  $^1\text{H}$ - $^1\text{H}$  COSY NMR spectrum of compound [4]Cl dissolved in  $\text{CD}_3\text{CN}$ .



**Figure AIII.16.**  $^1\text{H}$ - $^1\text{H}$  COSY NMR spectrum at 2.0-4.0 ppm of compound [4]Cl dissolved in  $\text{CD}_3\text{CN}$ . The correlation of the  $\text{H}_2\text{N}-\text{CH}_2-\text{CH}_2-\text{Se}$  (about 3.6 ppm) with  $\text{H}_2\text{N}-\text{CH}_2-\text{CH}_2-\text{Se}$  (about 2.2 ppm) is shown.

**Table AIII.1.** Crystallographic data for all crystals in the present work.

	[1]	[2]	[4]Cl
Chemical formula	C <sub>28</sub> H <sub>32</sub> Cl <sub>4</sub> Co <sub>2</sub> N <sub>6</sub> Se <sub>2</sub> · C <sub>4</sub> H <sub>10</sub> O	C <sub>16</sub> H <sub>16</sub> CoN <sub>5</sub> S <sub>2</sub> Se	C <sub>23</sub> H <sub>22</sub> CoN <sub>4</sub> OSe· 2(CHCl <sub>3</sub> )·Cl
<i>M<sub>r</sub></i>	944.29	480.35	782.52
Crystal system	Triclinic	Orthorhombic	Monoclinic
Space group	<i>P</i> −1	<i>Pbca</i>	<i>P</i> 2 <sub>1</sub> / <i>n</i>
Cell lengths ( <i>a</i> , <i>b</i> , <i>c</i> ) (Å)	8.3598(3) 13.7008(6) 17.2414(14)	11.1298(4) 16.5289(5) 19.6469(7)	13.5307(3) 13.2033(3) 17.4772(4)
Cell angles (α, β, γ) (°)	91.225(5) 101.881(4) 92.102(3)	90 90 90	90 105.487(3) 90
Cell volume (Å <sup>3</sup> )	1930.31(19)	3614.3(2)	3008.93(13)
<i>Z</i>	2	8	4
μ (mm <sup>−1</sup> )	3.06	3.20	2.43
Crystal size (mm)	0.22 × 0.13 × 0.03	0.21 × 0.14 × 0.06	0.26 × 0.22 × 0.04
Temperature (K)	110	110	110
Diffractometer	SuperNova, Dual, Cu at zero, Atlas detector	SuperNova, Dual, Cu at zero, Atlas detector	SuperNova, Dual, Cu at zero, Atlas detector
Radiation type	Mo <i>K</i> α	Mo <i>K</i> α	Mo <i>K</i> α
<i>T</i> <sub>min</sub> , <i>T</i> <sub>max</sub>	0.470, 1.000	0.552, 1.000	0.467, 1.000
No. of measured, independent and observed [ <i>I</i> > 2σ( <i>I</i> )] reflections	25557, 7594, 5429	32659, 4155, 3485	39269, 6915, 5863
<i>R</i> <sub>int</sub>	0.071	0.049	0.048
(sin θ/λ) <sub>max</sub> (Å <sup>−1</sup> )	0.617	0.650	0.650
<i>R</i> [ <i>F</i> <sup>2</sup> > 2σ( <i>F</i> <sup>2</sup> )], <i>wR</i> ( <i>F</i> <sup>2</sup> ), <i>S</i>	0.048, 0.105, 1.04	0.026, 0.058, 1.06	0.030, 0.068, 1.03
No. of reflections	7594	4155	6915
No. of parameters	426	226	443
No. of restraints	−	−	289
H-atom treatment	H-atom parameters constrained	H-atom parameters constrained	H-atom parameters constrained
Δρ <sub>max</sub> , Δρ <sub>min</sub> (e Å <sup>−3</sup> )	0.88, −0.55	0.59, −0.37	0.94, −0.81



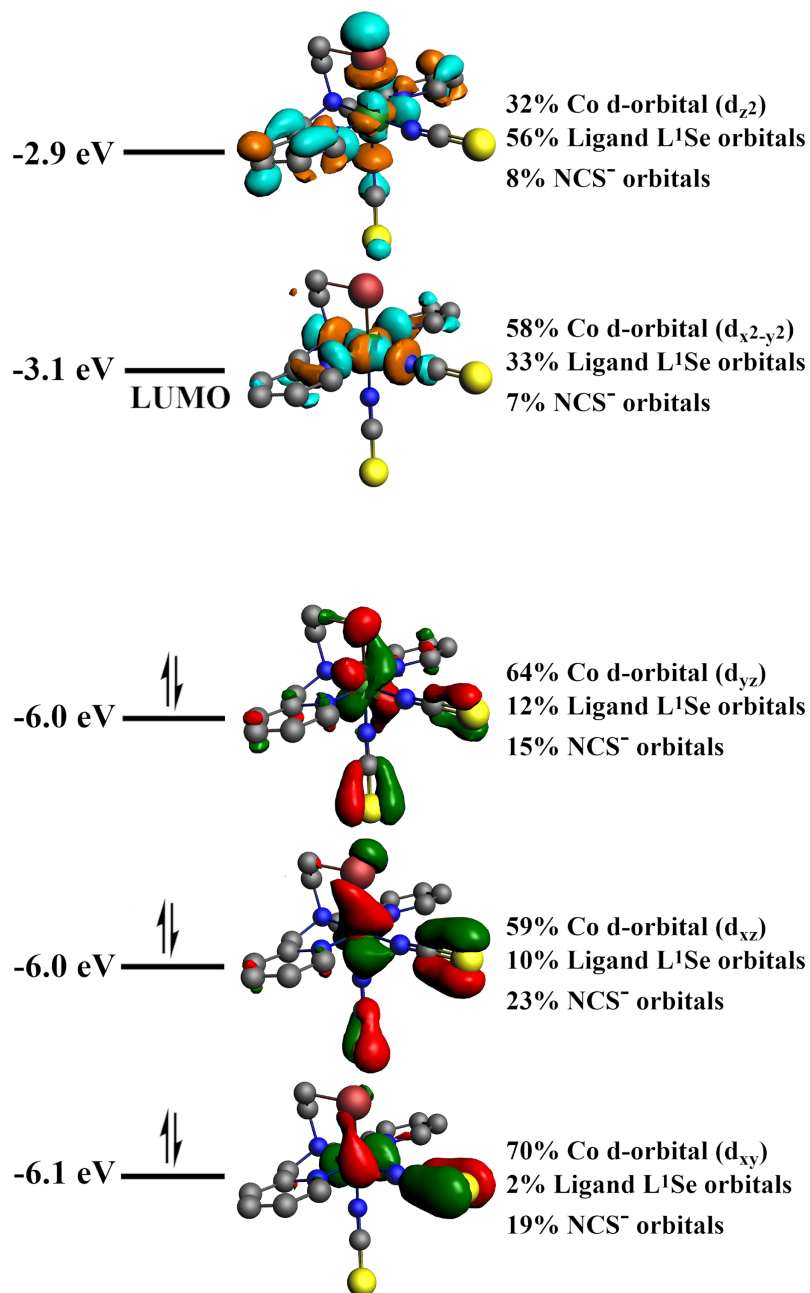


**Figure AIII.17.** Several frontier orbitals of [2] associated with Co *d*-orbitals along with their energies, orbital visualization, and orbital composition.

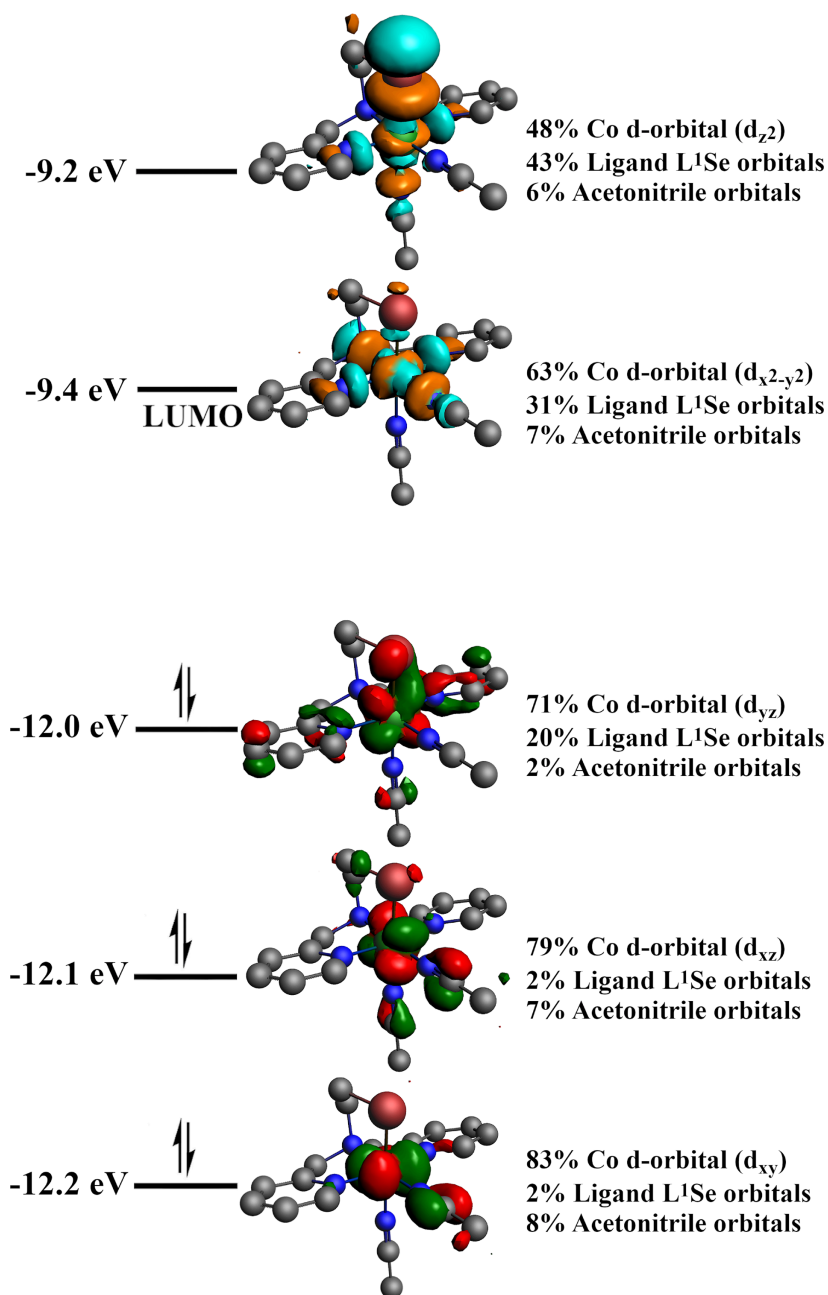


**Figure AIII.18.** Several frontier orbitals of  $[3]^{2+}$  associated with Co  $d$ -orbitals along with their energies, orbital visualization, and orbital composition.

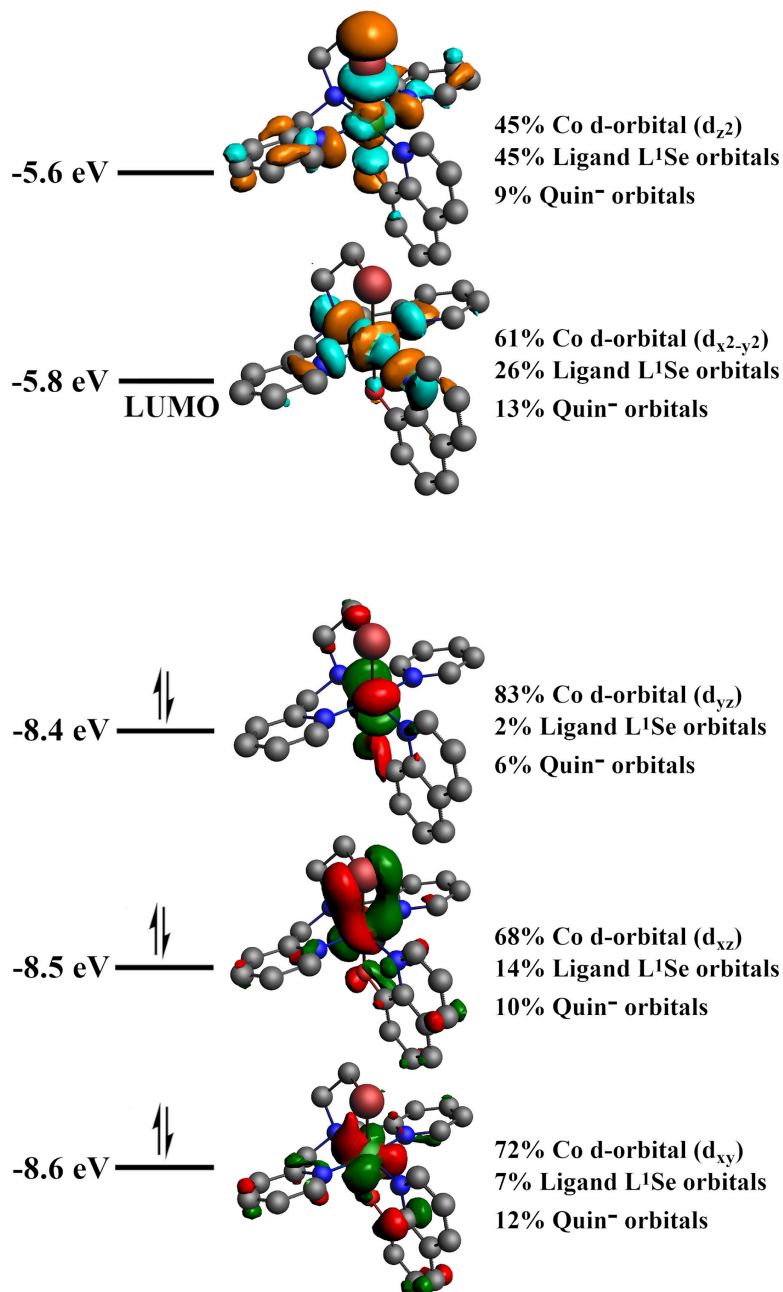


**Figure AIII.19.** Several frontier orbitals of  $[4]^+$  associated with Co  $d$ -orbitals along with their energies, orbital visualization, and orbital composition.

# Appendix IV

## Supplementary Information for Chapter 5

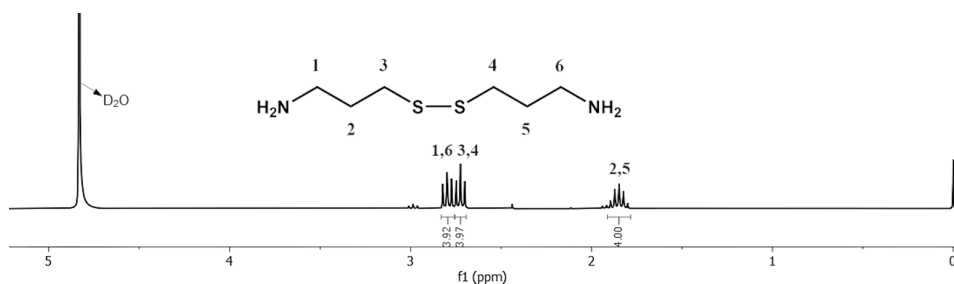


**Figure AIV.1.**  $^1\text{H}$ -NMR spectrum of bis(3-aminopropyldisulfide) in  $\text{D}_2\text{O}$ .

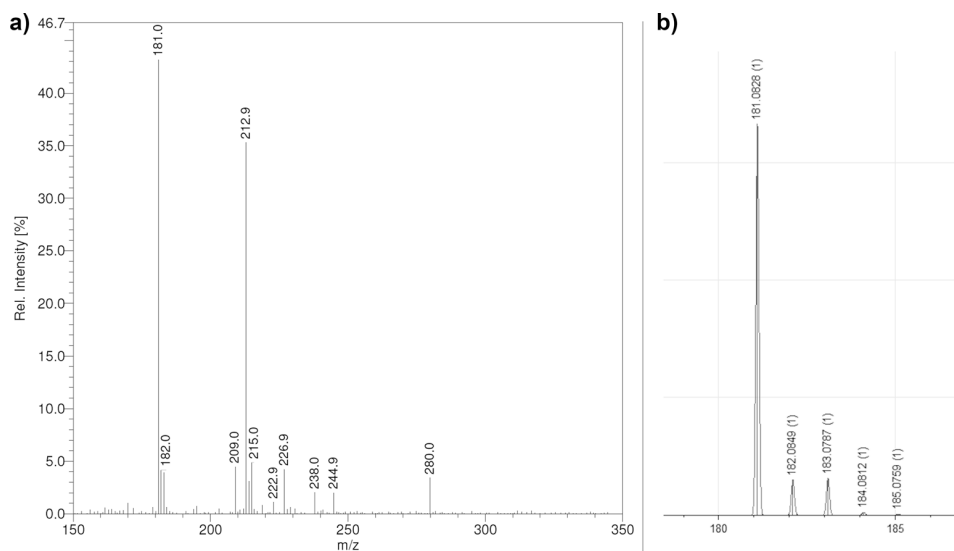


**Figure AIV.2.** ESI-MS spectrum of a) bis(3-aminopropyldisulfide) dissolved in  $\text{H}_2\text{O}$ ; b) simulated spectrum at  $m/z$  180–185. ESI-MS found (calcd.) for  $[\text{bis(3-aminopropyldisulfide)} + \text{H}]^+$   $m/z$  181.0 (181.08).

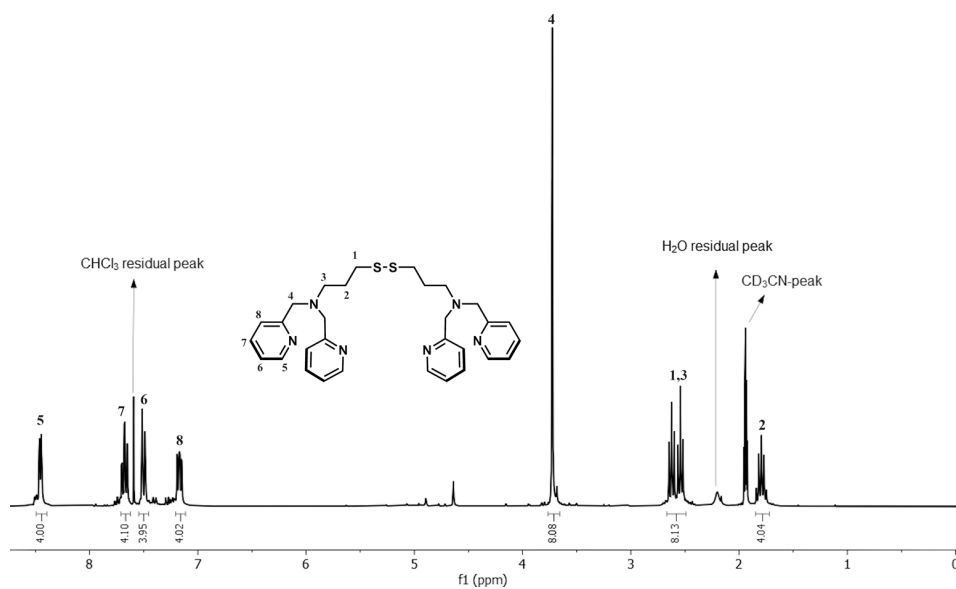


**Figure AIV.3.**  $^1\text{H}$ -NMR spectrum of  $\text{L}^{\text{p}}\text{SSL}^{\text{p}}$  in  $\text{CD}_3\text{CN}$ .

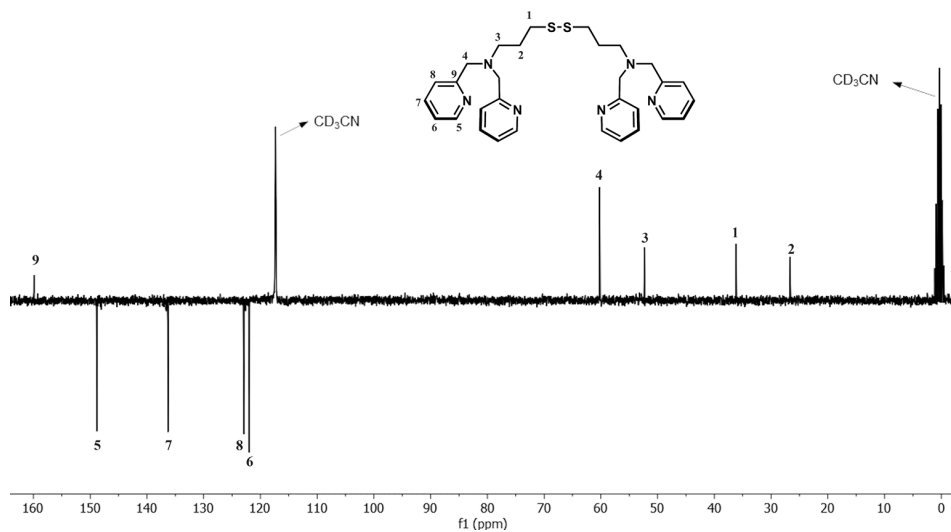


**Figure AIV.4.**  $^{13}\text{C}$ -NMR spectrum of  $\text{L}^{\text{p}}\text{SSL}^{\text{p}}$  in  $\text{CD}_3\text{CN}$ .

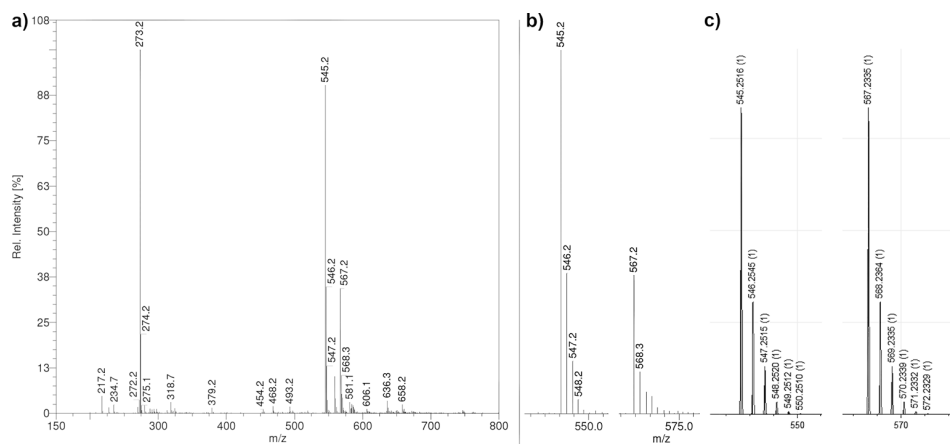


**Figure AIV.5.** ESI-MS spectrum of a) L<sup>p</sup>SSLP dissolved in methanol; b) the experimental isotopic distribution; c) simulated isotopic distribution at  $m/z$  540–575. ESI-MS found (calcd.) for [L<sup>p</sup>SSLP + Na]<sup>+</sup>  $m/z$  567.2 (567.2), for [L<sup>p</sup>SSLP + H]<sup>+</sup>  $m/z$  545.2 (545.2), for [L<sup>p</sup>SSLP + 2H]<sup>2+</sup>  $m/z$  273.2 (273.1).

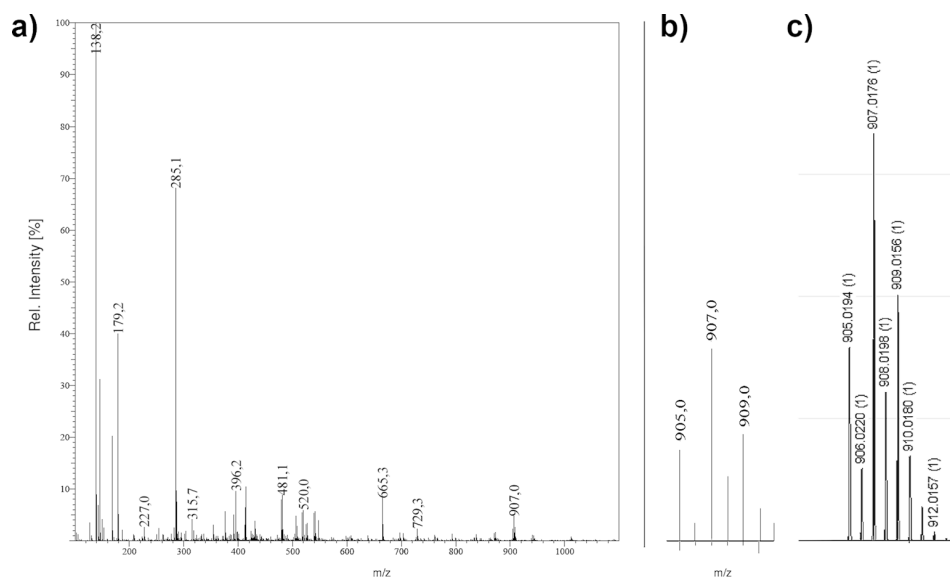


**Figure AIV.6.** ESI-MS spectrum of a) [1Br<sup>-</sup>] dissolved in acetonitrile; b) the experimental isotopic distribution; c) simulated isotopic distribution. ESI-MS found (calcd.) for [1Br<sup>-</sup> - 2Br<sup>-</sup> + HCOO<sup>-</sup>]<sup>+</sup>  $m/z$  907.0 (907.02) and for [1Br<sup>-</sup> - 3Br<sup>-</sup> + HCOO<sup>-</sup>]<sup>2+</sup>  $m/z$  414.1 (413.5).

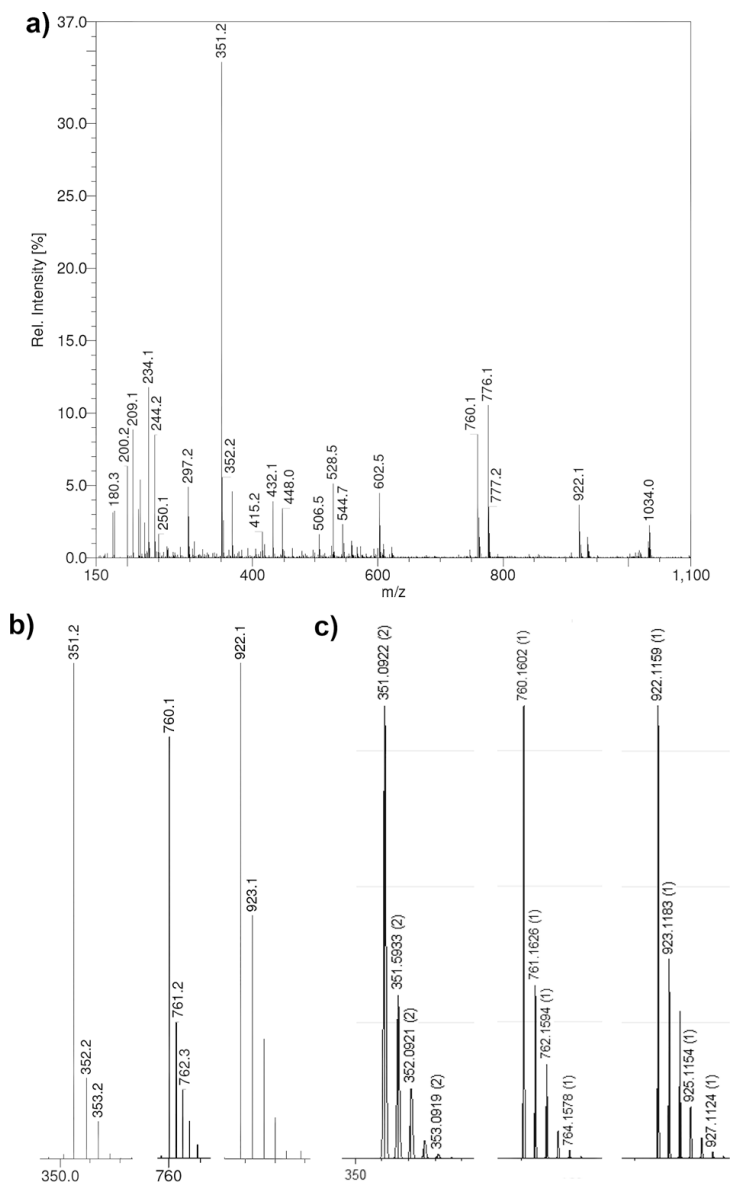


**Figure AIV.7.** ESI-MS spectrum of a) [1NCS] dissolved in methanol; b) the experimental isotopic distributions; c) simulated isotopic distributions at different  $m/z$ . ESI-MS found (calcd.) for [1NCS - NCS<sup>-</sup> + HCOO<sup>-</sup> + H<sup>+</sup>]<sup>+</sup>  $m/z$  922.1 (922.1), for [1NCS - 3NCS<sup>-</sup>]<sup>+</sup> (partial reduction from the ESI-MS)  $m/z$  760.1 (760.16), and for [1NCS - 4NCS<sup>-</sup>]<sup>2+</sup> (partial reduction from the ESI-MS)  $m/z$  351.09 (351.1).

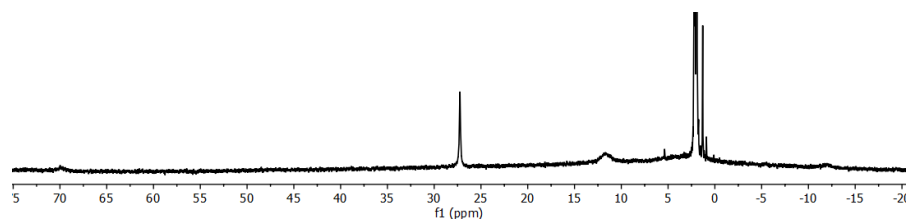


**Figure AIV.8.**  $^1\text{H}$ -NMR spectrum of  $[\mathbf{1}_{\text{NCS}}]$  dissolved in  $\text{CD}_3\text{CN}$ .

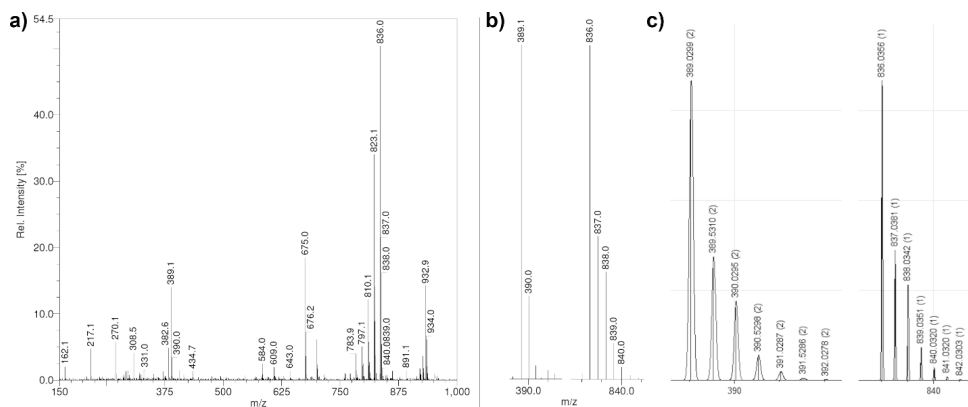


**Figure AIV.9.** ESI-MS spectrum of a)  $[\mathbf{2}_{\text{NCS}}]$  dissolved in acetonitrile; b) the experimental isotopic distribution of the main signals; c) simulated isotopic distribution of the main signals. ESI-MS found (calcd.) for  $[\mathbf{2}_{\text{NCS}} - \text{NCS}]^+ m/z$  836.0 (836.0), for  $[\mathbf{2}_{\text{NCS}} - 2\text{NCS}]^{2+} m/z$  389.1 (389.0).

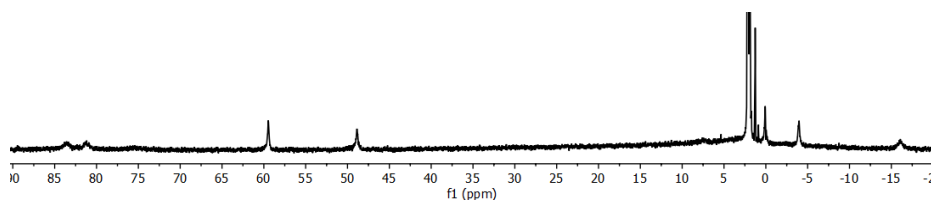


**Figure AIV.10.**  $^1\text{H}$ -NMR spectrum of  $[\mathbf{2}_{\text{NCS}}]$  dissolved in  $\text{CD}_3\text{CN}$ .



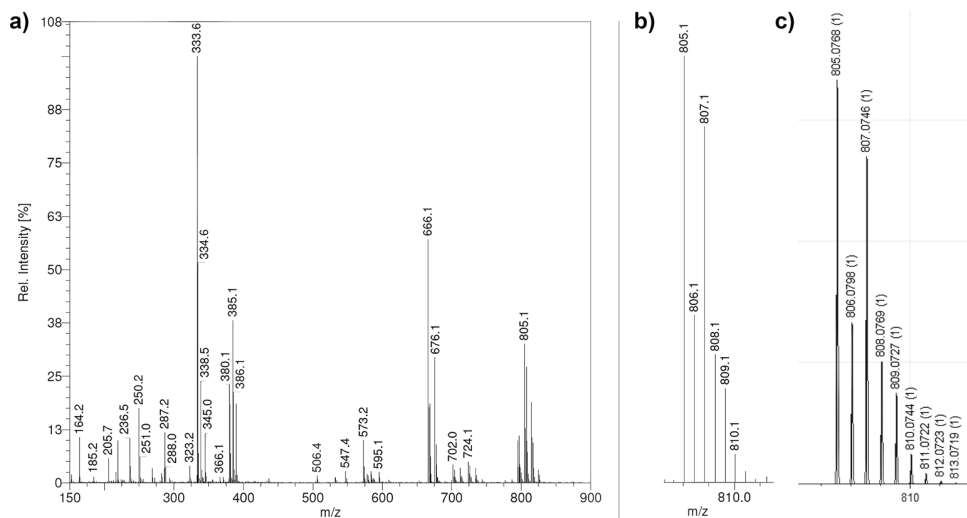


**Figure AIV.11.** ESI-MS spectrum of compound a) [3Cl] dissolved in methanol; b) the experimental isotopic distribution; c) simulated isotopic distribution at  $m/z$  800–815. ESI-MS found (calcd.) for  $[3\text{Cl} - 2\text{Cl}^- + \text{HCOO}^-]^+$   $m/z$  805.1 (805.08), for  $[3\text{Cl} - 3\text{Cl}^- + \text{HCOO}^-]^{2+}$   $m/z$  385.1 (385.1), and for  $[3\text{Cl} - 2\text{Cl}^-]^{2+}$   $m/z$  380.1 (380.04).

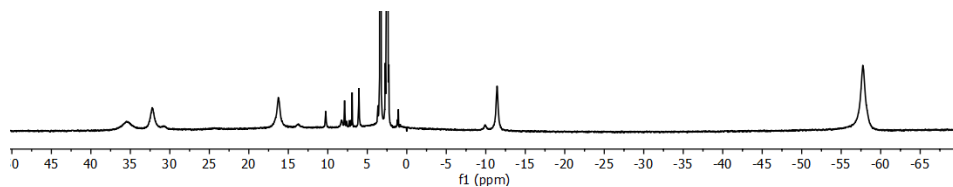


**Figure AIV.12.**  $^1\text{H}$ -NMR spectrum of compound [3Cl] dissolved in  $(\text{CD}_3)_2\text{SO}$ .

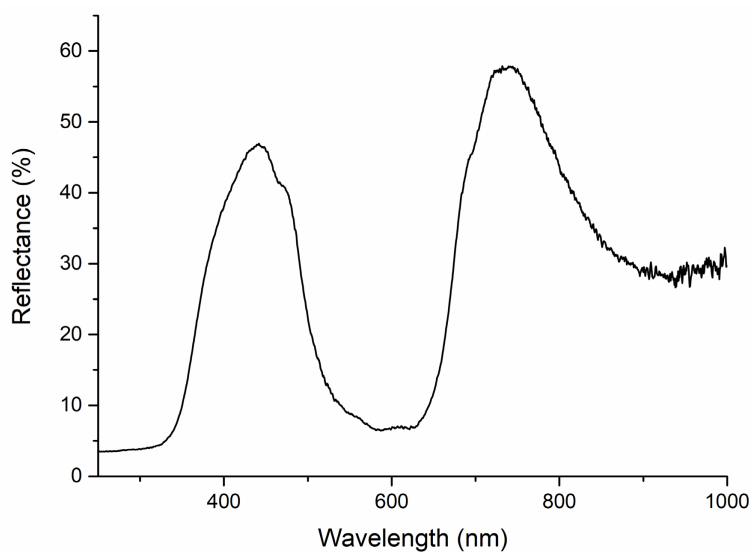


**Figure AIV.13.** Solid state reflectance spectrum of compound [1Br].

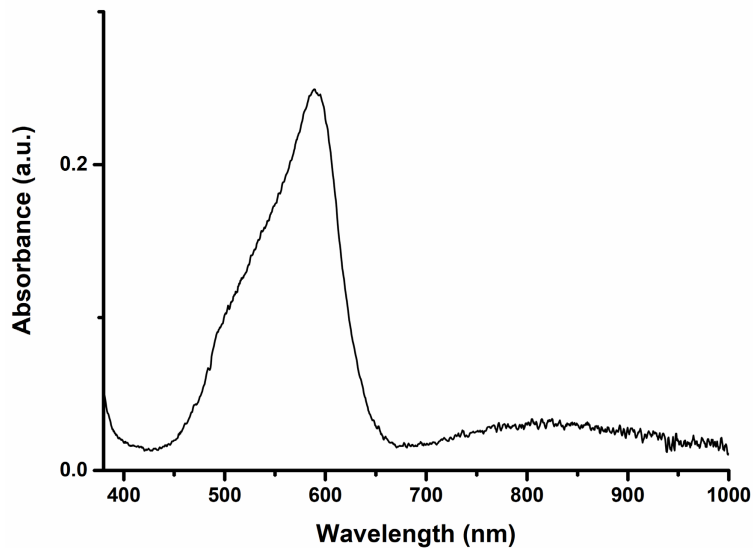


**Figure AIV.14.** UV-Visible spectrum of 2.5 mM solution of [1NCS] in acetone, recorded using a transmission dip probe with path length of 1.4 mm.

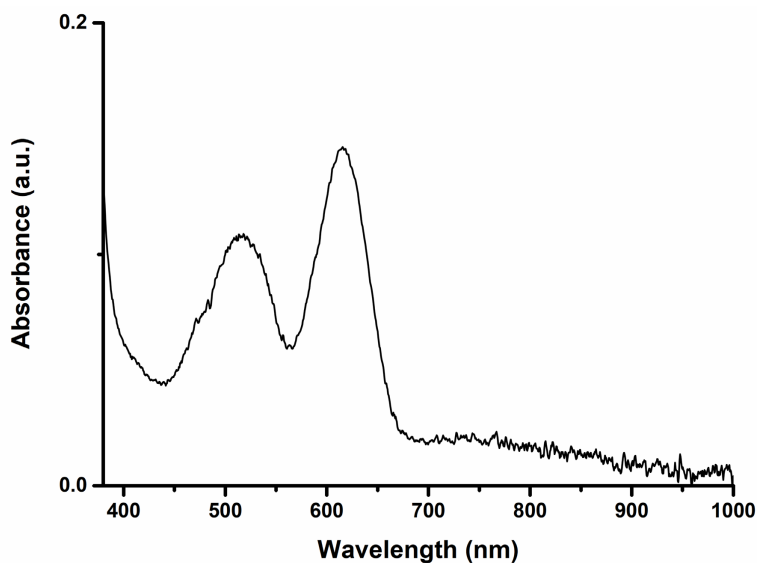


**Figure AIV.15.** UV-Visible spectrum of 2.5 mM solution of  $[2_{\text{NCS}}]$  in acetone, recorded using a transmission dip probe with path length of 1.4 mm.

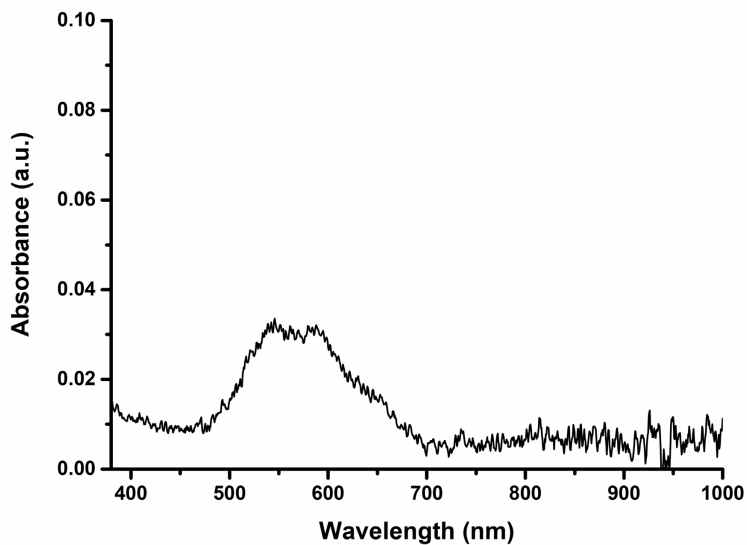


**Figure AIV.16.** UV-Visible spectrum of 2.5 mM solution of  $[3_{\text{Cl}}]$  in acetonitrile, recorded using a transmission dip probe with path length of 1.4 mm.

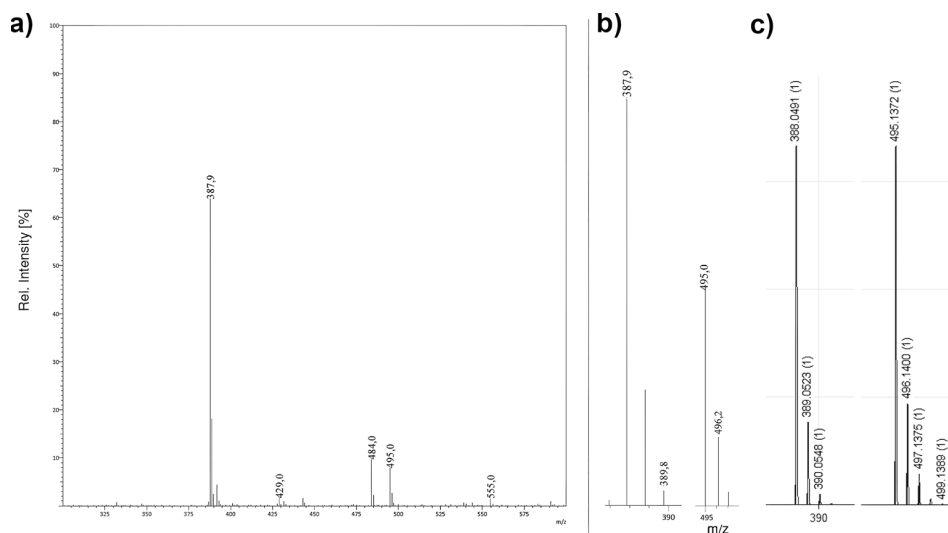


**Figure AIV.17.** ESI-MS spectrum of a) the reaction of Hquin,  $K_2CO_3$ , and *in situ* formed  $[Co_2(L^{mpz}SSL^{mpz})(Br)_4]$  dissolved in acetonitrile; b) the experimental isotopic distribution; c) simulated isotopic distribution. ESI-MS found (calcd.) for  $[Co(L^{mpz}S)(quin)]^+$   $m/z$  495.0 (495.1), for  $[Co(quin)_2(MeCN)]^+$   $m/z$  387.9 (388.0).

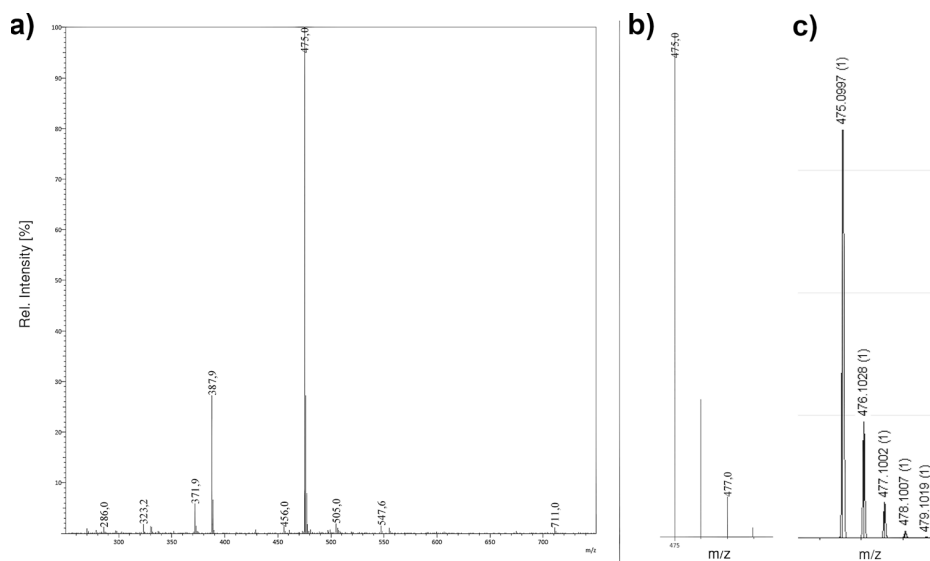


**Figure AIV.18.** ESI-MS spectrum of a) the reaction of Hquin,  $K_2CO_3$ , and *in situ* formed  $[Co_2(L^pSSL^p)(Cl)_4]$  dissolved in acetonitrile; b) the experimental isotopic distribution; c) simulated isotopic distribution. ESI-MS found (calcd.) for  $[Co(L^pS)(quin)]^+$   $m/z$  475.0 (475.1), for  $[Co(quin)_2(MeCN)]^+$   $m/z$  387.9 (388.0).

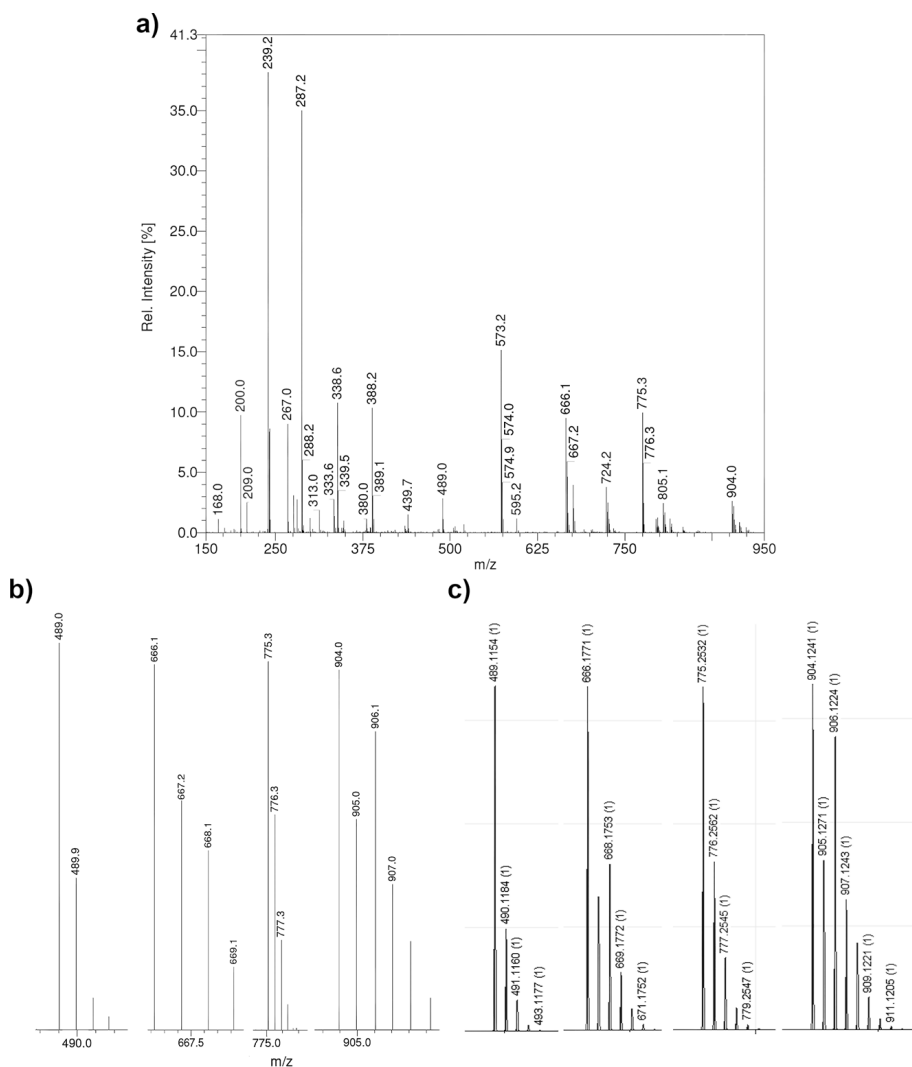


**Figure AIV.19.** ESI-MS spectrum of a) the reaction of Hquin,  $K_2CO_3$ , and *in situ* formed  $[Co_2(L^3SSL^3)(Cl)_4]$  dissolved in methanol; b) the experimental isotopic distribution; c) simulated isotopic distribution spectra. ESI-MS found (calcd.) for  $[Co(L^3S)(quin)]^+$   $m/z$  489.0 (489.1), for  $[Co(quin)_2(MeCN)]^+$   $m/z$  387.9 (388.0), for  $[L^3SSL^3 + H^+]^+$   $m/z$  573.2 (573.3), for  $[L^3SSL^3 + 2H^+]^{2+}$   $m/z$  287.2 (287.2), for  $[L^3SSL^3 + Co + Cl]^+$   $m/z$  666.1 (666.2), for  $[L^3SSL^3 + Co + quin]^+$   $m/z$  775.3 (775.3), and for  $[Co_2(L^3SSL^3)(Cl)_2(quin)]^+$   $m/z$  904.0 (904.1).

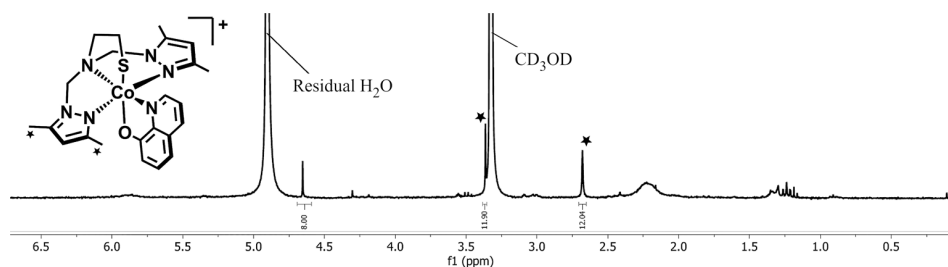


**Figure AIV.20.**  $^1\text{H}$ -NMR spectrum of the brown powder of presumably  $[\text{Co}(\text{L}^{\text{mpzS}})(\text{quin})]\text{Br}$  dissolved in  $\text{MeOD}_4$ . The aromatic region contains no signal.

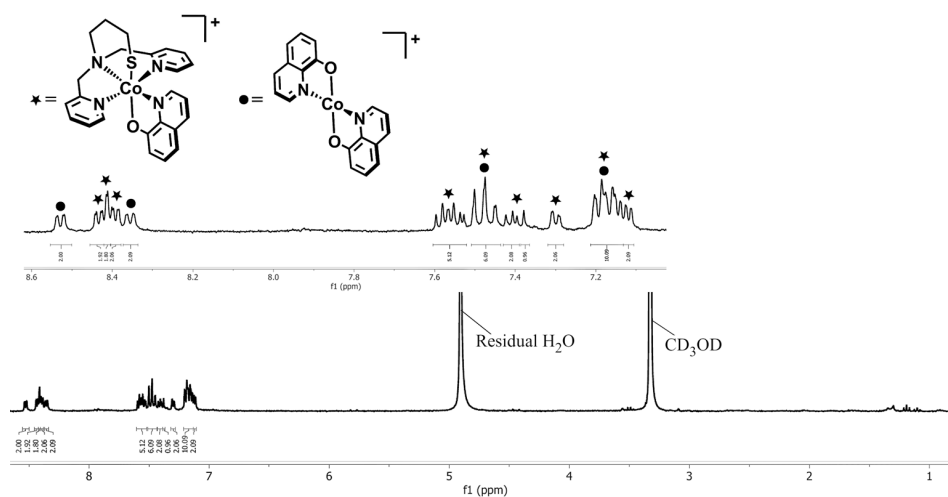


**Figure AIV.21.**  $^1\text{H}$ -NMR spectrum of the brown powder of presumably  $[\text{Co}(\text{L}^{\text{pS}})(\text{quin})]\text{Cl}$  dissolved in  $\text{MeOD}_4$ . Inset shows the peaks in the aromatic region (between 7.0 – 8.6 ppm). The peaks assigned are for the species  $[\text{Co}(\text{L}^{\text{pS}})(\text{quin})]^+$  and  $[\text{Co}(\text{quin})_2]^+$ . However, the aliphatic peaks of the ligand  $\text{L}^{\text{pS}}$  are missing.

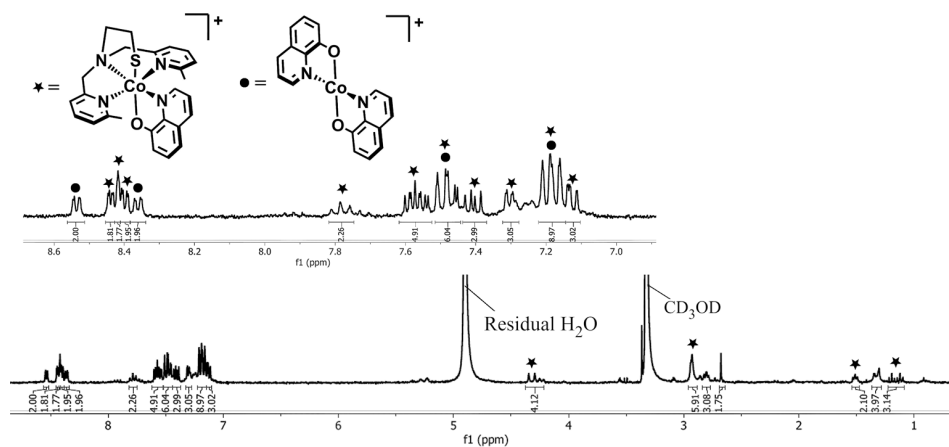


**Figure AIV.22.**  $^1\text{H}$ -NMR spectrum of the brown powder of presumably  $[\text{Co}(\text{L}^3\text{S})(\text{quin})]\text{Cl}$  dissolved in  $\text{MeOD}_4$ . Inset shows the peaks in the aromatic region (between 7.0 – 8.6 ppm). The peaks assigned are for the species  $[\text{Co}(\text{L}^3\text{S})(\text{quin})]^+$  and  $[\text{Co}(\text{quin})_2]^+$ .

**Table AIV.1.** Crystallographic data for compound [1<sub>NCS</sub>] and [1<sub>Br</sub>].

	[1 <sub>NCS</sub> ]	[1 <sub>Br</sub> ]
Chemical formula	C <sub>32</sub> H <sub>44</sub> Co <sub>2</sub> N <sub>14</sub> S <sub>6</sub> ·2(C <sub>2</sub> H <sub>3</sub> N)	C <sub>28</sub> H <sub>44</sub> Br <sub>4</sub> Co <sub>2</sub> N <sub>10</sub> S <sub>2</sub>
$M_r$	1017.14	1022.35
Crystal system	Monoclinic	Triclinic
Space group	$C2/c$	$P-1$
Cell lengths ( $a$ , $b$ , $c$ ) (Å)	27.4033 (3), 10.05127 (11), 19.6772 (3)	8.6620 (3), 14.5167 (4), 15.3806 (4)
Cell angles ( $\alpha$ , $\beta$ , $\gamma$ ) (°)	90, 101.5415 (11), 90	82.892 (2), 82.030 (2), 89.653 (2)
Cell volume (Å <sup>3</sup> )	5310.26 (12)	1900.49 (10)
$Z$	4	2
$\mu$ (mm <sup>-1</sup> )	7.43	5.22
Crystal size (mm)	0.38 × 0.28 × 0.22	0.14 × 0.07 × 0.04
Temperature (K)	110	110
Diffractometer	SuperNova, Dual, Cu at zero, Atlas detector	SuperNova, Dual, Cu at zero, Atlas detector
Radiation type	Cu $K\alpha$	Mo $K\alpha$
$T_{\min}$ , $T_{\max}$	0.180, 0.396	0.632, 0.976
No. of measured, independent and observed [ $I > 2\sigma(I)$ ] reflections	21714, 5193, 4734	32103, 7468, 6234
$R_{\text{int}}$	0.033	0.039
$(\sin \theta/\lambda)_{\text{max}}$ (Å <sup>-1</sup> )	0.616	0.617
$R[F^2 > 2\sigma(F^2)]$ , $wR(F^2)$ , $S$	0.035, 0.090, 1.04	0.038, 0.094, 1.03
No. of reflections	5193	7468
No. of parameters	276	423
H-atom treatment	H-atom parameters constrained	H-atom parameters constrained
$\Delta\rho_{\text{max}}$ , $\Delta\rho_{\text{min}}$ (e Å <sup>-3</sup> )	0.45, -0.40	2.45, -1.37



**Table AIV.2.** Crystallographic data for compound [2<sub>NCS</sub>] and [3<sub>Cl</sub>].

	[2]	[3]
Chemical formula	C <sub>34</sub> H <sub>36</sub> Co <sub>2</sub> N <sub>10</sub> S <sub>6</sub>	C <sub>32</sub> H <sub>40</sub> Cl <sub>4</sub> Co <sub>2</sub> N <sub>6</sub> S <sub>2</sub> ·2(C <sub>2</sub> H <sub>3</sub> N)
<i>M<sub>r</sub></i>	894.95	914.59
Crystal system	Monoclinic	Monoclinic
Space group	<i>P</i> 2 <sub>1</sub> / <i>c</i>	<i>I</i> 2/ <i>a</i>
Cell lengths ( <i>a</i> , <i>b</i> , <i>c</i> ) (Å)	13.3213 (3), 11.5322 (3), 26.3107 (7)	15.3973 (3), 8.62095 (19), 31.1728 (6)
Cell angles (α, β, γ) (°)	90, 98.684 (2), 90	90, 97.3686 (19), 90
Cell volume (Å <sup>3</sup> )	3995.62 (18)	4103.69 (15)
<i>Z</i>	4	4
μ (mm <sup>-1</sup> )	1.18	1.21
Crystal size (mm)	0.20 × 0.16 × 0.07	0.32 × 0.09 × 0.06
Temperature (K)	110	110
Diffractometer	SuperNova, Dual, Cu at zero, Atlas detector	SuperNova, Dual, Cu at zero, Atlas detector
Radiation type	Mo <i>K</i> α	Mo <i>K</i> α
<i>T<sub>min</sub></i> , <i>T<sub>max</sub></i>	0.645, 1.000	0.613, 1.000
No. of measured, independent and observed [ <i>I</i> > 2σ( <i>I</i> )] reflections	47666, 9172, 7483	36703, 4706, 4209
<i>R<sub>int</sub></i>	0.037	0.031
(sin θ/λ) <sub>max</sub> (Å <sup>-1</sup> )	0.650	0.650
<i>R</i> [ <i>F</i> <sup>2</sup> > 2σ( <i>F</i> <sup>2</sup> )], <i>wR</i> ( <i>F</i> <sup>2</sup> ), <i>S</i>	0.037, 0.094, 1.06	0.029, 0.075, 1.06
No. of reflections	9172	4706
No. of parameters	469	313
No. of restraints	-	171
H-atom treatment	H-atom parameters constrained	H-atom parameters constrained
Δρ <sub>max</sub> , Δρ <sub>min</sub> (e Å <sup>-3</sup> )	0.74, -0.56	0.75, -0.30

**Table AIV.3.** Complete bond distances and bond angles in [1Br].

Atoms	Distance (Å)	Atoms	Bond angles (°)	Atoms	Bond angles (°)
Co1–S1	2.6084(12)	S1–Co1–N1	81.46(9)	N2–Co2–N32	74.37(13)
Co1–N1	2.264(3)	S1–Co1–N12	91.93(10)	N2–Co2–N42	74.51(13)
Co1–N12	2.129(3)	S1–Co1–N22	76.37(9)	N2–Co2–Br3	88.32(9)
Co1–N22	2.165(3)	S1–Co1–Br1	170.98(3)	N2–Co2–Br4	173.84(9)
Co1–Br1	2.4860(7)	S1–Co1–Br2	88.11(3)	Br4–Co2–N32	101.20(10)
Co1–Br2	2.5299(7)	Br1–Co1–N1	93.23(9)	Br4–Co2–N42	103.85(10)
Co2–N2	2.378(4)	Br1–Co1–N12	93.77(10)	Br4–Co2–Br3	97.83(3)
Co2–N32	2.072(4)	Br1–Co1–N22	95.31(9)	N32–Co2–N42	113.02(15)
Co2–N42	2.060(4)	Br1–Co1–Br2	97.18(2)	N32–Co2–Br3	129.64(12)
Co2–Br3	2.4242(7)	N1–Co1–N12	75.34(12)	N42–Co2–Br3	106.78(10)
Co2–Br4	2.4419(8)	N1–Co1–N22	75.77(12)		
S1–S2	2.0454(14)	N1–Co1–Br2	169.56(9)		
Co2–S2	6.090(1)	N12–Co1–N22	150.12(13)		

**Table AIV.4.** Complete bond distances and bond angles in [1ncs].

Atoms	Distance (Å)	Atoms	Bond angles (°)
Co1–N1	2.3701(17)	N1–Co1–N12	74.71(6)
Co1–N12	2.0444(17)	N1–Co1–N22	74.79(6)
Co1–N22	2.0400(17)	N1–Co1–N3	87.66(7)
Co1–N3	1.9788(18)	N1–Co1–N4	174.40(7)
Co1–N4	1.9952(19)	N4–Co1–N12	102.43(8)
S1–S1	2.0396(10)	N4–Co1–N22	102.70(7)
Co1–S1	6.0600(7)	N4–Co1–N3	97.94(8)
Co1–Co1	11.6906(6)	N3–Co1–N12	119.70(7)
		N3–Co1–N22	112.80(7)
		N12–Co1–N22	116.76(7)

**Table AIV.5.** Complete bond distances and bond angles in [2ncs].

Atoms	Distance (Å)	Atoms	Bond angles (°)	Atoms	Bond angles (°)
Co1–N1	2.2785(19)	N1–Co1–N11	77.09(7)	N2–Co2–N31	77.37(7)
Co1–N11	2.0661(19)	N1–Co1–N21	77.60(7)	N2–Co2–N41	78.38(8)
Co1–N21	2.0530(19)	N1–Co1–N51	174.26(8)	N2–Co2–N71	174.77(8)
Co1–N51	2.018(2)	N1–Co1–N61	87.42(8)	N2–Co2–N81	89.66(8)
Co1–N61	1.990(2)	N51–Co1–N11	99.20(8)	N71–Co2–N31	101.27(9)
Co2–N2	2.2337(19)	N51–Co1–N21	100.04(8)	N71–Co2–N41	97.35(9)
Co2–N31	2.032(2)	N51–Co1–N61	98.11(9)	N71–Co2–N81	95.44(9)
Co2–N41	2.0509(19)	N61–Co1–N11	113.19(9)	N81–Co2–N31	116.85(8)
Co2–N71	1.995(2)	N61–Co1–N21	127.31(8)	N81–Co2–N41	130.82(8)
Co2–N81	1.993(2)	N11–Co1–N21	112.01(7)	N31–Co2–N41	106.76(8)
S1–S2	2.0272(9)				
Co1–S1	6.2951(7)				
Co2–S2	5.6117(8)				
Co1–Co2	7.0894(7)				

**Table AIV.6.** Complete bond distances and bond angles in [3C].

Atoms	Distance (Å)	Atoms	Bond angles (°)
Co1–N1	2.1406(14)	N1–Co1–N11	79.18(6)
Co1–N11	2.1631(14)	N1–Co1–N21	78.41(6)
Co1–N21	2.1918(15)	N1–Co1–Cl1	112.91(4)
Co1–Cl1	2.3235(5)	N1–Co1–Cl2	123.28(4)
Co1–Cl2	2.2976(5)	N21–Co1–N11	157.28(6)
S1–S1	2.0311(12)	N21–Co1–Cl1	95.81(4)
Co1–S1	4.8457(9)	N21–Co1–Cl2	93.52(4)
		N11–Co1–Cl1	96.29(4)
		N11–Co1–Cl2	95.63(4)
		Cl1–Co1–Cl2	123.78(2)

# Samenvatting

## *Inleiding*

Onderzoek naar synthetische modellen van actieve plaatsen van enzymen heeft veel begrip opgeleverd van de chemische processen die plaatsvinden in deze enzymen, zoals de katalytische mechanismes of de rol van een specifiek onderdeel in de actieve plaatsen. Gedurende dit soort onderzoek wordt regelmatig unieke reactiviteit van dit soort synthetische modellen gevonden. Één van de vele soorten reactiviteit die in de laatste twintig jaar gevonden is, is de redoxinteractie tussen disulfideliganden en overgangsmetaalionen. Deze redoxinteracties kunnen zodanig te beïnvloed worden dat veranderingen in de oxidatietoestand van het zwavelligand en het overgangsmetaalion plaatsvindt. Dit is bekend onder de naam redoxconversiereactie. Deze redoxconversiereacties zijn belangrijk omdat ze kunnen leiden tot begrip van de redoxreacties die veel voorkomen in de natuur.

Ondanks het belang van redoxconversiereacties van metaal-disulfide- en metaal-thiolaatcomplexen zijn er tot nu toe slechts enkele studies gerapporteerd hierover. De meerderheid van deze studies waren gericht op koper-gebaseerde disulfide/thiolaat conversies. Recent zijn er verschillende studies gerapporteerd die kobalt(II)-disulfide en kobalt(III)-thiolaatcomplexen betreffen. In lijn met de waarnemingen in de op koper-gebaseerde systemen, wordt de kobalt-disulfide/thiolaat conversie beïnvloedt door kleine veranderingen in de coördinatieomgeving, echter zijn er meer voorbeelden nodig om het reactiemechanisme te begrijpen. In Hoofdstuk 1 wordt een uitgebreide uiteenzetting gegeven van relevante, nieuwe redoxconversiereacties.

## *Het Belang van Ligandveldsterkte en Ligandoriëntatie in de Redoxconversie van Co(II)-disulfide- naar Co(III)-thiolaatcomplexen*

Ondanks een aantal recente voorbeelden van kobalt(II)-disulfide naar kobalt(III)-thiolaat redoxconversiereacties, is er een beperkt begrip van hoe de coördinatieomgeving van het metaalion deze reactie beïnvloedt. In de Hoofdstukken 2 en 3 zijn resultaten beschreven van onze zoektocht naar begrip van deze reactie door de ligandveldsterkte van de toegevoegde liganden in beschouwing te nemen. Hiervoor zijn de liganden 2,2'-bipyridine (bpy) en

8-quinolinolaat ( $\text{quin}^-$ ) gebruikt. Beide worden beschouwd als een ligand met een relatief hoge ligandveldsterkte. Daarnaast zou de negatieve lading op het  $\text{quin}^-$  ligand de positieve lading van het kobalt(III)-thiolaatcomplex kunnen stabiliseren.

Wanneer bpy wordt toegevoegd aan het kobalt(II)-disulfidecomplex  $[\text{Co}_2(\text{L}^1\text{SSL}^1)(\text{Cl})_4]$  leidt dit tot de vorming van het kobalt(III)-thiolaatcomplex  $[\text{Co}(\text{L}^1\text{S})(\text{bpy})]^{2+}$ , zoals beschreven in Hoofdstuk 2. Tegen de verwachting in werden ook de bijproducten  $[\text{Co}_2(\text{L}^1\text{SSL}^1)(\text{bpy})_2(\text{Cl})_2](\text{Cl})_2$  en  $[\text{Co}(\text{bpy})_3]^{n+}$  gevormd. In Hoofdstuk 3 wordt gerapporteerd dat de reactie met  $\text{quin}^-$  leidt tot het product  $[\text{Co}(\text{L}^1\text{S})(\text{quin})]^+$  in nagenoeg kwantitatieve opbrengst, zonder dat de chloride liganden verwijderd hoeven te worden. Daarnaast leidt het gebruik van  $\text{quin}^-$  tot de omzetting van het complex  $[\text{Co}_2(\text{L}^2\text{SSL}^2)(\text{Cl})_4]$ . Verschillende pogingen om ligand  $\text{L}^2\text{SSL}^2$  met kobalt(II) in de redoxconversiereactie te gebruiken zijn gerapporteerd, maar tot nu toe bleek de vorming van het Co(III)-thiolaatcomplex niet te gebeuren. In dit geval werd echter ook een bijproduct gevonden, namelijk  $[\text{Co}_2(\text{L}^2\text{SSL}^2)(\text{quin})_2(\text{Cl})_2]$ .

Niettemin geven de kristalstructuren van deze bijproducten waardevolle inzichten in hoe de omzetting van een kobalt(II)-disulfide- naar een kobalt(III)-thiolaatcomplex verloopt. In de structuur van het bijproduct  $[\text{Co}_2(\text{L}^1\text{SSL}^1)(\text{bpy})_2(\text{Cl})_2]^{2+}$  zijn de stikstofatomen in een faciale oriëntatie, wat het naderen van de disulfidegroep naar het kobaltcentrum verhindert. In tegenstelling tot de structuur van  $[\text{Co}_2(\text{L}^1\text{SSL}^1)(\text{bpy})_2(\text{Cl})_2]^{2+}$ , zijn in de structuur van  $[\text{Co}_2(\text{L}^2\text{SSL}^2)(\text{quin})_2(\text{Cl})_2]$  de stikstofatomen in een meridionale oriëntatie wat het naderen van de disulfidegroep wel toestaat. Dit maakt een efficiënte elektronenoverdracht mogelijk.

Er zijn DFT berekeningen uitgevoerd om een inschatting te verkrijgen van de ligandveldsterkte van de liganden in de complexen. Molecuulorbitaalanalyses laten zien dat de geschatte  $d$ -orbitaalsplittingsenergie van het vereenvoudigde Co(II)-disulfidecomplex zeker kleiner is dan die van de Co(III)-thiolaatcomplexen. De geschatte  $d$ -orbitaalsplittingsenergie van  $[\text{Co}(\text{L}^1\text{S})(\text{bpy})]^{2+}$  lijkt kleiner te zijn dan die van  $[\text{Co}(\text{L}^1\text{S})(\text{MeCN})_2]^{2+}$ , wat suggereert dat bpy zorgt voor een kleinere ligandveldsplitsing dan acetonitril. Naast dat er een overmaat aan acetonitril aanwezig is in de reactie, kan dit ook de bijproducten verklaren die gevonden worden als bpy gebruikt wordt. De geschatte  $d$ -orbitaalsplittingsenergie voor het complex  $[\text{Co}(\text{L}^1\text{S})(\text{quin})]^+$  lijkt iets hoger te zijn dan die

van  $[\text{Co}(\text{L}^1\text{S})(\text{bpy})]^{2+}$ , wat in overeenstemming is met de experimentele resultaten. Een vergelijking van de geschatte *d*-orbitaalsplitsing van  $[\text{Co}(\text{L}^1\text{S})(\text{quin})]^+$  en  $[\text{Co}(\text{L}^2\text{S})(\text{quin})]^+$  liet zien dat het ligand  $\text{L}^2\text{SSL}^2$  een kleinere ligandveldsplitsing veroorzaakt dan  $\text{L}^1\text{SSL}^1$ . Ondanks het elektronendonende effect, is er gerapporteerd dat *ortho*-methylering van pyridinegroepen in  $\text{L}^2\text{SSL}^2$  zorgt voor een verminderd donerend vermogen van de pyridinestikstofatomen. Dit is voornamelijk een sterisch effect, resulterend in grotere metaal-stikstof afstanden, en dus een kleinere ligandveldsplitsing.

De resultaten beschreven in Hoofdstukken 2 en 3 laten zien dat ook de oriëntatie van het toegevoegde ligand en van het disulfideligand de redoxconversie beïnvloeden. In Hoofdstuk 2 is het toegevoegde ligand bpy een symmetrisch, bidentaat ligand. Daarom is in dit geval het effect van de oriëntatie van het disulfideligand onderzocht met computationele methodes. Hieruit is gebleken dat het hoogste SOMO niveau van het hypothetische intermediair waarin de stikstofdonoren van het disulfideligand meridionaal gebonden zijn meer gedestabiliseerd is dan dat van het faciale intermediair die in de kristalstructuur is gevonden. Dit duidt erop dat elektronenoverdracht van Co naar S makkelijker gaat wanneer de stikstofatomen van het ligand  $\text{L}^1\text{S}$  in een meridionale oriëntatie zitten. In tegenstelling tot bpy is het ligand  $\text{quin}^-$  uit Hoofdstuk 3 asymmetrisch; vandaar dat in dit geval de invloed van de oriëntatie van  $\text{quin}^-$  aan kobalt theoretisch onderzocht is. Het complex  $[\text{Co}(\text{L}^1\text{S})(\text{quin})]^+$  is energetisch meer stabiel wanneer de negatief geladen zuurstofdonor *trans* gebonden is ten opzichte van het zwavelatoom vergeleken met wanneer die *trans* zit tot de stikstofdonor van het tertiaire amine. Kwantumchemische analyses lieten zien dat coördinatie van de zuurstofdonor van  $\text{quin}^-$  tegenover het zwavelatoom van het ligand  $\text{L}^1\text{S}$  voordeel heeft van een hogere elektrostatistische interactie van de aromatische ringen van  $\text{quin}^-$  en het positiefgeladen fragment  $[\text{Co}(\text{L}^1\text{S})]^{2+}$ .

#### *De Gelijkenis tussen Selenium en Zwavel in de Redoxconversiereactie*

We hebben onze studie uitgebreid naar selenium, waarvan bekend is dat het vergelijkbare eigenschappen heeft als zwavel, met name ook in redoxreacties. De eerste redoxconversiereactie voor een Co(II)-diselenide- naar Co(III)-selenolaatcomplex is beschreven in Hoofdstuk 4. Het Co(II)-diselenidecomplex  $[\text{Co}_2(\text{L}^1\text{SeSeL}^1)(\text{Cl})_4]$  is verkregen met het ligand  $\text{L}^1\text{SeSeL}^1$ , een nieuw ligand dat vergelijkbaar is met het ligand  $\text{L}^1\text{SSL}^1$  dat

beschreven is in de Hoofdstukken 2 en 3. De spectroscopische eigenschappen van het diselenidecomplex  $[\text{Co}_2(\text{L}^1\text{SeSeL}^1)(\text{Cl})_4]$  lijken op die van het disulfideanaloog  $[\text{Co}_2(\text{L}^1\text{SSL}^1)(\text{Cl})_4]$ . De vorming van Co(III)-selenolaatcomplexen werd bewerkstelligd door de reactie van  $\text{L}^1\text{SeSeL}^1$  met  $\text{Co}(\text{SCN})_2$ , wat resulteerde in  $[\text{Co}(\text{L}^1\text{Se})(\text{NCS})_2]$ , door verwijdering van chloride-ionen van  $[\text{Co}_2(\text{L}^1\text{SeSeL}^1)(\text{Cl})_4]$  in een acetonitril oplossing wat resulteerde in  $[\text{Co}(\text{L}^1\text{Se})(\text{MeCN})_2]^{2+}$ , of door de toevoeging van  $\text{quin}^-$  aan  $[\text{Co}_2(\text{L}^1\text{SeSeL}^1)(\text{Cl})_4]$ , waardoor  $[\text{Co}(\text{L}^1\text{Se})(\text{quin})]^+$  verkregen werd; deze producten vertonen sterke overeenkomsten met de thiolaatanalogen beschreven in Hoofdstukken 2 en 3. Er is echter vastgesteld dat de kobalt(III)-selenolaatcomplexen vrij onstabiel zijn in oplossing. DFT berekeningen gaven de indicatie dat de selenolaatdonor zorgt voor een kleinere ligandveldopsplitsing dan de thiolaatdonor. In combinatie met de opgedane kennis uit de Hoofdstukken 2 en 3, duiden deze resultaten erop dat de omzetting van Co(II)-diselenide naar Co(III)-thiolaat niet moeilijker is dan voor de zwavelanalogen, maar dat de selenolaatverbindingen minder stabiel zijn in oplossing. Deze resultaten laten zien dat selenium en zwavel vergelijkbaar zijn in de redoxconversiereactie, maar duiden ook op de verschillen die relevant kunnen zijn voor verdere studies met betrekking tot de kinetiek van de reactie.

#### *Ligandmodificatie en Stabilisatie van Co(III)-thiolaatcomplexen*

In Hoofdstuk 5 zijn de resultaten beschreven van het gebruik van drie verschillende disulfideliganden in pogingen om hiermee de bijbehorende Co(III)-thiolaatcomplexen te verkrijgen. In het ligand  $\text{L}^3\text{SSL}^3$  zijn alle vier de pyridinegroepen ten opzichte van ligand  $\text{L}^1\text{SSL}^1$  gemethyleerd. Het ligand  $\text{L}^p\text{SSL}^p$  lijkt op  $\text{L}^1\text{SSL}^1$  maar bevat twee propyleen structuren tussen de tertiaire amines en de disulfidegroepen. Het ligand  $\text{L}^{\text{mpz}}\text{SSL}^{\text{mpz}}$  verschilt aanzienlijk verschillend van  $\text{L}^1\text{SSL}^1$  aangezien het dimethylpyrazoolgroepen in plaats van pyridinegroepen bevat.

Een reeks van Co(II)-disulfidecomplexen met deze drie verschillende liganden zijn geïsoleerd en gekarakteriseerd. Het ligand in de verbinding  $[\text{Co}_2(\text{L}^{\text{mpz}}\text{SSL}^{\text{mpz}})(\text{Br})_4]$  coördineert onverwachts asymmetrisch; één van de disulfidezwavelatomen is gecoördineerd aan één van de kobaltcentra, terwijl het andere zwavelatoom niet coördineert. De reactie tussen het ligand  $\text{L}^{\text{mpz}}\text{SSL}^{\text{mpz}}$  met  $\text{Co}(\text{SCN})_2$  geeft het kobalt(II)-disulfidecomplex

$[\text{Co}_2(\text{L}^{\text{mpz}}\text{SSL}^{\text{mpz}})(\text{NCS})_4]$ , wat een indicatie is dat de ligandveldsterkte van het pyrazoolligand te klein is door om de anionen met een relatief sterk ligandveld gecompenseerd te kunnen worden. Onverwachts leverde de reactie tussen  $\text{L}^{\text{p}}\text{SSL}^{\text{p}}$  en  $\text{Co}(\text{SCN})_2$  ook een kobalt(II)-disulfidecomplex op.

Gebaseerd op de opgedane kennis in de vorige Hoofdstukken, is geprobeerd om Co(III)-thiolaatcomplexen te vormen van de liganden  $\text{L}^{\text{mpz}}\text{SSL}^{\text{mpz}}$ ,  $\text{L}^{\text{p}}\text{SSL}^{\text{p}}$ , en  $\text{L}^3\text{SSL}^3$  door de toevoeging van  $\text{quin}^-$ . De vorming van de Co(III)-thiolaatcomplexen leek succesvol aangezien de ESI-MS spectra signalen vertoonden die toegekend konden worden aan de verwachte producten. In de meeste pogingen werd echter minstens één bijproduct gevormd en het bleek onmogelijk om de gewenste thiolaatverbindingen zuiver te verkrijgen. Over het algemeen duiden deze resultaten de erop dat de ligandveldsterkte van  $\text{L}^{\text{mpz}}\text{SSL}^{\text{mpz}}$ ,  $\text{L}^{\text{p}}\text{SSL}^{\text{p}}$ , en  $\text{L}^3\text{SSL}^3$  niet groot genoeg is om de Co(II)-disulfidecomplexen om te zetten naar de Co(III)-thiolaat redoxisomeren.





# Summary in Indonesian (Ringkasan)

## *Pengantar*

Penelitian mengenai situs aktif dari enzim dengan bantuan model senyawa telah membuahkan banyak hasil dalam pemahaman tentang proses-proses kimia seperti mekanisme katalitik enzim atau peran dari gugus tertentu dalam sebuah situs aktif. Seringkali selama proses penelitian tersebut, ditemukan beberapa reaktivitas baru yang sangat menarik. Salah satu dari beberapa reaktivitas baru yang ditemukan dalam kurun waktu dua dekade terakhir ialah interaksi redoks ligan disulfida dengan ion-ion logam transisi. Interaksi redoks tersebut dapat dikontrol untuk mengubah keadaan redoks dari sulfur sebagai ligan maupun ion-ion logam transisi. Hal tersebut kini lebih dikenal dengan nama reaksi pengubahan-redoks. Reaksi-reaksi pengubahan-redoks ini sangat penting karena berkaitan dengan reaksi transfer-elektron yang sering diamati di alam.

Hingga saat ini, hanya terdapat beberapa studi yang telah dilaporkan mengenai reaksi pengubahan-redoks dari senyawa-senyawa kompleks logam-disulfida dan logam-tiolat. Mayoritas dari studi-studi sebelumnya memiliki fokus pada pengubahan senyawa disulfida/tiolat berbasis tembaga. Walaupun demikian, beberapa contoh reaksi pengubahan-redoks berbasis kobalt mulai bermunculan pada dua dekade terakhir. Walaupun untuk saat ini pemahaman tentang mekanisme pengubahannya masih belum berkembang, pengubahan senyawa disulfida/tiolat berbasis kobalt dapat dikontrol dengan mengubah lingkungan kimia dari senyawa tersebut. Pada Bab 1, perkembangan terbaru dalam reaksi pengubahan-redoks telah dibahas dengan detail.

## *Peranan Kekuatan Medan-Ligan dan Orientasi Ligan dalam Reaksi Pengubahan-redoks Senyawa Kompleks Kobalt(II)-disulfida ke Kobalt(III)-tiolat*

Walaupun terdapat beberapa contoh reaksi pengubahan-redoks senyawa kobalt(II)-disulfida menjadi kobalt(III)-tiolat, pemahaman mengenai pengaruh lingkungan kimia dari senyawa kompleks masih sangat terbatas. Pada Bab 2 dan Bab 3, pemahaman reaksi pengubahan-redoks telah dijabarkan dengan fokus kepada kekuatan medan-ligan dari ligan

eksternal. Dalam penelitian ini, ligan 2,2'-bipyridine (bpy) dan 8-quinolinolate ( $\text{quin}^-$ ) yang merupakan ligan dengan medan-ligan kuat digunakan untuk menghasilkan senyawa kobalt(III)-tiolat. Selain itu, muatan negatif dari ligan  $\text{quin}^-$  diduga dapat membantu menstabilkan muatan positif senyawa kompleks kobalt(III)-tiolat.

Penambahan bpy pada senyawa kobalt(II)-disulfida  $[\text{Co}_2(\text{L}^1\text{SSL}^1)(\text{Cl})_4]$  menghasilkan senyawa kobalt(III)-tiolat  $[\text{Co}(\text{L}^1\text{S})(\text{bpy})]^{2+}$ . Walaupun demikian, produk samping yaitu  $[\text{Co}_2(\text{L}^1\text{SSL}^1)(\text{bpy})_2(\text{Cl})_2](\text{Cl})_2$  dan  $[\text{Co}(\text{bpy})_3]^{n+}$  ternyata juga terbentuk. Pada bab 3, senyawa kobalt(III)-tiolat  $[\text{Co}(\text{L}^1\text{S})(\text{quin})]^+$  dapat terbentuk menggunakan reaksi dengan ligan  $\text{quin}^-$  dengan hasil yang kuantitatif tanpa menyingkirkan ligan klorida. Terlebih lagi, penggunaan ligan  $\text{quin}^-$  mampu menginduksi pengubahan-redoks senyawa kompleks  $[\text{Co}_2(\text{L}^2\text{SSL}^2)(\text{Cl})_4]$ , yang sebelumnya tidak dapat dilakukan. Walaupun demikian, produk samping  $[\text{Co}_2(\text{L}^2\text{SSL}^2)(\text{quin})_2(\text{Cl})_2]$  juga terbentuk dalam kasus ini.

Meskipun merupakan produk samping, hasil elusidasi struktur produk samping yang terbentuk memberikan wawasan tentang bagaimana proses pengubahan kobalt(II)-disulfida menuju kobalt(III)-tiolat terjadi. Pada struktur senyawa  $[\text{Co}_2(\text{L}^1\text{SSL}^1)(\text{bpy})_2(\text{Cl})_2]^{2+}$  atom donor nitrogen dari ligan  $\text{L}^1\text{SSL}^1$  tersusun mengikuti orientasi *facial* sehingga menghambat proses koordinasi gugus disulfida menuju atom pusat kobalt. Sebaliknya, pada struktur  $[\text{Co}_2(\text{L}^2\text{SSL}^2)(\text{quin})_2(\text{Cl})_2]$  atom donor nitrogen dari ligan  $\text{L}^2\text{SSL}^2$  tersusun mengikuti orientasi *meridional* sehingga memungkinkan pendekatan gugus disulfida kepada kobalt untuk proses transfer elektron yang lebih efisien.

Melalui pendekatan kimia komputasi dengan metode DFT, kekuatan medan-ligan di dalam senyawa-senyawa tersebut dapat diperkirakan. Analisis orbital molekul menunjukkan bahwa perkiraan energi pembelahan orbital-*d* pada senyawa kobalt(II)-disulfida dipastikan lebih rendah daripada pada senyawa kobalt(III)-tiolat. Menariknya, perkiraan energi pembelahan orbital-*d* pada senyawa  $[\text{Co}(\text{L}^1\text{S})(\text{bpy})]^{2+}$  juga terlihat lebih rendah daripada senyawa  $[\text{Co}(\text{L}^1\text{S})(\text{MeCN})_2]^{2+}$ . Hal ini mengindikasikan ligan bpy memiliki medan-ligan yang lebih lemah daripada asetonitril. Terlepas dari jumlah asetonitril dalam reaksi yang berlebih di dalam reaksi (sebagai pelarut), hasil ini mendukung pembentukan produk samping ketika bpy digunakan dalam reaksi. Sesuai dengan hasil eksperimen, perkiraan energi pembelahan orbital-*d* pada senyawa  $[\text{Co}(\text{L}^1\text{S})(\text{quin})]^+$  lebih besar daripada  $[\text{Co}(\text{L}^1\text{S})(\text{bpy})]^{2+}$ . Selain itu,

perbandingan perkiraan energi pembelahan orbital-*d* pada  $[\text{Co}(\text{L}^1\text{S})(\text{quin})]^+$  dan  $[\text{Co}(\text{L}^2\text{S})(\text{quin})]^+$  mengindikasikan ligan  $\text{L}^2\text{SSL}^2$  memiliki medan-ligan yang lebih lemah daripada  $\text{L}^1\text{SSL}^1$ . Meskipun terdapat efek donasi-elektron, dengan adanya gugus metil pada posisi orto pada piridin, diketahui dapat menurunkan kemampuan donasi dari nitrogen pada piridin dikarenakan rintangan sterik.

Pada bab 2 dan 3 juga dijelaskan bahwa, selain orientasi ligan disulfida, orientasi ligan eksternal juga mempengaruhi reaksi pengubahan-redoks. Pada bab 2, ligan bpy adalah ligan bidentat yang simetris, sehingga hanya orientasi ligan disulfida yang berpengaruh dan dapat diteliti lebih lanjut dengan metode komputasi. Tingkat energi tertinggi dari SOMO (*singly occupied molecular orbital*) pada senyawa hipotetikal dengan orientasi ligan disulfida yang *meridional* terbukti lebih tinggi daripada orientasi *facial* (dimana orientasi ini ditemukan pada struktur kristal). Hal ini menunjukkan bahwa transfer elektron dari atom Co kepada atom S akan lebih mudah terjadi jika konformasi ligan  $\text{L}^1\text{S}$  adalah *meridional*. Setelah mengetahui bahwa konformasi ligan yang optimal adalah *meridional*, ligan  $\text{quin}^-$  yang asimetris dapat memiliki dua mode ikatan / orientasi, dimana pembahasan lebih dalam mengenai hal ini terdapat pada Bab 3. Metode komputasi menunjukkan bahwa senyawa  $[\text{Co}(\text{L}^1\text{S})(\text{quin})]^+$  lebih stabil secara energi ketika atom oksigen dari  $\text{quin}^-$  terkoordinasi secara *trans* terhadap atom sulfur dari ligan  $\text{L}^1\text{S}$  dibandingkan ketika koordinasi tersebut *trans* terhadap atom nitrogen dari amina tersier. Hal ini dikarenakan lebih kuatnya interaksi elektrostatik antara cincin aromatik dari  $\text{quin}^-$  dan muatan positif dari fragmen  $[\text{Co}(\text{L}^1\text{S})]^{2+}$ .

#### *Kemiripan Selenium dan Sulfur pada Reaksi Pengubahan-redoks*

Lingkup studi reaksi pengubahan-redoks telah kami perluas dengan menguji unsur selenium yang memiliki sifat serupa dengan sulfur, terutama dalam reaksi-reaksi redoks. Untuk pertama kalinya, reaksi pengubahan-redoks dari senyawa kobalt(II)-diselenida menuju kobalt(III)-diselenolat dijabarkan di bab 4. Senyawa kobalt(II)-diselenida  $[\text{Co}_2(\text{L}^1\text{SeSeL}^1)(\text{Cl})_4]$  diperoleh dengan menggunakan ligan  $\text{L}^1\text{SeSeL}^1$  yang merupakan ligan baru yang serupa dengan ligan  $\text{L}^1\text{SSL}^1$  pada bab 2 dan 3. Sifat-sifat spektroskopi dari senyawa  $[\text{Co}_2(\text{L}^1\text{SeSeL}^1)(\text{Cl})_4]$  menyerupai senyawa  $[\text{Co}_2(\text{L}^1\text{SSL}^1)(\text{Cl})_4]$ . Pembentukan senyawa kobalt(III)-selenolat dapat dilakukan dengan cara yang serupa dengan pembentukan senyawa kobalt(III)-tiolat, yaitu melalui reaksi antara  $\text{L}^1\text{SeSeL}^1$  dengan  $\text{Co}(\text{SCN})_2$

(menghasilkan  $[\text{Co}(\text{L}^1\text{Se})(\text{NCS})_2]$ ), dengan menyingkirkan ion-ion klorida dalam larutan asetonitril (menghasilkan  $[\text{Co}(\text{L}^1\text{Se})(\text{MeCN})_2]^{2+}$ ), atau dengan penambahan ligan  $\text{quin}^-$  kepada  $[\text{Co}_2(\text{L}^1\text{SeSeL}^1)(\text{Cl})_4]$  (menghasilkan  $[\text{Co}(\text{L}^1\text{Se})(\text{quin})]^+$ ). Namun, kami menemukan bahwa senyawa-senyawa kobalt(III)-selenolat kurang stabil dalam bentuk larutan. Metode komputasi dengan DFT mengindikasikan lebih lemahnya atom donor selenium dibandingkan dengan atom donor sulfur dalam energi pembelahan orbital- $d$ . Berdasarkan informasi yang telah diperoleh di bab 2 dan bab 3, hasil penelitian menunjukkan bahwa sebenarnya reaksi pengubahan-redoks senyawa kobalt(II)-diselenida menuju kobalt(III)-selenolat tidak sulit dilakukan jika dibandingkan dengan analog sulfurnya, namun sayangnya senyawa-senyawa yang mengandung selenium ini kurang stabil dalam bentuk larutan. Hasil eksperimen kami menunjukkan bahwa tak hanya kemiripan selenium dan sulfur pada reaksi pengubahan-redoks yang ditemukan, namun juga perbedaannya yang berpotensi sebagai topik penelitian di masa mendatang.

#### *Modifikasi Ligan dan Stabilisasi Senyawa Kompleks Kobalt(III)-tiolat*

Pada bab 5, kami mendeskripsikan tiga ligan disulfida yang berbeda untuk memperoleh senyawa kobalt(III)-tiolat, yakni  $\text{L}^3\text{SSL}^3$ ,  $\text{L}^p\text{SSL}^p$ , dan  $\text{L}^{\text{mpz}}\text{SSL}^{\text{mpz}}$ . Pada ligan  $\text{L}^3\text{SSL}^3$ , keempat gugus piridin dari ligan  $\text{L}^1\text{SSL}^1$  telah dimetilasi, sementara pada ligan  $\text{L}^p\text{SSL}^p$  yang juga mirip dengan ligan  $\text{L}^1\text{SSL}^1$ , terdapat dua gugus propilen antara gugus disulfida dan gugus amina tersier. Ligan  $\text{L}^{\text{mpz}}\text{SSL}^{\text{mpz}}$  adalah ligan yang sangat berbeda dengan  $\text{L}^1\text{SSL}^1$  karena gugus piridin digantikan fungsinya oleh gugus dimetilpirazol. Berdasarkan penggunaan ketiga ligan tersebut, beberapa senyawa kobalt(II)-disulfida telah didapatkan dan dikarakterisasi. Senyawa  $[\text{Co}_2(\text{L}^{\text{mpz}}\text{SSL}^{\text{mpz}})(\text{Br})_4]$  menunjukkan pola koordinasi yang asimetris, dimana salah satu atom donor sulfur terkoordinasi kepada atom pusat kobalt sedangkan atom sulfur yang lainnya tidak terkoordinasi. Reaksi ligan yang sama dengan  $\text{Co}(\text{SCN})_2$  menghasilkan  $[\text{Co}_2(\text{L}^{\text{mpz}}\text{SSL}^{\text{mpz}})(\text{NCS})_4]$ . Hal ini mengindikasikan bahwa kekuatan medan-ligan dari gugus pirazol terlalu rendah sehingga anion  $\text{NCS}^-$  pun tidak cukup kuat untuk menghasilkan kobalt(III)-tiolat. Sayangnya, kedua ligan  $\text{L}^p\text{SSL}^p$  dan  $\text{L}^3\text{SSL}^3$  belum berhasil untuk menstabilkan kobalt(III)-tiolat dengan ligan halida maupun  $\text{NCS}^-$ .

Dengan informasi yang didapatkan dari bab-bab sebelumnya, kami mencoba untuk mendapatkan kobalt(III)-tiolat dengan ligan  $L^{mpz}SSL^{mpz}$ ,  $L^pSSL^p$ , dan  $L^3SSL^3$  dengan cara menambahkan ligan  $quin^-$ . Senyawa kobalt(III)-tiolat terbukti dapat terbentuk, yang dibuktikan dari hasil karakterisasi spektroskopi massa. Sayangnya, pada semua percobaan kami menemukan bahwa terdapat setidaknya satu produk samping yang terbentuk. Secara umum, hasil ini mengindikasikan bahwa kekuatan medan-ligan dari ligan  $L^{mpz}SSL^{mpz}$ ,  $L^pSSL^p$ , dan  $L^3SSL^3$  tidak cukup besar untuk mampu menstabilkan kobalt(III)-tiolat tanpa pembentukan produk samping, meskipun telah dibantu dengan ligan  $quin^-$  yang terbukti memiliki medan-ligan yang kuat.

### *Kesimpulan*

Secara singkat, kami telah menunjukkan bahwa terdapat hubungan antara kekuatan medan-ligan dengan proses pengubahan-redoks yang terjadi. Struktur ligan disulfida menjadi salah satu faktor yang sangat berpengaruh dalam reaksi pengubahan-redoks. Selain itu, dengan meningkatkan kekuatan medan-ligan dan memanfaatkan ligan eksternal, reaksi pengubahan-redoks juga dapat terjadi. Berdasarkan hasil penelitian, dapat disimpulkan bahwa terdapat empat faktor yang mempengaruhi pembentukan produk samping dalam proses pengubahan-redoks yaitu besarnya kekuatan medan-ligan, muatan dari ligan eksternal, orientasi ligan-ligan dalam senyawa kompleks, dan konstanta pembentukan produk samping relatif terhadap pembentukan senyawa kompleks kobalt(III).



# Curriculum Vitae

Christian Marvelous was born in Malang, East Java, Indonesia, on the 9<sup>th</sup> of March 1994. In August 2012, he moved to Bandung, West Java, to pursue a BSc in chemistry at Institut Teknologi Bandung (ITB). During his studies, he was involved in several extracurricular activities such as the chemistry student association ‘HMK ‘AMISCA’ ITB’, as well as being a leader of the chemistry class of 2012. In July 2016 he obtained a BSc degree *cum laude* with a thesis entitled “Novel Cobalt(II)-Mannich Base Compound as A New Potent Anticancer” under the supervision of Dr. Irma Mulyani and Dr. Deana Wahyuningrum. After finishing his BSc, he started fast-track MSc studies in Inorganic Chemistry at the same university. In January 2017, he started his research internship at University of Groningen, The Netherlands, under the supervision of Dr. Bart Crielgaard with the thesis entitled “Synthesis, Characterization, and Cellular Interactions of Iron Oxide Nanoparticles and Gold-Coated Iron Oxide Nanoparticles”. In October 2017, he graduated *cum laude* and received the best poster award for the final thesis from Chemistry Department Institut Teknologi Bandung.

On the 11<sup>th</sup> of April 2018, he started his PhD in the Metals in Catalysis, Biomimetics, and Inorganic Materials group at Leiden University under supervision of Prof. Dr. Elisabeth Bouwman and Prof. Dr. Célia Fonseca Guerra. During his PhD studies, he supervised several practical courses, six *Leren Onderzoeken 1* students, two BSc students, and one MSc student. He followed a number of courses offered by the Holland Research School of Molecular Chemistry (HRSMC) as well as the Graduate School of Leiden University, including “Scientific Conduct”, “Anxiety, Stress, and Courage”, “Physical Methods in Inorganic Chemistry”, “Molecular Modelling”, and “High Impact Writing”.

The results reported in this thesis were presented at several conferences as listed below:

**Poster Presentation** Netherlands’ Chemistry and Catalysis Conferences (NCCC) XX – XXI, 2019–2020, Noordwijkerhout, The Netherlands

**Poster Presentation** HRSMC Symposium, 2019, Amsterdam, The Netherlands

**Poster Presentation** NWO CHAINS Conference 2019, Veldhoven, The Netherlands



**Oral Presentation** NWO CHAINS Conference 2021, Online, The Netherlands

**Oral Presentation** HRSMC Symposium, 2022, De Duif, Amsterdam, The Netherlands

**Oral Presentation** Netherlands' Chemistry and Catalysis Conference XXIII, 2022, Noordwijkerhout, The Netherlands

# List of Publications

“Cobalt(II)-disulfide compounds with the unusual  $\text{PF}_2\text{O}_2^-$  anion. Ligand-dependent redox conversion to a cobalt(III)-thiolate complex”

F. Jiang<sup>#</sup>, C. Marvelous<sup>#</sup>, A.C. Verschuur, M.A. Siegler, S.J. Teat, and E. Bouwman, *Inorganica Chimica Acta*, 2022, **535**, 120880.

<sup>#</sup>Equal contributions

## Chapter 2

“Probing The Redox Interconversion of Co(II)-disulfide / Co(III)-thiolate Complexes: The Effect of Ligand Field Strength”

C. Marvelous, L. de Azevedo Santos, M.A. Siegler, C. Fonseca Guerra, and E. Bouwman, *Dalton Transactions*, 2022, **51**, 8046-8055

## Chapter 3

“Cleaner and Stronger: How 8-quinolinolate Facilitates Formation of Co(III)-thiolate from Co(II)-disulfide Complexes”

C. Marvelous, L. de Azevedo Santos, M.A. Siegler, C. Fonseca Guerra, and E. Bouwman, *submitted*.

## Chapter 4

“Redox-conversion Reactivity of The Chalcogen Family: Selenium vs Sulfur”

C. Marvelous, M.A. Siegler, C. Fonseca Guerra, and E. Bouwman, *manuscript in preparation*.

## Chapter 5

“Structural Investigations and Reactivity of Cobalt(II)-Disulfide Complexes”

C. Marvelous, M.A. Siegler, and E. Bouwman, *manuscript in preparation*.



# Acknowledgements

The past four years are the most challenging years yet the most sensational and unforgettable years of my life. Being more than ten thousand kilometers away from home, I have grown personally as well as scientifically, and I owe that to people with whom I interacted during the four years of my PhD.

First and foremost, I would like to express my gratitude to Prof. Dr. Elisabeth Bouwman and Prof. Dr. Célia Fonseca Guerra for the opportunity to perform this PhD study. Their scientific guidance has shaped me to be meticulous and keep pushing myself to become a better scientist. The most valuable thing that I have learned from Lies and Célia is how important it is to be critical of my own work. I would like to thank Dr. Maxime A. Siegler, as, without his contribution, this thesis would not contain as many crystal structures as it does now. I am also grateful to Dr. Trevor Hamlin and Dr. Lucas de Azevedo Santos, for their help with DFT studies as well as their scientific contributions to the chapters. I sincerely appreciate Prof. Dr. Sylvestre Bonnet and Dr. Dennis Hetterscheid for the scientific discussions and suggestions during this study. I thank Fons and Karthick for their assistance in operating the NMR spectrometers.

To my previous office mates Feng Jiang and Hans de Bruijn, thank you for all the fun in the lab as well as outside the lab (having dinner and playing games together was fun!). To my current office mates Ashok, whom I can talk to about everything; Dennis who kindly provided the *samenvatting* for me; and Irene who is always bubbly; my gratitude for all the jokes and every discussion that we had, whether it was a serious scientific discussion or just some random topic, I had my share of fun with you guys. Thank you to Sipeng, not only for the ESI-MS measurements but also for the crazy comments and ideas that made me laugh during coffee breaks. Furthermore, to all students whom I supervised, it was great to work with you. Thank you to all the people from MCBIM for making these four years wonderful: Andrea, Aleksandar, Erik, Michael, Anja, Corjan, Ehider, David, Chengyu, Agnese, Valeriia, Vasiliki, Liyan, Ramu, Xuequan, Selda, Sina, Ludovic, Aswin, Yurii, Lan, Wessel, Bas, Daan, Michiel, Nicole, Silvia, Sjoerd, Dana, Kyra, Ross, Phebe, Marleen, Shengxiang, and others which I cannot possibly mention here.

In 2020, when the COVID-19 hit hard and we had to be in a lockdown situation, there were friends who accompanied me even when they are in other parts of the world. I am sincerely grateful for them: Felix, Eunike, Dhimaz, Donny, Novita, Farhan, Della, Zaid, Siwi, Daniel, Danang, Fauzi, Banyu, Rachman, Yovin, Mora, and Yasifa. Special thanks to my best friends Jack and Nicodemus for weekly online meetings and trying to do podcasts and business, even in these hard times.

To my family, their endless support and never-ending love mean a lot to me. Talking to them every weekend motivates me to finish this long journey to my PhD degree. Finally, to Veronica Grace, thank you for being with me since my undergraduate studies and for your encouragement and love for the past (almost) 9 years. I am delighted to have you in my life.

Christian Marvelous